THE GEOCHEMISTRY OF PYRITIC SHALE WEATHERING WITHIN AN ACTIVE LANDSLIDE

by

Alwyn Vear

Submitted in fulfilment of the requirements
for the Degree of Doctor of Philosophy

Departments of Geography and Geology,
University of Sheffield.

November, 1981.

"It's time something was done about that road!"

SUMMARY

Intense chemical weathering accompanies physical instability at the site of a repeatedly active landslide in North Derbyshire. In order to describe and quantify the chemical weathering, a programme of water sampling and analysis was devised. A sequence of reactions are proposed, based on theresults of this work, to account for the observed concentrations of chemical species in the drainage waters.

It is thought that pyrite oxidation, accelerated by the presence of catalytic bacteria, is responsible for the considerable acidity of these waters. Additional reactions involving carbonates and silicates occur at strictly comparable rates and consume over 99% of the acidity prior to the water's emergence in a number of ochre-precipitating springs.

Analysis of the solid reactants and products confirms the suggested sequence of events and suggests a number of ways in which chemical weathering might be related to slope stability. Clay minerals appear to be little affected by weathering, and the growth of precipitate minerals such as gypsum in joints and on bedding planes might be a more important mechanism in shale breakdown. After this initial rapid physical disintegration, chemical weathering, at the surface, proceeds relatively slowly.

Chemical processes build up stresses within the rocks and possibly help to maintain any inherent planes of weakness. Ultimately landslide movement is triggered by increases in porewater pressures brought about by fluctuations in local ground water levels.

ACKNOWLEDGEMENTS

I wish to thank Dr. Charles Curtis for his continued encouragement, enthusiasm and invaluable criticism throughout.

Professor R.S. Waters gave considerable support, and the Natural Environment Research Council provided the necessary funds.

Special thanks also to Margaret, Rod, Villy and Pat - and many others too numerous to mention - of the Geography and Geology Departments, University of Sheffield.

CONTENTS

LIST OF FIGURES

LIST OF PLATES

LIST OF TABLES

1. INTRODUCTION

1.1 Objectives

1.1.1 Physical Background

Mam Tor, in North Derbyshire, is notorious both locally and nationally as the site of an extremely active landslide (Plate 1). Episodes of movement possibly date back some ten or eleven thousand years to the end of the last glaciation in this country.

The precise dating of ancient mass-movement is difficult unless organic material can be found beneath the landslide and subjected to radiometric dating. No such material has been found at Mam Tor, but the landslide does rest on solifluction deposits dated as late Pleistocene, for this region, by McArthur (1970) and Said (1969), which places a maximum age on the landslide of 10,000 years B.P. The presence of an Iron Age hill fort on the summit, which appears to have been dissected by the landslip scar, would suggest a minimum age of at least 2.5 to 3 thousand years.

Recent archaeological excavations, however, have uncovered Bronze Age artifacts from within the 16 acre site and it is thought that occupation may go back still further (Coombs, 1971). Also it is not known for certain that the fort was not originally constructed using the landslide scar as a natural defensive flank; in which case the initiation of landsliding is pushed back still further into prehistory.

In 1802, a major highway was constructed across the landslide (now the A625) by the Manchester to Sheffield Turnpike Company to by-pass the older route through Winnats Pass which has a gradient of one-in-five. The Peak Park Joint Planning Board (1977) observe that since the road was opened in 1802: "Records show that the slip has been more or less continually active and repairs have been carried out annually since its

PLATE 1: A general view of the Mam Tor Landslide looking west from the village of Castleton.

opening which in turn have caused closure of the road on an almost regular basis." More recently the route has been closed for major repairs in 1912, 1933, 1946, 1952 and 1966 (Reed, 1977). In the latter case the rate of landslide movement, and of certain sections of the road, exceeded 0.5 m day^{-1} (Brown, 1977) and the road was closed for two weeks. Following similar movements in March, 1977, the A625 was reduced to a single lane controlled by traffic lights and closed to heavy traffic which, it was believed at the time, contributed to the repeated failure of certain sections. After two years of weight restrictions, however, the road was severely damaged once again, and in January 1979 the route was permanently closed to all through traffic when parts of the road were displaced vertically by more than one metre.

An alternative route is still being sought (see Dunn, 1979).

1.1.2 Chemical Background

Prior to the commencement of this research it was noticed by Curtis (1977, personal communication),and no doubt by others, that in addition to this repeated physical instability Mam Tor is also the site of considerable chemical activity. The evidence for this lies in the fact that certain streams draining the landslide precipitate ochre upon mixing with atmospheric oxygen or with other streams. Further up on the major slipped units of the landslide, where bedrock is exposed due to fracturing, gypsum ($CaSO_4$) can be seen in hand specimen as a major constituent of the rocks. Clearly this mineral could not have been an original component of the sediment (Middle Carboniferous mudstone) as no evaporite deposits of this age are known in the area.

1.1.3 Initial Objectives

The above observations led, at the outset, to the formulation of the two principal objectives of this research. Firstly, the subsequent work

should attempt to describe and possibly even quantify the geochemical reactions taking place within the landslide and giving rise to these somewhat unusual products. Secondly, since both intense physical and chemical activity are occurring in the same small area, the research should investigate the possibility of links between chemical weathering and certain aspects of the geomorphology.

Prior to a discussion of the experimental procedures followed and results obtained, a review of the existing body of literature concerning certain related topics will help to place this research in its wider scientific context.

1.2 Literature Review

1.2.1 Landslides

Mass movements in general, and landslides in particular, have been studied for many years. All too often such studies are essentially descriptive and have been conducted after a major disaster has occurred; such as that at Aberfan in 1966 (see Bishop et al., 1969). Certain workers, however, have studied the actual mechanisms which cause landslide movement and even investigated the possibilities of predicting landslides in any given situation (Hutchinson, 1968; Terzaghi, 1950).

Much of the research on landslides comes from the discipline of civil engineering, where damage to structures (or, more precisely, the prevention of such damage) is the prime concern. An early, and somewhat classic,work dealing with the geological and geomorphological aspects of landslides is presented by Sharpe (1938, reprinted 1960).

More recently Piteau (1970) looks at certain geological controls on landsliding and stresses the importance of discontinuities in bedrock such as bedding and, in particular, jointing. Piteau notes that weathering products often accumulate in joints and the stability of the landslide

mass as a whole is then dependent on the shear strength of this gouge material. The weakest link of all may be at the gouge/bedrock interface.

Similarly, Nonveiller (1967) in a study of the Zalesina and Vajont landslides in Yugoslavia and Italy, respectively, concludes that: "The investigation of stability conditions of rock slopes should be based on a study of the systems of jointing and their relation to possible failure surfaces as well as on comprehensive investigation of the strength parameters of the decomposed material filling the joints".

Most workers are agreed that the ultimate cause of slope failure is an increase in porewater pressure in the bedrock. In an excellent and up-to-date review of work on landslides, Cooke and Doornkamp (1974) note that "there is seldom only one cause of slope instability". They envisage a sequence of events resulting in landsliding only when "The forces creating movement exceed those resisting it (shear strength of materials)". It is important, therefore, to distinguish between factors contributing to increased shear stress (disturbing forces) and those contributing to low shear strength(resisting properties). Cooke and Doornkamp list four factors which produce shear stress:

1. The removal of lateral or underlying support (especially by weathering)
2. Increased disturbing forces.
3. Transi tory earth stresses (e.g. earthquakes)
4. Increased internal pressure (particularly porewater pressure).

Three factors which lead to decreased shear resistance are given as:

1. Properties of materials (degree of fracturing, jointing, etc.).
2. Weathering changes (particularly water absorption by clay minerals).
3. Porewater pressure increase.

The ultimate stability of a slope is thus given by the Safety Factor:

$$F_S = \frac{\Sigma \textit{Forces Resisting Slope Failure}}{\Sigma \textit{Disturbing Forces}} \qquad (1)$$

Clearly, if $F_S \geq 1$, the slope is stable (or conditionally stable), and when $F_S < 1$ it is unstable and failure is imminent. Terzaghi (op.cit.) believes that by performing engineering tests on materials the value of such a Stability Factor can be calculated and the stability (or otherwise) of a given slope determined.

In his paper of 1950, Terzaghi also discusses the lubricating effect of water on slip planes; a mechanism generally thought to be responsible for the initiation of movement. He shows, however, that many common minerals, such as calcite and quartz, actually increase their resistance to sliding if they become wet. In addition, the author points out that only a very thin film of any lubricant is needed to produce the full lubricating effect, and the required amount is nearly always present in bedrock anyway, even in relatively arid areas. It would seem, therefore, that lubrication is not nearly so important a control as changes in porewater pressure; a fact which is demonstrated using a model landslide by Curtis and Williams (1978).

Terzaghi ends his discussion of the mechanisms responsible for landslide movement with a plea for more co-operation between engineers and geologists, since their two disciplines approach a common problem from different origins. With the continued growth of engineering geology as a subject in its own right since the 1950's, some common ground seems finally to have been established.

1.2.2 Chemical Weathering - General

Weathering: *"Changes in the degree of consolidation and in composition which take place in the earth's crust within the sphere of influence of atmospheric and hydrospheric agencies."* (Jackson and Sherman, 1953).

A considerable volume of literature concerning chemical weathering of rocks has been produced both prior and subsequent to Goldich's (1938) classic paper, describing a weathering sequence of common rock-forming minerals ('stability series') which is essentially the reverse of Bowen's reaction series (Bowen, 1928). This article, however, in common with the vast majority of others, is concerned with the weathering of igneous and metamorphic rocks. Comparatively few studies until recently have paid attention to sediments. Of these, most are devoted to carbonate rocks and in particular to the development of karst features. Loughnan (1962) believes that Goldich's stability series is in agreement with a classification of silicates based on the number of silicon-oxygen bonds. He considers mineral structure to be one of two factors which influence weathering, the other being the mobilities of the bonding cations. The solubility of these cations is said to be a function of five inter-related environmental factors: pH, Eh, leaching potential, time and fixation.

Perhaps the most common approach to chemical weathering - because of the ease with which laboratory simulation can be conducted - is the study of interactions between individual minerals and aqueous solutions. Wilson (1975) reviews such studies in relation to soil formation and fertility, with special reference to the influence of crystal structure on the conversion of micas to kaolinite (see also Andersson and Wiklander, 1975). Similarly Correns (1961; 1963) uses individual minerals, first ground to a fine powder in order to increase the active surface area, and then placed in a continuous-flow apparatus. He concludes that: "Dissolution is affected by the speed with which the solution moves through the soil or weathering product".

A more realistic attempt at simulating the natural weathering environment is made by Barnhisel and Rotromel (1974) in their study of the weathering of clay minerals in a coal mine spoil bank. This is done by subjecting the

material to dilute acid solutions for periods of up to six months. The mode of attack of the acid is found to be at the edges of the clay minerals whereupon Al, Fe, K and Si ions are released into solution. The authors conclude that: "Even though the drastic acid conditions in strip-mine spoils may dissolve the clay minerals and release potentially toxic ions such as Al^{3+}, the relative mineralogic composition as a result of this chemical weathering should not change significantly." This presumably is because the rates of dissolution of the original minerals (micas) and weathered products (kaolinite) are essentially the same.

In recent years work on geochemical weathering has tended to move away from descriptive studies and attempts at simulating the weathering environment (which often left much to be desired) towards a more systematic and mechanistic approach. Detailed input/output analyses on a well-defined (therefore, usually small) catchment area, such as those described by Bricker et al. (1968) and Cleaves et al. (1970) for the Hubbard Brook experimental catchment, are typical of the systematic approach. Laboratory weathering of the same rocks which underlie the catchment (in this case pelitic schists) accompany field based experiments. Agreement between the two sets of data is generally very good. The results of these studies have shown that silicate-water reactions are much more rapid than previously thought, although the calculation of erosion rates for certain valley features does not take into account drastic climatic changes which have occurred over the millennia.

Thermodynamic approaches to chemical weathering are aimed at describing reactions using standard free energy data. Krauskopf (1967, Chapter 8) defines the free energy change for a given reaction as being the sum of the free energies of formation of all the reaction products minus the sum of the free energies of the reactants (in their standard states). This may be represented by:

$$\Delta G^{o}_{r} = \Delta G^{o}_{f}\ (products) - \Delta G^{o}_{f}\ (reactants) \qquad (2)$$

where ΔG^{o}_{r} is the standard free energy of reaction and ΔG^{o}_{f} the free energy of formation. If ΔG^{o}_{r} is negative (due to the conventional way of writing thermodynamic equations) the reaction will be spontaneous since it requires no external energy for initiation. The likely extent of a reaction and even the 'rate' or intensity can be estimated from further considerations of free energies and 'activation energies'.

In such a thermochemical approach to weathering Curtis (1976) considers the "special position" of oxidation reactions. An example quoted is the oxidation of pyrite in the presence of water:

$$2FeS_2 + 4H_2O + 7\tfrac{1}{2}O_2 \rightarrow Fe_2O_3 + 4SO_4^{2-} + 8H^{+} \qquad (3)$$

The free energy of reaction (from Equation 1) is -17.68 k cal g.atom^{-1} which Curtis notes as being "of the same order of magnitude as hydrocarbon combustion" (approximately -20 k cal g.atom^{-1}).

1.2.3 Chemical Weathering: Sediments

Very few studies have been conducted concerning the weathering of natural sediments, other than carbonates. Mudrocks in particular have received little attention. When considered at all the weathering environments described, or the experimental conditions set-up, are invariably far removed from those of the 'natural' situation.

One such work is the comparative study of Laguros, et al. (1974) of natural and simulated shale weathering. The ultrasonic disaggregation technique they employ can only be of use in predicting the durability of shales in engineering tests, and the authors concede that: "it is not a predictive test where the mineralogical characteristics are of significance".

Spears and Taylor (1972) investigate the weathering of shales in coal mine spoil heaps. In their study they suggest that the mechanism of weathering

in the natural, rather than simulated, environment is different from that proposed by Barnhisel and Rotromel (op.cit.). Spears and Taylor believe that after an initial relatively rapid breakdown along bedding and laminations the material remains largely unaffected by chemical weathering. In another paper, the same authors note that the rates of chemical weathering are controlled by this physical disintegration which increases the surface area of particles (Taylor and Spears, 1970). They consider the expansion of mixed-layer clays to be a more likely mechanism in breakdown than actual 'dissolution' as suggested by Barnhisel and Rotromel. It is reasonable to believe that the disintegration, particularly of fine-grained and finely laminated rocks can result from clay mineral expansion - an essentially physical process. Another mechanism is the growth of secondary minerals between the laminations and in joints. This action combines both chemical and physical processes of crystal growth and expansion leading ultimately to the build-up of stresses in the rocks. The actual growth of crystals from saturated pore solutions can occur against pressures of up to 47 bars, and the expansion of these crystals on hydration against 63 bars (Goudie et al., 1970; Cooke and Smalley, 1968). Since the tensile strength of rocks is commonly between 20 and 200 bars Goudie et al. believe disintegration as a result of these processes to be highly likely, especially close to the surface where the overburden is slight. In one of the few reported weathering experiments to include mudrocks these authors find that strong salt solutions are not necessarily needed to cause splitting. During the course of their wetting-drying/heating-cooling procedure the only fresh shale samples to split were the controls which had been treated only with distilled water.

Volume increases accompanying the formation of weathering products often occur in sulphide-bearing shales. As early as 1920 damage to certain structures was recognised as being caused by sulphide mineral expansion

(Anon, 1960) and much has since been written concerning the problem of 'heave'. This phenomenon seems to be particularly prevalent in Pennsylvania where pyritic shales underlie the foundations of many buildings in the Pittsburgh area (Dougherty and Barsotti, 1972).

Numerous possible mechanisms for causing these shales to heave have been suggested, but Coveney and Parizek (1977) believe that "gypsum formation is the prime cause". They observe that in parts of Kansas City's underground development sites the floor has risen in places as much as 6-8 inches over a period of several years since excavation. They further state that: "Major mineral constituents of the weathered or the fresh Hushpuckney Shale are similar but the minor mineral constituents are quite different. Most notable is the presence of abundant gypsum which occurs in fractures or partings in the shale". Dougherty and Barsotti also attribute heaving to crystal growth on bedding planes of fissile shales which force the bedding apart and cause overlying rocks to buckle. If there is sufficient overburden (10 feet seems adequate) heaving is not detected. When the authors tried to simulate such crystal growth in the laboratory, however, they failed to precipitate gypsum on bedding planes. It is felt that this is a function of the equipment used (the shale samples were not completely confined) since gypsum did form in other parts of the apparatus. When the samples were successively wetted and dried with dilute H_2SO_4 an uplift pressure of 500 pounds per square foot was noted.

Coveney and Parizek (op.cit.) observe that the sulphur bearing minerals in weathered rock occupy nearly twice the volume of the primary sulphides in fresh rock (due to the different densities of gypsum (SG = 2.36) and pyrite (SG = 5.02)). Fassiska et al. (1974) study changes in the molecular packing arrangements during the pyrite-gypsum transformation. They note "an approximate volume increase of 350%" which was increased further by hydration and the addition of bulky water molecules.

These volume expansions and resultant pressure increases agree well with the cases of salt weathering quoted by Goudie et al. (1970) and are not dissimilar to the process of physical breakdown proposed by Spears and Taylor (1972). Many more examples of shale heaving due, in the first instance, to chemical weathering of sulphides can be found in the literature of engineering geology. The interested reader is referred to Grattan-Bellew and Eden, 1975; Quigley and Vogan, 1970.

1.2.4 Weathering and Slope Stability

Extensive exposures of Tertiary mudstones occur throughout Japan. The close association of these rocks with landslides has prompted research into possible links between bedrock weathering and slope stability.

Geologists commonly believe that the association is simply due to the fact that changes in the position of the water table induce changes in porewater pressures, lowering the overall strength of the material and leading ultimately to failure.

This connection has indeed been shown to exist, although the mechanistic steps are more complex.

Nakano (1967) demonstrates that certain shales slake more readily if repeated wetting and drying takes place (this is somewhat similar to the findings of Goudie et al., op.cit.). Such a process operates continually in the zone of fluctuating groundwater level.

In a study of 185 landslides in the Nagano Prefecture, Nakano shows that a strong correlation exists between frequency of landslides and the occurrence of mudstones which slake on wetting. He believes that heavy rainfall (and particularly snow melt) and increased pore pressures simply act as a trigger mechanism on sliding surfaces which have already developed due to weathering of the shales.

Similarly Yoshioka (1975) believes that the formation of clay minerals by weathering (of a tuff layer between more consolidated rocks) leads to a lowering of cohesive strength through expansion and weakening of the constituent minerals and leads ultimately to landsliding. In a study of the same area (the Kamenose landslide) Kitano et al. (1967) describe how the solute content of the groundwater gives an indication of the degree of weathering of the bedrock and the likelihood of landslides occurring. They do not, however, consider the weathering reactions producing the solutes.

Little direct work has been done, outside Japan (where the standard of research often leaves a great deal to be desired) on the links between weathering and slope stability and examples from the existing literature often appear to be contradictory.

For example, in a consideration of factors causing landslides, Cooke and Doornkamp (op.cit.) suggest that the free flow of water through joints "prevents the build-up of locally excessive water pressures, and thus decreases the likelihood of instability". If such water is chemically reactive, however, secondary minerals may precipitate in the joints (as described by Piteau, op.cit.) and cause increased stress. The subsequent dissolution of these minerals (salt, gypsum, dolomite, etc.) at a later date or in another part of the landslide may even decrease the shear resistance and, consequently, the safety factor.

It is hoped that the work described in the following sections might help to resolve some of these differences of opinion and present a generally acceptable view of links between chemical weathering and slope instability.

1.3 Experimental Design

1.3.1 Geochemistry

The chemically-charged streams draining the Mam Tor landslide hold the key to weathering reactions taking place at depth - the products of such

reactions inevitably being carried away in solution. By sampling and subsequently analysing the drainage waters on a regular basis the proportions of the various dissolved species can be determined. Reactions between groundwater and bedrock can then be suggested to account for the observed composition. Therefore, a detailed sampling strategy was developed, including control sites from the surrounding area, which is described in more detail in Section 4.

In order to fulfil the first objective of this research (Section 1.1) it was considered necessary also to monitor the precipitation input to the landslide and stream discharge from it. If the quantities of dissolved solids at each stage can be determined then a solute budget-type study can be undertaken and the overall rates of chemical weathering calculated (see Bricker, et al. and Cleaves et al., op.cit.).

Precipitation totals are easily monitored using a standard Meteorological Office rain gauge. Such an instrument was installed at Mam Tor prior to the commencement of the main sampling programme. Recordings were checked against those obtained daily at the Meteorological Office Station No.106852 at the nearby village of Hope (GR. 4168.3822).

The quantitative assessment of solute inputs to a catchment from rainfall, however, is more difficult to achieve than a simple volume estimate. Specially designed rainfall samplers constructed from chemically inert plastics must be used to intercept and store the rainfall until chemical analyses can be performed. Contamination of samples held in such apparatus is reported by many workers (Allen et al., 1968; Gore, 1968) and measures taken to prevent birds perching on the rim of the collecting funnel, or insects falling in, generally prove unsatisfactory.

In addition, there is no secure site for such an obtrusive structure as a rainfall sampler (out of the reach of inquisitive cattle, sheep and tourists)

anywhere on the Mam Tor landslide. In view of these problems it was decided that continuous monitoring of rainfall quality would not be conducted. Spatial variations in the chemistry of rainfall in Britain are in any case slight (Stevenson, 1968) and the quantitites of solutes likely to be added are considered small in comparison to the amounts contained in the Mam Tor streamwaters (which must be highly concentrated in order to precipitate ochre and gypsum, as noted in Section 1.1.2). Average compositions of precipitation in the Pennines are well documented in the literature (see Allen et al., 1968; Crisp, 1966; Rippon, 1980).

Stream discharge is most easily monitored using some standard gauging device such as a flume or weir. These structures restrict the natural flow of a stream, confining it to a narrow channel or to emerge through a restricted opening. The 'head' of water behind the structure (in the case of a weir) is proportional to the discharge, measured in litres per second or cubic metres per second - "CUMECS". British Standard No. 3680 gives details of the construction of flumes and weirs (B.S.I. 1965).

Ideally the discharge at several streams on Mam Tor should be monitored and small, easily removable 'V'-notch weirs were designed for this purpose. However, the National Trust (who own over 90% of the land at Mam Tor) would not grant permission for the excavation of small approach channels or the installation of the weirs, and the work could not go ahead.

Since the majority of the 'streams' are in fact just shallow seepages none of the other standard methods of discharge measurement which use a velocity-area technique could be employed. The only alternative remaining was to estimate discharge by a 'dilution gauging' method. Details of this technique are given in Section 5.4.2, but it should be noted at this stage that dilution gauging could not be conducted at many of the stream sites, particularly during the period of streamwater analysis. The problem lies in the principle of the technique, which requires the injection of a

saturated salt solution into the streamwater. Clearly if this same water is being sampled for chemical analysis such a procedure might seriously affect the results. Also, since many of the streams precipitate secondary minerals the addition of such a concentrated solution might lead to supersaturation and cause further deposits to form. In view of such possibilities discharge measurements were only made after the main period of study had been completed, and then at only one of the sampling sites (see Section 5.4).

Consequently, a quantitative solute budget study such as that conducted by Cleaves (op.cit.) could not be undertaken at Mam Tor. It should also be noted that a further difficulty would have been encountered in delimiting the catchment area, since the Mam Tor landslide forms only a small part of a much larger drainage basin. What is more Cleaves et al. state that sources of water, other than precipitation falling within the catchment, must be small and preferably known (determined during base-flow conditions). At Mam Tor, however, it would seem that there is a considerable supply of groundwater from outside the immediate area. This possibility is considered in detail in Section 5.4.3.

1.3.2 Engineering Properties

In order to fulfil the second objective of this research - to investigate links between chemical weathering and slope stability - it is necessary to examine the solid material which is being weathered. Ideally this examination should include both mineralogic investigations of 'fresh' and 'weathered' bedrock and analysis of the relative strength of these materials.

The mineralogy of the rocks (principally the Edale Shales) was determined using X-ray diffraction techniques. Other materials, such as carbonates and the ochre and gypsum precipitates, were also analysed in this way to verify their identification.

The engineering properties of rocks are most commonly assessed by performing triaxial or shear-box tests. Triaxial testing, however, requires that the material be largely homogeneous (such as in the case of a granular intrusive igneous rock) so that there is no inherent 'weak' direction. Finely laminated mudstones which are frequently jointed, interbedded with diagenetic carbonates, and even highly fractured due to landslide activity such as are present at Mam Tor, are clearly not amenable to this type of investigation.

Shear-box testing is more usually applied to weaker rocks and soils. This type of strength test describes the tendancy of materials to shear under stresses operating in opposite directions on different parts of the mass. Shear-testing would appear to be particularly useful in a landslide context where the rocks are moving on discrete rupture surfaces. The material making up the Mam Tor landslide, however, is of such a highly fragmented and inhomogeneous nature that the testing of any single small sample will not give results representative of themass as a whole.

In such cases Nonveiller (1967) recommends that: "Tests should be carried out on large samples of rock, the size of which must be so large that the influence of defects on the test result may be regarded as giving a statistical average, characteristic of the domain which is investigated. This leads to the necessity to test very large samples in cases where exceptionally large volumes of rock are involved, as in the study of stability of rock slopes". Facilities for testing the strength of very large rock samples (over 1 m^3) were not available in this study. After consulting engineering geologists familiar with the problems of strength testing (J. Cripps, 1979; C. Gribble, 1980 - personal communications) it became apparent that no suitable alternative for materials of this type exists. Consequently engineering tests were not carried out on the Mam Tor rocks.

A further consideration which was taken into account is the lack of any suitable supply of unweathered Edale Shale for comparison. Material from within the landslide, even at considerable depth, is badly weathered. The only place where fresh rock can easily be obtained is from a cement-works quarry at Hope, 4 km east of Mam Tor, where the beds being exploited are somewhat lower in the succession.

2. THE STUDY AREA

2.1 Location

Mam Tor is known locally as the 'Shivering Mountain', presumably because of its repeated movement. The hill is located close to the Derbyshire village of Castleton, itself some 24 km west of Sheffield (see inset, Figure 5) and the summit at 1695 feet is encircled by a double ditch and mound which marks the position of an ancient hill fort.

On the east side of Mam Tor a landslide extends on to the floor of the Hope Valley at its westernmost end. To the north lies the gritstone ridge of Back Tor-Lose Hill separating it from the parallel-running Vale of Edale. To the south steep slopes of reef limestone mark the northernmost limit of the Derbyshire limestone massif. The stream draining eastwards out of the Hope Valley joins with the River Noe flowing out of Edale to become a tributary of the Derwent.

As noted previously, the A625 Sheffield to Manchester (via Chapel-en-le-Frith) road runs along the Hope Valley from Castleton and twice crosses the landslide on its ascent of Mam Tor before continuing westwards along Rushup Edge.

The area described above is located towards the centre of Sheet 110 of the Ordnance Survey's 1:50,000 Series (First Edition).

2.2 Geology

2.2.1 Edale Shales

Sheet SK18 of the Geological Survey's 1:25,000 series shows the Mam Tor landslide to be one of many in this area, which are usually located where Kinderscout Grit or Shale Grit overlie steep shale slopes. At Mam Tor it is the Mam Tor Beds and underlying Edale Shales that are affected by slipping (see Figure 1).

FIGURE 1: Geology and Landslides of the Edale-Mam Tor Area. (Source: Geological Survey Sheet SK18, 1:25,000 Series)

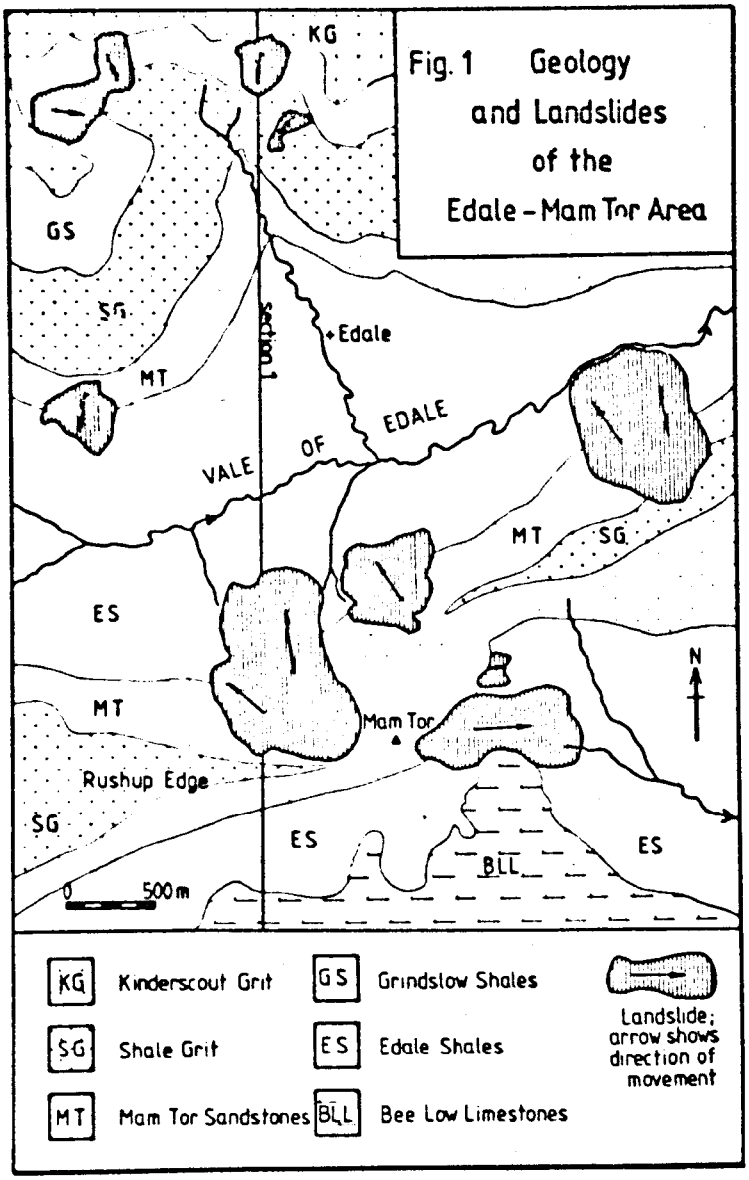
Fig. 1 Geology and Landslides of the Edale - Mam Tor Area
KG
GS
SG
MT
ES
BLL
Edale
EDALE
VALE OF
section 1
Mam Tor
Rushup Edge
N
0 500m
Kinderscout Grit
Grindslow Shales
Shale Grit
Edale Shales
Mam Tor Sandstones
Bee Low Limestones
Landslide; arrow shows direction of movement

Section 1

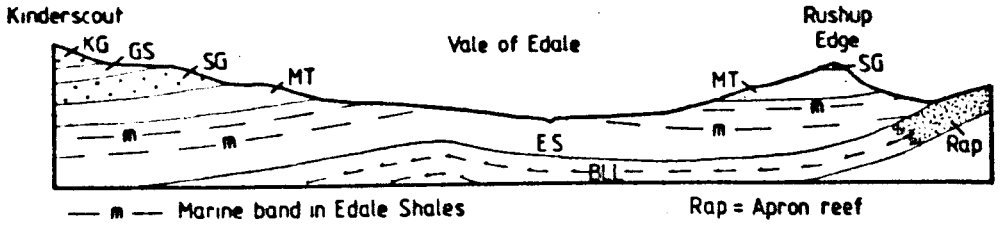
Kinderscout
KG
GS
SG
MT
Vale of Edale
Rushup Edge
MT
SG
m
ES
BLL
Rap
— m — Marine band in Edale Shales
Rap = Apron reef

As the geological section in Figure 1 shows, the Edale Shales rest unconformably on the Dinantian limestones and vary in thickness considerably as a result. In the Vale of Edale to the north, these beds are in excess of 200 m thick. In the Hope Valley at Castleton successively higher strata overlap the lowest beds (*Cravenoceras leion*) as the edge of the limestone shelf is approached. AT Mam Tor the Edale Shales consist mainly of mudstones, but occasionally siltstones and diagenetic carbonates occur. The latter may take the form of continuous beds or discrete concretions of dolomitic composition (see X-ray analysis in Appendix C). The concretions vary in size considerably from a few centimetres to two metres across (Plate 2a) and many show calcite-lined septaria.

These carbonates, on a fresh surface, are very dark - almost black - and extremely hard. A weathered surface skin, however, exists on both bands and concretions which is very variable in character. In places this rind is a light grey-brown colour and can easily be removed with a fingernail, having a soft and chalky texture. Elsewhere a very hard crust has formed which is characteristically purple or red-brown, suggesting the presence of hematite or other iron oxides. Gypsum crystals frequently encrust the surface of these carbonates, which are easily distinguished at a distance from the surrounding shales by an overall red-and yellow-brown colouration.

The shales are equally variable in appearance from place to place and depending upon the degree of weathering. Fresh rock, from Hope Cement Works or (rarely) from borehole cores, appears dark grey and largely homogeneous. This rock is extremely fine-grained and splits along relatively few bedding planes, which seem to contain a higher proportion of mica or carbonaceous material. In thin section this observation is confirmed (Plate 2b) and small (<0.25 mm) subhedral grains of an opaque mineral, possibly pyrite, can also be seen.

PLATE 2a: A carbonate concretion from the retrogressive unit above Site 7.

PLATE 2b: Photomicrograph of 'fresh' Edale Shale. Sample BH88, x 20.

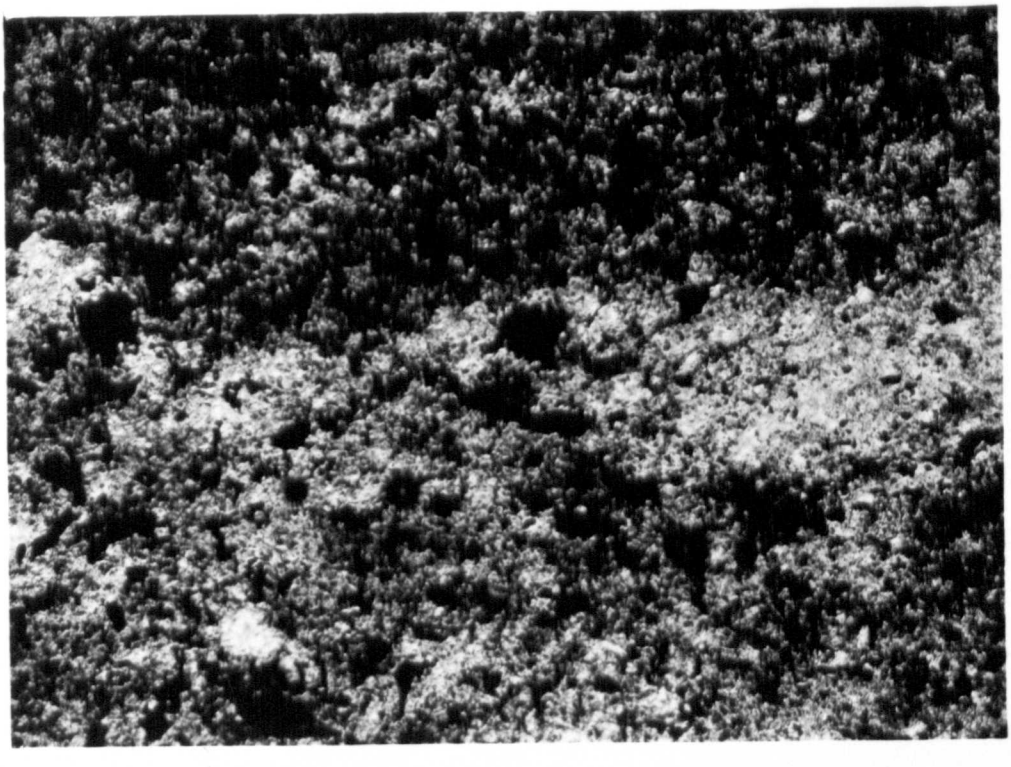

PLATE 3a: Photomicrograph of 'weathered' Edale Shale. Sample G2, x 20. The white areas are gypsum.

PLATE 3b: Detail from thin section of sample G2, x 25.

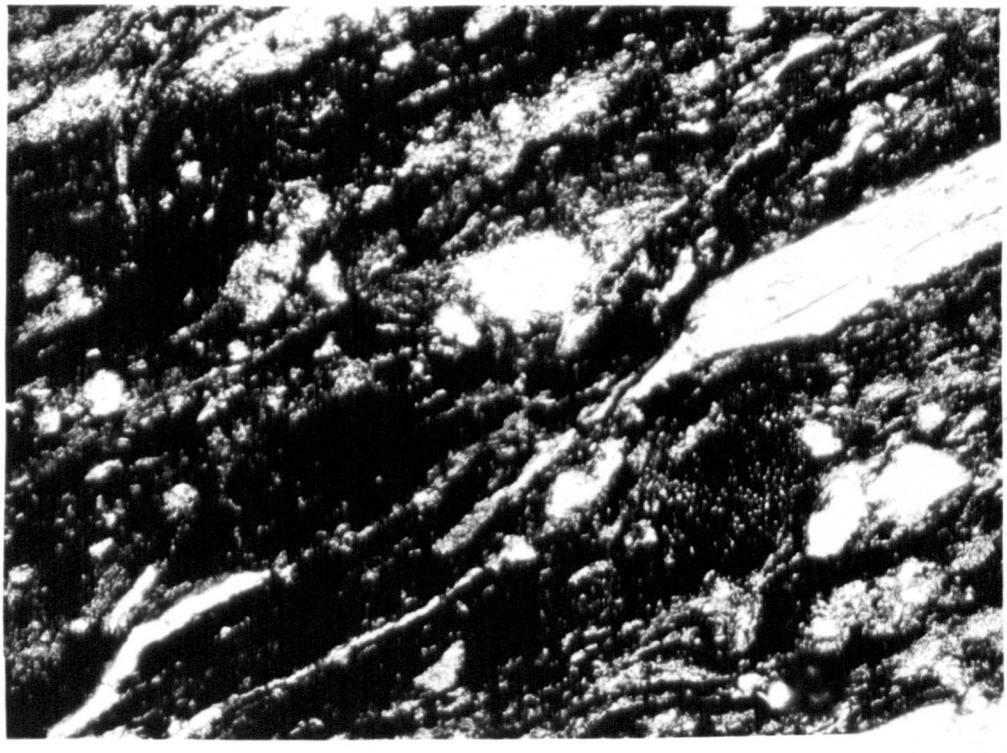

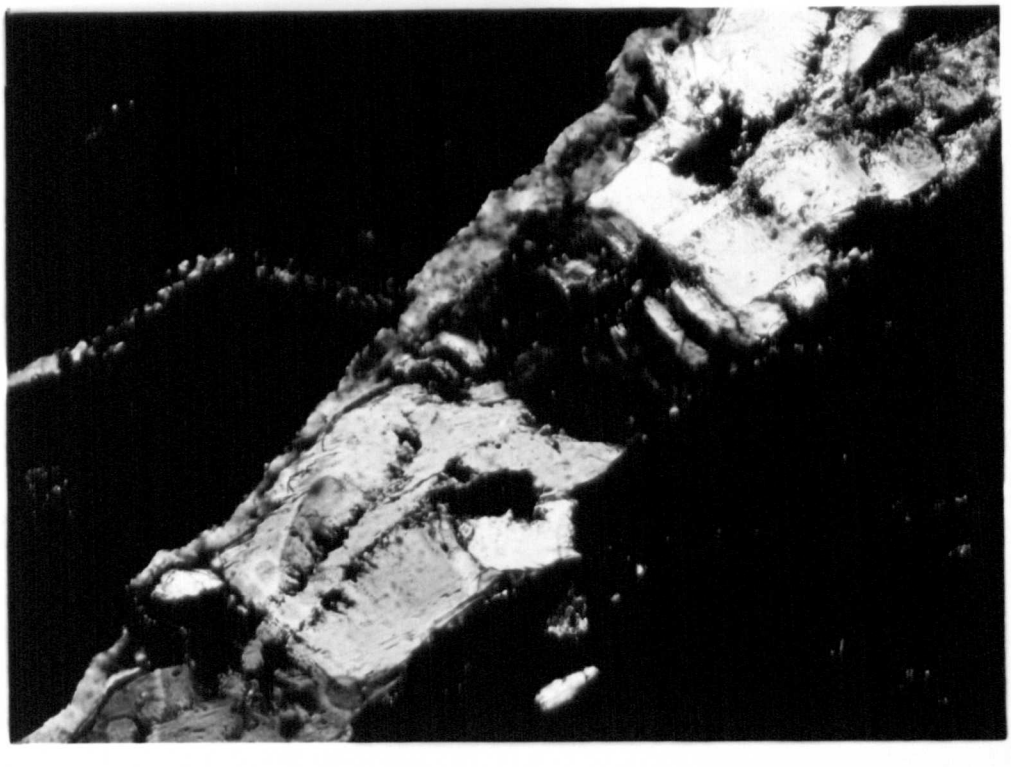

PLATE 4a: Euhedral gypsum crystals in thin section of sample G2, x 25.

PLATE 4b: Hand specimen of Edale Shale showing euhedral gypsum crystals.

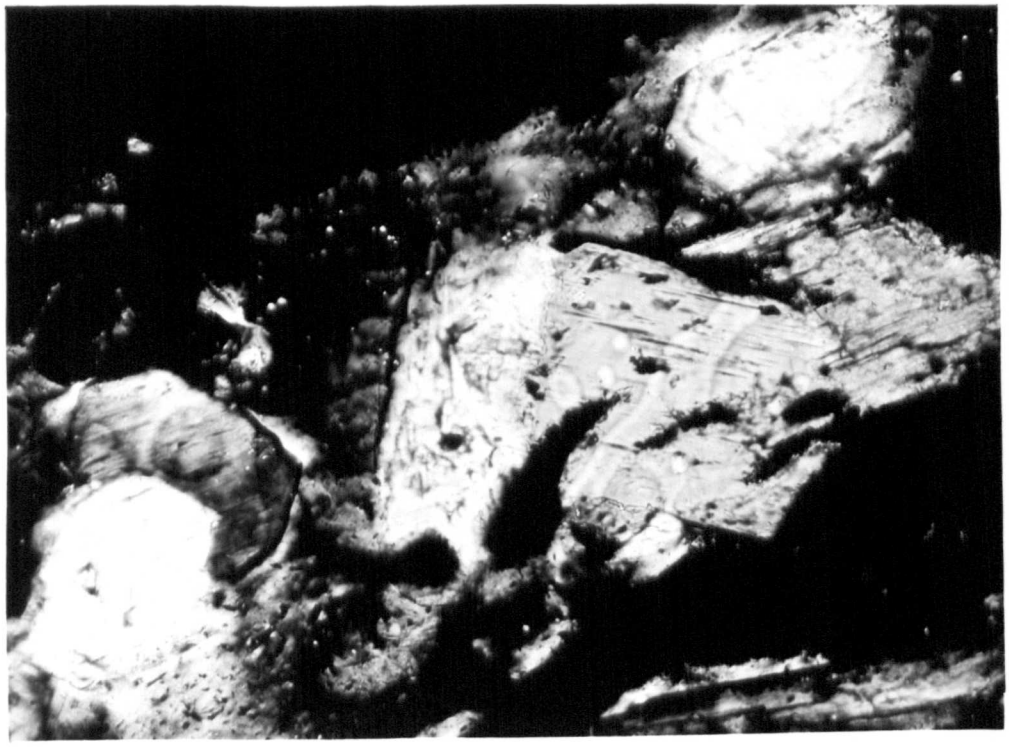

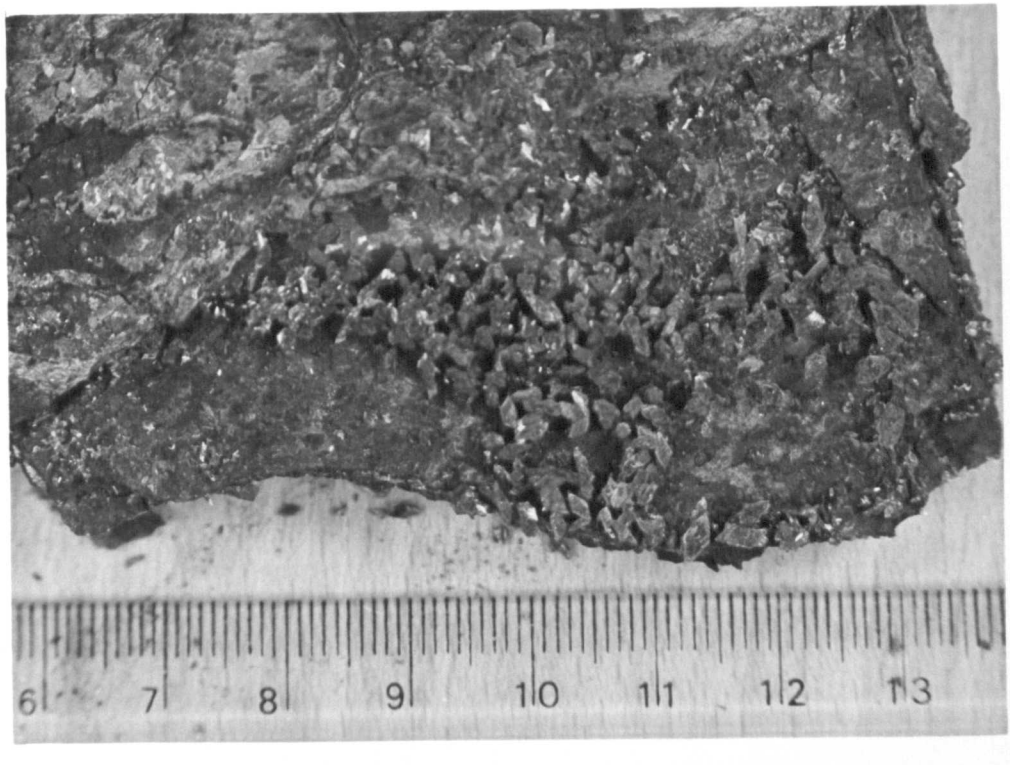
6
7
8
9
10
11
12
13

Weathered Edale Shale has a completely different appearance. In the field bedding and laminations can be seen at 1 or 2 mm intervals throughout the exposure, and at least two joint sets are noticed. These laminations and joints appear to be widened in places and filled with euhedral crystals of gypsum. The presence of gypsum is confirmed in resin-impregnated thin-sections of weathered shale such as those shown in Plates 3 and 4a. These crystals vary in size from less than 1 mm to several cm and occur both as small rosettes and single large tabular forms (Plates 4b and 5). They are frequently discoloured on the surface by a powdery red-brown or sometimes yellow overgrowth. A powdery yellow mineral which resembles sulphur is closely associated with the gypsum on joints and bedding surfaces.

Cracks running at about 60^{o} to bedding are also present (see Plates 21 and 22b) and the result is that most exposures are surrounded by material which has broken along these cracks, bedding planes and joints into small, angular fragments less than 5 cm across. Indeed the shales in this highly weathered state offer little resistance even to slight finger pressure and disintegrate easily. The resulting blocks accumulate as scree below the exposures where continued breakdown further reduces their size. Typical Edale Shale scree material is shown in Plate 6a and can be seen to comprise platy particles less than 1 cm across and 1 mm or less thick. The fragments of carbonate, once they have acquired their protective weathered rind, remain relatively large. When the scree material is disturbed a sulphurous smell is noticed.

The Edale Shales are deep basinal mudstones and as such contain an abundant marine fauna comprising both thick and thin-shelled goniatites, *Pectinoid* bivalves, brachiopods and trilobites. Diagenetic pyrite occurs throughout the succession as small, disseminated grains (Amin, 1979).

PLATE 5: Single large gypsum crystal (and numerous smaller ones) on a bedding plane in weathered shale.

CM

Pyrite is known to be a common constituent of many sedimentary rocks, particularly mudstones, where it is almost always associated with organic matter.

Thermodynamic calculations show that pyrite is only stable in the absence of oxygen and in the presence of dissolved sulphide (Garrels and Christ, 1964). Such conditions are found in modern sediments where organic matter first accumulates and subsequently decomposes as a result of bacterial action. Kaplan et al. (1963) however, have shown that not enough organically derived sulphur exists in sediments to produce the observed quantitites of pyrite. Consequently Berner (1970) believes that high pyrite contents are a result of "Continuous diffusion of dissolved sulfate into sediments where it is reduced to H_2S and reacted with iron minerals". The first-formed phase in this process is seldom pyrite and laboratory experiments show that non-crystalline FeS, mackinawite ($Fe_{1.5}S$) and greigite (Fe_3S_4) are an intermediate step (Berner, 1964; Rickard, 1969).

Berner (1970) notes that most of the pyrite is formed in the top 10 cm of the accumulating sediment in the following sequence of events:

1. Organic matter and iron are deposited.
2. Dissolved oxygen is removed from the sediment by aerobic metabolism and anaerobic bacterial sulphate reduction occurs. H_2S is also formed.
3. H_2S reacts with the iron minerals to form the monosulphides.
4. Sulphate diffusion from the overlying water occurs. Sulphate reduction and Fe to FeS conversion continues.
5. Some H_2S is oxidised to elemental sulphur.
6. This sulphur combines with the monosulphide to form pyrite ($FeS+S = FeS_2$) which crystallises as minute 'framboidal microspheres'.

Berner concludes that "The time for complete transformation of FeS to FeS_2, in the presence of abundant H_2S and elemental sulfur, is in the order of several years".

For more detailed accounts of the geology of the Edale Shales the reader is referred to Hudson and Cotton (1945) and Stevenson and Gaunt (1971). The ajoining limestone massif is also adequately described elsewhere (see Eden et al., 1964; Stevenson, 1967).

2.2.2 Mam Tor Beds

The Edale Shales pass upwards, with no conspicuous change in lithology, into the Mam Tor Beds which are at their thickest - 140 m - in the vicinity of Mam Tor itself. These beds were first described in detail by Jackson (1927) who referred to them as the "Mam Tor Sandstones". Allen (1960) and Mason (1961) have also documented the succession in considerable detail. It is apparent from these works that the beds are typical distal turbidites and true sandstones are often not well developed. As a consequence Stevenson and Gaunt (1971) suggest that the name Mam Tor *Beds* is in fact more appropriate.

On passing out of the Edale Shales and up into the turbidites the only detectable change is that one or two more silty horizons are encountered. Here the shales yield *Reticuloceras reticulatum* which places the base of the Mam Tor Beds in the R_{1c} zone. Above these lower, dominantly shaly horizons, the cyclicity typical of turbidites is apparent and alternating shales, siltstones and fine-grained sandstones become gradually coarser towards the top of the exposure (Plate 6b).

White mica flakes are conspicuous both in the shales and sandstones, andthe former fracture along bedding planes containing a greater proportion of coarse flakes. The sandstones often show graded bedding, in addition to penecontemporaneous deformation structures such as slumpball structures,

PLATE 6a: Typical Edale Shale scree material.

PLATE 6b: General view of the turbidite succession, Mam Tor Beds, main scarp face. Note the increasing proportion of shale towards the base.

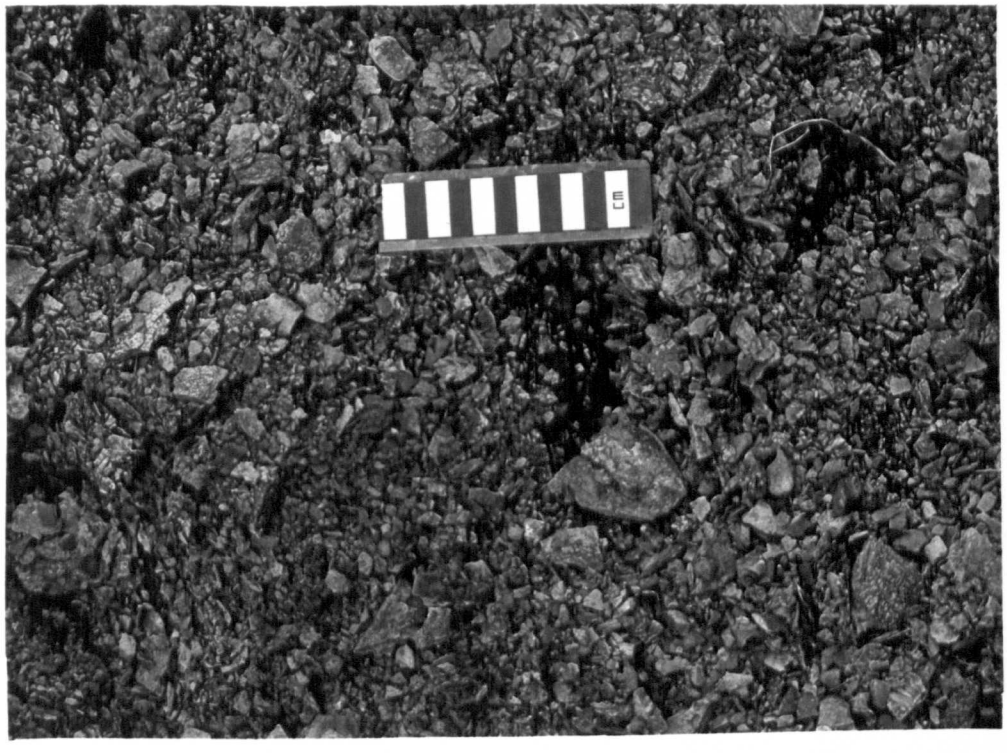
CM

PLATE 7a: Sole marks on the underside of a coarse sandstone unit.

PLATE 7b: The scarp face of Mam Tor showing the geological boundary. Mam Tor Beds above (a), Edale Shales below (b).

PLATE 7a: Sole marks on the underside of a coarse sandstone unit.

PLATE 7b: The scarp face of Mam Tor showing the geological boundary. Mam Tor Beds above (a), Edale Shales below (b).


cm


a
b
a
b

corrugated bedding, convolute and crumpled bedding (Mason op.cit.). The undersides of many sandstones exhibit excellent groove casts, flute casts, load casts, trail casts and burrows (see Plate 7a). These indicate a general derivation from the north-east.

Each cyclothem of the Mam Tor Beds from sandstone through siltstone to shale can vary in thickness from 7 cm to 3 m, yet even the thinnest are remarkably laterally persistent. None are seen to wedge out across the entire width of the scarp face; a distance of some 300 m. These turbidites are interpreted by Allen (op.cit.) as having been laid down on the lower slopes of a Namurian delta, and as such represent the first coarse clastic material to be deposited in the southern part of the Central Pennine Basin (Walker, 1966). It is interesting to note that further north the stratigraphically-equivalent beds are older, marking the advance of the delta into the southern part of the Basin (Reading, 1964).

In a geochemical investigation of Namurian rocks from the Pennine Basin, Amin (1979) notes that pyrite is only a very minor constituent of the Mam Tor Beds, occurring largely in the non-marine shale horizons in association with plant remains and siderite. This is in marked contrast with the Edale Shales which contain abundant pyrite.

Both the Edale Shales and Mam Tor Beds dip gently north-westwards at about 5^{o} in the vicinity of the landslide. This 'dip into slope' situation commonly accompanies deep-seated, concave failures of the type discussed in Section 3.1. The angle of dip steepens considerably as the limestone to the south is approached.

Shale Grit, the next highest formation in the succession, is not present at Mam Tor, but can be seen in exposure both to the east and west at Lose Hill and Rushup Edge, respectively, where this hard, resistant rock forms conspicuous tors. More detailed descriptions of the succession above the Edale Shales can be found in Allen (1960), Collinson and Walker (1967) and Walker (1967).

Plate 7b shows the face of Mam Tor as viewed from the east. The dashed line indicates the position of the geological boundary between the Mam Tor Sandstone s (A) and Edale Shales (B). Sandstone units in the turbidites, being more resistant to erosion than the interbedded shales, form conspicuous ledges on the main scarp face of Mam Tor and these can be easily identified from the photograph. The Edale Shales are best exposed in the minor scarp face of 'Little Mam Tor' (Plate 8), but can also be seen in the retrogressive units (Plate 9). The foot and toe areas of the landslide contain both lithologies. This material is so highly disrupted by centuries of movement, however, that relationships between the two cannot be established and the whole area is a jumble of sandstone and carbonate blocks set in highly fragmented black shales.

2.3 History (Mining)

Some consequences of economic mineral exploitation can be seen on and around the Mam Tor landslide. A worked-out mineral vein, the Odin Rake, parallels the south side of the landslide where it moves against the reef limestones of Treak Cliff (Plate 10a). The most important mineral that the Odin Rake contained was galena (PbS), although sphalerite (ZnS) was a common associate. Today traces of these minerals can be found in the fine tailings from Odin Mine although their weathered carbonate forms, cerussite and smithsonite, are more common. Isotope dates place the injection of the hydrothermal liquids from which these minerals crystallised at about 180 million years ago during the Jurassic (Ford and Rieuwerts, 1975). The famous variety of fluorspar called Blue John (from the French 'bleue-jaune') has also been mined at Treak Cliff for centuries and is often found in close association with the sulphide minerals.

Lead mining has a long history in Derbyshire and galena has probably been worked since Roman times. Odin Mine at Mam Tor is the earliest named

PLATE 8: Little Mam Tor showing sample locations.


MT1
MT2
MT4
MT5
MT6

PLATE 9: The area of retrogressive units showing sample locations. Spring No. 7 is located just beyond the two figures.


soil pit
MT 7
MT 8
G2
MT 9

PLATE 10a: Odin Mine and Gank Mouth Cave. The near-vertical cleft on the right is the worked out Odin vein. The drain at top centre carries water from Site 11 to the Odin Sitch, which flows from left to right through the trees.

PLATE 10b: The crushing circle and Knowles Engine Shaft (surrounded by a fence at top left). The ridge in the foreground is the right flank of the land slide.

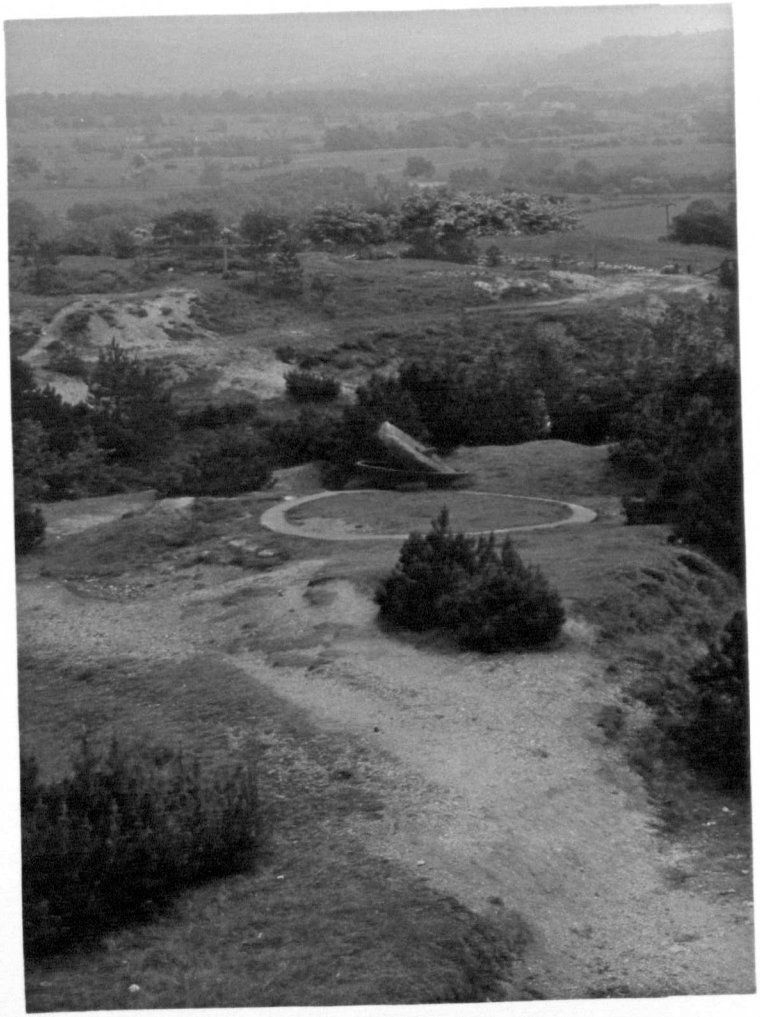

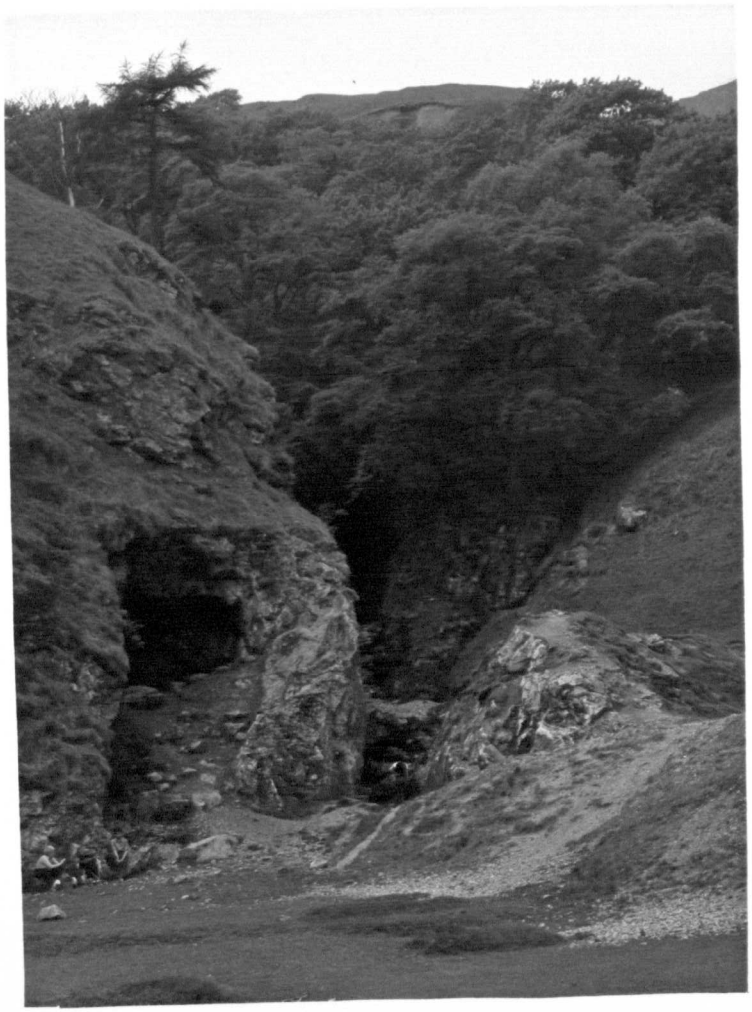

PLATE 11a: The artificial channel of the Odin Sitch.

PLATE 11b: The Odin Sitch 20 m further downstream, below the mixing site. Note the white precipitate coating the stream bed.

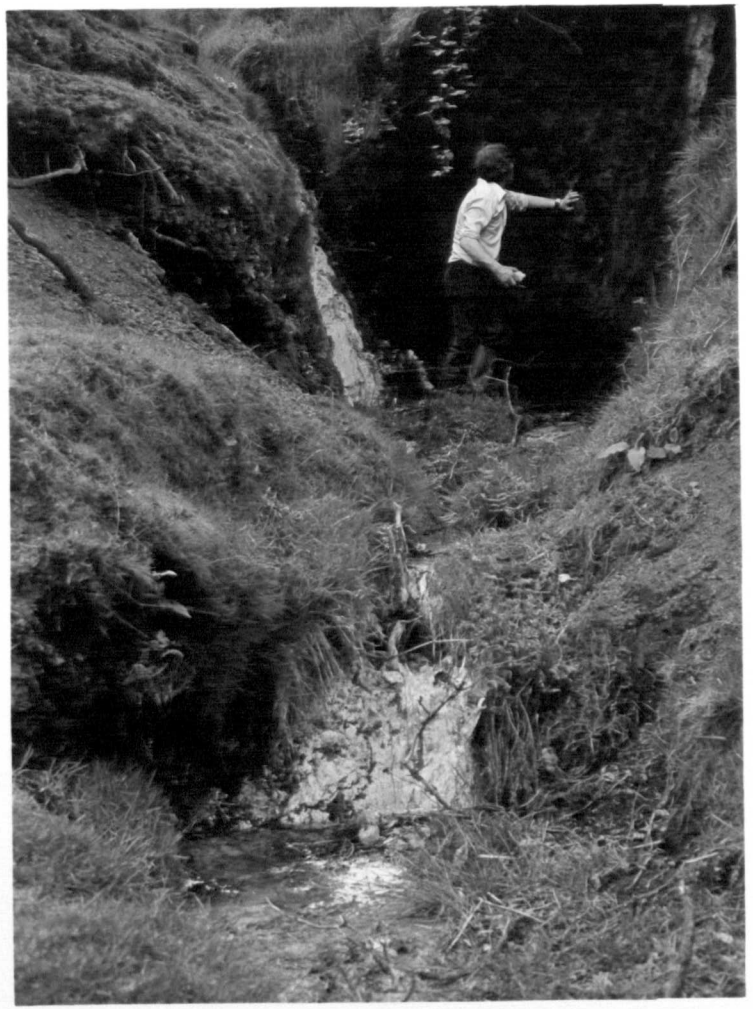

mine in the area, being first mentioned in print around 1280 A.D. (Ford and Rieuwerts, 1976). The effects of this mine on the landscape of Mam Tor have been considerable, particularly on the south side of the toe. This was for centuries the location of the mine's waste hillocks which have continually been built up, levelled, re-worked for gangue minerals and ultimately landscaped as a picnic site. Much of the waste was finally removed for ballast during road maintenance operations in the 1940's and 1950's.

A solitary shaft reaching to the old workings (the now flooded Knowles Engine Shaft) can still be seen close to the lead ore crushing circle, erected in 1823, and shown in Plate 10b. Many of these relics of the lead mining industry can be seen from the air (Plate 12).

A further consequence of mining operations was the diversion of the stream known as Odin Sitch. This stream flowing off the limestone would naturally have taken the easiest course down the gorge which marks the former position of the Odin Rake, here following the line of a fault. To avoid flooding of the workings this stream was diverted during the 18th century to flow north and then east around the mine and on to the landslide (Plate 11). This channel is still the most prominent feature of the drainage at Mam Tor today. Some consequences of re-routing these karst waters onto the landslide will be discussed in Section 7.4.3.2.

It is possible that concentrations of ions in streams draining the south flank of the landslide may be partly indicative of waste hillock mineralogy. It is not possible, though, that weathering of lead and zinc sulphide minerals associated with the Odin Rake can contribute sulphate ions to streams on the landslide. This is because any remaining mineralisation is located well below the Edale Shales, deep in the underlying limestones. In addition, a complex system of underground drainage channels (known as 'soughs') draws water down from the old workings,

FIGURE 2: Schematic section through the shafts and soughs of Odin Mine. (After Ford and Rieuwerts, 1976).

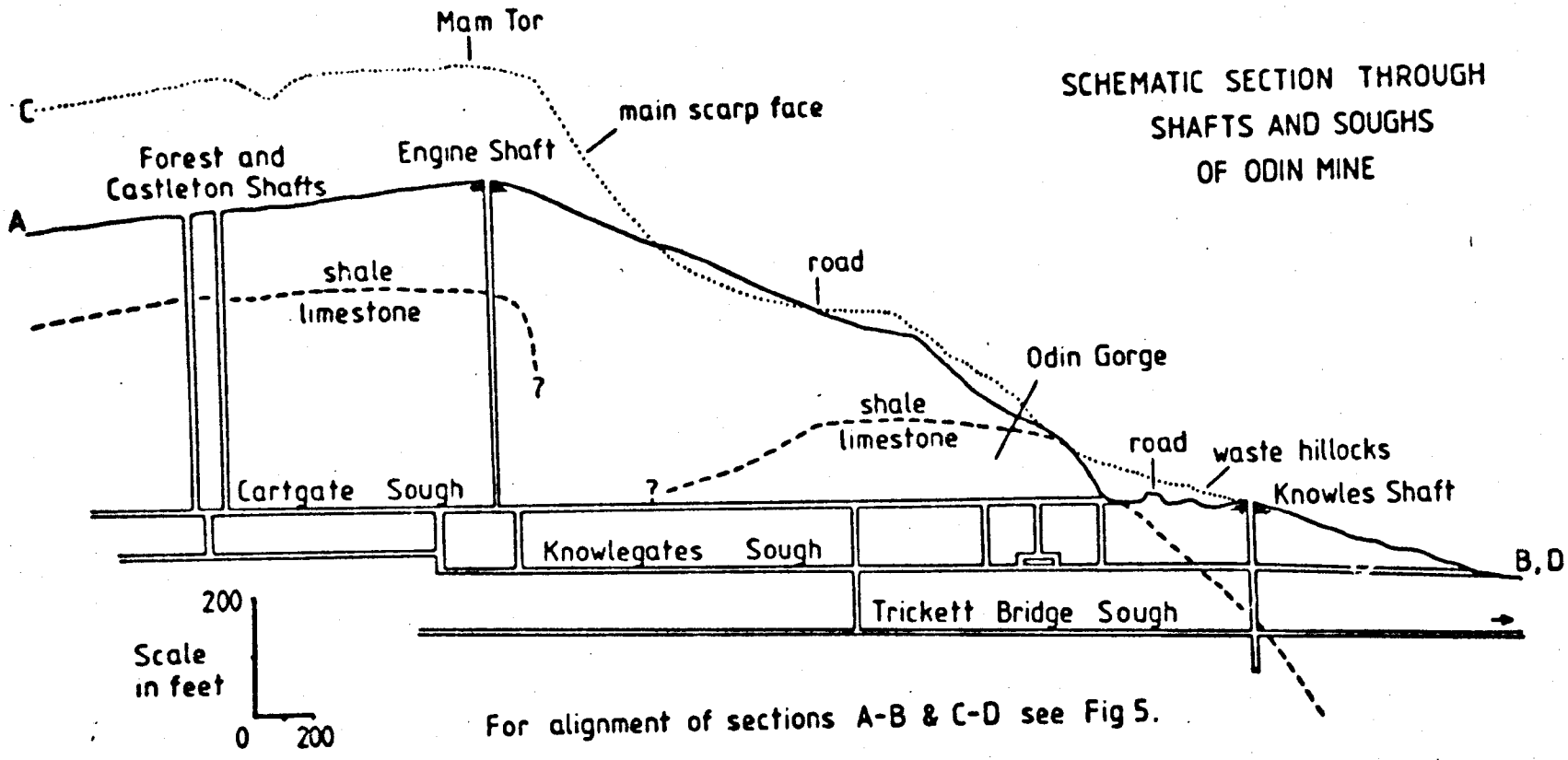

SCHEMATIC SECTION THROUGH
SHAFTS AND SOUGHS
OF ODIN MINE

For alignment of sections A-B & C-D see Fig 5.

several hundred feet below the surface, to finally emerge well to the east of the landslide close to Castleton village. Figure 2 is a diagrammatic representation of the underground soughs in relation to the landslide.

3. GEOMORPHOLOGY OF THE LANDSLIDE

3.1 Landslide Classification

Engineers and geomorphologists alike have produced many landslide classifications. Two of the most widely used, and most relevant here, are those of Hutchinson (1968) and Varnes (1958). According to Hutchinson "rotational landslips occur principally in slopes largely formed of, or underlain by, a fairly thick and relatively homogeneous deposit of clay or shale". This is certainly the case at Mam Tor, which according to Hutchinson would comprise an upper zone of 'rotational slip' and a lower zone of 'translational slide'. Similarly Varnes' model (Figure 4) considers an upper area of 'rotational slumping' in bedrock giving way to a lower area of 'earth flow'. Figure 3 is a general outline of Varnes' classification scheme.

Although Varnes' model more closely describes the Mam Tor landslide his terminology concerning the toe region is somewhat out-dated. The term 'translational slide' is preferred in this study.

By comparing Figures 4 and 5 it can be seen just how closely Varnes' diagram fits the Mam Tor slide; many features are identical in both figures. For example, there is a distinct main scarp, the main slipped unit shows reversed slope and increased dip of the strata (up to 55^{o} in places), minor scarps are clearly developed (such as that of 'Little Mam Tor'), there are numerous transverse ridges on the foot of the slide, and the toe is very clearly defined. Several of these geomorphological features can be seen on Plates 1, 8 and 12.

The retrogressive units on the south side of the main unit at Mam Tor are not shown on the diagram of Varnes. It would seem that these features result from secondary flank failures which occurred some time after the main unit itself rotated away from the face, leaving the side

FIGURE 3: Landslide classification scheme
(After Varnes, 1958)

Type of Movement			Type of Material		
I. Falls			Bedrock		Soils
			Rockfall (A)		Soilfall (A)
II. Slides	A. Material in motion is not greatly deformed		Rotational Slump (C-E) Planar Block Glide (C)		Rotational Slump (C-E) Planar Block Glide (D) Lateral Spreading (A)
	B. Material in motion greatly deformed		Rockslide (A-E)		Debris Slide (B-E) Lateral Spreading (A)
III. Flows			Unconsolidated		
			Large Rock Fragments	Sorted Sand or Silt	Mixed Rocks, Clay, Soil, etc.
		Dry ↓	Rock Fall/Avalanche (A) ↓ Rapid Earthflow (A) ↓	Sand Run (A-B) Loess Flow (A) ↓ Debris Avalanche (A) ↓ Debris Flow (A) Sand or Silt Flow (A)	↓ Slow Earthflow (B-D) ↓
		Wet	Mudflow (B)	Mudflow (B-C)	Mudflow (B-C)
IV. Complex Landslides			Movement is by a combination of one or more of the three types of movement described above (see Figure 4)		

Approximate Ranges of Rates of Movement

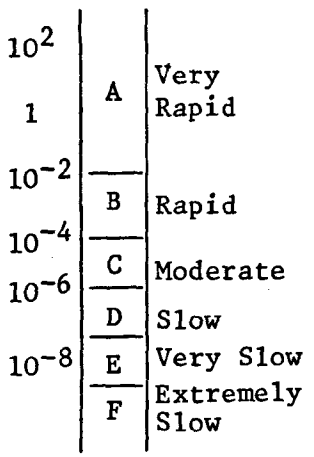

(Arrow indicates gradational series)

FIGURE 4: The major features of a rotational slump (After Varnes, 1958)

The Major Features of a Rotational Slump

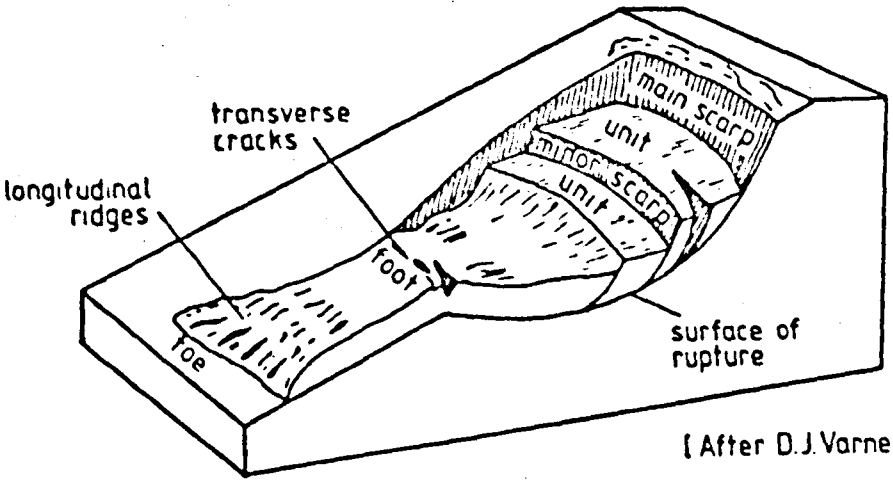

[After D.J. Varnes, 1958]

Main Scarp — The exposed surface of the main shear plane

Minor Scarp — The exposed surface of a subsidiary shear plane within the slump

Foot — The intersection of the main shear plane and original ground surface

Toe — The lowest margin of moved material

FIGURE 5: Location and major geomorphological features of the landslide at Mam Tor, Derbyshire.
(A.B.C.D. refer to lines of section on Figure 2).

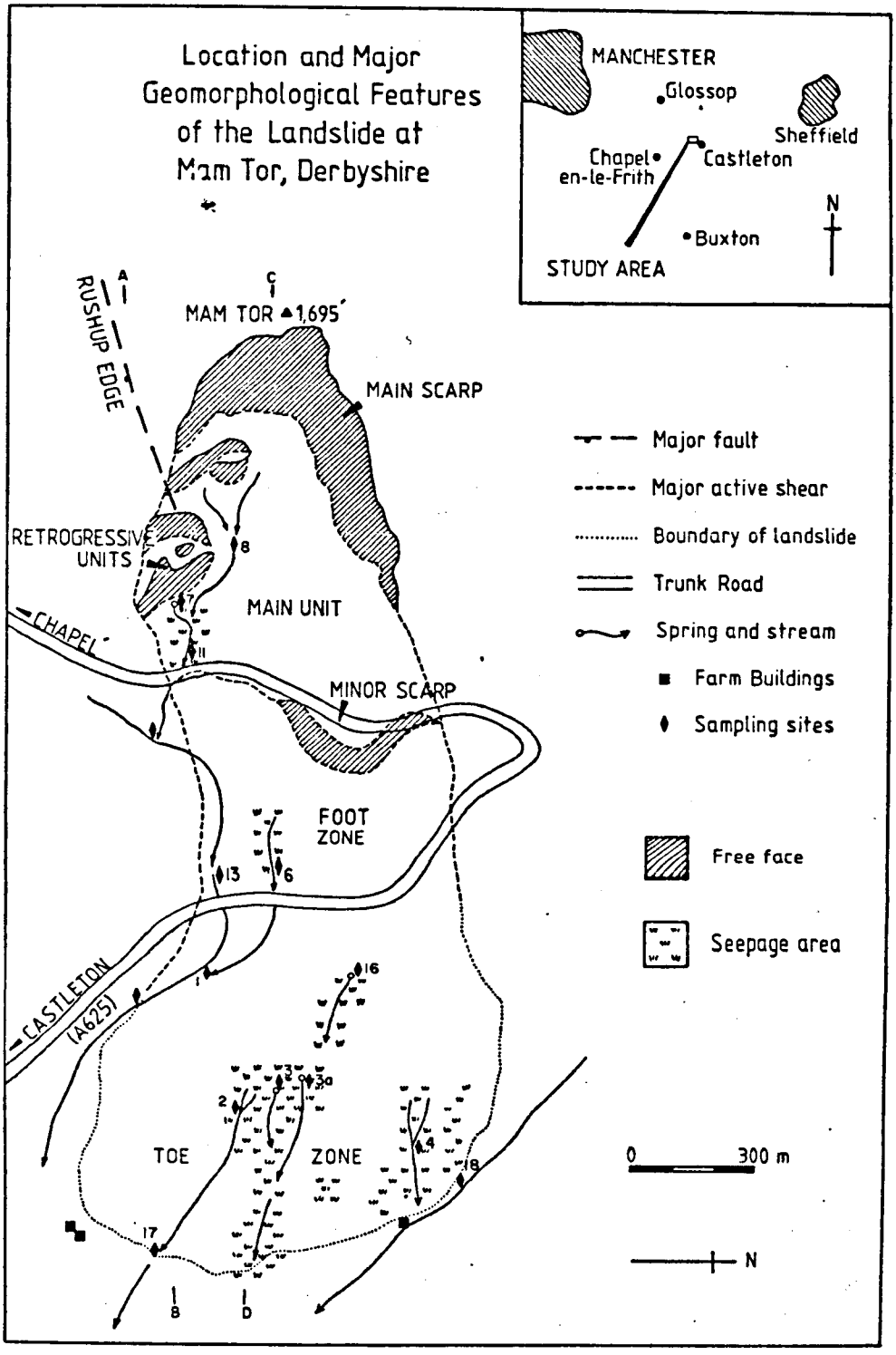
Location and Major Geomorphological Features of the Landslide at Mam Tor, Derbyshire
MANCHESTER
Glossop
Sheffield
Chapel en-le-Frith
Castleton
Buxton
STUDY AREA
N
A
C
RUSHUP EDGE
MAM TOR ▲1,695'
MAIN SCARP
RETROGRESSIVE UNITS
MAIN UNIT
CHAPEL
MINOR SCARP
FOOT ZONE
CASTLETON (A625)
TOE ZONE
Major fault
Major active shear
Boundary of landslide
Trunk Road
Spring and stream
Farm Buildings
Sampling sites
Free face
Seepage area
0 300 m
N

FIGURE 6: Longitudinal section through the landslide and retrogressive units. Plane of section is west (A) to east (B). Broken line indicates dip of strata.

FIG 6 LONGITUDINAL SECTION THROUGH THE LANDSLIDE

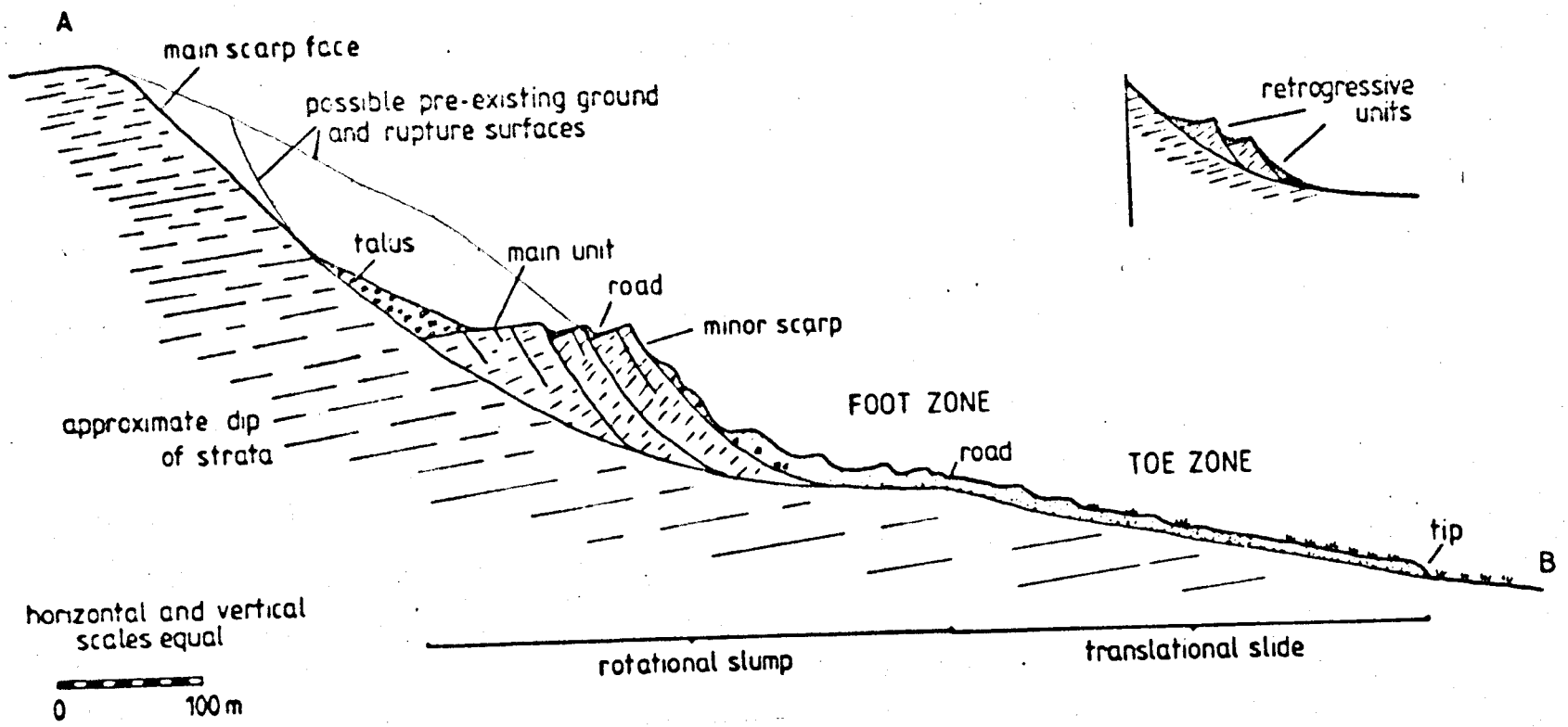

TABLE 1: Comparative Dimensions of Mam Tor and 21* Edale Landslides (After Brown, 1977)

	Mam Tor	*Mean Edale	Range Edale
Area (ha)	34.5	10.0	0.4- 63.0
Maximum Length (m)	950	340	110 -1130
Maximum Width (m)	550	301	75 - 840
Height of Main Scarp (m)	105	34	9 - 75

wall unsupported. The smaller cross-section in Figure 6 is drawn through these retrogressive units, which can be seen to have an identical structure to the main landslide but are on a much smaller scale.

3.2 Description of the Mam Tor Landslide

In terms of dimensions, Mam Tor is one of the largest landslides in the area covered by Sheet SK18, and is certainly the most elongate (due to the translational slide component beyond the foot). The figures given in Table 1 help to illustrate this point. The total volume of material which has moved is probably around 25 million cubic metres (Brown, 1977).

The most conspicuous feature of this landslide, which can easily be seen on Plate 1 and from the air (Plate 12), is the main scarp face. This rises to a height of 105 m above the main slipped unit. Horizontal banding on the face, which can be seen in more detail on Plate 6b, can also easily be discerned on the aerial photograph. This scarp appears generally light-toned due to the lack of covering vegetation, which is due to highly active erosion rather than a lack of suitable niches.

As a result of this continuous removal of material from the face thick 'scree' deposits have accumulated at its base. This is not true 'scree' as usually defined, since it contains a large proportion of very fine material which binds the mass together. In this way it falls somewhere between scree and colluvium. Whatever terminology is preferred this area is also easily distinguished from the air and frequently displays gully and levee-like features on its surface, particularly after heavy rain.

Beneath this 'scree' lies buried the main surface of rupture on which the landslide is moving. After particularly rapid movements, such

PLATE 12: Aerial photograph of the Mam Tor landslide. Contact scale 1:7,000. (Numbers refer to location of boreholes 7 and 8).

as those in 1977, the uppermost part of this surface is exposed as the main unit moves downslope, taking the 'scree' with it. After a time material falling from the face begins to accumulate and the surface becomes covered again. Plate 13a shows the uppermost portion of this surface with 'scree' material in the foreground. Slickensides indicate the direction of landslide movement and the polished appearance is due to the alignment of clay minerals under pressure, parallel with the rupture surface (Plate 13b).

Another bare rock/scree surface can be seen on Plate 12 just below the upper section of road. This is the minor scarp face known as 'Little Mam Tor' and is the result of activity on a second major shear plane which roughly parallels the upper section of road (see Figure 5). Here the inclined banding in the face (Plate 8) is due to the presence of carbonate horizons in the Edale Shale.

The appearance of this minor scarp face is not unlike the retrogressive units, which can also be picked out as light tonal areas on Plate 12, above the top road on the main unit.

Lying roughly between the two road sections is the 'foot zone' of the landslide. Movement upslope is greater than on the 'toe' and as a result material comprising the foot becomes rucked-up and a complex arrangement of ridges and hollows can be seen from the air.

Below the bottom section of road the toe of the landslide can be seen to spread out onto the solifluction-mantled footslopes of the Hope Valley. The fact that no solifluction material is found on top of the landslide material means that the landslide must have been activated after the last period of glaciation had ended.

On the toe, movement of material *en masse* along failure surfaces gradually dies out and is replaced by much slower translational slide. Roughly, the lowest point on the failure surface marking the right flank

PLATE 13a: The main failure surface exposed at the base of the scarp face.

PLATE 13b: A portion of the slickensided failure surface.


OLYMPUS

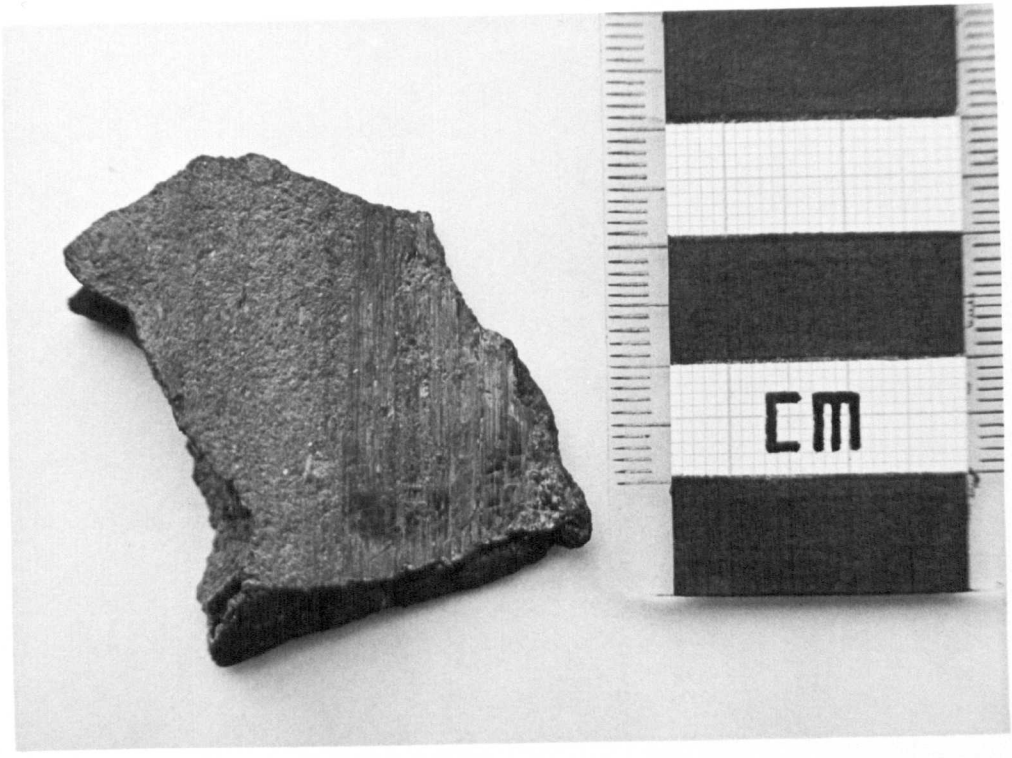
CM

of the landslide can be seen forming the slight ridge in the foreground of Plate 10b. As a result of slowing movement downslope this region is also characterised by a network of ridges and hollows. In many of these hollows exist seepage areas where waters upwell from the landslide material and precipitate ochre.

The vegetation of these boggy seepages is very different from the surrounding grass and bracken, and as a result they can be easily discerned as dark-tone patches on the air-photo. The position of the seepages must be constantly changing as the toe material creeps downslope since several isolated patches of ochre can be found which attest to the former positions of iron-precipitating springs. Plate 14 shows the characteristic appearance of these seepages.

The actual rate of movement on this lowest part of the landslide is minute in comparison with the often rapid rates recorded higher up. Tilted and displaced trees, fences and even telegraph poles indicate that movement is nevertheless still taking place. This is particularly evident at the very tip of the landslide and at one locality a farm building, Blacketley Barn, has periodically to be excavated to prevent it from being totally engulfed (see Plates 15a and b).

Easily distinguished, also, are the flanks of the landslide. In the upper part this is due to a line of tears in the turf due to the shearing movement, and in certain places sections of walls have been displaced considerable distances relative to each other on either side of the shear. These flank shears are most spectacularly developed where the road crosses from stable ground on one side onto the landslide on the other.

On the upper road section the moving material has been displaced downwards relative to the stable ground on either side (Plate 16). On the lower portion of road the landslide material has been pushed up (Plate 17). This in itself is conclusive evidence that the slipped mass is moving on a concave,

spoon-shaped surface. Further down on the landslide the flanks are defined where the toe debris rests with convexity on the valley floor.

Severe road damage has also occurred along the transverse shear plane described above as being responsible for the scarp of Little Mam Tor. In places the road surface has been constructed directly on top of this highly active shear and the carriageway is split in two during periods of activity (Plate 18a). Vast quantities of limestone ballast have been laid down along this shear in short-term attempts at re-grading and, therefore, stabilising the road. These are seen as the lightest patches on the aerial photograph. Further results of movement on this shear plane can be seen in Plates 18b and 19.

One feature which is common to all highly active landslides, and Mam Tor is certainly no exception, is the lack of an integrated surface drainage network. The artificial drainage ditches on the main unit never contain water, even after periods of intense rainfall. This is due to the fact that they become sheared after movement of the landslide and thereafter precipitation soaks rapidly into the highly permeable covering of scree and subsequently into the network of failure surfaces, and cracks, below. Some of this deeper drainage may also find its way into the underground drainage soughs, originally intended to drain the workings of the Odin Mine, and never re-emerge in the toe seepages as much of the shallower drainage does. Downstream from these seepages the water does begin to flow in well defined channels which link with each other and with streams draining the surrounding area beyond the landslide toe.

The only large drainage channel, which permanently carries water, on the entire landslide is the man-modified stream known as Odin Sitch. This water eventually finds its way into the area of lead-mine spoil near Knowlegates Farm. This is also the point of emergence of Knowlegates Sough draining the workings of Odin Mine.

PLATE 14a: Seepage at Site 16.

PLATE 14b: Seepage at Site 3.

PLATE 15a: Encroachment at Blacketley Barn.

PLATE 15b: Tilting of fences due to movement at the toe.

PLATE 16: Downward movement of the road on the upper section.

PLATE 17: Upward movement of material in the foot zone.

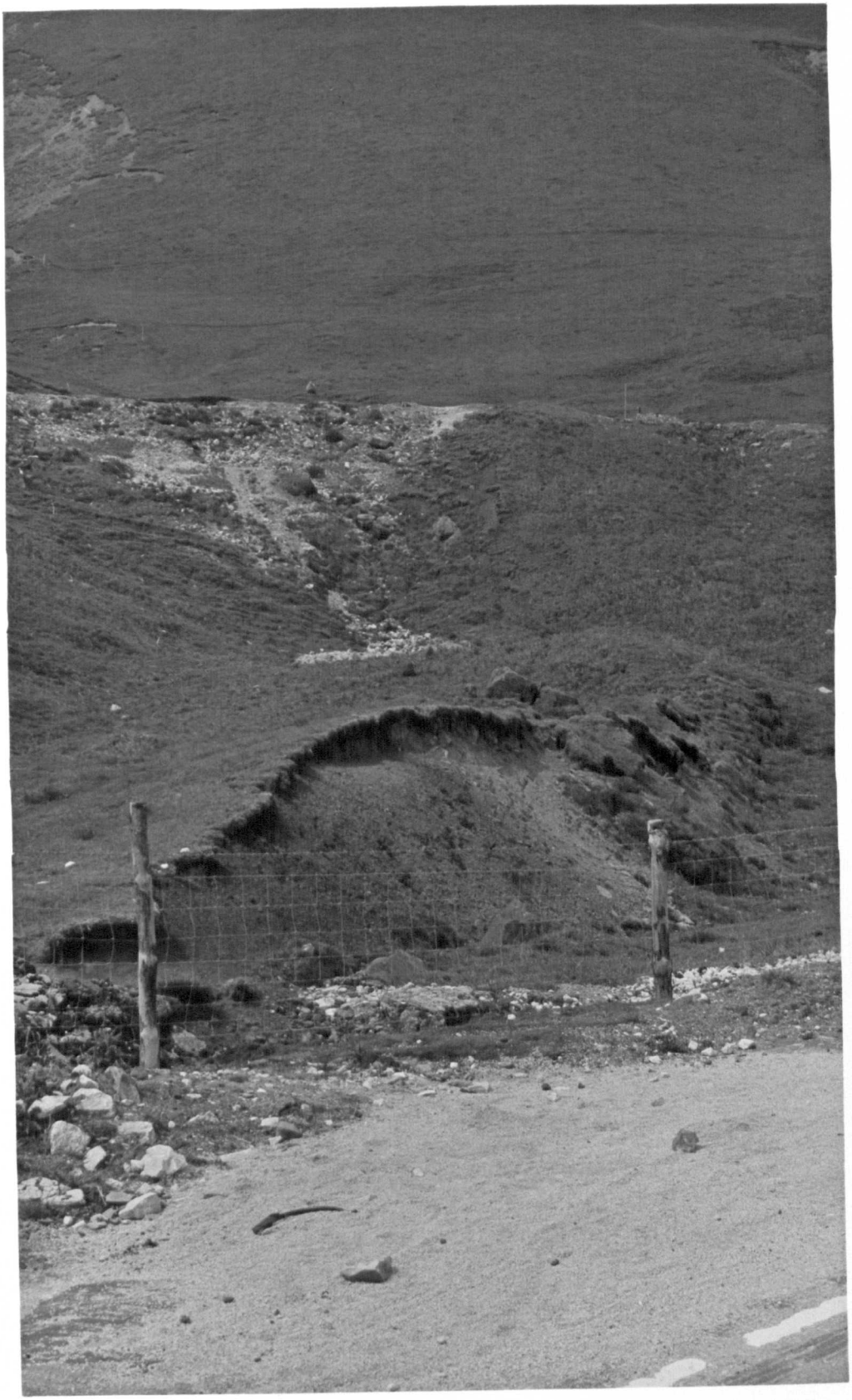

PLATE 18: Further examples of road damage.

PLATE 19: Severe road damage and tarmac stratigraphy.

3.3 Landslide Management

During studies of the large scale and rapid movements of the Mam Tor landslide, which were referred to in Section 1.1, it was noted that the maximum rate of movement (in the order of 0.5 m per day) is usually maintained at most for two or three days (Brown, 1977). Subsequently the rate diminishes gradually and returns to the 'normal' minimum of less than 1 mm per day. This abrupt transition from slow creep to rapid failure and a return to steady creep corresponds closely with the observations of Terzaghi (1950) concerning 'threshold behaviour'.

The resulting disruptions of the road surface present highway engineers with perplexing problems. Should a long-term but permanent solution be found, or is it sufficient to simply 'patch up' the damage each time it is incurred? The latter approach to management has been chosen in the past at Mam Tor and maintenance operations have been carried out on the worst-affected sections of the road nearly every year since 1802 (when the present road was first opened). These 'maintenance operations' consist simply of laying down fresh surfacing material (and hardcore if necessary) over the cracks and ridges and as a consequence an impressive stratigraphy of tarmac has built up over the years. At least two metres of this material can be seen below the photographer's feet in Plate 19.

Many more permanent solutions to landsliding have been described including the installation of giant retaining structures, the regrading of slopes, or even the artificial acceleration of movement to produce a more stable configuration (see Forbes, 1947; Cooke and Doornkamp, 1974). All of these are too costly and unsightly (in a National Park) to be practicable at Mam Tor, and the latter scheme might even make the situation worse by removing support for the main face which would itself then become

unstable. Royster (1979) advocates the complete removal of material in cases of slipping such as this, although the landslides he describes are somewhat smaller than Mam Tor.

One method of management which was seriously considered by Derbyshire County Council was deep drainage of the entire area. As Cooke and Doornkamp (op.cit.) note, with regard specifically to rotational slips "The back tilting at the head of the mobile mass forms hollows in which water can collect. This tends to drain down the rupture surface and maintain permanently high pore pressures. By this means it may be self-perpetuating as an area of instability".

As a precursor to drainage several boreholes were put down (under the direction of A.W. Skempton and R.J. Chandler of Imperial College, London) through the landslide in 1978, in order to determine the position of the water table and the location of any failure surfaces. The subsequent report from the team of consultants is still not available. One can only assume that the results were inconclusive.

The proposed scheme was to consist of a network of four-foot diameter drains bored horizontally into the slope. The consultants suggested that this would reduce infiltration and run-on, drawing water away from the slip planes. Such deep drainage has proved successful in stabilising other landslides (Forbes, 1947; Early and Skempton, 1972), where the major input of water is from precipitation falling within the bounds of the moving mass. At Mam Tor, however, there seems to be an additional source of water, irrespective even of the position of the local water table. The possibility of groundwater upwelling from a fault is discussed in detail in Section 5.4.3. The point made here is simply that such a drainage scheme would not necessarily render the slide more stable. Indeed it may even make the situation worse by improving throughflow and aeration and increasing the rate of chemical weathering within the landslide material.

Due to an immediate lack of funds and pressure from local inhabitants the plans for drainage have been shelved. Rather than trying to keep the existing road open (which was becoming increasing more costly and difficult) the County Council have proposed a route for a new road which will by-pass Mam Tor on the more stable limestone plateau to the south (Peak Park Planning Board, 1977). The date of commencement for building the road has not been definitely agreed. In the meantime the A625 remains open for access to farm premises, but use as a through-route is impossible due to the extensiveness of the recent damage.

4. WATER SAMPLING AND ANALYSIS

4.1 Sampling Design and Procedure

As noted in Section 1.1.2, certain springs on the Mam Tor landslide, notably those of the seepage areas on the toe, precipitate ochre. The presence of these accumulations of iron hydroxide suggests that the emergent waters contain a high proportion of dissolved ferric iron. Also, in dry weather, the stems of plants in the seepages become coated with gypsum crystals in fine fibrous habit (Plate 20). This suggests that the stream waters are also concentrated in calcium and sulphate ions. Capillary rise of the solutions up the plant stems and subsequent evaporation leads to crystallisation of the gypsum ($CaSO_4$).

In view of these observations it was decided to sample, on a regular basis, any waters draining the landslide area with a veiw to determining their overall chemical composition. A pilot study was conducted in the Spring of 1978 when water from six streams was collected and removed to the laboratory for analysis. Detectable quantities of several cations and anions were found and there was considerable variation between samples. A more thorough sampling network was established on the basis of this pilot study and the main sampling programme commenced in October 1978, lasting for twelve months.

Originally every distinct site of flowing water on the landslide was sampled, in addition to one surface runoff site located on Rushup Edge to the west, and two sites in the village of Castleton to the east. The latter two sites were located where streams emerge from the limestone cave system of the area to the south and west of the village. These acted as 'controls', representing the 'normal' karst waters of the region. The number of sites originally totalled twenty-eight.

PLATE 20: Gypsum precipitation on plants in the seepages

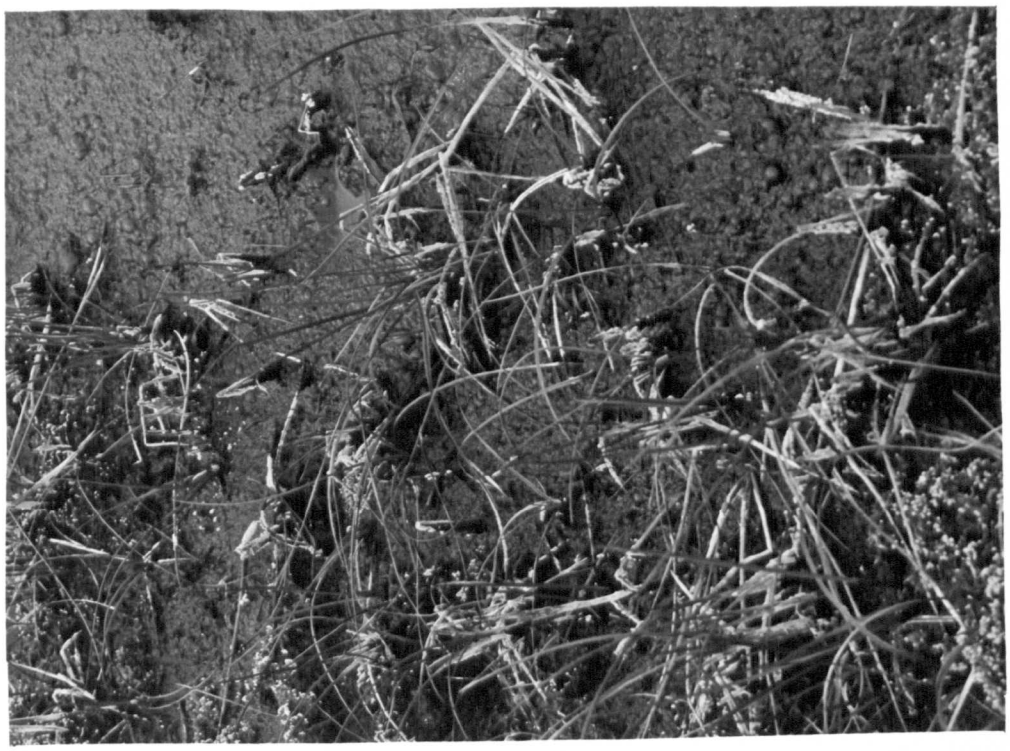

This total was reduced,however, during the course of the year and data are presented here for fifteen sites only. A number of the original twenty-eight sites dried up after thefirst few weeks of analysis, or else froze for long periods during the winter. Indeed the weather was so severe during January and February, 1979, that Mam Tor was cut-off and impossible to reach for periods of up to three weeks. During this time the rain gauge was buried by snow for seven weeks in all, and data from the Hope Meteorological Office station is used in Appendix Bii. Other sites are obviously linked hydrologically with ones nearby (although this is not apparent from the surface drainage pattern), giving identical analytical results. Sampling at such sites was also discontinued after a time, resulting in a total reduction of thirteen sampling sites. The fifteen remaining sites are shown on Figure 5.

In large channels, different velocities in different parts of the flow can lead to cross-channel variations in chemical composition, and bulk sampling is often necessary. Since the flow of water at most of these fifteen sites,however, is in the form of shallow seepage or turbulent flow in a narrow channel (ensuring adequate mixing) it was decided that single depth-integrated samples from the centre of flow would be sufficiently representative of the stream as a whole (Rainwater and Thatcher, 1960).

New or acid-cleaned 250 ml. polythene bottles with air-tight caps were used to collect the water samples. These were filled completely, by immersion in the stream, so that no air space was left in the bottle above the solution. Each bottle and its cap was rinsed two or three times in the water downstream from the actual sampling site before taking the sample. Careful handling of the bottles at all times until capped was necessary to prevent contamination, especially by salts from the fingers. Each sample bottle was clearly marked with a site number and a letter corresponding to the date of collection; this was necessary to avoid confusion in the laboratory

when handling large numbers of otherwise identical bottles. Initially samples were taken from each of the sites at seven-day intervals. In order to standardise this procedure the samples were taken every Tuesday morning between the hours of 8.00 a.m. and 10.30 a.m. (1½ hours was needed to visit all the sites). Such standardisation is often important when taking samples of natural waters since chemical changes (most easily detected by monitoring fluctuations in pH) take place throughout the day, particularly during warm sunny days where plants and other organisms are living in the water (Golterman et al.,1978).

As stated in Section 1.3.1 rainfall quality was not regularly determined. Two samples were taken, however, during storm events on 21st August, 1979, and 2nd October, 1979. Full chemical analyses were performed on these two samples and the results are given in Table 7.

4.2 Sample Storage

During the pilot study it was noticed that samples from certain streams produced an orange deposit on the insides of the sample bottles even if left unopened for only a matter of hours. If left overnight the amount of precipitate was considerable. Since the whole aim of collection is to transfer the sample from stream to place of analysis with minimal chemical alteration this precipitation is clearly undesirable.

It is reasonable to assume that iron in solution is responsible since the orange precipitate forms only in samples from those streams which deposit ochre in the field. Many chemical preservatives for natural water samples have been suggested (see Zobell and Brown, 1944) but acidification is the most common method of preventing the precipitation of iron and other metals. Since the amounts of chloride and sulphate ions were to be determined at a later date the use of HCl or H_2SO_4 for acidification was precluded. HNO_3 was, therefore, used instead, 0.5 ml. being added to

TABLE 2: The Effects of Sample Storage and Acidification on Water Quality

Sample Number	Date of Analysis	Days After Sampling	Solute Content				
			Ca^{2+}	Mg^{2+}	Na^{+}	K^{+}	Fe^{t}
1B	10.10.78	0	111	30	50	3.1	8.2
1B	17.10.78	7	114	31	49	3.2	0.6
1B	24.10.78	14	111	30	61	3.2	0.3
2B	10.10.78	0	188	41	37	5.7	23.3
2B	17.10.78	7	190	42	34	6.0	22.1
2B	24.10.78	14	191	41	43	6.0	22.0
7B	10.10.78	0	408	201	13	5.1	89.5
7B	17.10.78	7	427	197	13	5.6	31.5
7B	24.10.78	14	422	206	17	5.6	26.1
8B	10.10.78	0	24	14	10	2.7	1.1
8B	17.10.78	7	24	15	5	2.8	0.7
8B	24.10.78	14	21	13	14	2.7	0.1
11B	10.10.78	0	223	122	11	4.1	43.3
11B	17.10.78	7	260	124	11	4.3	31.0
11B	24.10.78	14	252	114	15	4.3	23.3
13B	10.10.78	0	100	31	26	2.0	5.9
13B	17.10.78	7	113	47	30	2.0	3.1
13B	24.10.78	14	95	37	33	2.0	2.2
1Ba	10.10.78	0	109	29	51	3.1	8.2
1Ba	17.10.78	7	137	31	64	3.2	8.2
1Ba	24.10.78	14	120	31	61	3.2	8.4
2Ba	10.10.78	0	186	40	37	5.5	23.0
2Ba	17.10.78	7	190	41	34	6.0	22.7
2Ba	24.10.78	14	190	40	40	5.8	22.5
7Ba	10.10.78	0	410	206	13	5.2	90.0
7Ba	17.10.78	7	416	197	8	5.5	93.0
7Ba	24.10.78	14	419	200	12	5.4	92.1
7Ba	02.10.79*	357	426	209	15	5.4	88.4
8Ba	10.10.78	0	20	12	9	2.6	1.4
8Ba	17.10.78	7	20	14	8	2.7	0.9
8Ba	24.10.78	14	19	14	11	2.8	0.2
11Ba	10.10.78	0	250	137	11	4.0	49.7
11Ba	17.10.78	7	256	121	7	4.3	49.1
11Ba	24.10.78	14	252	131	11	4.6	49.9
11Ba	02.10.79*	357	255	126	12	4.0	48.0
13Ba	10.10.78	0	99	30	26	1.9	6.0
13Ba	17.10.78	7	99	31	23	2.0	5.8
13Ba	24.10.78	14	102	39	30	2.0	5.7

a Samples acidified prior to analysis

* Samples analysed approximately 12 months after collection

each sample on arrival back at the laboratory. This reduced the pH of all samples to the range 1.7-2.0. Table 2 shows the effects of acidifying samples. The most noticeable improvement in storage efficiency is observed for total iron content, which is remarkably constant over twelve months, when the sample is acidified but decreases rapidly in the control.

Coarse particulate and organic matter was removed from the samples prior to acidifying by passing each solution through a 'Whatman' 541 (hardened, ashless) filter-paper. This procedure undoubtedly causes some extremely fine particulate iron and aluminium hydroxides to be recorded as solutes, but the amounts are small compared with the truly ionic species present.

Samples were kept for a maximum of fourteen days prior to analysis although storage for several months was found to have little effect on composition (Table 2). During the two weeks of storage the samples were kept at room temperature out of direct sunlight (see Slack and Fisher, 1975).

4.3 Sample Analysis

Analysis of the water samples was conducted in two phases. Firstly the temperature, pH, and electrical conductivity of the waters was measured in the field at the time of sample collection. After the samples had been removed to the laboratory, filtered and acidified as described in Section 4.2, they were analysed for ten major ions and a number of trace metals. Details of standard conditions and procedures for these chemical analyses are given in Appendix A, but a brief outline follows here.

4.3.1 Temperature, pH, and Electrical Conductivity

Stream water temperature at the point of sampling was measured by immersing a mercury thermometer in the flow. The thermometer was left to equilibrate while the 250 ml. sample was being taken as described in Section 4.1. Temperature was recorded to the nearest $0.1^{o}C$ and entered into a field

notebook along with readings of pH and conductivity and any relevant notes concerning flow conditions (i.e. 'very low', 'heavy', etc.).

pH (the negative log of the hydrogen ion concentration) was measured in the field using a portable battery-operated pH meter - Walden Precision Instruments model WPA C6. Since the pH of most samples was in the range 3.0-6.0 a buffer solution of pH 4.0 was used to check the instrument. The accuracy of the measurements was in the order of $\pm$ 0.1 units, and all values were correct for the temperature of the water. pH is readily converted to H^+ activity, $[H^+]$, by taking the antilog and changing the sign.

Electrical conductance is a measure of the ability of a conductor, in this case a dilute aqueous solution, to convey electricity. The conductance of water is measured between two parallel platinum or carbon plates and is directly proportional to plate area and inversely proportional to plate separation. Results are expressed as if for plates of 1 cm^2 separated by 1 cm. When standardised in this way the measure becomes independent of the measuring system and is a property particular to the water sample. The units of this measure of conductivity are Ω^{-1} cm^{-1}, or more commonly, S cm^{-1} ('S' for Siemens). The older name of 'specific conductance' with units of µmho cm^{-1} is now obsolete (Golterman and Clymo, op.cit.). The instrument used to measure conductivity in this study, by immersion of the electrode in the stream, was manufactured by Electronic Switchgear (model MC 1, mark V). This particular model incorporates a temperature compensation dial (conductivity readings are quoted at 25°C). By taking measurements of conductivity both in the field and on return to the laboratory it was discovered that differences of less than 5% occurred between the two, and very often there was no difference at all. Therefore, it was decided to take measurements immediately upon return, thereby eliminating the need to carry heavy field equipment from site to site.

4.3.2 Cations: Al^{3+}, Fe^{3+}, Fe^{2+}, Ca^{2+}, Mg^{2+}, Na^{+}, K^{+}, H^{+}

The quantities of six cations (the only ones present in significant amounts in the pilot study samples) were determined each week by a variety of methods. Ca^{2+}, Mg^{2+}, Na^{+} and K^{+} were measured by atomic absorption spectrophotometry, total Fe(Fe^{2+} + Fe^{3+}) by a colorimetric method, and H^{+} indirectly from pH as described in Section 4.3.1. At the outset Al^{3+} was not thought to be present but later was measured from time to time by atomic absorption spectrophotometry. Samples which were high in total Fe (those precipitating ochre) were occasionally analysed for Fe^{2+} separately, by titration. This had to be done prior to acidification since this process oxidises iron to the ferric (Fe^{3+}) form. In this way the proportions of ferric to ferrous ions could be determined.

Principles and applications of atomic absorption techniques will not be discussed here. The text by Christian and Feldman (1970) is recommended to the interested reader; Chapter 4 on 'interferences' is considered particularly useful.

4.3.3 Anions: HCO_3^-, Cl^-, SO_4^{2-}

The only anions detected during the pilot study were HCO_3^-, Cl^- and SO_4^{2-}. Bicarbonate ions were, however, only found in the waters from the Peak Cavern resurgence in Castleton. Since these waters are of no direct consequence to the work at Mam Tor the bicarbonate titration was discontinued and Cl^- and SO_4^{2-} only were measured on all samples, by silver nitrate titration and barium chloride turbidimetry, respectively.

4.3.4 Trace Metals: Cd, Cr, Cu, Mn, Ni, Pb, V, Zn

Black shales commonly contain heavy metals in trace amounts (Vine and Tourtelot, 1970; Holland, 1979). Since the waters at Mam Tor are draining an area of fragmented black mudstones it seemed likely that the waters might also contain certain trace metals and that these could eventually

co-precipitate in the seepages with the ochre since iron hydroxide is a well-known 'scavenger' of other metals (see Section 7.6.3). As a result, eight samples were selected to cover the range of site types from ochre seepages to surface runoff and these were analysed for Cd, Cr, Cu, Mn, Ni, Pb, V, and Zn by atomic absorption using a high temperature carbon arc furnace attachment.

4.4 Results

A complete table of results obtained from the chemical analyses is given in Appendix B. There follows here a brief description of the results overall, which leads on to a more detailed discussion of their significance in Chapter 5.

4.4.1 Temperature, pH and Electrical Conductivity

At the commencement of the main study in October, 1978, the temperatures of all the streams, springs and seepages were in the range 8-9°C. Temperatures rose slightly during this month, which was remarkably mild, but then fell consistently until the end of the year. By January the temperature of most streams had reached or closely approached 0°C. There were two notable exceptions.

Waters draining the limestone region and emerging at Peak Cavern stayed relatively warm and the temperature never fell below 5.6°C. At sampling site No.7, below the retrogressive units on the south side of the landslide, the total fall in temperature throughout the period October to February was only 0.9°C. The lowest temperature recorded at this site was 8.7°C.

Throughout the Spring of 1979 stream temperatures began to rise and by May had reached their October level. The highest temperatures of the year were recorded during a very hot spell of weather in June when some sites became dry and one (Site No.4) was not to flow again during the period of study. The highest temperature of all, recorded at Site No.3a, was 24.2°C.

TABLE 3: Summary of Water Temperature Data

Site	1	2	3	4	6	7	8	11	13	16	17	18	100	101	3a
Minimum Temperature (°C)	0.9	1.4	4.3	0.1	2.5	8.7	0.4	1.9	1.1	3.2	0.0	1.6	4.5	5.6	0.4
Maximum Temperature (°C)	13.9	17.2	14.0	16.7	12.9	10.2	22.7	16.8	16.2	14.8	15.1	13.7	12.8	9.5	24.2
Mean Temperature (°C)	7.7	7.8	8.5	6.7	10.2	9.5	9.1	8.5	7.7	8.7	7.8	7.9	8.6	8.1	8.1
Standard Deviation from Mean	4.3	4.7	2.8	4.9	3.2	0.5	5.6	3.9	4.5	3.2	5.0	3.9	2.2	1.1	6.6

From February until June, as the temperature at most sites was rising steadily, that of the water at Site 7 rose by only 1.3 degrees to 10.0°C. The Peak Cavern water remained cooler and reached only 9.5°C during August. In this same month the temperature at Site 7 attained its maximum value of 10.2°C.

Temperatures fluctuated considerably during the unsettled summer but all lay within the range 8-10°C once again by October, 1979.

Table 3 is a summary of the data given in Appendix Bi, and clearly shows the constancy of Sites 7 and 101 (Peak Cavern).

The vast majority of pH readings fell in the range 3.0-3.7, a fact which can clearly be seen on Figure 11. Surface runoff sites and waters draining the limestone area have slightly higher pH values, approaching neutrality. Variations in pH seem in no way related to time of year. On two occasions during the winter months air temperatures were so low that the pH 4 buffer solution froze and the field meter ceased to operate.

During May, 1979, the conductivity meter which had been used throughout the study was so severly damaged that repair was impossible. A second identical model was acquired and used for the remainder of the sampling period. It is not known if the two meters would have given identical readings for the same sample. There was no systematic variation in conductivity according to the season, but levels were generally higher at the end of the twelve months of sampling than they were at the start. It is hoped that this observation is not the result of having changed meters.

A considerable range in conductivities can be noted in Appendix Biii between the two extremes of Site 7 and Site 100. The mean values at these two sites are 2265 and 92 $\mu S\ cm^{-1}$ respectively.

Differences in conductivity between samples reflect differences in the concentration of ions in solution. Thus, conductivity is a rapidly obtained measure of the total *ionic concentration* or *activity* of a water sample.

FIGURE 7: Total dissolved solids-conductivity relationship.

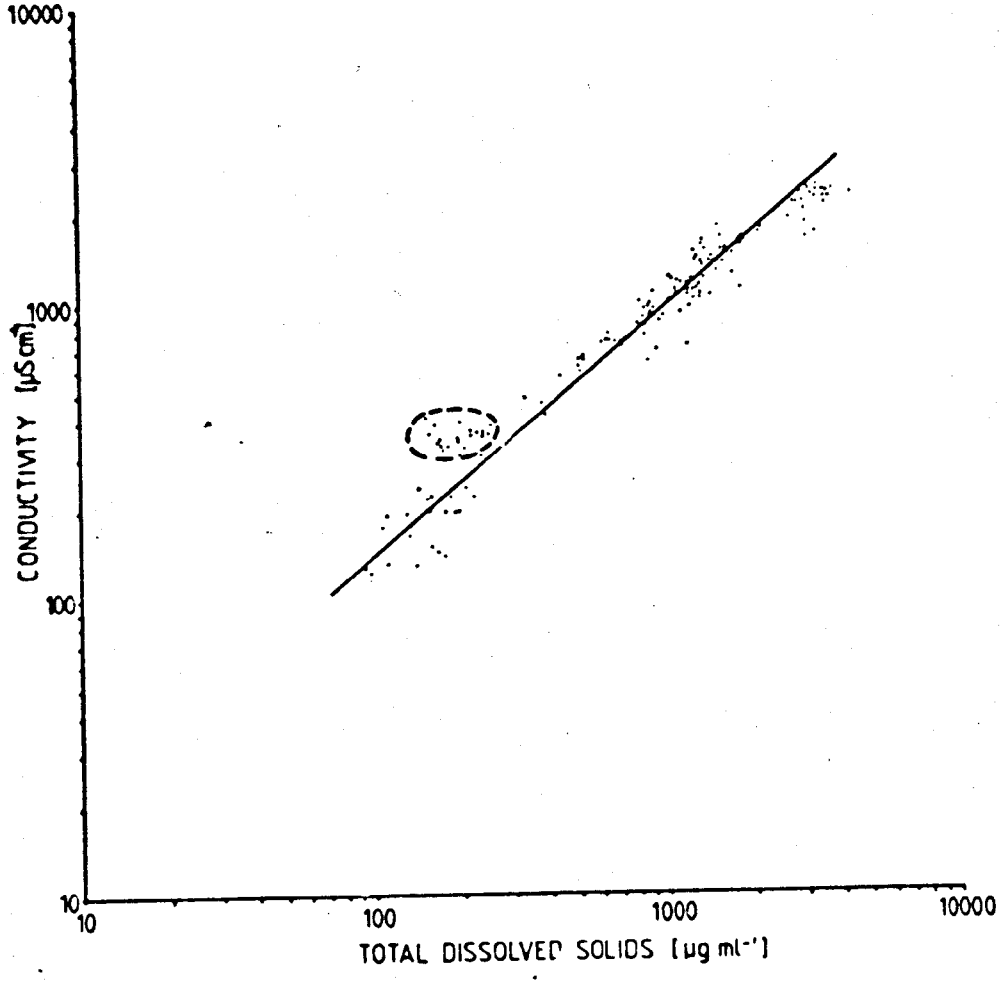
10000
1000
100
10
CONDUCTIVITY [µScm⁻¹]
10
100
1000
10000
TOTAL DISSOLVED SOLIDS [µg ml⁻¹]

Lind (1970) shows that there is a log-log relationship between conductivity and ionic strength, both for natural water samples and laboratory-prepared salt solutions. A similar relationship seems to exist for the Mam Tor samples, shown in Figure 7, between conductivity and total dissolved solids (TDS). One group of points, however, lies off the 'best fit' line. This group (circled) consists of samples which are known to contain the ion HCO_3^-, although this was not included in the chemical analyses (see Section 4.3.3). If bicarbonate had been measured, although the conductivity would remain the same, the TDS content would be higher and the points would lie closer to the line.

4.4.2 Cations

Calcium in solution is often assumed to indicate alkaline conditions. The site with the highest pH in this study is Site No.101 issuing from Peak Cavern. Yet the data in Appendix Biv clearly indicate that this site has one of the lowest Ca^{2+} concentrations. Much higher concentrations of this ion are to be found in the acidic (pH 3-3.5) streams and, in particular, Site 7 where values in excess of 400 $\mu g\ ml^{-1}$ are frequently recorded.

Similarly Mg^{2+} concentrations are highest in the Site 7 water and are often double the values for the next most concentrated site (No.11). The extreme values are 239 $\mu g\ ml^{-1}$ (9.1.79, Site 7) and 1.0 $\mu g\ ml^{-1}$ (5.6.79, Site 101).

Concentrations of Na^+ and K^+ ions are given in Appendix Bvi and Bvii. Sodium levels show a dramatic increase during the winter months in sites located close to the road. These fluctuations correlate closely with periods of road gritting conducted by the County Council. Potassium levels are generally low at all sites, but are possibly slightly higher-than-average in the ochre-precipitating seepages.

Total Fe concentrations (Appendix Bviii) vary considerably from site to site. The lowest levels are recorded in surface runoff and karst waters

TABLE 4: The Changing Proportions of Ferrous:Ferric Iron on Storage

Sample	A Total Fe (ug ml^{-1})	B Fe^{2+} (ug ml^{-1})	C Fe^{3+} (A-B)	D $Fe^{2+}:Fe^{3+}$ (C/B)
3P	88	13	75	5.8
7P	114	85	29	0.3
11P	121	16	105	6.6
16P	97	17	80	4.7
After twenty-four hours				
3P	88	10	78	7.8
7P	114	61	53	0.9
11P	121	7	114	16.3
16P	97	2	95	47.5
After forty-eight hours				
3P	88	7	81	11.6
7P	114	56	58	1.0
11P	121	0	121	-
16P	97	0.2	96.8	484

(< 1.0 μg ml^{-1}) and are once again highest at Site 7 and in the ochre springs (often > 100 μg ml^{-1}). Ferrous iron is only present in a handful of sites (all ochre-precipitating) and the proportion of Fe^{3+} to Fe^{2+} varies considerably between sites (see Table 4). The highest concentration of 85 μg ml^{-1} Fe^{2+} was recorded at Site 7.

Ferrous iron was not determined every week and the overall variation in concentration is not known.

Similarly Al^{3+} was not analysed for on a regular basis, but Appendix Bix lists the analyses for five consecutive weeks samples. Again aluminium is most abundant at Site 7.

4.4.3 Anions

Levels of chloride ions as given in Appendix Bx are generally quite high and it is thought that this may be due to an intrinsic fault in the method of analysis (see Appendix A). However, variations in concentration can be seen between sites and throughout the year. Ochre springs are generally highest in chloride, with the exception of Site 7; this apparent deviation from the 'norm' may be due to interference, from other ions, with the analysis.

An identical response to that shown by Na^{+} is noticed for streams close to the road (Figures 15 and 18) and a large contribution of sodium and chloride ions from road salt in winter seems inevitable.

Sulphate is by far the most concentrated ion in solution at Mam Tor. 'Background' levels of 20-30 μg ml^{-1} are recorded from surface and karst waters but values of around 3000 μg ml^{-1} are found in Site 7 water (Appendix Bxi). This fact coupled with the low pH here justifies the use of the term 'acid sulphate' to describe these waters.

As can be seen from Table 5, the measured concentrations of the various ions in solution, together with sample temperature and conductivity, are not

TABLE 5: Basic Statistics for Water Variables

Variable	Number of Observations	Minimum	Maximum	Mean	Standard Error	Standard Deviation	Skewness	Kurtosis
Calcium	374	1	521	148.826	5.679	109.823	0.845	0.333
Magnesium	399	1	239	44.221	2.381	47.526	1.987	3.670
Sodium	399	2	110	34.965	1.132	22.611	0.619	-0.671
Potassium	399	0.6	11.0	3.709	0.106	2.115	0.402	-0.627
Total Iron	399	0	123	33.440	2.048	40.909	0.926	-0.801
Chloride	398	14	170	70.191	1.939	38.684	0.293	-1.083
Sulphate	398	18	3320	622.055	31.721	632.836	1.823	3.366
pH	354	2.7	7.9	4.385	0.065	1.220	0.475	-1.134
Temperature (^{o}C)	359	0	24.2	8.22	0.211	4.001	0.041	0.288
Conductivity (μScm^{-1})	369	60	2600	922.390	31.554	606.128	0.607	-0.144

normally distributed about the mean. Large standard deviations attest to the considerable spread of values while 'skewness' and 'kurtosis' are measures of the shape and peakedness of the frequency distribution relative to a normal curve.

Skewness is calculated as the 'third moment about the mean' (i.e. the average of the sum of the cubes of the deviations) divided by the standard deviation cubed:

$$Skewness = \frac{\frac{\Sigma(x - \bar{x})^3}{n}}{\left[\sqrt{\frac{\Sigma(x - \bar{x})^2}{n}}\right]^3} \quad \text{(Gregory, 1963)} \qquad (4)$$

For a normal curve the skewness index is zero. Here the data are clearly positively skewed with a 'tail' on the high side caused by the exceptionally high values recorded in the Site 7 samples.

Kurtosis is defined as the 'fourth moment about the mean' divided by the standard deviation raised to the fourth power:

$$Kurtosis = \frac{\frac{\Sigma(x - \bar{x})^4}{n}}{\left[\sqrt{\frac{\Sigma(x - \bar{x})^2}{n}}\right]^4} \quad \text{(Gregory, 1963)} \qquad (5)$$

A perfectly normal distribution yields a kurtosis value of 3. Here most variables show a lower degree of peakedness (a greater spread).

Table 6 shows the calculated Pearson's product-moment correlation coefficients for every possible combination of variables. Particularly high (>0.8) positive correlations are obtained for the following ion-pairs: Ca-Mg; Ca-Fe; Ca-SO_4; Mg-SO_4; Na-Cl.

TABLE 6: Correlation Matrix for Water Variables

	Calcium	Magnesium	Sodium	Potassium	Total Iron	Chloride	Sulphate	pH	Temperature
Magnesium	0.905								
Sodium	0.202	-0.043							
Potassium	0.969	0.483	0.384						
Total Iron	0.809	0.766	-0.017	0.595					
Chloride	0.299	0.039	0.901	0.541	0.089				
Sulphate	0.905	0.969	-0.025	0.534	0.781	0.072			
pH	-0.677	-0.555	-0.237	-0.789	-0.644	-0.391	-0.602		
Temperature	0.167	0.181	-0.088	-0.017	0.192	0.073	0.170	0.100	
Conductivity	0.954	0.898	0.223	0.696	0.814	0.337	0.914	-0.717	0.223

The close relationship between calcium and magnesium, and to a lesser degree iron, suggests that these ions are derived from the same source (diagenetic dolomite and ankerite). This also applies to the Na-Cl correlation, confirming the belief that these ions are derived from road salt.

The strong $Ca-SO_4$ and $Mg-SO_4$ correlations perhaps suggests that the precipitates forming from solution in the seepages are not only gypsum ($CaSO_4.2H_2O$) but also epsomite ($MgSO_4.7H_2O$), although similar examples from the literature could not be found. Not surprisingly the dependent variable, conductivity, shows a high degree of correlation with four of the most concentrated dissolved species - Ca^{2+}, Mg^{2+}, Fe^{t} and SO_4^{2-}.

4.4.4 Trace Metals

Trace metal analysis was conducted on an additional set of water samples collected from eight sites on January 23rd, 1980. Appendix Bxii gives the full table of results.

Of the eight metals for which analysis was performed, only manganese was present in sufficiently large quantities to have been detected by normal 'flame' techniques (see Appendix A). Lead, zinc and vanadium were easily picked up but only very minor amounts of copper, nickel, chromium and cadmium were found. As for the greater proportion of major constituents the trace metals were in the greatest concentrations in the Site 7 waters.

High Pb and Zn concentrations were also observed at Mam Tor by Ford (1976), in a number of geochemical traverses across the area. These anomalies were noted, however, in soil and stream sediment samples above the position of the underground extension of Odin Vein. They were detected despite the vein being covered by about 500 feet of shale. Unfortunately Ford does not give quantitative details of measurements made and a comparison of values with those obtained from stream water samples cannot be made.

TABLE 7: Median monthly bulk precipitation concentrations, 1959-64 (after Stevenson, 1968) compared with values for two samples from Mam Tor collected on 21st August, 1979(a) and 2nd October, 1979(b)

Station	Ca^{2+}	Mg^{2+}	Na^{+}	K^{+}	Cl^{-}	SO_4^{2-}	Number of Observations
Aberdeen	1.1	0.6	4.6	0.4	5.7	2.1	70
Aldergrove	0.8	0.6	5.2	0.5	6.0	2.4	47
Belmullet	1.8	-	16.0	0.7	24.5	2.1	70
Birr	1.3	-	3.3	0.2	4.4	0.9	71
Camborne	0.8	0.6	7.7	0.4	11.3	1.9	57
Clones	0.6	-	2.7	0.2	3.6	1.0	72
Dublin	2.5	-	4.0	0.4	6.3	2.6	70
Edinburgh	1.8	0.3	3.8	0.3	3.0	1.7	68
Eskdalemuir	0.3	0.2	1.8	0.2	2.8	1.2	59
Leeds	2.7	1.0	2.3	0.5	5.3	3.9	63
Lerwick	2.0	3.2	22.5	1.1	32.3	3.3	61
Malin	2.1	-	21.0	0.9	33.0	2.6	71
Newton Abbot	1.5	0.6	5.5	0.7	6.3	2.9	59
Rosslare	1.7	-	14.8	0.7	22.0	2.3	69
Rothamsted	1.4	0.3	1.8	0.5	3.1	2.1	59
Stornoway	1.1	1.9	17.0	0.9	28.0	2.4	56
Valentia	0.9	-	8.0	0.3	12.7	1.4	72
Mam Tor - a	2.0	1.0	7.0	0.3	9.0	3.0*	1
Mam Tor - b	2.0	1.2	6.7	0.3	11.0	3.0*	1

*At lower detection limit of method used

5. INTERPRETATION OF THE WATER CHEMISTRY DATA

5.1 Environmental Responses

5.1.1 Rainfall

After several weeks of analysis it was observed that high concentrations of ions in the stream waters occur at times of low flow. Conversely, the lowest concentrations are measured after periods of heavy rainfall. It appears therefore, that the waters are simply diluted by a large input of atmospheric precipitation which is much less concentrated, in respect of all ions, than the stream water.

Levels of dissolved solids in rain and snow fall are generally very low over the British Isles (Stevenson, 1968), especially when compared with the high concentrations present in the Mam Tor drainage waters. Analyses of the two rainfall samples taken at Mam Tor during storm events are given in Table 7. These compare favourably with average values for this part of the country, as given by Crisp (1968) and by Gore (1968). A study of rainfall quality at Ladybower Reservoir, only 10 km northeast of Mam Tor, is described by Rippon (1980). A full chemical analysis was not made but Rippon's values for SO_4^{2-} of between 3 and 5 $\mu g\ ml^{-1}$ agree well with others in Table 7. Rippon attributes the excess sulphate in drainage water to additional input from dry fallout. Since stratigraphically similar beds to those present at Mam Tor underlie the area, however, it seems that a geologic source similar to that discussed in Section 6 is more feasible.

The concentrations of ions in rainfall is usually somewhat higher during heavy storms than during persistent light rain, and individual ions can vary dramatically from one storm to the next; Ca^{2+} is supplied from agricultural areas being limed, Na^{+}, Mg^{2+} and Cl^{-} from storms at sea,

and SO_4^{2-} from industrial pollution (see Cryer, 1976a). Overall it is considered that the supply of solutes to most of the Mam Tor waters from atmospheric precipitation is minimal.

In other systematic studies of solute inputs to catchment areas (notably the detailed modelling at the Hubbard Brook experimental catchment in New Hampshire, USA) similar inverse relationships to those found at Mam Tor between stream discharge and ion concentrations have been observed. These relationships are generally attributed to the mixing of rain or surface water with deeper soil water (Johnson et al., 1969). During the course of the Hubbard Brook study it was noted that some ions, particularly H^+ and Al^{3+} actually showed an *increase* in concentration with increased throughput. This is certainly not the case at Mam Tor, where without exception, all ions show a decrease after heavy rainfall in streams supplied partly by surface and rain water.

It must be remembered, however, that in the Mam Tor study there was often a considerable time-lag between a rainfall event and the stream-water sample being taken. It may be that immediately following heavy rainfall the concentration of some, if not all, constitutents does increase as weathering products are 'flushed' out of pore spaces. This initial increase, which may last for only a matter of hours or minutes, is then followed by a progressive decrease in concentration over the next few days, producing the observed dilution effect. Such a rise and fall in concentration with the flood hydrograph has been noted by Cryer (1976b) and by Trexler et al. (1975).

Having stated that the Mam Tor stream waters are diluted by inputs of precipitation, it should not be thought that all the streams show a similar degree of dilution. As Johnson (op.cit.) notes, if a stream is supplied with half of its water from surface runoff and half from deep flow the effects of increased rainfall input will be felt much more strongly than at another site which receives nearly all of its water from the surface.

At Mam Tor most sites show a moderate dilution response. One site (No.11), however, shows very dramatic reductions in solute levels at high flow and peaks during base-flow conditions. Still others (notably Sites 7 and 101) show very little or no response to changes in precipitation input. Implications of these facts will be discussed shortly in examining the various origins of the drainage waters in Section 5.4.

5.1.2 Temperature

Pitty (1976) defines five factors which influence the temperature of stream water. These may be summarised as follows:

1. Air temperature at sink (limestone areas).
2. Air temperature at emergence.
3. Time of travel underground.
4. Mixing of underground waters.
5. Season (controls the effect of increased runoff).

Pitty concludes that air temperatures possibly play the major role in determining the final temperature of most stream waters. Thus, it might be expected that air temperatures during the Mam Tor study, although not measured, will closely parallel the changes in water temperature given in Appendix Bi.

At times of low flow, when the travel time of deep waters is increased, stream water temperatures will be affected more by conditions underground (Factors 3 and 4 of Pitty's scheme). Smith and Lavis (1975) note that reductions of 4-5^{o}C can occur during such times, and temperatures tend to equilibrate at about 7^{o}C.

At Mam Tor the various streams respond differently to changes in ambient temperatures. Shallow, surface streams show the most dramatic fluctuations, ranging from winter freezing to summer drying. Clearly such streams are influenced entirely by air temperatures at the time of emergence.

Others show very little response to such seasonal changes, remaining relatively warm in winter and cool in summer. Streams draining the limestone cave system and emerging at Peak Cavern in Castleton (the control sites) are such an example. These waters travel deep underground from the swallet system at Perryfoot(GR. SK.101.812) to the resurgence at Peak Cavern (GR. SK.148.827),a distance of 5 km. Pitty (op.cit.),using temperature-lag data, estimates that the waters take some twenty-eight days to travel this distance. Simpson (1954), however, records tests made by North Derbyshire Water Board "which indicate a flow-through time of six days from Perryfoot". It is likely that considerable variations from a few days to several weeks occur depending on precipitation conditions.

The least variation of any stream at Mam Tor is shown by the waters emerging below the retrogressive units at Site 7 (Fig. 5). In addition, the waters here are much warmer than the 7°C quoted by Smith and Lavis (see Table 3). Again the importance of these observations will be discussed further in Section 5.4.

5.2 Cluster Analysis

The degree of response to environmental variables discussed in the last section was neither unique at each site nor the same for all sites. Rather the sites seem to fall into a number of groups with strong intra-group similarities and distinct inter-group differences. Similar groups could also be distinguished on the basis of actual *quantities* of ions present in solution (Section 4.4). Although it is easy 'by eye' to divide the sites into groups on the basis of one or two attributes, it is difficult to do so objectively and virtually impossible when dealing with more than a handful of variables. There now exists a considerable volume of literature concerned with statistical methods of multivariate analysis (see, for example, Johnston, 1978) and after considering the possibilities

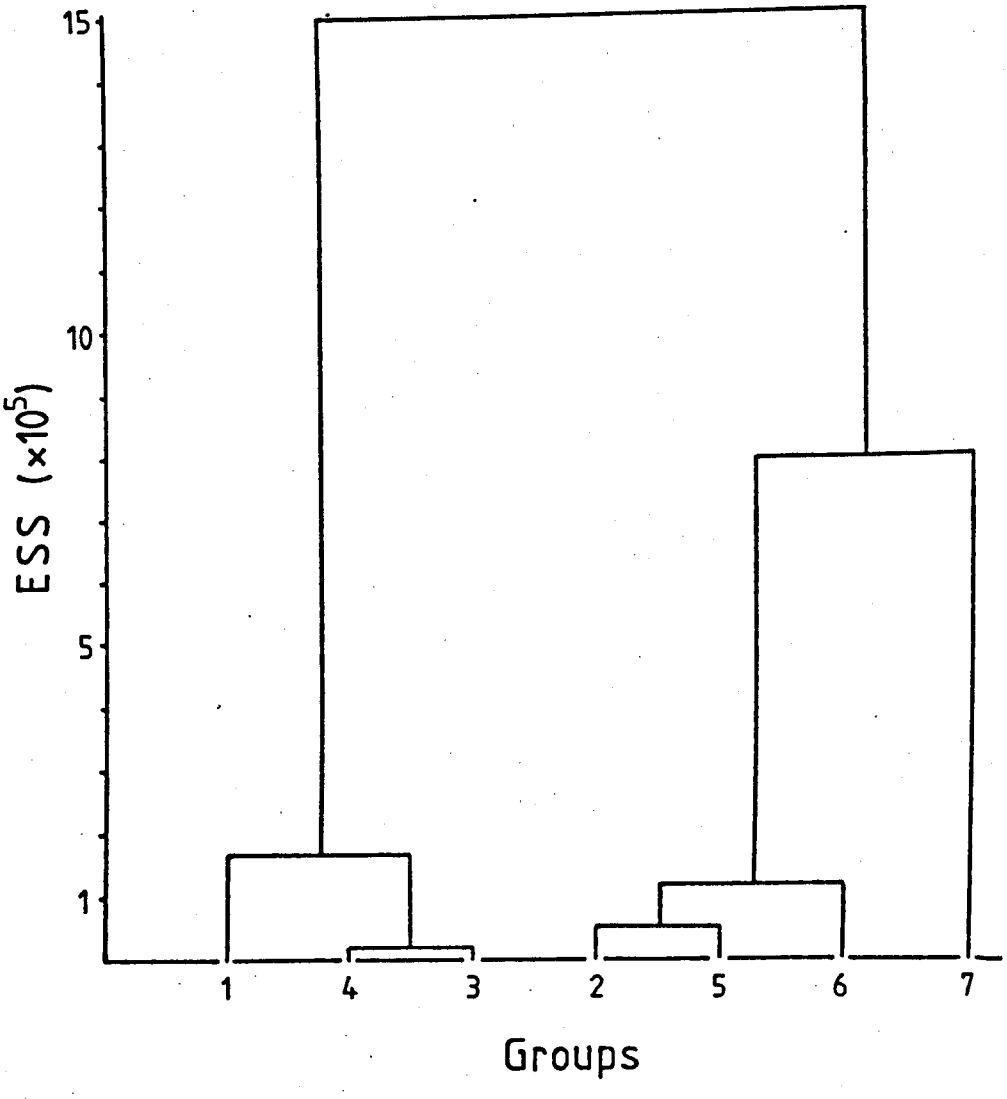
15
10
5
1
ESS (×10^5)
1
4
3
2
5
6
7
Groups

FIGURE 8: Cluster analysis hierarchy based on annual mean data.
ESS = Ward's error-sum-of-squares distance measure.
Numbers 1 to 7 refer to the cluster groups of Table 8.

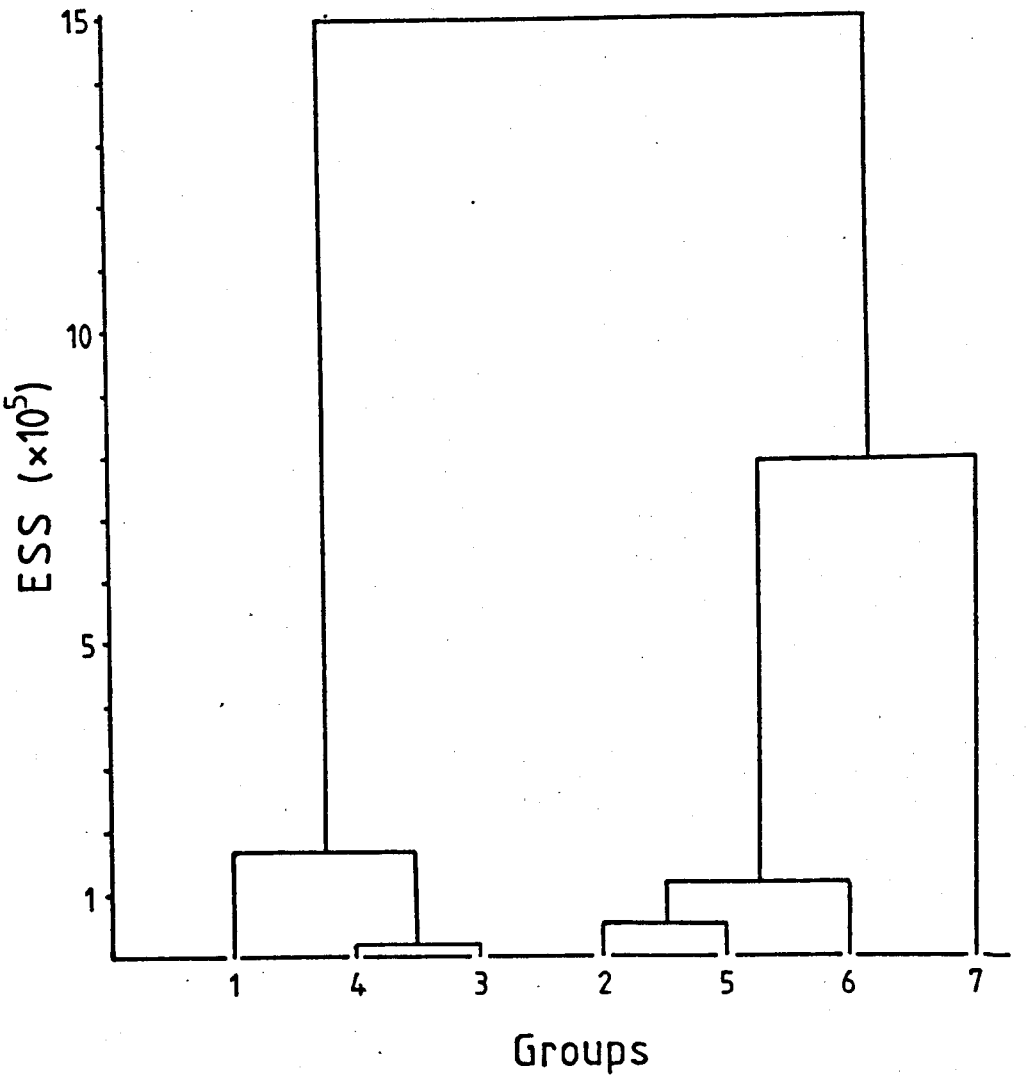
15
10
5
1
ESS (×10^5)
1
4
3
2
5
6
7
Groups

TABLE 8: Characteristics of the Seven Cluster Analysis Groups

Group	Sites	Description
1	1, 6, 13	Stream sites of Odin Sitch and south flank of the landslide.
2	2, 4, 17	Non ochre-precipitating seepages on landslide toe.
3	8, 18, 100	Surface runoff sites.
4	101	Limestone waters of the Peak Cavern resurgence.
5	3, 16, 3a	Ochre-precipitating seepages on landslide toe.
6	11	Mixture of deep and surface derived water.
7	7	Deep origin water emerging at base of retrogressive units.

available it was decided that 'cluster analysis', a technique of hierarchical classification, would be used in this case to produce an objective grouping of the sampling sites. In this way it was hoped to reduce the amount of data so that trends and responses to independent variables might be more easily distinguished.

Various methods of cluster analysis are available on the ICL 1906S computer at Sheffield University, under the package name of CLUSTAN. For the number and type of variables to be used here (seven numeric variables with the same units - Ca, Mg, Na, K, Fe, Cl and SO_4 concentrations - and three with different units - pH, temperature and conductivity) it was decided that a most suitable method of analysis was that first described by Ward (1963). Ward's method utilises an error-sum-of-squares distance measure to calculate individuals dissimilarity and gives the values of this measure at which each group of individuals fuses to the next. The results are best understood when represented in graphical form. Figure 8 is such a cluster analysis hierarchy produced for yearly average data from each of the fifteen sites. Essentially similar classifications were produced when data for individual weeks analyses were used.

The most obvious split in the cluster analysis hierarchy is at a very high level. This means that the groups on the left hand side of the classification are quite dissimilar to those on the right. Table 8 shows which sites make up the various groups.

Groups 1, 3 and 4, on the left of the hierarchy, contain surface run-off sites on the landslide and the 'control'sites on Rushup Edge and in Castleton (see Figure 5). The water at all seven of these sites has a pH of 5.0 or above, and relatively low conductivity (low solute content). Groups 2,5,6 and 7, however, comprise eight landslide sites whose waters have a low pH and high ionic strength, most of which precipitate ochre.

The most distinctive 'group' of all - that which branches from the hierarchy at the highest level - is Group 7 which in fact contains only one site. This is Site No.7, which was noted previously as being different from the rest in terms of quantities of ions in solution and response to temperature and rainfall fluctuations.

Table 8 shows that of the seven cluster analysis groups four contain three sites and three contain only one site. For the three-site groups the arithmetic mean value of every variable was calculated for each week. In this way the data matrix was reduced in size from 10-by-15 to 10-by-7 (ten variables at seven 'sites'). The following series of graphs (Figures 10 to 19) show these group-averaged data plotted against time. Letters along the abcissa correspond to the sampling dates given throughout Appendix B.

Rainfall data obtained from the on-site rain gauge are given in Appendix Bii and shownas a histogram in Figure 9. Differences between totals recorded by the Mam Tor gauge and that of the Meteorological Office at Hope, 3 km east of the landslide, were slight (< 5%) and showed no systematic variation. It might be expected that the Mam Tor gauge would consistently record less precipitation than the one at Hope due to the positioning of the rain gauge in the lee of the main scarp face in a slightly sheltered site surrounded by trees (close to Site No.1, Figure 5). This, however, was not the case and the two sets of data agree very closely.

Readings taken at the Hope station are used in Figure 9 between 09.01.79 and 27.02.79 as the Mam Tor gauge was buried beneath several feet of snow during this period.

The responses of the group-averaged data to changes in precipitation can be seen by comparing Figures 10 to 19 with the rainfall histogram. Weeks with considerably less-than-average rainfall (e.g. J, S, CC) correspond with sharp peaks on most of the other graphs. Conversely, sharp

FIGURE 9: Rainfall histogram for the entire study period. Letters refer to sampling dates used in Appendix B.

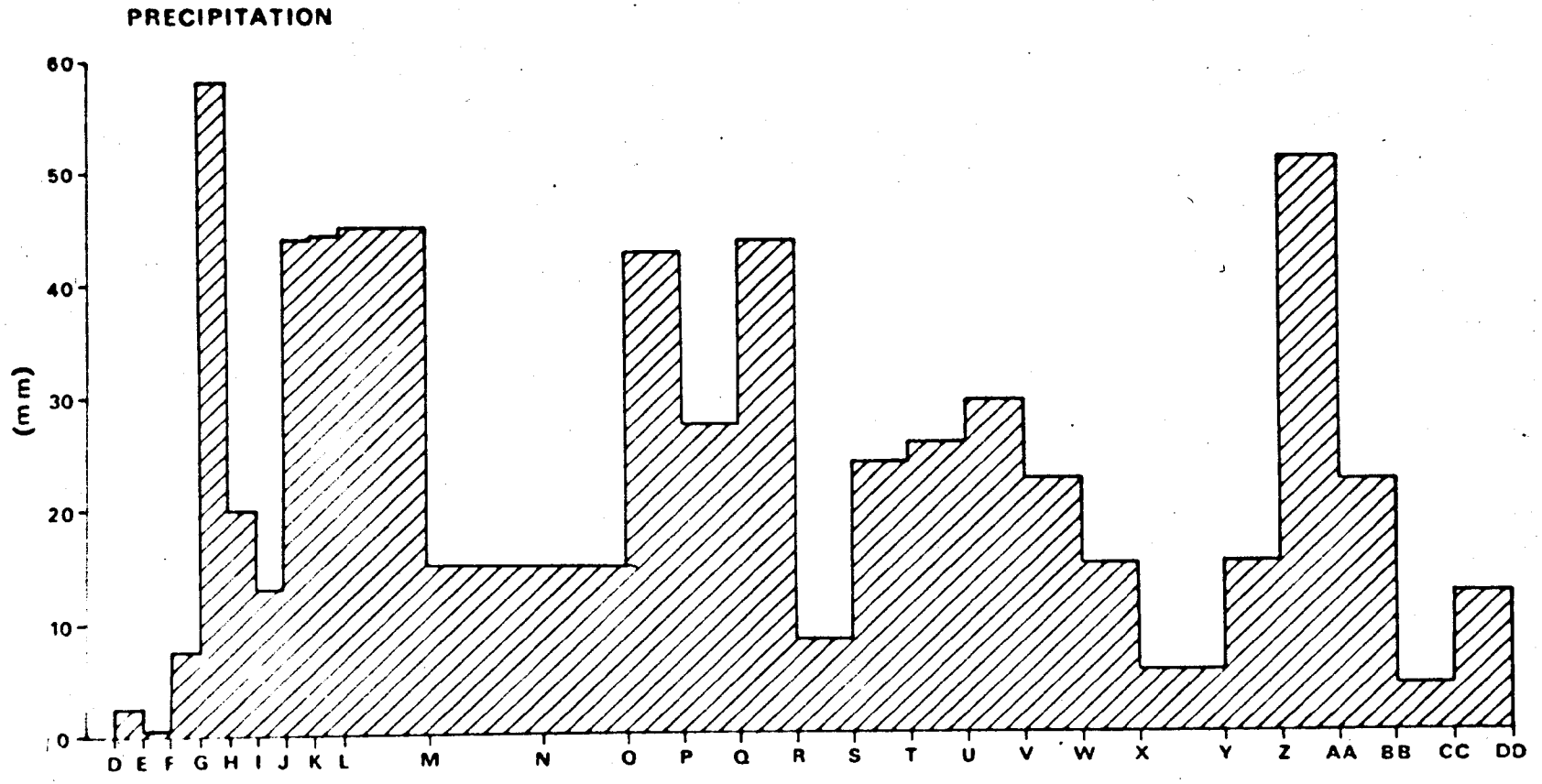
PRECIPITATION
(mm)
60
50
40
30
20
10
0
D E F G H I J K L M N O P Q R S T U V W X Y Z AA BB CC DD

KEY FOR FIGURES 10-19

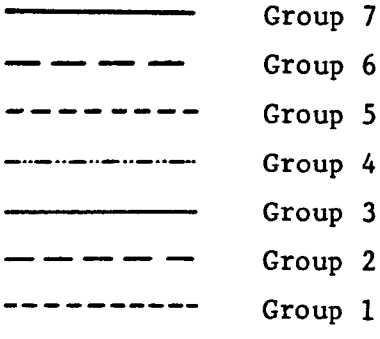

FIGURE 10: Variations in stream water temperature. Group averaged data used.

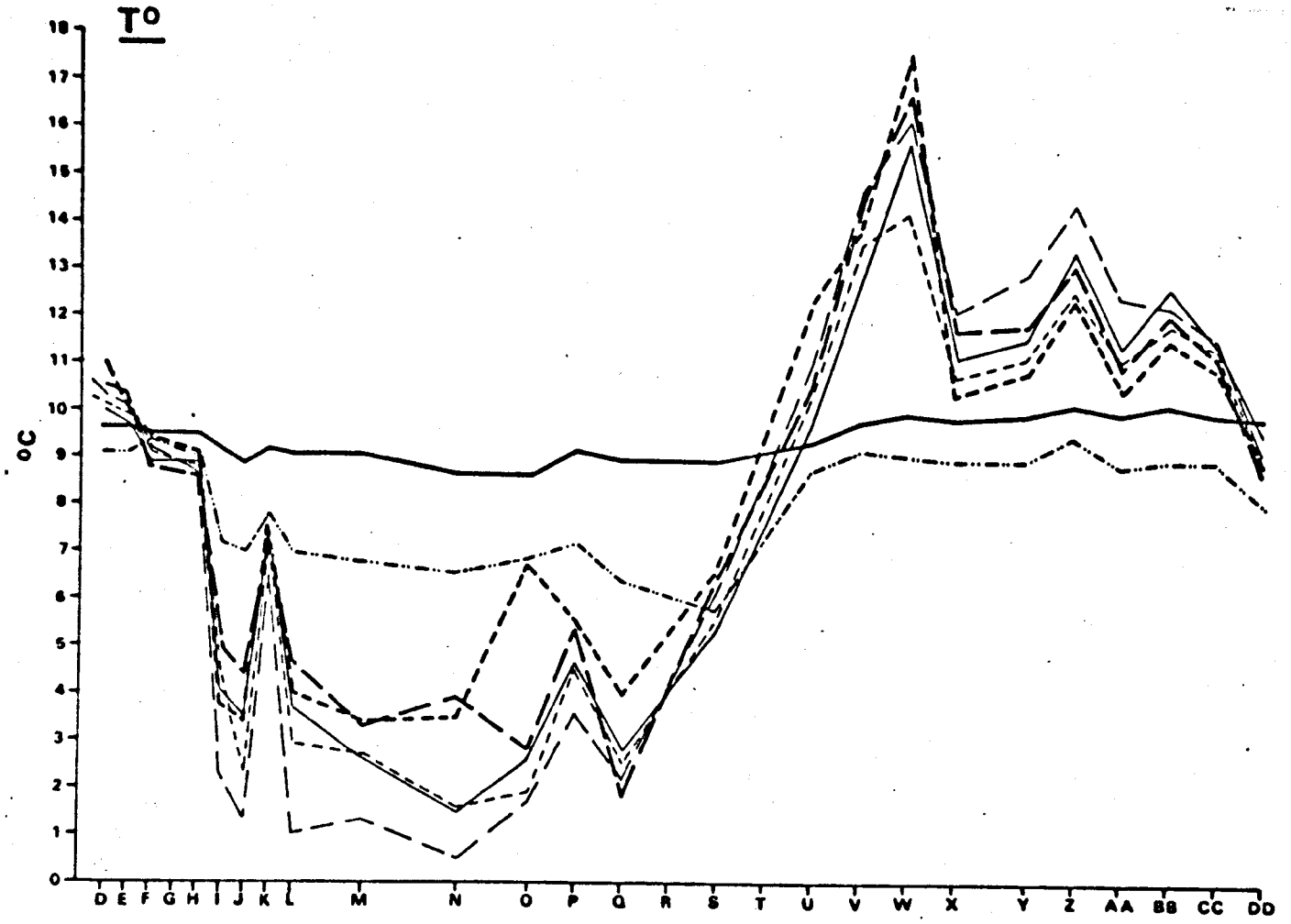
T°
°C
0
1
2
3
4
5
6
7
8
9
10
11
12
13
14
15
16
17
18
D E F G H I J K L M N O P Q R S T U V W X Y Z AA BB CC DD

FIGURE 11: Variations in stream water pH.

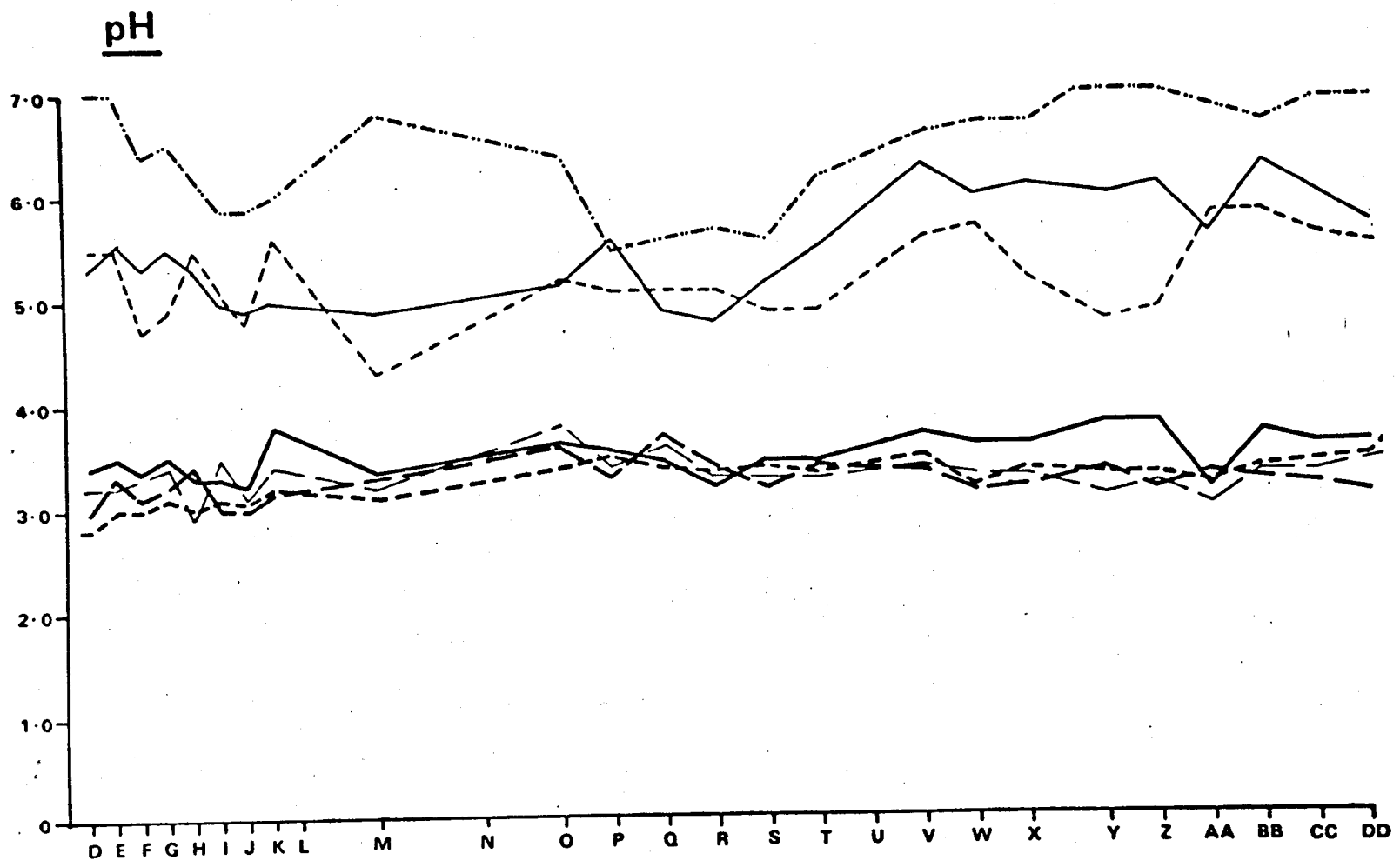
pH
7·0
6·0
5·0
4·0
3·0
2·0
1·0
0
D E F G H I J K L M N O P Q R S T U V W X Y Z AA BB CC DD

FIGURE 12: Variations in electrical conductivity.
($\mu S\ cm^{-1}$, $25^{o}C$)

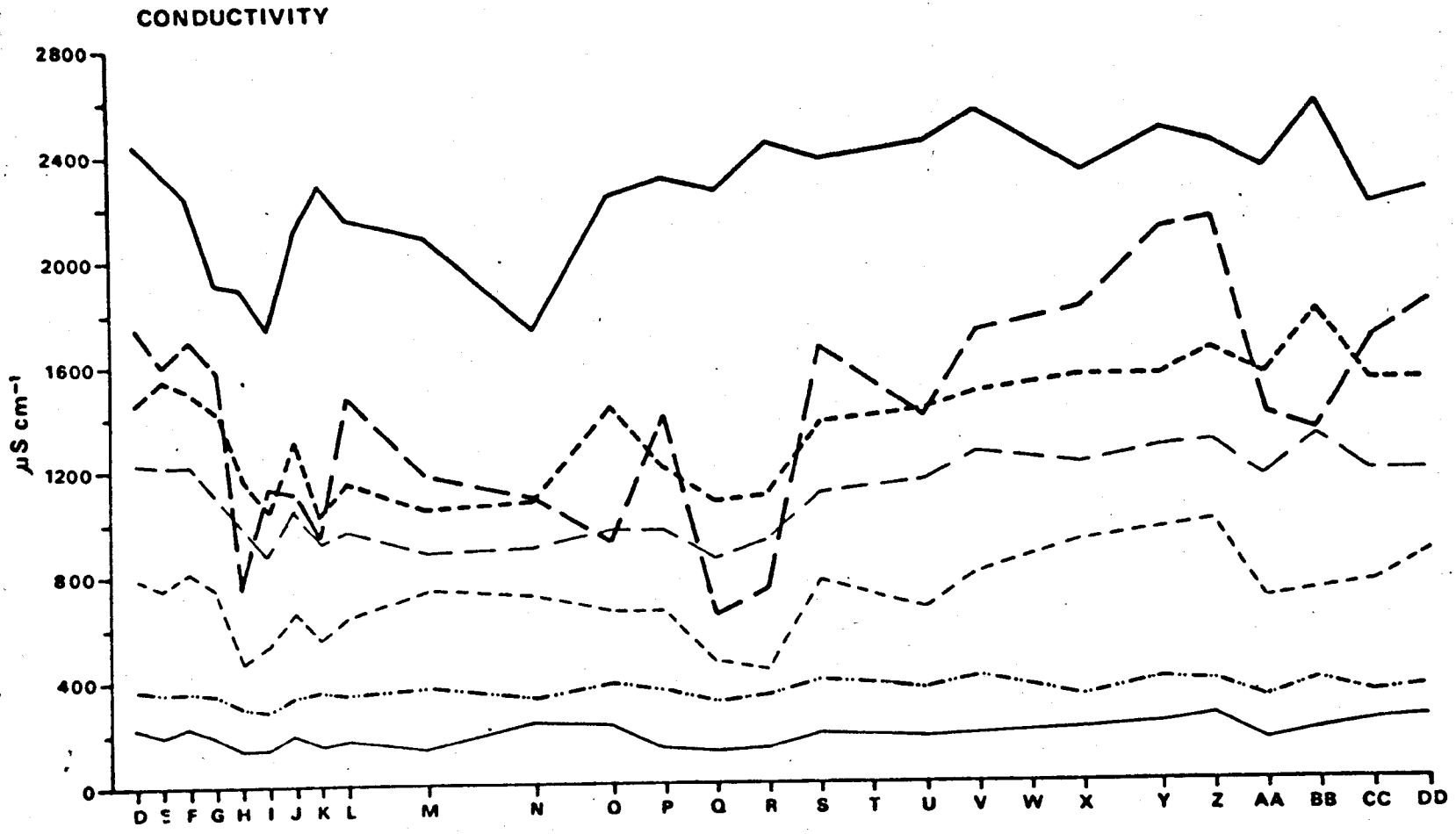
CONDUCTIVITY
2800
2400
2000
1600
1200
800
400
0
µS cm⁻¹
D
E
F
G
H
I
J
K
L
M
N
O
P
Q
R
S
T
U
V
W
X
Y
Z
AA
BB
CC
DD

FIGURE 13: Variations in calcium content of stream waters.

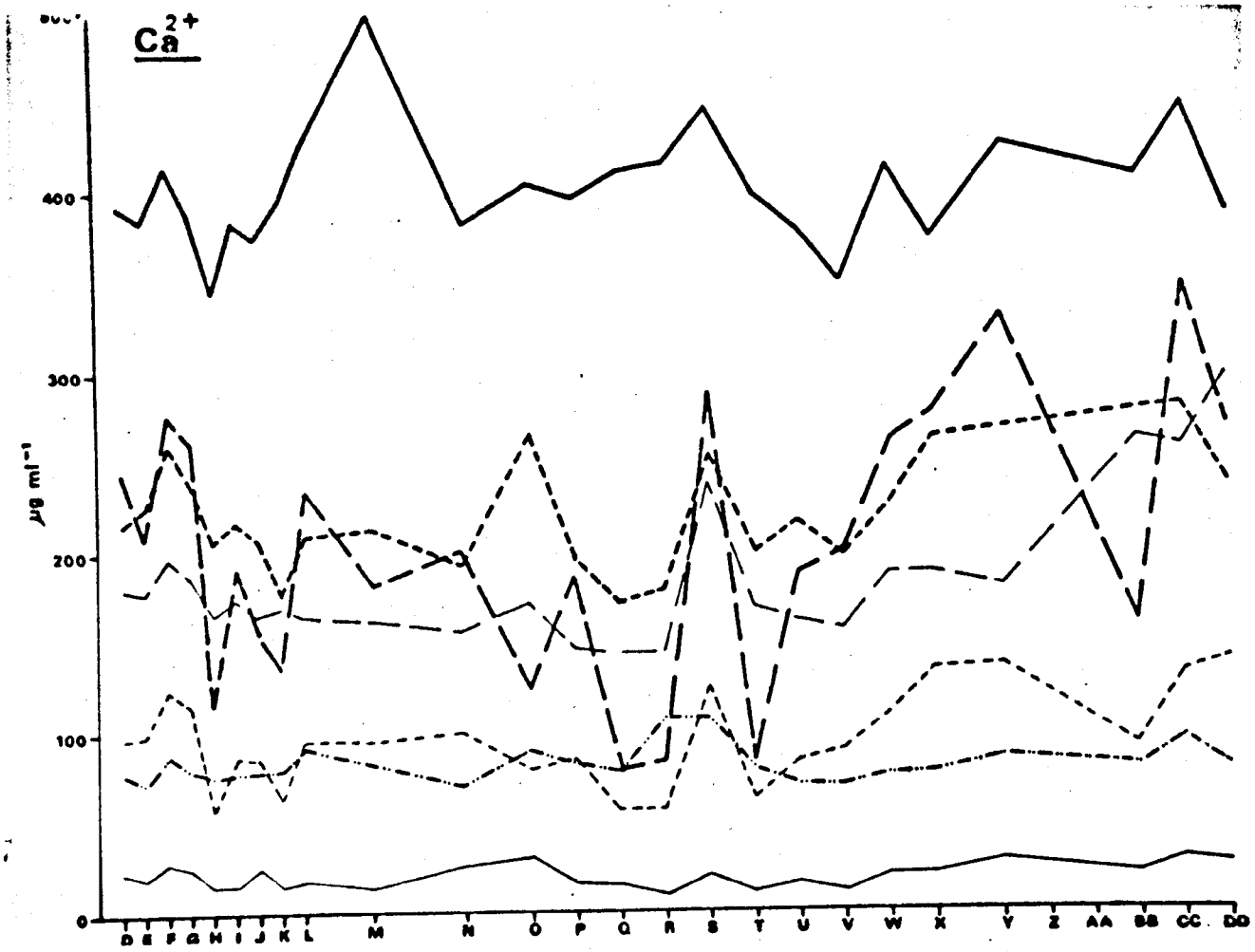
Ca^{2+}
400
300
200
100
0
µg ml⁻¹
D E F G H I J K L M N O P Q R S T U V W X Y Z AA BB CC DD

FIGURE 14: Variations in magnesium content of stream waters.

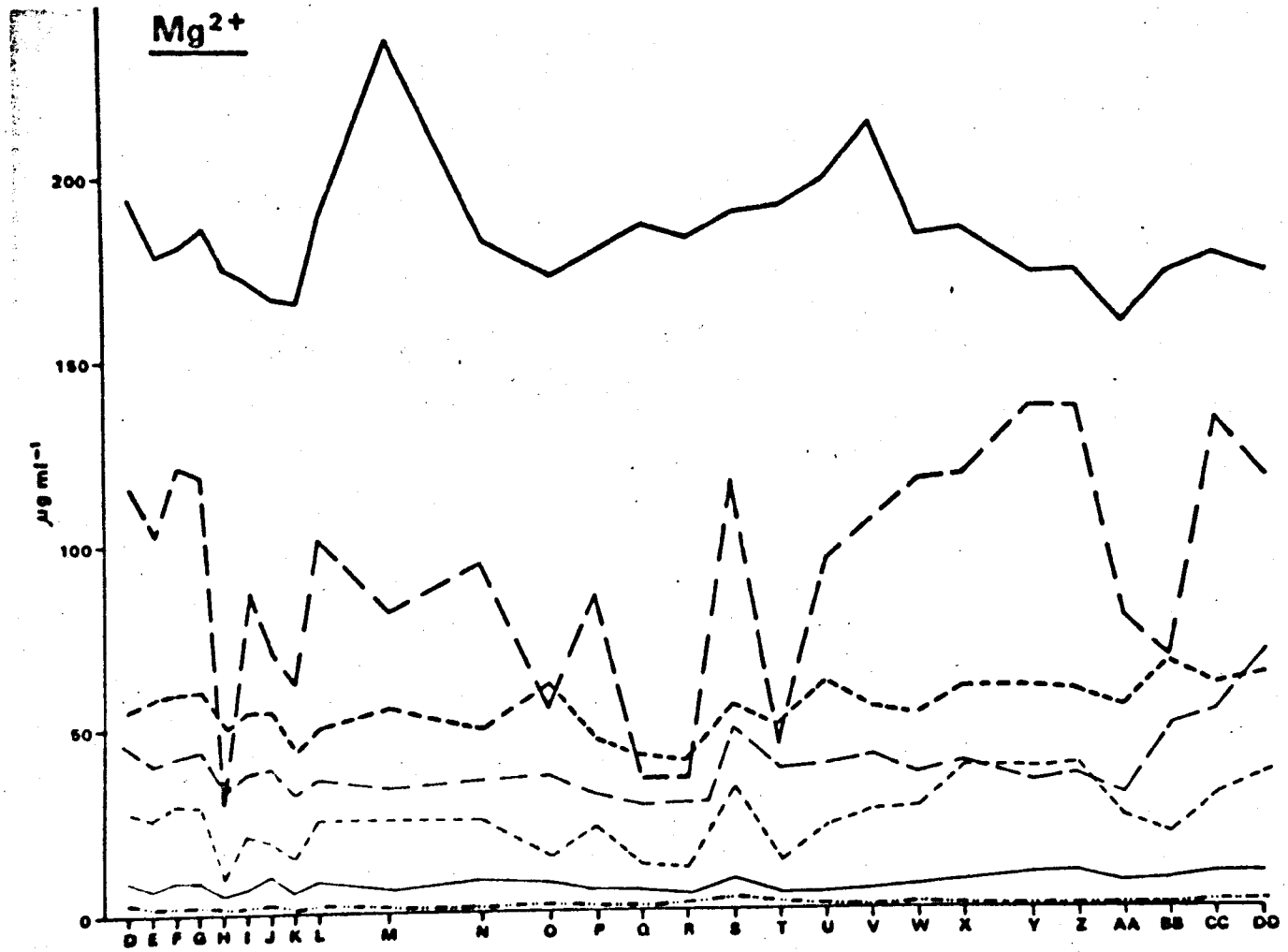
Mg2+
200
150
100
50
0
µg ml-1
D E F G H I J K L M N O P Q R S T U V W X Y Z AA BB CC DD

FIGURE 15: Variations in sodium content of stream waters.

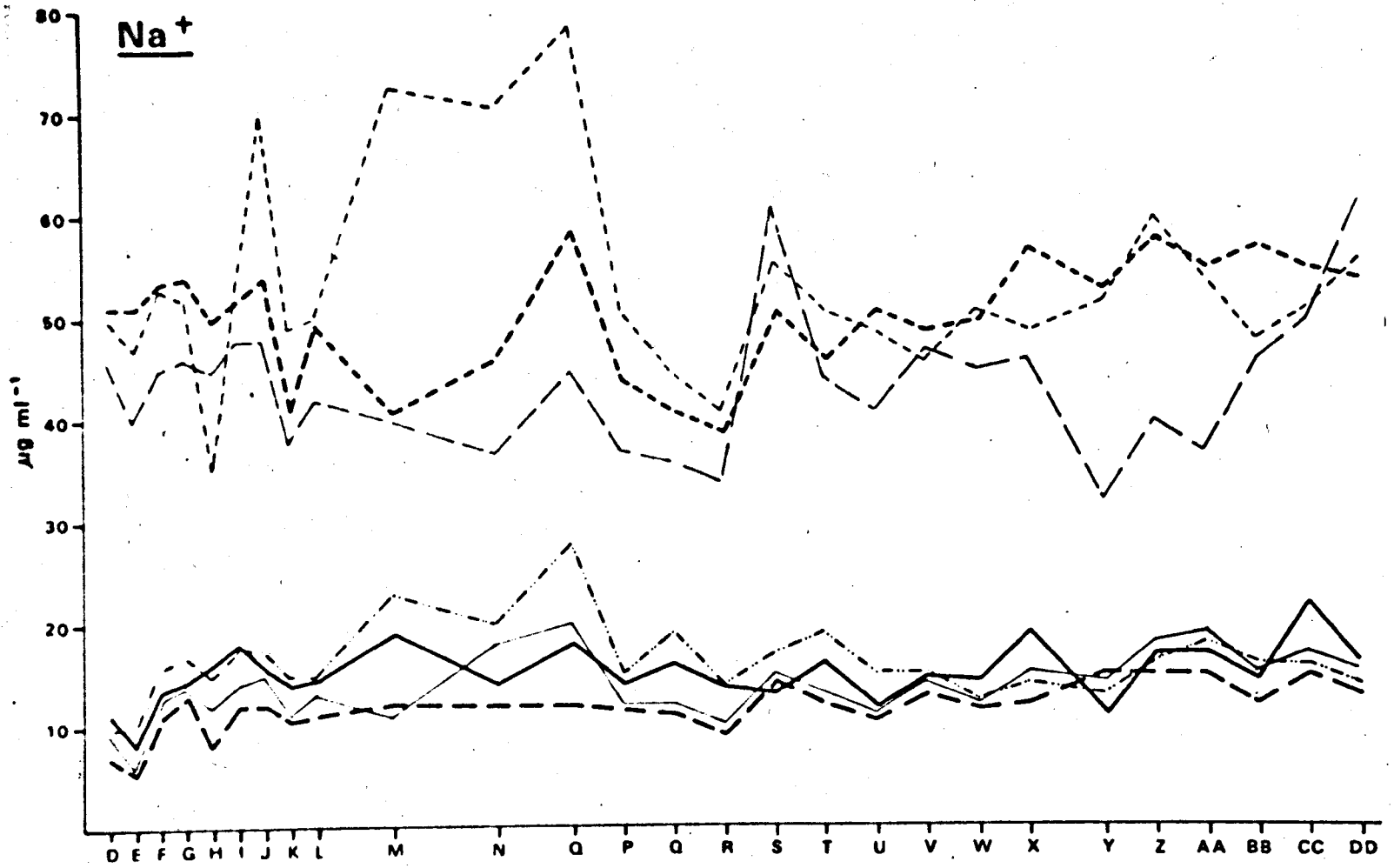
Na+
80
70
60
50
40
30
20
10
µg ml-1
D E F G H I J K L M N O P Q R S T U V W X Y Z AA BB CC DD

FIGURE 16: Variations in potassium content of stream waters.

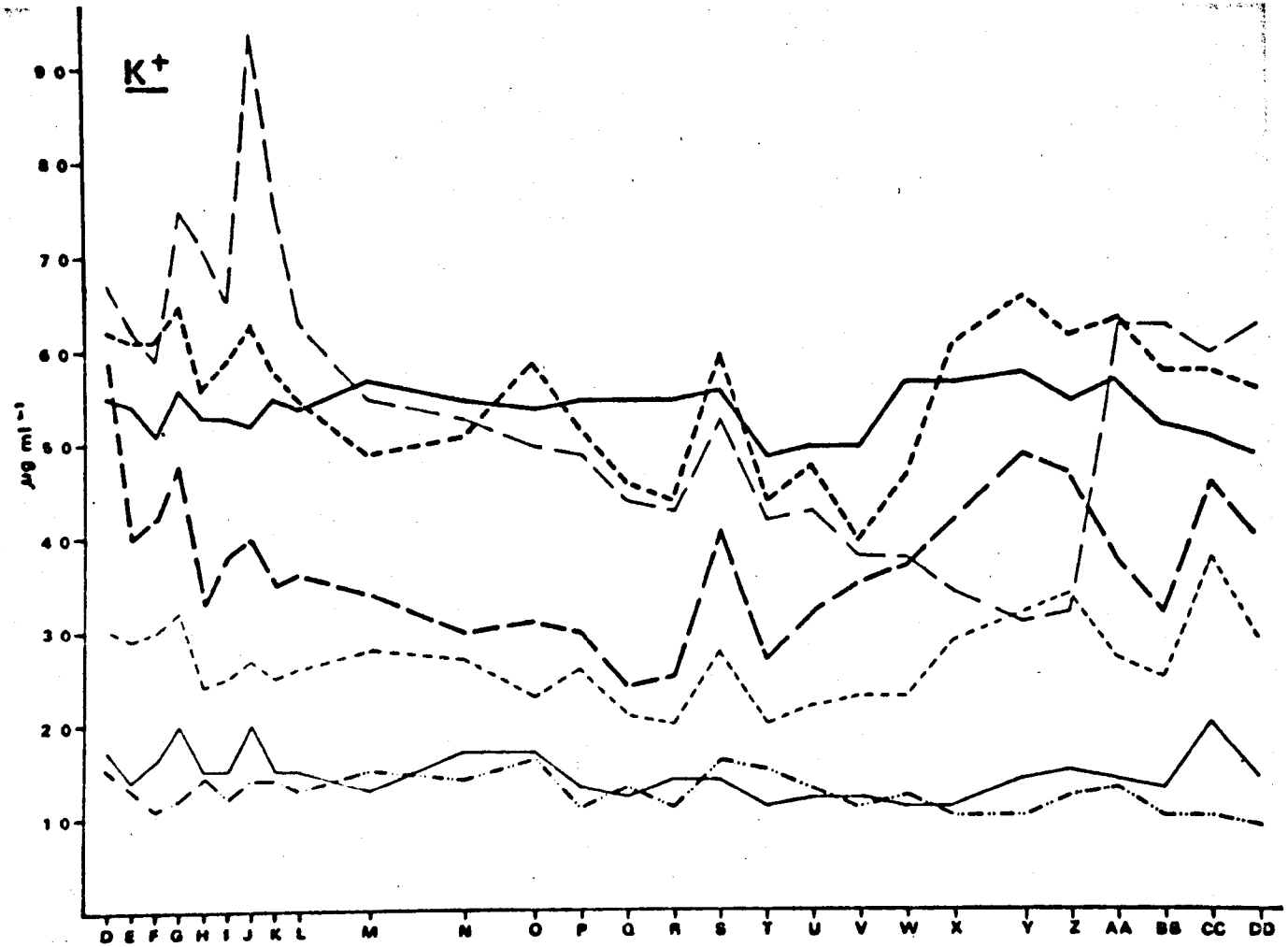
K+
90
80
70
60
50
40
30
20
10
µg ml⁻¹
D E F G H I J K L M N O P Q R S T U V W X Y Z AA BB CC DD

FIGURE 17: Variation in total iron content of stream waters.

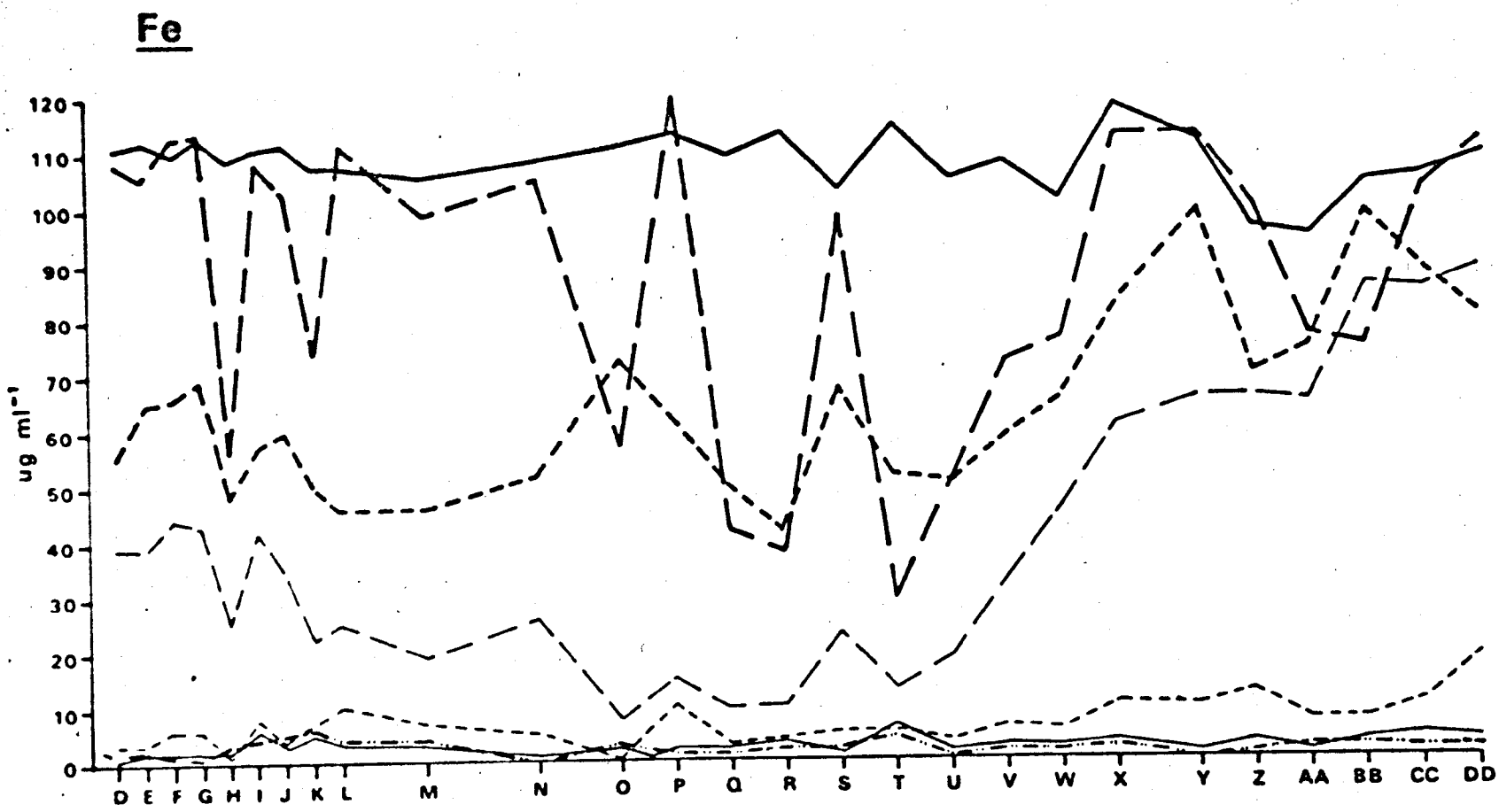
Fe
ug ml⁻¹
120
110
100
90
80
70
60
50
40
30
20
10
0
D E F G H I J K L M N O P Q R S T U V W X Y Z AA BB CC DD

FIGURE 18: Variations in chloride content of stream waters.

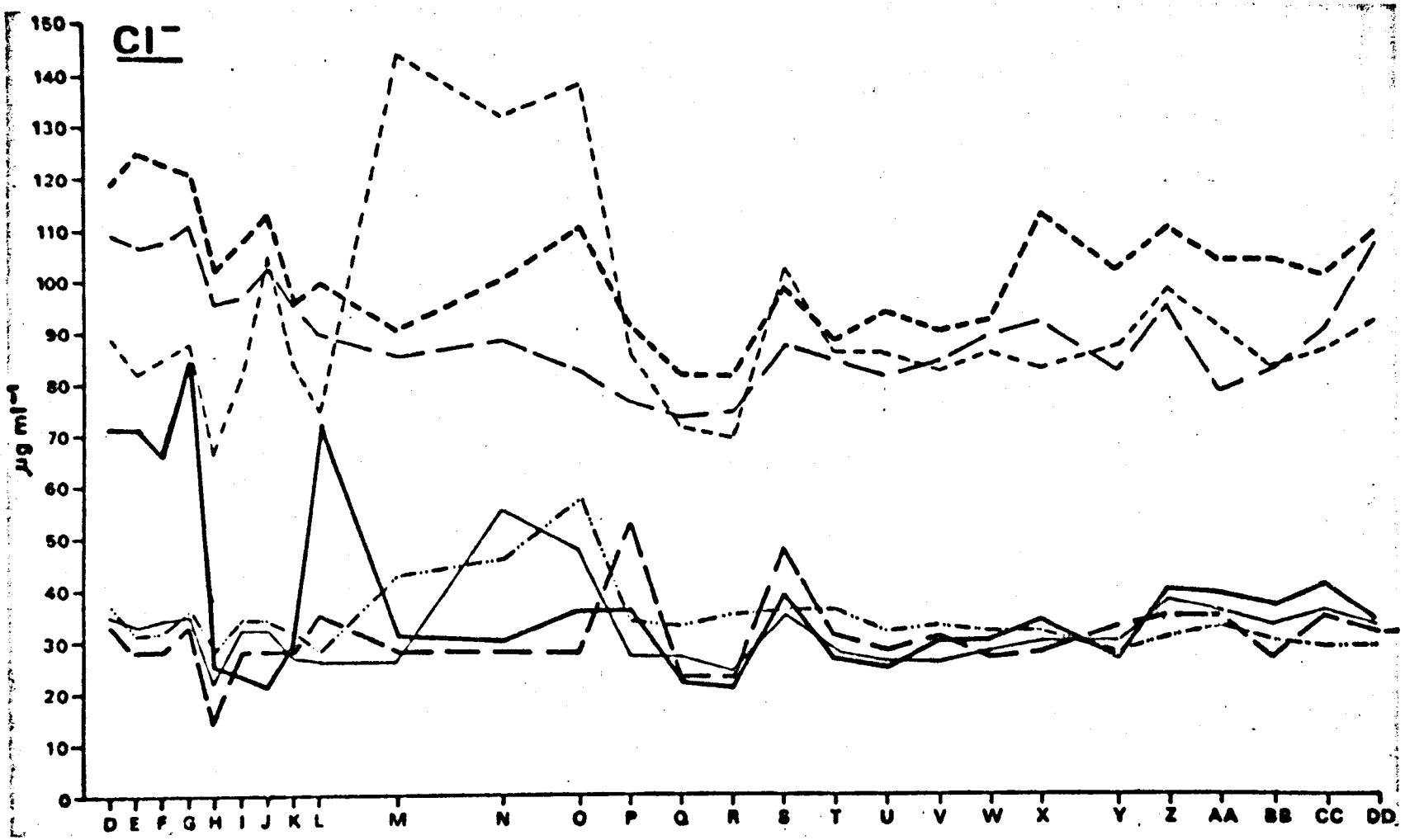
Cl⁻
150
140
130
120
110
100
90
80
70
60
50
40
30
20
10
0
mg/l
D E F G H I J K L M N O P Q R S T U V W X Y Z AA BB CC DD

FIGURE 19: Variations in sulphate content of stream waters.

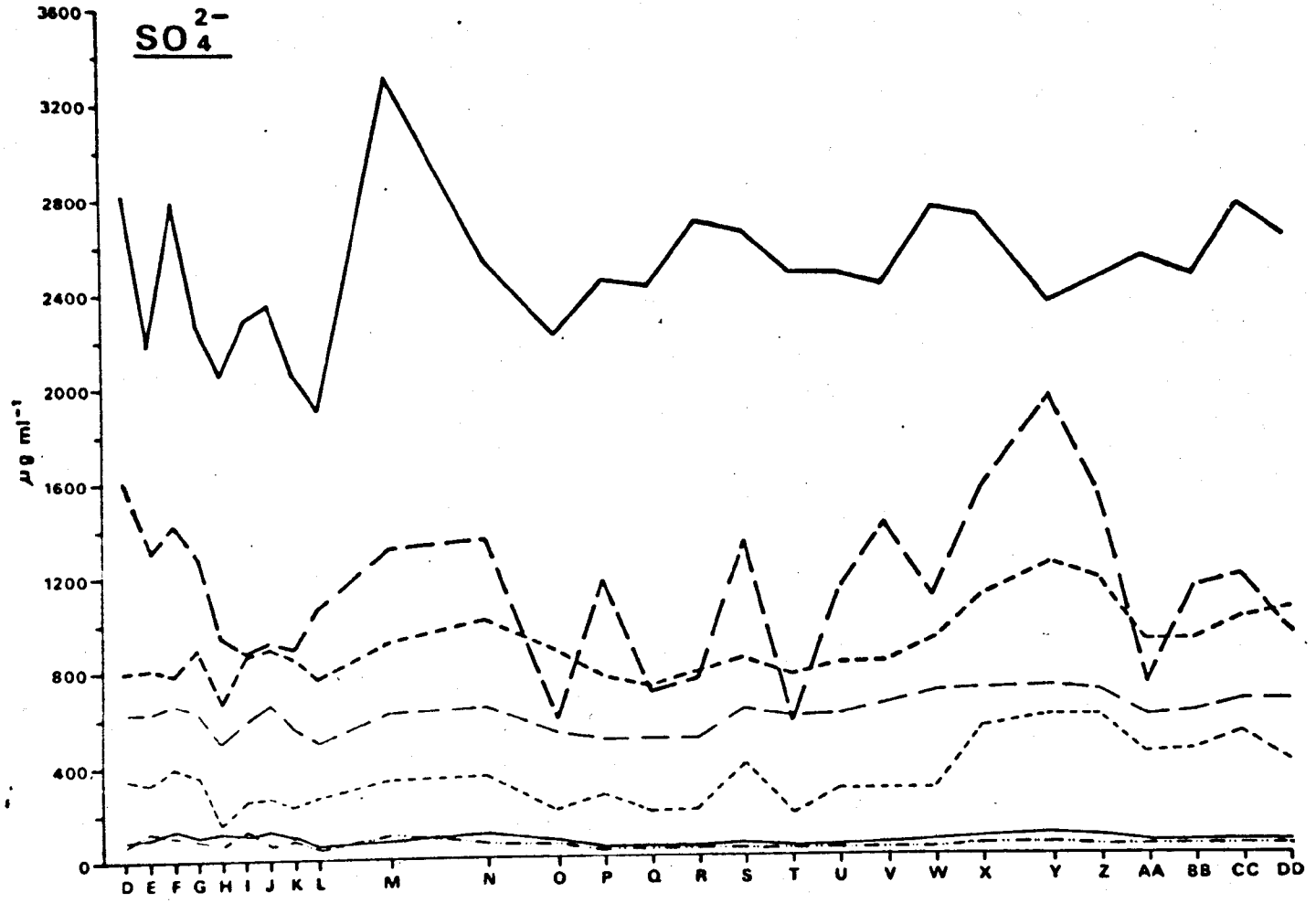
SO_4^{2-}
3600
3200
2800
2400
2000
1600
1200
800
400
0
µg ml⁻¹
D E F G H I J K L M N O P Q R S T U V W X Y Z AA BB CC DD

drops in solute content occur when precipitation is high (e.g. H, K, AA).

Temperature variations throughout the year are considerable (Figure 10). The only exceptions, as noted previously, being 'Groups' 4 and 7 (Sites 101, and 7, respectively). The remarkable consistency of the latter is clearly evident. So too is the clustering of pH values around 3.0-3.5 in Figure 11, which suggest that a natural buffering system is operating on certain waters (see Section 8.3).

5.3 Charge Balance

In any ionic solution the overall net charge must be zero. This is to say that the positive charge contributed by the cations must be exactly balanced by a negative anion charge. The charge attributable to any single ion can be calculated by dividing the amount of that ion present by its atomic or molecular weight and then multiplying by the valency. For example, the charge contributed by 100 µg calcium (Ca^{2+}) is given by:

$$\frac{100}{40.08} \cdot (+2) = +4.99\mu E \qquad (\mu E = \text{microequivalent})$$

and that by 100 µg sulphate (SO_4^{2-}) by

$$\frac{100}{96.06} \cdot (-2) = -2.08\mu E$$

In this study the quantitites of five cations (Ca^{2+}, Mg^{2+}, Na^{2+}, K^{+} and total Fe) and two anions (Cl^{-} and SO_4^{2-}) were determined each week. A charge balance can be calculated for every water sample based onthese seven variables. H^{+} is present in such small amounts, even in pH 3.0 waters, that its contribution to the balance will be very slight and is omitted here. It is assumed for the purpose of these calculations that any iron present is in the ferrous (Fe^{2+}) form.

TABLE 9: Charge Balances Calculated for Group Averaged Data (all values in microequivalents)

Week	Group						
	1	2	3	4	5	6	7
D	-0.310	0.032	-0.413	2.113	-0.323	-8.308	-20.554
E	0.012	-0.779	-1.093	1.714	0.340	-5.044	-8.906
F	0.743	0.243	-0.798	2.440	2.848	-1.987	-19.867
G	0.781	0.444	-0.378	2.054	-0.446	-0.293	-9.901
H	-0.072	0.956	-1.077	2.349	1.520	-9.486	-7.076
I	1.295	0.618	-0.714	1.908	-1.490	2.425	-12.585
J	0.776	-1.544	-0.365	2.646	-2.426	-1.985	-12.363
K	-0.473	-0.604	-0.832	2.330	-4.251	-4.287	-5.692
L	1.945	1.076	0.228	3.773	-0.235	1.593	0.001
M	-0.758	-1.884	-0.684	2.425	-3.006	-8.243	-20.617
N	-0.588	-2.376	-0.893	1.796	-5.990	-6.708	-14.728
O	0.740	0.783	0.412	2.959	2.352	0.207	-7.839
P	0.894	-0.417	0.279	3.233	-0.696	-4.456	-12.232
Q	0.070	-0.984	0.149	3.178	-1.650	-6.243	-10.291
R	-0.422	-1.054	-0.297	4.535	-3.018	-7.371	-15.973
S	0.603	4.548	0.319	4.947	1.787	-0.718	-15.837
T	0.548	-0.441	0.106	3.551	-0.357	-3.431	-11.637
U	0.043	-0.869	0.012	2.748	0.372	-4.569	-12.415
V	-1.127	-1.193	-0.048	2.600	-0.972	-8.441	-16.350
W	-0.117	-2.128	0.101	2.918	-1.454	2.746	-17.792
X	-1.041	-0.237	0.187	3.153	-2.373	-4.351	-18.077
Y	-2.047	-1.328	0.412	3.465	-4.280	-8.744	-9.108
Z	-	-	-	-	-	-	-
AA	-	-	-	-	-	-	-
BB	-2.779	7.708*	0.401	3.378	6.751=	-7.421	-12.810
CC	-1.283	6.745*	0.689	4.150	1.211=	-7.511	-16.424
DD	0.318	10.348*	0.836	3.224	-2.164=	-7.216	-16.901
Mean	-0.090	-0.325	-0.127	2.943	-1.079	-4.395	-13.040
Mean Sum Cations	8.786	15.476	2.351	4.920	19.841	21.236	38.561
Mean Sum Anions	8.444	15.555	3.059	2.725	20.369	24.856	50.679

- Calcium values missing, balance not calculated

* Site No. 4 dried up

= Site No.3a dried up

} Values excluded from mean calculations

Table 9 shows the values of $\Sigma cation\ charge$ minus $\Sigma anion\ charge$ as calculated for the group data. The calculations were made using a 'Commodore PET' mini-computerusing a program written for the purpose in BASIC language.

Group 1 waters show only a very slight deviation from the actual charge balance of 0.00. The mean value of -0.09 μE is only 1% of the total cation or anion charge. This value is considerably better than that quoted by Rainwater and Thatcher (1960). In their experiments, using only very dilute solutions (T.D.S. = 30 μg ml^{-1}) the best charge balance they could obtain was ± 5%.

Groups 2, 3 and 5 also show a good balance, 2%, 5% and 5% respectively. The charges do not balance, however, for the remaining three groups. The waters of Group 4 show an apparent excess positive charge which is probably balanced by additional anions not included in the analyses. Indeed it was noted during the course of pilot study (p. 40) that HCO_3^- ions were present in these karst waters (this also accounts for deviations in the T.D.S.-CONDUCTIVITY curve shown in Figure 7).

In contrast, a large excess negative charge is the characteristic feature of Groups 6 and 7. This is partly explained by the fact that iron was assumed to be in the ferrous form. It is known that some also exists as trivalent ferric iron (p. 44) and this would increase the positive charge if taken into account in the calculations. Another trivalent ion known to be present in the waters of Groups 6 and 7 is Al^{3+} and again calculations would be improved by its inclusion.

Thus it appears that the calculation of charge balance serves as a useful 'check' on the analyses. If the inbalance is constantly to one side (positive or negative) for any given stream then the analysis of that water is probably incomplete or is in error. It would seem that the use of only seven ions in this study is sufficient for all but three of the sites, and in these cases the 'missing' ions are known.

TABLE 10: A Quantitative Mixing Model for Group 6 Waters

	(A) $\bar{x}$ Group 3	(B) $\bar{x}$ Group 7	(C) $\bar{x}$ Group 6	(D) (A + B) ÷ 2	(E) C∿D	(F) % Error $(\frac{E}{D} \times \frac{100}{1})$
Ca^{2+}	20	404	204	212	8	4
Mg^{2+}	7	185	92	96	4	4
Na^{+}	14	14	11	14	3	27
K^{+}	1.4	5.4	3.8	3.4	0.4	10
Fe	2.6	109	88	56	32	36
Cl^{-}	32	42	31	37	6	20
SO_4^{2-}	73	2486	1141	1279	138	12

All values in $\mu g\ ml^{-1}$

Many other ions will be present in the waters sampled and all will contribute to the charge balance (unless species with zero charge occur). The additional quantitites of ions and charges will be small, however, in comparison to the ten or so major ions considered here.

5.4 Origin of Drainage Waters

5.4.1 Deep and Surface Components

As noted in Section 5.2, the various groups of waters show different responses to variations in precipitation. Following the model of Johnson et al. (1969), it would appear that if the water emerging at any particular site shows a strong dilution after rainfall then the water at that site is derived partly from deep flow and partly from surface runoff supplied by the rainfall event. In this study the waters of Groups, 1,2,5 and 6 can be thought of as originating in this way. The deep flow component comprises waters which have reacted with the rocks within the landslide to give their characteristic chemical composition. Differences in responses and overall water quality between these four groups reflect different proportions of deep to surface flow.

A quantitative mixing model can be derived by trial and error if it is assumed that simple proportions of deep and surface water mix at any given site and provided analyses of the two components are available. At Site 11 (Group 6), on Figure 5, water from Site 7 (Group 7) and Site 8 (Group 3) meet and mix. The chemical compositions at all three are known, and Table 10 shows the results of a simple theoretical mixing of equal volumes of Group 3 (surface)and Group 7(deep) waters.

Yearly average data are used at all times. The percentage differences between the theoretically 'mixed' waters and the true composition of Group 6 are quite small considering the simplistic approach adopted. Sodium and chloride values are in error presumably due to unknown supplies from road

salt. Also iron may be involved in precipitation and re-solution between Sites 7 and 11. 'Mixing' these waters in different proportions (60:40, 20:40 etc.) produces worse results than the simple 50:50 mix discussed here.

There appears to be no dilution of the deep flow component by surface runoff in the case of Group 7 waters. This results in the lack of response to precipitation and temperature changes and consistently high solute concentrations noted in Section 4.4

One interesting feature of Site 7 is that the flow rate does not appear to fluctuate from week to week. At all the other sampling sites variations in discharge could be observed, albeit subjectively, throughout the period of study. For the reasons outlined in Section 1.3, it was not possible to regularly monitor discharge from the Mam Tor streams. Since Site 7 appears to be so distinctive, however, it was decided that discharge measurements by the rather laborious technique of 'diluting gauging' should be made, if not at all the sites, then at least here.

The very low solute content of the Group 3 waters results from them being almost totally derived from surface runoff, with no deep flow component. Any reactions taking place here involve relatively unmodified precipitation and soil minerals/organics.

The control waters of Group 4 are chemically very distinct from any other group. Their chemical composition is entirely due to reactions involving carbonates as they pass through the limestone. These waters and reactions in which they are involved are not central to the arguments to be put forward in this study and need not be considered further.

Figure 20 summarises the likely mode of derivation of each of the seven groups.

FIGURE 20: Flow diagram showing the derivation of the seven groups of waters.

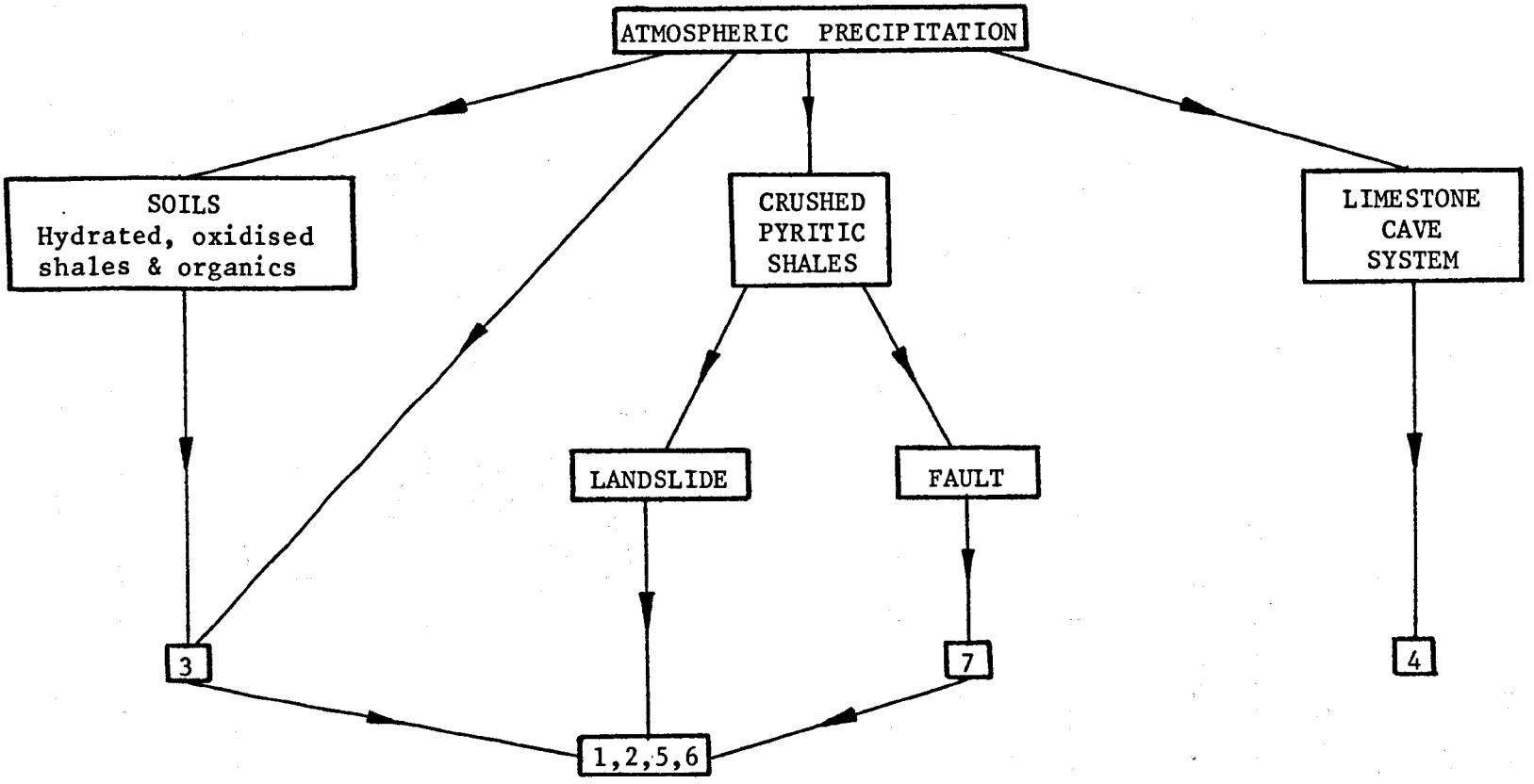
ATMOSPHERIC PRECIPITATION
SOILS
Hydrated, oxidised
shales & organics
CRUSHED
PYRITIC
SHALES
LIMESTONE
CAVE
SYSTEM
LANDSLIDE
FAULT
3
7
4
1,2,5,6

5.4.2 Dilution Gauging

Dilution gauging is most easily carried out using a constant rate injection method (see B.S.I., 1964). The principle of this technique is that if a chemical tracer solution is added to a stream at a constant rate then an increase in concentration of the solution's constituents in the streamwater will eventually become apparent at a downstream sampling point. For a given tracer solution the increase in concentration will be inversely proportional to streamdischarge. It has to be assumed that the tracer solution mixes completely with the streamwater, and hence a sampling point located a considerable distance downstream from the injection point is desirable. If complete mixing is achieved a constant, raised level of concentration is observed downstream and this 'plateau' is maintained as long as the upstream injection continues. The discharge of the stream is calculated in the following way:

$$Qs = Qt \cdot \frac{Ct - Cds}{Cds - Cus} \qquad (6)$$

where:

Qs = stream discharge
Qt = tracer discharge
} ($1\ sec^{-1}$)

Ct = tracer concentration ($mg\ l^{-1}$)

Cds = streamwater concentration at sampling point ($mg\ l^{-1}$)

Cus = streamwater concentration above injection point ($mg\ l^{-1}$)

The tracer solution used in this case was NaCl and a constant rate of injection was achieved using a Mariotte Bottle. This simply is a constant head device of about 20 litre capacity shown in diagrammatic form by Figure 21c. Sodium chloride was chosen as the tracer because the concentration of Na^+ and Cl^- ions in solution at Site 7 are low and certainly very much less than in the saturated NaCl solution in the Mariotte Bottle.

FIGURE 21: The principles of dilution gauging.
See text for explanation.

a)

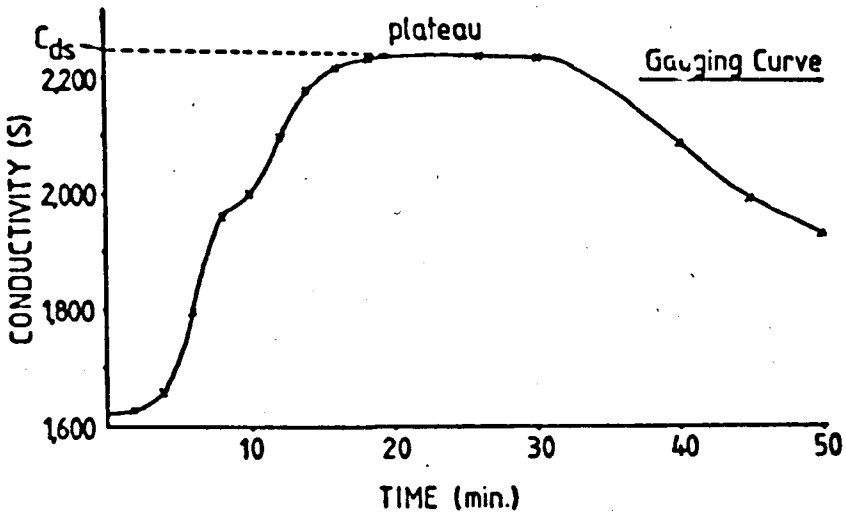

b)

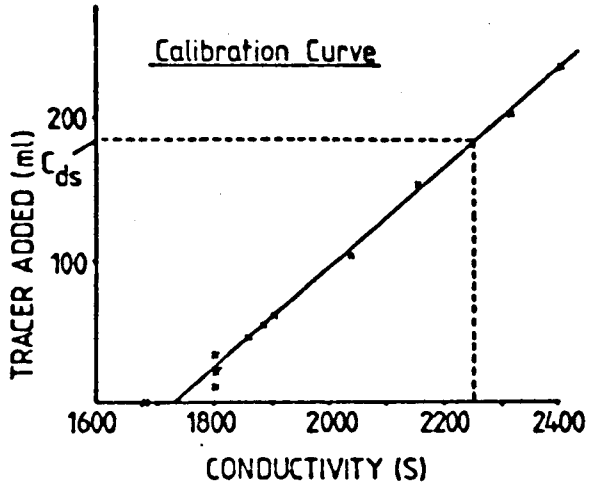

c)

Mariotte Bottle

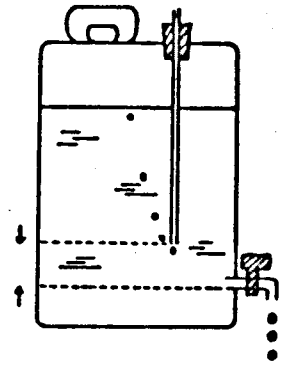

C_t = 760g NaCl in 20l
= 38000 mg l^{-1}

Q_t = 2l in 8min
= 0.004 l s^{-1}

C_{ds} = 2250 S = 185 ml tracer
= 7030 mg in 20l
= 350 mg l^{-1}

Thus Cus → zero and Ct is also much greater than Cds. Equation 6 can, therefore, be conveniently reduced to:

$$Qs = \frac{Qt.Ct}{Cds} \qquad (7)$$

Qt can be preset by opening the tap to give a convenient flow rate and calculated simply by timing the filling of a beaker of known volume. Ct is known from the mixing of the original solution. Cds is most accurately measured by titration of streamwater samples taken during the 'plateau' phase but a more suitable field method is to estimate Cds from simple conductivity measurements made at the downstream sampling point using the field apparatus described in Section 4.3.

This is done by firstly preparing a calibration curve of conductivity against concentration by adding successive volumes of tracer solution (say 10 ml) to a large, known volume of streamwater. The conductivity of the mixture is recorded after each addition. Once the calibration curve is constructed the tracer concentration in streamwater can be found by measuring only conductivity at the sampling point (see Figure 21b).

A conductivity meter was, therefore, placed on the stream bank approximately 30 m downstream from the injection point with the electrodes immersed in the streamwater. Readings were taken every two minutes and the resulting graph is shown in Figure 21a.

The discharge at Site 7 was calculated from Equation 7, as follows:

$$Qs = \frac{Qt.Ct}{Cds} \qquad (7)$$

$$= \frac{0.004 \times 38000}{350}$$

$$= 0.43 \text{ l sec}^{-1}$$

The discharge at Site 7 was, in fact, measured on two separate occasions. The first, for which the above data are given, was on 1st November, 1979, when it was noted that the other streams and seepages were flowing at well below their usual rates. The second occasion followed a week of almost continual light rain, and on 20th December, 1979, a discharge of 0.44 l sec^{-1} was recorded.

Although only two quantitative measurements were made they do attest to the constancy of flow at this particular site under different climatic conditions. When visiting the site regularly for a period of twelve months differences in flow rate from week to week can be recognised. As noted in Section 1.3.1 qualitative information regarding changes in discharge at each site was entered into a field notebook. The only notes recorded at Site 7 read 'no change' and it is believed that the flow rate of approximately 0.4 l sec^{-1} is maintained virtually constantly throughout the year.

5.4.3 Additional Inputs

The constant flow rate discussed in the preceding Section poses an interesting problem regarding the origin of the Site 7 waters. A discharge of 0.4 l sec^{-1} is not very great but would certainly require a catchment area greater than that present to maintain it throughout the year. The maximum reasonable area which might contribute water to this site is the ground above and including the retrogressive units. This immediate catchment has a maximum area of 6,400 m^2 as measured from the air photo (Plate 12). Total rainfall received during the period of study was 1,137 mm, giving a volume of water supplied to this area of approximately 7.28×10^6 l.

A stream flowing at 0.43 l sec^{-1}, however, removes some 13.37×10^6 litres in a year. Therefore, an additional 6.09×10^6 litres (46% of the total discharge) must be supplied from elsewhere. It must be remembered

that this figure is a maximum since it is assumed that all the water falling within this catchment (which is also probably an over-estimate of the actual contributing area) arrives at Site 7. From considerations of the geology and topography of the retrogressive units this seems highly unlikely. The dip of the beds into the main scarp face would tend to channel water away from the site, and evaporation losses from such an area of bare, often fragmented, shale must be large. Also it is unlikely that all the water held in the area of the retrogressive units should emerge at only this one site. Indeed after heavy rainfall water has been observed to seep out of the shales and move in the direction of an ephemeral stream which flows between Sites 8 and 11 (Figure 5).

A larger catchment area than that of 6,400 m^2 quoted here for Site 7 seems unlikely. Above the retrogressive units surface water would naturally be channelled northwards, due to thegradient, on to the main unit. Any deep water present here would be carried westwards and northwards, down-dip, away from Site 7. Similarly the dip of the beds off the landslide area to the southwest is in the 'wrong' direction (c. 5^{o} northwest), and surface water in this region can be seen on the air photo to be flowing in gullies and shallow seepages parallel with the south flank of the landslide towards the Odin Sitch.

The most feasible alternative to a larger catchment area is that over 6 million litre of water annually are supplied by groundwater recharge. One feature, clearly visible as a distinct break of slope on the air photo, and also marked on Figure 5, which might channel such groundwater towards the retrogressive units is the fault running along Rushup Edge in a west-southwest-east-northeast direction.

Such a fault, which here cuts through the uppermost horizons of the Edale Shales, would normally be associated with an area of highly fragmented or brecciated rock - the fault crush zone - which acts like a 'sponge',

attracting groundwater largely by capillary forces. The groundwater could thus be drawn from a considerable area, and might possibly upwell from great depths (the vertical extent and throw of the fault are not known) into the fault crush prior to emergence at Site 7.

Since the eastern end of the fault is so closely associated with the retrogressive units it might even be related to the initiation of movement of this area after the main unit had itself slipped. This could have occurred by re-activation of the fault during recent geologic times or, more likely, the structural weakening of the rocks by its presence.

If the groundwater is uprising from depth towards Site 7 in this way it may account for the elevated and constant temperatures which have been observed (Section 5.1.2). A long residence time deep underground, where the geothermal gradient is higher, is easily envisaged. Alternatively, the observed temperature and chemical anomalies at Site 7 might be due to exothermic reactions taking place between groundwater and minerals of the fault crush. Such reactions are considered in detail in the following Section.

6. DEVELOPMENT OF A WEATHERING MODEL

In the previous two Sections, the results of chemical analyses of the water samples were discussed and the extreme composition of spring 7 was noted. It is intended in this Section to account for the proportions of ions in the Site 7 water by reference to reactions taking place at depth, possibly within a fault crush zone, between percolating ground waters and solid mineral phases.

By considering each major ion in turn, starting with the most abundant, sulphate, the most likely reactions responsible for their liberation can be put together in sequence and quantitative values ascribed at each stage.

In order to do this it is assumed that all the sulphate generated in the first reaction remains in solution and does not participate in further mineral transformations prior to emergence at Site 7. This assumption will be qualified towards the end of the Section before considering some of the wider implications of the model.

6.1 Weathering Reactions

6.1.1 Pyrite Oxidation

Since many of the streams draining the Mam Tor landslide precipitate ochre and gypsum, the waters must be highly concentrated in iron, sulphate and calcium. A possible source of the former two components is the oxidation of pyrite by percolating waters charged with dissolved oxygen. Since the Edale Shales, which comprise the bulk of the landslip material, are known to contain abundant pyrite and the mass as a whole is highly fractured by landslide movement (Section 2.2.1) the contact between such waters and minerals is inevitable.

There is considerable disagreement, judging from published work, as to the actual mechanism of pyrite oxidation, which is most frequently

written as:

$$2FeS_2 + 4H_2O + 7\tfrac{1}{2}O_2 = Fe_2O_3 + 4SO_4^{2-} + 8H^+ \quad (8)$$

In an early paper by Winmill (1915) this equation is given as:

$$2FeS_2 + 7O_2 + 2H_2O = 2H_2SO_4 + 2FeSO_4 \quad (9)$$

or

$$4FeS_2 + 15O_2 + 2H_2O = 2Fe_2(SO_4)_3 + 2H_2SO_4 \quad (10)$$

depending on whether ferrous or ferric sulphate is formed.

The true mechanism of pyrite oxidation is probably far more complex than these reactions suggest. Banerjee (1971) describes thermoanalytical techniques of investigating the various steps involved and intermediate products formed. Much of this work, however, is conducted at high temperature and such experiments are clearly of little consequence in weathering studies. An earlier article by Mapstone (1954) describes the reaction as taking place by several steps even at low temperatures. Although some of these steps seem a little unlikely the sequence of five reactions does account for virtually all the possible direct products of oxidation. The sequence is written by Mapstone as follows:

1. Oxygen is absorbed on pyrite surfaces, liberating sulphur dioxide in the presence of moisture:

$$FeS_2 + O_2 \rightarrow FeS + SO_2 \quad (11)$$

2. The reactive ferrous sulphide is directly oxidised to sulphate:

$$FeS + 2O_2 \rightarrow FeSO_4 \quad (12)$$

3. The sulphur dioxide of step 1 is oxidised to sulphuric acid:

$$2SO_4 + O_2 + 2H_2O \rightarrow 2H_2SO_4 \quad (13)$$

4. The interaction of ferrous sulphide with the acid liberates hydrogen sulphide:

$$FeS + H_2SO_4 \rightarrow FeSO_4 + H_2S \quad (14)$$

5. Interaction of this with the sulphur dioxide gives free sulphur:

$$2H_2S + SO_2 \rightarrow 3S + 2H_2O \qquad (15)$$

Saksela (1952) and Nambu (1957) suggest alternative mechanisms for the reaction, neither of which entirely agree with other literature. Steger and Desjardins (1978) also note that: "Previous studies on weathered pyrite ... do not show a consensus on either the products or nature of the oxidation".

In an attempt to settle the dispute these authors oxidise three sulphide minerals - pyrite, chalcopyrite and pyrrhotite - in a constant temperature/humidity chamber at 52°C and 68% RH (conditions which do not entirely represent those of most weathering situations). They note that: "The major difficulty encountered in the study of the oxidation of sulphide minerals at temperatures less than 100°C is the identification of the small amounts of products formed during reasonable periods of time".

Steger and Desjardins found that (in their experiments) the oxidation of pyrite proceeds to give the metal sulphate as the predominant product. Some metal thiosulphate which also forms is later oxidised to sulphate:

$$2FeS_2 + 3O_2 \rightarrow 2FeS_2O_3 \qquad (16)$$

or

$$2FeS_2 + 3O_2 \rightarrow 2FeSO_3 + 2S^o \text{ (or } SO_2 \uparrow) \qquad (17)$$

In most natural situations where pyrite is being oxidised, however, water is present and the chief product then is an acid iron sulphate solution. Garrels and Thompson (1960), therefore, quote the reaction as:

$$FeS_2 + 8H_2O + 14Fe^{3+} \rightarrow 15Fe^{2+} + 2SO_4^{2-} + 16H^+ \qquad (18)$$

Although in their weathering experiments Garrels and Thompson use solutions of extreme acidity (pH 0-2) it does seem likely, where ferric iron is present in solution, that this mechanism will predominate over direct oxidation by atmospheric oxygen.

Despite this lack of agreement as to the detailed mechanism of pyrite oxidation the final products are reasonably well known. Much of the work on sulphide mineral weathering has been conducted in the mining districts of Colorado, in North America. Here pyrite, in close association with copper sulphide, is ubiquitous throughout most geologic formations, occurring as disseminated grains, in veins, and as large discrete crystals in rocks which otherwise show no effects of hydrothermal alteration (Harrer and Tesch, 1959). Much of this pyrite is presumably of diagenetic origin. Here in a temperate region with moderate annual rainfall totals, the chief minerals formed as a result of rock weathering are 'limonite' and geothite.

Hanshaw (1974) describes the geochemical evolution of a geothite deposit in Colorado formed where waters percolating through the pyritic rocks emerge in springs and seepages very similar to those at Mam Tor. Hanshaw states that the de-oxygenated waters, on emergence, first form 'limonite' according to the reaction:

$$2Fe^{2+} + \tfrac{1}{2}O_2 + 5H_2O \rightarrow 2Fe(OH)_3 + 4H^+ \qquad (19)$$

This 'limonite' then dehydrates with time to form the oxyhydroxide geothite:

$$Fe(OH)_3 \rightarrow HFeO_2 + H_2O \qquad (20)$$

Most of the oxidation reactions cited above have one product in common - acidity. This is represented by either large quantities of hydrogen ions (Garrels and Thompson, Equation 18) or a combination of these and sulphate ions, sulphuric acid (Winmill, Equation 9 and 10).

As stated previously, much of the work on this subject has been conducted in mining areas. Whether these be sulphide mineral mining or coal

mining areas (pyritic rocks are commonly found in association with coal seams) a common descriptive term is now applied to the water produced. It is simply known as 'acid mine drainage'. A vast body of literature has emerged on this topic since Winmill's (1915) time, particularly from such mining areas as the Appalachian region of the USA where the problem is particularly acute and considerable environmental pollution has resulted.

A discussion of the consequences and possible controls of acid mine drainage is contained in Section 6.2. It is sufficient to note here that such waters have a very similar chemical composition to those draining the Mam Tor landslide and that pyritic source rocks appear to be common to both situations.

6.1.2 Carbonate Dissolution

Ca^{2+} ions may be supplied to the Mam Tor waters by the weathering of diagenetic carbonates (described in Section 2.2.1) which occur in close association with pyrite in the Edale Shales.

The simplest and most frequently quoted carbonate dissolution reaction is given by:

$$CaCO_3 + H_2CO_3 = Ca^{2+} + 2HCO_3^- \qquad (21)$$

where carbonic acid, formed by the solution of atmospheric CO_2 in rainwater, attacks limestone (calcite) to produce Ca^{2+} and more stable bicarbonate ions.

The Mam Tor carbonates are commonly composed of dolomite or ankerite, minerals which are less soluble in carbonic acid (Krauskopf, 1967, page 109). In a more concentrated acid solution - such as acid mine drainage - the dissolution of dolomite can be represented by:

$$Ca_{1.1}Mg_{0.9}(CO_3)_2 + 4H^+ = 1.1Ca^{2+} + 0.9Mg^{2+} + 2H_2O + 2CO_2\uparrow \qquad (22)$$

This reaction yields Ca^{2+} and Mg^{2+} ions in roughly the correct proportions, as found in the Mam Tor waters. Streams draining the limestone area to the south have ratios at least fifty times greater than this (see Appendices Biv and Bv) although the actual quantitites of ions are much smaller.

It should be pointed out that the above formula for dolomite represents an ideal composition. The actual proportions of calcium and magnesium can vary considerably; many sedimentary dolomites contain far more calcium. Iron substitution for magnesium is also common and where Fe > Mg the mineral is known as *ankerite* (Read, 1970, page 277).

Since the exact proportions of Ca, Mg and Fe are not known for the Edale Shale dolomites an ideal formula is used.

6.1.3 Clay Mineral Transformation

The only additional major mineral constitutents of the Edale Shales, assuming the gypsum and iron oxides are weathering products and not primary components, are clay minerals.

Cation exchange is the main mechanism of metal-ion release in clay mineral weathering and the exchange of hydrogen ions in, for example, an illite to kaolinite transformation, can be represented by:

$$K_2Al_4\left[Si_2Al_2O_{20}\right](OH)_4 + 2H^+ + 3H_2O$$
$$= 3Al_2Si_2O_5(OH)_4 + 2K^+ \qquad (23)$$

where an ideal muscovite formula is used. This is not true'exchange' since the process is irreversible, but nevertheless potassium ions are released into solution; these constitute yet another component of the Mam Tor waters (Appendix Bvii).

Kaolinite is invariably the stable end-product of silicate weathering (as examplified by the formation of china clay deposits after the weathering

of Cornish granites). In extremely acid solutions, however, kaolinite itself may be dissolved according to the reaction:

$$Al_2Si_2O_5(OH)_4 + 6H^+ = 2Al^{3+} + 2Si(OH)_4 + H_2O \quad (24)$$

this in turn consumes more H^+ ions and liberates Al^{3+}. Minor amounts of other cations, including Ca^{2+}, Mg^{2+}, Fe^{2+} and Na^+, may also be released during such clay mineral transformations.

Na^+ and Cl^- ions are not considered in this model since the greatest proportion is supplied by road salt (Section 4.4.2).

6.1.4 A Quantitative Weathering Model

The net result of pyrite oxidation, irrespective of the various possible mechanistic steps, can be summarised by the two end-member reactions:

$$2FeS_2 + 14(O) + 2H_2O = 2Fe^{2+} + 4SO_4^{2-} + 4H^+ \quad (25)$$

$$2FeS_2 + 15(O) + H_2O = 2Fe^{3+} + 4SO_4^{2-} + 2H^+ \quad (26)$$

depending on the degree of oxidation. Since most of the iron in the Mam Tor waters is in the ferric form, the second equation is probably more useful. If it is assumed that one product of this reaction remains in solution and does not participate in further chemical reactions prior to emergence in the springs and seepages quantitative values can be assigned to the various reactants and products based on the molar quantities present.

In reaction 26, SO_4^{2-} is most likely to remain in solution as a simple ion. Therefore if the quantity of sulphate is determined the amount of pyrite destroyed per litre of water can be calculated.

Waters emerging at Site 7 are least affected by mixing and dilution (Section 5.4). Therefore, the sulphate content of these waters is probably most indicative of the reactions taking place at depth. The mean annual

SO_4^{2-} concentration at Site 7 is 2486 μg ml^{-1} or 25.880 mM l^{-1} (the annual mean value, calculated from Appendix Bxi).

Thus if some 26 mM l^{-1} SO_4^{2-} are produced in Equation 26, then $\frac{26}{2}$ mM l^{-1} pyrite must be consumed (since 2 moles sulphate are produced for every mole of pyrite).

$$\frac{26}{2} \text{ mM pyrite} = \frac{26}{2} \times (\text{molecular weight of pyrite}) \text{ μg ml}^{-1}$$

$$= 13 \times 119.97$$

$$= 1559.6 \text{ μg ml}^{-1}$$

$$= \underline{1.5596 \text{ g l}^{-1}}$$

Thus some 1.5 g pyrite are destroyed by every litre of water in liberating 2.486 g sulphate. Similar calculations show that, in addition, 0.7260 g Fe^{3+} and 0.0131 g H^+ are produced.

If all the iron in solution in the Site 7 water is assumed to be in the ferric form (for the purpose of these calculations), then the average concentration, from Appendix Bviii, is 0.109 g l^{-1}. This is considerably less than the amount produced by pyrite oxidation. Therefore, it is postulated that some of this iron (0.617 g l^{-1}) must be precipitated prior to emergence as either 'limonite' or goethite according to the reactions:

$$2Fe^{3+} + 6H_2O = Fe_2O_3 \cdot 3H_2O + 6H^+ \quad (27)$$

or

$$2Fe^{3+} + \tfrac{1}{2}O_2 + 5H_2O = 2HFeO_2 + 2H_2O + 4H^+ \quad (28)$$

If 'limonite' is precipitated according to the first equation 1.1804 g hydroxide are precipitated and 3.34×10^{-2} g H^+ are liberated. According to the second equation some 0.9816 g goethite would precipitate and 2.23×10^{-2} g H^+ would be liberated.

Such calculations balance the ferric ions but precipitation of ochre in this way liberates further hydrogen ions, making the waters even more acid. If the amounts of H^+ ions present at this stage are summed the following observations are noted:

Quantity of H^+ ions from pyrite oxidation = 1.31×10^{-2} g l^{-1}

Quantity of H^+ ions from ochre precipitation = 3.34×10^{-2} g l^{-1}

Total = 4.65×10^{-2} g l^{-1}

This concentration represents a pH value of 1.33. The mean pH of the Site 7 waters however, is only 3.49 which corresponds to a H^+ concentration of 3.2×10^{-4} g l^{-1}.

Therefore, over 99% of the acidity generated by pyrite oxidation and ochre precipitation must be consumed in further mineral reactions before these waters emerge at the surface.

Clay mineral transformations of the type discussed in Section 6.1.3 (Equations 23 and 24) would consume some 2×10^{-4} and 9.7×10^{-3} g H^+, respectively, and produce a solution 0.2 mM with respect to K^+ and 3.2 mM with respect to Al^{3+}. These values, corresponding to solution concentrations of 7.8 µg ml^{-1} K^+ and 86 µg ml^{-1} Al^{3+}, agree closely with the observed mean concentrations of 5.4 and 77 µg ml^{-1} (Appendices Bvii and Bix).

An excess of hydrogen ions (0.0366 g) still remains. The acid decomposition of dolomite, as discussed in Section 6.1.2 (Equation 22) could account for this discrepancy. 3.66×10^{-2} g H^+ would destroy 1.688 g dolomite, yielding 0.4002 g Ca^{2+} and 0.1986 g Mg^{2+} (9.98 and 8.17 mM, respectively). Once again these values agree well with measured concentrations at Site 7 of 0.404 g l^{-1} Ca^{2+} and 0.185 m l^{-1} Mg (Appendices Biv and Bv).

It would appear, therefore, that a very simple weathering model based on only five or six reactions and the water analyses described in Section

FIGURE 22: Sequence of chemical reactions affecting the composition of water at Site 7. Figures at the bottom indicate calculated and, in parenthesis, observed concentrations of ions in g l^{-1}. Values with an asterisk are those used in calculations.

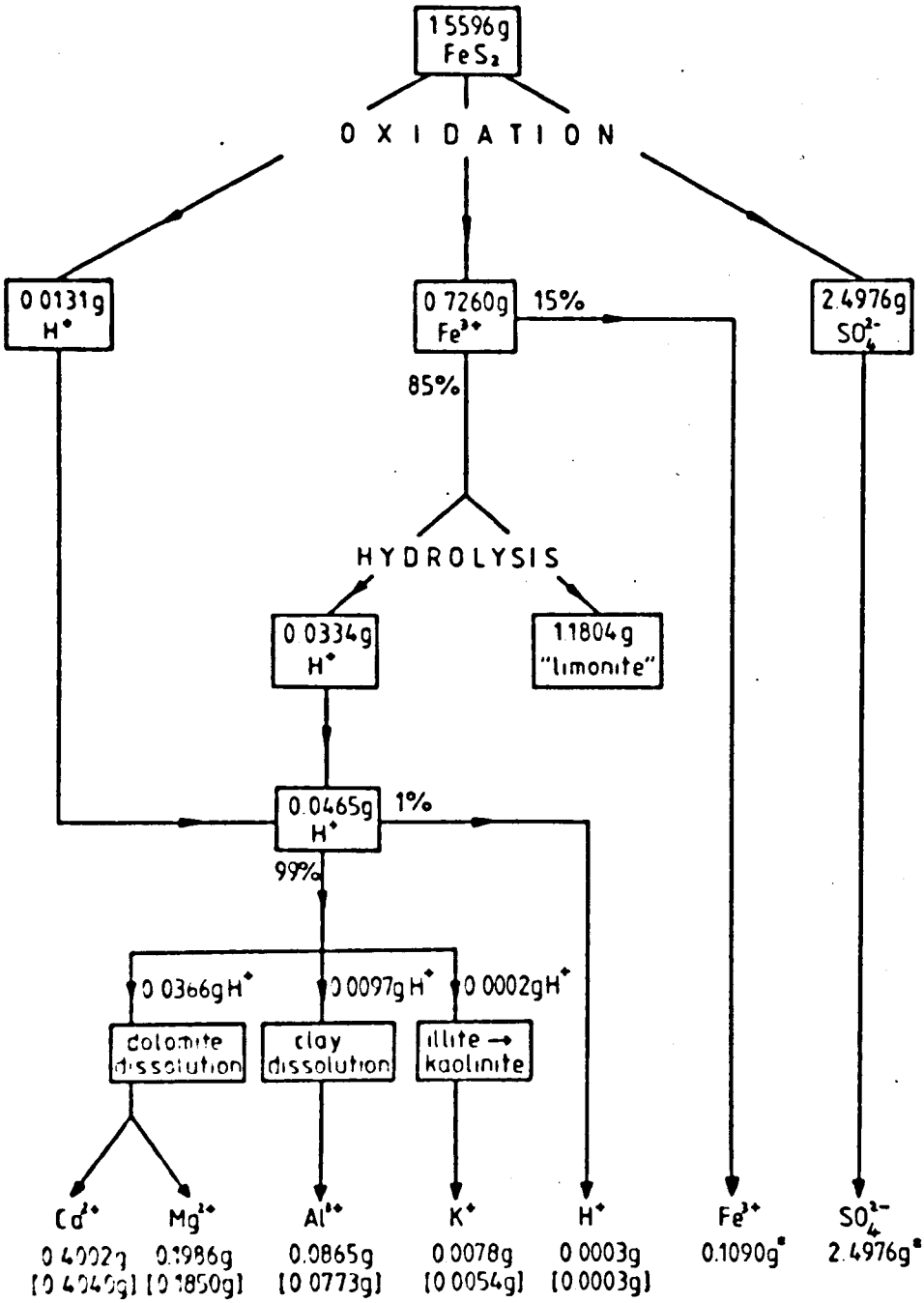
1.5596g FeS2
OXIDATION
0.0131g H+
0.7260g Fe3+
15%
2.4976g SO4 2-
85%
HYDROLYSIS
0.0334g H+
1.1804g "limonite"
0.0465g H+
1%
99%
0.0366g H+
0.0097g H+
0.0002g H+
dolomite dissolution
clay dissolution
illite → kaolinite
Ca2+
Mg2+
Al3+
K+
H+
Fe3+
SO4 2-
0.4002g [0.4040g]
0.1986g [0.1850g]
0.0865g [0.0773g]
0.0078g [0.0054g]
0.0003g [0.0003g]
0.1090g*
2.4976g*

4 can account for the observed water quality at this site. Figure 22 summarises the various steps involved.

It is interesting to note that if a flow rate of 0.43 l sec^{-1} is maintained throughout the year at Site 7 (Section 5.4) and each litre of water has oxidised 1.56 g pyrite, then some 21 tonnes of pyrite are consumed per annum. Similarly, 23 tonnes of carbonate are destroyed and 13 tonnes of goethite are precipitated.

6.1.5 The Sulphate Problem

The results of mineralogical analyses are not considered until Section 7.3 but it must be mentioned at this stage that the sulphate minerals gypsum ($CaSO_4.2H_2O$) and jarosite ($KFe_3(SO_4)_2(OH)_6$) are found in samples of shale from Mam Tor. The former is only found in surface outcrops of Edale Shale but jarosite often occurs at considerable depth within the landslide. The significance of this deep jarosite formation is that the process consumes sulphate ions which would otherwise remain in solution. Since SO_4^{2-} concentration of the Site 7 waters was the basis for all calculations in the preceding Section, the quantitites of minerals given in Figure 22 must be *under-estimates* and more than 21 tonnes of pyrite must be consumed annually.

Since some K^+ is also consumed in this reaction more must be leached from the clays in the first place. This may, in fact, account for the discrepancy between the observed and calculated values of K^+ in Figure 22.

If some iron and sulphate is used up in jarosite formation the components of Equation 26 can be divided, in molar terms, as follows. The equation must first be multiplied by a factor of 6 in order to produce the 24 millimoles (approximately) per litre of SO_4^{2-} in the Site 7 water:

$$12FeS_2 + 90(0) + 6H_2O = 12Fe^{3+} + 12H^+ + 24SO_4^{2-} \qquad (29)$$

This is the scale of the reaction necessary for the original weathering model. More pyrite must be oxidised, however, in order to form jarosite. This can be represented, schematically by:

$$14FeS_2 + 105(O) + 7H_2O = 14H^+ + 14Fe^{3+} + 28SO_4^{2-} \qquad (30)$$

$$\begin{array}{ccccc} 8 & & 6 & 4 & 24 \\ 8FeOOH & & 2KFe_3(SO_4)_2(OH)_6 & & 24SO_4^{2-} \\ \text{(goethite)} & & \text{(jarosite)} & & \text{(stream)} \end{array}$$

Thus, 15% more pyrite is oxidised and 15% more iron precipitated. Approximately 60% of this iron is in the form of goethite and 40% is precipitated as jarosite.

6.2 Wider Implications of the Weathering Model

6.2.1 Catalysts

Curtis (1976) notes that the 'activation energy' of a reaction is closely related to reaction rate. If a reaction can proceed via more than one mechanism (which, from the discussion in Section 6.1.1, certainly seems possible for pyrite oxidation) there will be several possible 'activation energies'.

According to Curtis "catalysts induce acceleration of reactions by providing an alternative reaction mechanism with lower 'activation energy'".

There is considerable debate in the literature of both microbiology and water resources concerning the role of chemosynthetic autotrophic bacteria as catalysts in sulphide oxidation (see Lau, et al. 1970). Such organisms, by definition, are able to build up their body substance from carbon dioxide and certain salts using chemical energy obtained by oxidising inorganic materials.

Quispel et al. (1952), were among the first to suggest that the autotroph responsible for pyrite oxidation is *Thiobaccillus thiooxidans*. Leathen et al. (1956), however, point out that this organism does not completely oxidise pure pyrite, and they suggest an alternative species, *Ferrobacillus ferrooxidans*, which apparently does, via the intermediate production of ferric iron. It is nowadays considered that Leathen's bacterium is really a variant of the species *Thiobacillus ferrooxidans* which was first 'discovered' by Temple and Colmer (1951).

Numerous studies suggest that bacteria may be more important in oxidising pyrite than oxygen. One proviso, however, would seem to be that the pyrite is of small particle size (Temple and Delchamps, 1953) as is the case when the mineral is disseminated throughout argillaceous rocks. Leathen et al. (op.cit.) for example, found that the large concentrations of ferrous iron (c. 200 mg l^{-1}) present in some mine drainage waters was completely oxidised by a culture of *T. ferrooxidans* in three days whereas the chemical oxidation of a sterile solution by atmospheric oxygen alone took more than two years.

Similarly Colmer and Hinkle (1947), before *Thiobacilli* had been positively identified as responsible, treated acid mine drainage with anticeptics and found a discrepancy in oxidation rates between the treated samples and controls. Bryner and Jamerson (1958) have even demonstrated a technique for the commercial extraction of metals from low grade pyrite ores using these bacteria.

Bloomfield (1972a) in considering the role of iron-oxidising bacteria in the formation of acid sulphate soils, describes an experiment whereby Alum Shale is oxidised in the laboratory. He finds that significantly more pyrite is oxidised in the shale when *Thiobacilli* are present and notes that the maximum pH at which these organisms can survive is 3.5 to 4.0

According to Kuznetsov et al. (1963) the growth of *T. ferrooxidans* cultures ceases above pH 4.5 and the optimum conditions lie between pH 2.0 and 4.0. They state that "Because of its ability to live under conditions of high acidity, *Thiobacillus ferrooxidans* can withstand the large concentrations of sulphuric acid that it forms as a result of metabolism" (see also Lazaroff, 1963).

Kuznetsov et al. also note that the fracturing of pyritic rocks produces favourable conditions for the development of micro-organisms by promoting the access of water and by creating larger surface areas for them to act upon. Nowhere do pyritic rocks become so fractured - except perhaps, within a landslide - as in mine workings, where bacterial oxidation can still proceed deep underground even though the supply of oxygen may be severely limited (Singer and Stumm, 1970).

6.2.2 Acid Mine Drainage

6.2.2.1 Formation

The number of publications concerned with acid mine drainage has increased dramatically over the last thirty years apparently in proportion with those on microbiological oxidation.

Colmer and Hinkle (op.cit.) were among the first to suggest that acid mine drainage is produced by the action of micro-organisms on sulphide minerals. During the 1950's, as further work on *Thiobacilli* was progressing, many more researchers saw the connection (see for example Temple and Delchamps, 1953; Ashmead, 1955). In the 1960's most of this research was conducted in the coal mining areas of North America (Barnes, et al. 1964) where in the Appalachian region alone some 6,000 miles ofstreams are polluted by mine drainage (Appalachian Regional Commission, 1969). More recently attention has focused on the more localised but more intense problems in areas of sulphide mineral extraction (Hanshaw, 1974; Potter, 1976; Wentz, 1974).

In a study of extremely toxic discharge from a lead/zinc mine in Idaho (see Table 11, sample 1) Trexler et al. (1975) note that in addition to high acidity and sulphate concentrations, aluminium, cadmium, copper, iron, lead and zinc are also present in undesirable quantitites. The problem of pollution on such a scale has become so acute in recent years that several attempts have been made at producing computer packages which can predict the volume and quality of acid mine drainage likely to be produced in any given situation (Ricca and Chow, 1974; Rae, 1977). Caruccio et al. (1976) even use depositional palaeoenvironments as a predictor of acid mine drainage characteristics.

Deep mines frequently discharge acid drainage into deep groundwaters and so cause little surface pollution. After centuries of mining, however, the vast accumulations of spoil above ground are now themselves a threat. Indeed some of the worst cases of acid mine drainage pollution are the result of leaching strip-mine overburden materials (Whaley et al. 1977; Anderson and Youngstrom, 1976).

6.2.2.2 Abatement

In a work concerned with the biochemical ecology of water pollution, Dugan (1972) devotes a chapter (Chapter 11) to the role of bacteria in controlling the rate of acid mine drainage production. This chapter ends with a discussion of various means of treatment and abatement of acid mine drainage. (The interested reader is also referred to a publication by the Ohio State University, 1971).

Dugan suggests that the use of heterotrophic anaerobic bacteria of the *Desulfovibrio* type might reduce the vast amounts of toxic sulphate generated in acid mine drainage. Their technique appears to work well in laboratory experiments but the development of anaerobic conditions and the supply of organic nutrients, necessary to provide the micro-organisms with

the energy and carbon they require, on a scale great enough to deal with most natural situations would be difficult to achieve.

Bloomfield (1972a) studies the possibilities of an alternative method of treatment. In experiments which lasted five months he examines the effects of adding lime to acid sulphate soils in order to raise the pH and, therefore, prevent the growth of iron-oxidising bacteria. He finds that the quantities of iron and sulphate in waters draining the soils are reduced slightly with the addition of a quantity of $CaCO_3$ equivalent to 14 tonnes per hectare, although the pH only rises by 0.4 units.

Hill (1974) examines the use of both lime and limestone to treat acid mine drainage in order to reduce acidity, remove heavy metals (which are less soluble at high pH) and lower the concentrations of ferrous iron and sulphate ions. He notes that in 1973 alone over 41,000 tonnes of lime were used in this way (Gutschick, 1974). Hill quotes the reactions involved in lime treatment as:

$$Ca(OH)_2 + H_2SO_4 \rightarrow CaSO_4 + 2H_2O \qquad (31)$$

$$Ca(OH)_2 + FeSO_4 \rightarrow Fe(OH)_2 + CaSO_4 \qquad (32)$$

or $$4Ca(OH)_2 + 4FeSO_4 + 2H_2O + O_2 \rightarrow 4Fe(OH)_3 + 4CaSO_4 \qquad (33)$$

depending on whether sulphuric acid or ferrous sulphate are the reactants and ferrous or ferric hydroxide the products.

Limestone treatment takes place according to the following reactions, again depending on the reactants involved:

$$CaCO_3 + H_2SO_4 \rightarrow CaSO_4 + H_2O + CO_2 \qquad (34)$$

or $$3CaCO_3 + Fe_2(SO_4)_3 + 3H_2O \rightarrow 3CaSO_4 + 2Fe(OH)_3 + 3CO_2 \qquad (35)$$

Most industrial treatment plants prefer the use of lime to limestone for the following reasons:

TABLE 11: Comparison of Five Acid Mine Drainage Waters

Sample	pH*	Ca^{2+}	Mg^{2+}	Na^{+}	Fe^{t}	Al^{3+}	Cl^{-}	SO_4^{2-}	Conductivity*
(1)	2.0	-	856	-	14000	228	-	-	45000
(2)	-	488	469	2480	39	-	2285	3066	-
(3)	-	260	49	13	143	12	-	1650	-
(4)	2.6	36	26	0.8	27	19	-	950	1274
(7)	3.5	404	185	14	109	77	42	2486	2332

(1) Bunker Hill Mine, Idaho; Trexler et al. (1975)

(2) River Dearne, South Yorkshire; Rae (1978)

(3) Victor Mine, Missouri; Hem (1970), after Emmons (1917)

(4) Babb Creek, Pennsylvania; Crouse and Rose (1976)

(7) Mam Tor, Site 7. Yearly mean value

+All values in $\mu g\ ml^{-1}$ except: pH(-log H^{+} activity), conductivity($\mu S\ cm^{-1}$)

(1) The carbon dioxide produced in equations 34 and 35 buffers the reaction and it is difficult to raise the pH sufficiently.

(2) Limestone is ineffective if the water has a high ferrous iron content.

(3) The size, characteristics and method of application of the limestone are critical.

(4) The treatment plant is more complex than for lime treatment.

Several different commercial schemes for limestone treatment are described in Hill and Wilmoth (1971).

Whichever method of treatment is used the 'neutralisation' of acid mine drainage has several shortcomings. For example the hardness of the water may be increased, the sulphate and iron content can still remain unacceptably high and vast quantities of waste sludge (mainly gypsum) are produced and must be safely disposed of. Hill (op.cit.) concludes that a split treatment of mine drainage by both lime and limestone may be the most cost-effective method, and suggests the use of limestone for reducing toxicity in surface spoil heaps (see also Deul, 1974).

6.2.3 Comparison with Mam Tor Drainage Waters

Table 11 shows that waters grouped together under the all-embracing term 'acid mine drainage' can in fact show considerable variation in quality. The water of analysis (1) is clearly exceptionally rich in total iron, a fact reflected by the conductivity value, while that of (2) is extremely saline. Features common to all such drainage waters are a low pH and high metal and sulphate concentrations.

It is interesting to note that the mean values given for Site 7 fall somewhere in between these two extreme samples and the other two waters included in the table.

It seems perfectly justified, therefore, to consider the Mam Tor waters as being a 'natural' example of acid mine drainage. This is the result of fracturing of rocks by landslide movement, rather than by mining activity, and the subsequent involvement of micro-organisms in the process of pyrite oxidation. It is likely that the production of acid sulphate waters in this way has been continuous since landslide initiation and as such the time-scale involved is perhaps an order of magnitude greater than for true mine drainage of similar composition.

Since the waters draining Mam Tor are not used for public supply and pose no threat to wildlife or fish stocks, there is no need for remedial measures, such as those discussed above, to be taken. It is an interesting academic point, however, to consider how such abatement could be achieved.

The use of sulphur-reducing bacteria as described by Dugan (op.cit.) would be precluded for the reasons given on page 75 . Limestone treatment would, presumably, also prove ineffective since the waters encounter carbonate material in any case on their passage through the Edale Shales and through road-fill; many hundreds of tons of limestone ballast have been used and subsequently scattered over a wide area during 180 years of road maintenance.

The most effective way of ameleorating this acid drainage would seem to be by natural processes which do not require man's intervention. Natural beneficiation of acid mine drainage has been discussed at length by Biesecker and George (1966) and Lovell and Lachman (1970). It has been noted that simple dilution as the acid streamsmix with larger, less concentrated, bodies of water cannot explain the observed fall in concentration of certain ions. Interactions between the acid waters and stream sediments (Crouse and Rose, 1976) and the effects of non-acid streams containing significant bicarbonate (Barnes and Romberger, 1968) are probably responsible. Chemically active stream sediments and karst waters are both present at and

TABLE 12: Species List for Selected Water Sampling Sites

	Higher Plants	Bryophytes and Mosses	Algae
SITE 2	*Carex nigra* *Deschampsia flexuosa* *Eriophorum angustifolium* *Holcus mollis* *Juncus acutiflorus* *Molinia caerulea* *Phragmites communis*	*Drepanocladus fluitans* *Sphagnum recurrum* *Sphagnum subsecundum*	*Euglena mutabilis* *Zygogonium* sp.
SITE 3	*Deschampsia flexuosa* *Eriophorum angustifolium* *Juncus actiflorus* *Phragmites communis* *Potentilla erecta*	*Drepanocladus fluitans* *Sphagnum recurrum*	*Euglena mutablis* *Zygogonium* sp.
SITE 6	*Agrostis tenuis* *Dactylis glomerata* *Deschampsia cespitosa* *Equisetum palustre* *Holcus mollis* *Juncus acutiflorus*		*Euglena mutabilis* *Zygogonium* sp.
SITE 7	*Agrostis tenuis* *Carex nigra* *Deschampsia flexuosa* *Juncus effusus*	*Drepanocladus fluitans* *Polytrichum commune*	*Chlamydomonas applanta,* var. *Acidophila* *Euglena mutablis* *Hormidium* sp. *Mougeotia* sp
SITE 8	*Agrostis camina* *Agrostis stolonifera* *Agrostic tenuis* *Anthozanthum odoratum* *Cardamine pratensis* *Cerastium holosteoides* *Cirsium palustre* *Deschampsia flexuosa* *Epilobium palustre* *Equisetum palustre* *Festuca ovina* *Galium palustre* *Galium saxatile* *Holcus mollis* *Juncus effusus* *Luzula campestris* *Molinia caerulea* *Poa pratensis* *Poa trivialis* *Ranunculus repens* *Rumex acitosa* *Sagine procumbens* *Trifolium repens* *Tussilago farfara* *Vaccinium oxycoccus* *Veronica beccabunge*	*Acrocladium cuspidatum* *Atricum undulatum* *Dicranella squarraso* *Drepanocladus fluitans* *Eurhynchium praelongum* *Philonotis fontana* *Polytrichum commune* *Rhytidiadelphus squarrosus*	*Hormidium* sp. *Spirogyra* sp.

in the vicinity of Mam Tor and the toxic constitutents of the waters have all been removed by the time the streams leave the village of Castleton (Sampling Site No. 102 was located below the confluence of waters draining Mam Tor and a karst stream). Some consequences of mixing waters of contrasting compositions are discussed in Section 7.6.1.

6.3 Environmental Considerations

6.3.1 Phytosociological Responses

Lackey (1938) provides a detailed list of organisms which he found to be living in acid mine drainage in Indiana and West Virginia. Unfortunately his account does not state whether or not the species are optimally adapted to the high acidity levels or even if they are actually growing. Species diversity in such waters is known to be low and algae are particularly restricted (Harrison, 1958; Steinback, 1966; Warner, 1968). Consequently, most workers have concentrated on the lower forms of biota.

Bennett (1969) for example, considers the algal floras in seventeen acid creeks where he finds no evidence that any chemical factors other than acidity are limiting or controlling. The total number of algal species in highly acidic streams in England is reported as being twenty-four (plus two moss species) by Hargreaves et al. (1975). An interesting conclusion of these authors is that the acid streams which have been in existence the longest appear to have a richer flora.

A list of the species of plants found at five sites on Mam Tor is given in Table 12.

Sites 2,3,6 and 7 are all acidic (pH 3.0-3.5) seepages and can be seen to contain, in total, only fourteen species of higher plants, four mosses and five algae. By contrast Site 8 (mean pH = 5.2) has twenty-five higher plants, eight moss or bryophyte and two algal species. The greater diversity at the latter site, which can readily be accounted for by lower acidity, is obvious. Phytosociological differences between acid sites are slight and all contain virtually the same communities of moss and algae.

Of the higher plants restricted to acid seepages one, *Phragmites communis*, is particularly interesting. Although this reed is commonly believed to grow only in neutral-pH environments this is the second site known to the author where it thrives in water of pH <3.5. Indeed at Parys Mountain on the Isle of Anglesey, North Wales, a large stand of *Phragmites* is the dominant community in water draining abandoned copper mines where the pH is often as low as 2.0 or less.

Of the plant species found at Mam Tor, those that are known to prefer acid conditions are *Juncus effusus*, *Deschampsia flexuosa*, *Agrostis tenuis* and *Carex nigra*. Of the mosses *Drepanocladus fluitans* and *Polytrichum commune* are tolerant of highly acidic waters. The former species has also been recorded in large numbers in an acid mine stream in Durham, England, by Whitton (1972). The algae of *Euglena*, *Chlamydomonas*, *Mougeotia* and *Zygogonium* species are all acidophilic and are commonly found in acid mine drainage (Hargreaves, 1975).

High concentrations of H^+ ions generally impare a plant's absorption of calcium, magnesium and phosphate and can increase the solubility and toxicity of aluminium, manganese and iron (Rorison, 1973). Mycorrhizal activity and cell division in young roots are also restricted.

Sulphate is not usually considered to have much effect on plant growth and nutrition, but at very high concentrations can prevent the uptake of nitrate and phosphate, adversely affect osmosis and generally stunt growth. Brock (1969) studies in detail the effects of extreme conditions on the lower forms of aquatic life.

It would be interesting to observe whether the acidophilic species, or indeed those not generally considered to survive in low-pH waters, at Mam Tor have adjusted over the millenia to the toxic conditions and if the species diversity is greater than that reported for true acid mine drainage

situations. Unfortunately there was insufficient time in the present study to conduct such an investigation and the author is not qualified to perform the necessary experiments. From casual observation, however, it would seem that some plants *are* growing in waters generally considered unsuitable and that some species, particularly mosses, are more diverse than reported by Hargreaves et al. (op.cit.).

Any interested reader would have the full co-operation of the author in undertaking such work and the streamwater chemical data presented here might prove invaluable in this event. It is thought that by using Mam Tor as an example of what happens after prolonged exposure to acid mine drainage possible ways of re-colonising areas devastated by pollution of this kind might be found. The examination of plant remains incorporated in the ochre deposits might yield evidence of past changes in plant communities in the seepages.

Examples of studies concerned with re-populating the aquatic environment of acid mine drainage areas could not be found. In a study of the recolonisation of black wastes from coal mining areas (very similar material to the fragmented black shale at Mam Tor) Schramm (1966) found that low pH was not the limiting factor. Nitrogen-fixing legumes and potentially ectotrophic mycorrhizal species such as pines, spruces, birches, aspens, oaks, and willows can tolerate a highly acid growing medium. High surface temperatures resulting from the low albedo of black shales are far more important.

Black shales exposed to the direct rays of the sun can reach a temperature in excess of 75°C at the surface; 25 mm below the surface this temperature can drop by as much as 18°C. Heat injury and even death both of seeds and seedlings can result purely from insolation and it is thought that the lack of vegetation cover on certain parts of the Mam Tor landslide (notably the black scree slopes of Little Mam Tor and the retrogressive units) may

be partly due to elevated surface temperatures which are observed on fine days, particularly on south and southwest facing slopes.

Several animal species can be found in the acid waters at Mam Tor including a large population of frogs and several insects (beetles, water-boatmen, etc.). Again it is not known if these animals are in some way adapted to the toxic conditions or if they are barely managing to survive.

6.3.2 Biological-Chemical Interactions

The concentration of some elements in streamwater can be predicted purely from abiotic chemical reactions of precipitation, complexing, and so on. Levels of others may be significantly influenced by biochemical reactions. According to Ruttner (1953), for example, "It is quite impossible to understand the chemistry of an aquatic biotope without taking into consideration the causal relationships in the metabolism of its community of organisms".

Higher plants and animals only become significant in influencing streamwater chemistry when their numbers are large. Because of the high surface area to volume ratio and the biochemical versatility of bacteria and microscopic plants and animals these generally play the dominant role.

In a study of the relation of biological activity to water composition Lee and Hoadley (1967) observe that the effects of such organisms are largely indirect. The number of free-living bacteria in natural waters is shown by these authors to be extremely low. Most are attached to particulate matter where they "create special localised conditions, permitting solution of mineral constituents or the metabolism of certain organic materials by altering the pH, redox potential, or by preventing dispersal of extracellular enzymes".

Changes in pH result from normal photosynthesis and can lead to precipitation of chemical species which are at or near saturation. The classic

example is the photosynthetic precipitation of $CaCO_3$ which is accelerated by the presence of certain bacteria (Lee and Hoadley, op.cit.).

Since concentrations of iron in water in excess of a few tenths of a milligram per litre can impart an unpleasant taste, and even stain materials with which it comes into contact, the solution characteristics of this element have probably been more closely studied than any other. The often-controlling influence of organisms,which all require iron to build up their body substance, on iron concentrations is well known. Perhaps the most comprehensive review of literature on this subject is that of Oborn (1960). While this work pays particular attention to microscopic forms that of Oborn and Hem (1962) concentrates on the effects of the larger aquatic organisms.

It is thought that at Site 7 at Mam Tor the filamentous green alga *Hormidium* is sufficiently abundant to influence oxygen levels during photosynthesis, thereby bringing about diurnal cycles in stream chemistry (Whitton, B.A., 1979; written communication). The filaments can also be seen to act as nuclei for the precipitation of iron oxide. Spring and summer growths of *Hormidium* at this site become completely encrusted with iron by the Autumn, and it is thought that this process may be in part responsible for the accumulation of ochre at this and other localities (Section 7.6.3). Sykora et al. (1972) have also noted that algae can act as nucleation sites for precipitating ferric hydroxide, which ultimately results in the death of the organisms.

The close association of algae and gypsum is also observed in the Mam Tor seepages, and can be seen in Plate 20.

6.4 Conclusions

The conclusions which can be drawn from this Section, concerned essentially with the chemical reactions taking place at Mam Tor, are summarised as follows:

Observations made in Sections 4 and 5 can now be explained in terms of quantitative chemical equations. Pyrite oxidation is the source of sulphate and iron, calcium and magnesium are derived from dolomite dissolution and silicate transformations give rise to the aluminium and potassium in the waters.

At least 99% of the acidity produced in pyrite oxidation and ochre precipitation is consumed before the solutions rise at Site 7. The residual 1% of H^+ ions leave the water considerably acid, at a pH of approximately 3.5. Over 20 tonnes of pyrite are consumed annually in the generation of this acidity.

The waters produced by these reactions closely resemble so-called 'acid mine drainage' and the involvement of chemoautotrophic iron oxidising bacteria as catalysts in their generation is suspected.

Pronounced vegetational differences occur between acid springs and surface drainage on the landslide. It is not known whether the organisms in the acid seepages have become adapted to the extreme conditions. Algae almost certainly act as nucleation sites in the precipitation of ferric hydroxide as well as raising the oxygen status of the waters.

The next logical step in this research would be to examine the above equations more carefully to see if they make sense, for example, in terms of chemical thermodynamics. Firstly, however, we will consider the other half of the descriptive story - the analysis of solid materials.

7. MINERAL ANALYSIS

The chemical weathering of individual mineral grains takes place by surface attack. Therefore, it seems logical to examine the finest fractions within a rock sample as the effective surface area is much greater than for coarse grains and the results of chemical alteration will be more readily detected.

Structural changes may also occur in the clay minerals as a consequence of weathering which might be particularly relevent here since an increase in the proportion of, say, expandable clays can affect the stability of the material as a whole. Consequently the separation and methods of analysis of very fine clays (< 0.5 μm) will be described in detail.

We are also interested, however, in overall compositional changes involving the removal of certain minerals and the precipitation of others. The identification of mineral phases and the detection of inter-sample variations or trends are facilitated by the use of powdered whole rock samples, as opposed to any particular size fraction. Both types of analysis - clay mineral and whole rock - will be discussed after brief consideration of the nature and location of the samples themselves. This Section ends with a broader discussion of the occurrence of gypsum, jarosite and ochre.

7.1 Sampling of Solid Materials

Appendix Ci gives a description of each sample taken for X-ray analysis. Essentially these samples can be split into three distinct sets; shales taken from surface exposures on the landslide, shales from borehole cores, and samples of various other surface materials. These will be discussed in more detail below, with a further division of the surface rock samples between the two principal sampling localities.

7.1.1 'Little Mam Tor'

Since the Edale Shales contain the various mineral phases thought to be responsible for the unusual drainage water quality, numerous samples of these mudstones were collected for analysis. The largest exposure of Edale Shales on the landslide is on the minor scarp face known as 'Little Mam Tor'.

Samples were not systematically located throughout the exposure here. Rather, materials which appeared visually distinctive were taken from various locations marked on Plate 8, in a general 'down slope' succession. The reason for this is that material being weathered on the face, falling off to accumulate as scree, and eventually becoming incorporated into the soil profile is undergoing progressive alteration. Any mineralogical variation produced by weathering, therefore, would be most easily detected between samples of relatively fresh shale on the scarp face and highly broken-down shale beneath the grass cover at its base.

As noted in Section 2.2.1, the Edale Shales at outcrop here are fractured considerably due to jointing and expansion along bedding planes. Consequently samples are easy to collect and can be picked from the face by hand. Occasionally a small geological hammer is necessary particularly for breaking off pieces of the carbonate bands which are much harder than the shales.

Samples collected in this way were placed in self-sealing polythene bags and marked with a number representing the sample location and date. Any relevant comments were recorded in a field notebook.

7.1.2 Retrogressive Units

Some of the highest beds in the Edale Shales succession outcrop in the area of retrogressive units (Plate 9). Here the rocks are even more highly fragmented and the enlarged joints and bedding planes are lined

PLATE 21: Joint filling material in the retrogressive units.

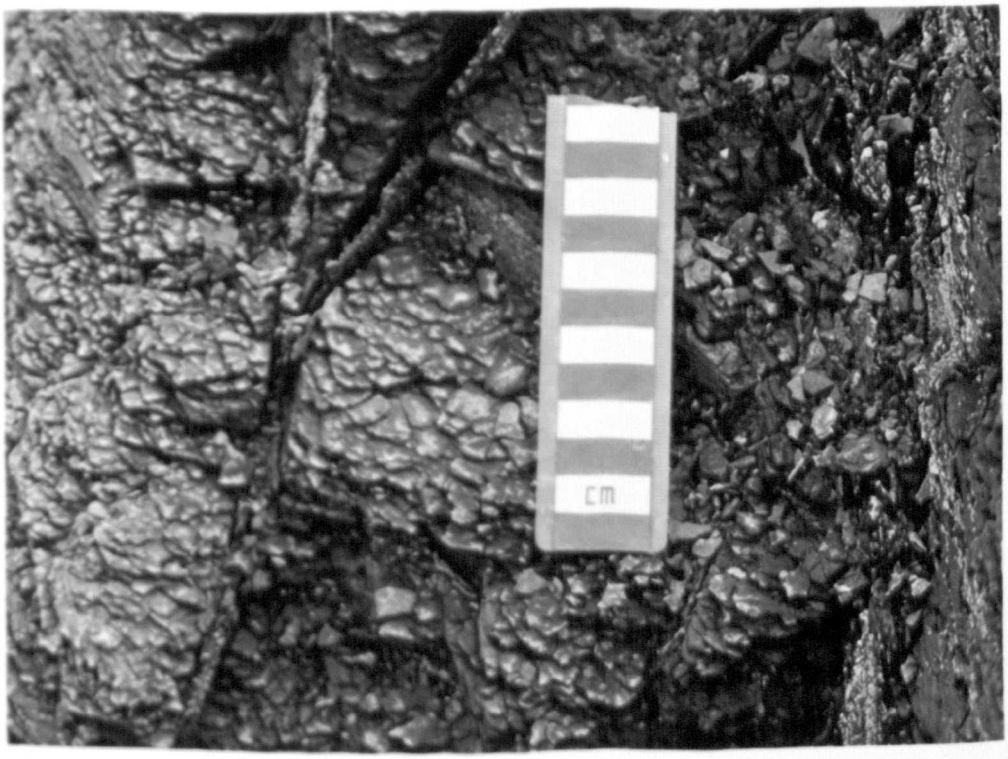
CM

FIGURE 23: Soil profile in a pit dug above Site 7 on the retrogressive unit.

Letters refer to soil horizons as defined by Cruikshank, 1972.

Fig 23 Soil Profile Above Retrogressive Units

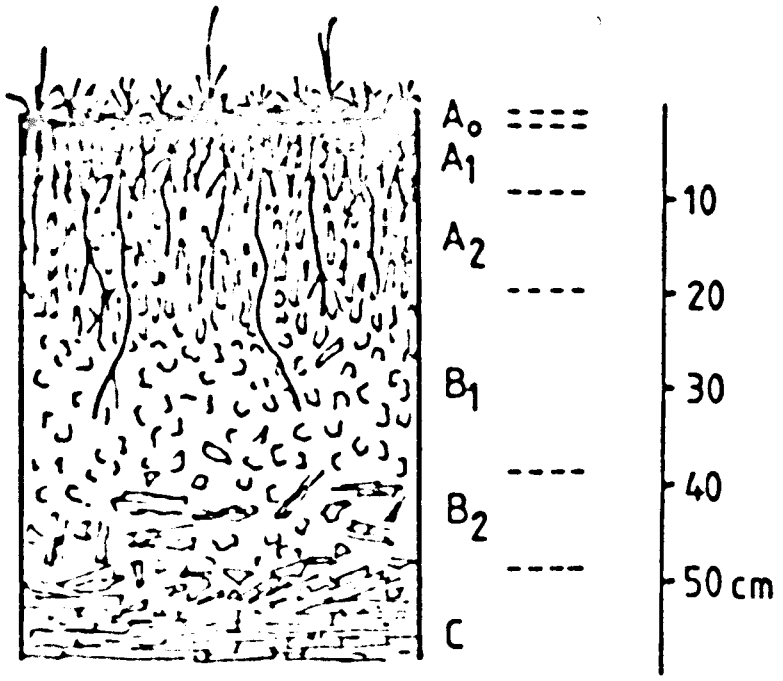

with gypsum and iron oxides (Plate 21). Discrete carbonate concretions are present in addition to continuous beds.

Samples of joint-fill material and highly weathered shale were collected from the face of the main retrogressive unit in addition to pieces of the concretions and carbonate bands.

A soil pit was dug on top of the main retrogressive unit. Plate 9 shows the location of this and other sampling points. Material collected from the soil pit ranges from very fine shale fragments in the turf layer to weathered bedrock at a depth of approximately 50 cm. Figure 23 shows the section in this pit.

7.1.3 Other Surface Materials

A piece of the main failure surface some 5 cm square, was removed from the base of the main scarp face in order to determine the mineralogy and to compare this with the other shale samples. In addition a large carbonate concretion (Plate 2a) was taken from the top of the main retrogressive face and returned to the laboratory where different types of surface coatings and oxide layers were carefully removed and separately analysed (Samples A to F, Appendix Ci).

Samples of precipitates from the seepage areas, previously described simply as 'ochre' were also taken. The ochre at Site 3 was sampled by inserting a barrel auger with a sharp cutting tip down into the stream bed with a corkscrew motion. The auger penetrated to a depth of about 40 cm and yielded a good intact core.

At the top of this core the ochre is a purplish-red colour and is very brittle despite having a high water content. Further down the ochre is reddish-orange with a high organic content (the remains of *Sphagnum* and *Polytrichum* moss), and at 40 cm depth it is yellow-brown, very hard and has a lower organic content. Sub-samples of these three distinctive ochre types were taken.

Gypsum crystals were removed both from the carbonate concretion and from plant stems in the seepages (Plate 20) and returned to the laboratory in stoppered glass bottles. A milky-white precipitate from the Odin Sitch (Plate 11b) was also collected for X-ray analysis and some of this material was precipitated in the laboratory for comparison by mixing water from Site 11 with karst water (see Section 7.6.1).

A sample of unweathered Edale Shale was collected from the quarry at Hope Cement Works. Unfortunately the management of the Works would not grant permission for more comprehensive sampling as they considered the existing quarry workings "too dangerous". The single sample was taken from a stock pile of recently quarried material. It is not known, therefore, from whereabouts in the succession it came, but it must be lower than any beds outcropping at Mam Tor.

7.1.4 Borehole Cores

In the Spring of 1978, Derbyshire County Council sank eight boreholes down through the landslide (see Section 3.3). The cores from these boreholes proved a useful source of material from depth within the landslide and small samples were obtained, with permission from the Council, from various depths in two of the cores. The location of these two boreholes is shown on Plate 12.

Borehole 7 penetrated to a depth of about 20 metres and samples of shaly material, some 'fresh' and some 'weathered' were collected at regular intervals down to 18 metres. The material was fragmented to varying degrees throughout this distance. It is not known for certain if the fracturing is due to coring procedure or to inherent cracks in the rock. It is thought likely, however, that since certain portions of the core were relatively undisturbed that much of the fracturing was the result of past landslide movements.

FIGURE 24: Location of samples in Boreholes 7 and 8. Correlation is made on distinctive units.

FIG 24 LOCATION OF SAMPLES IN BOREHOLES 7 & 8

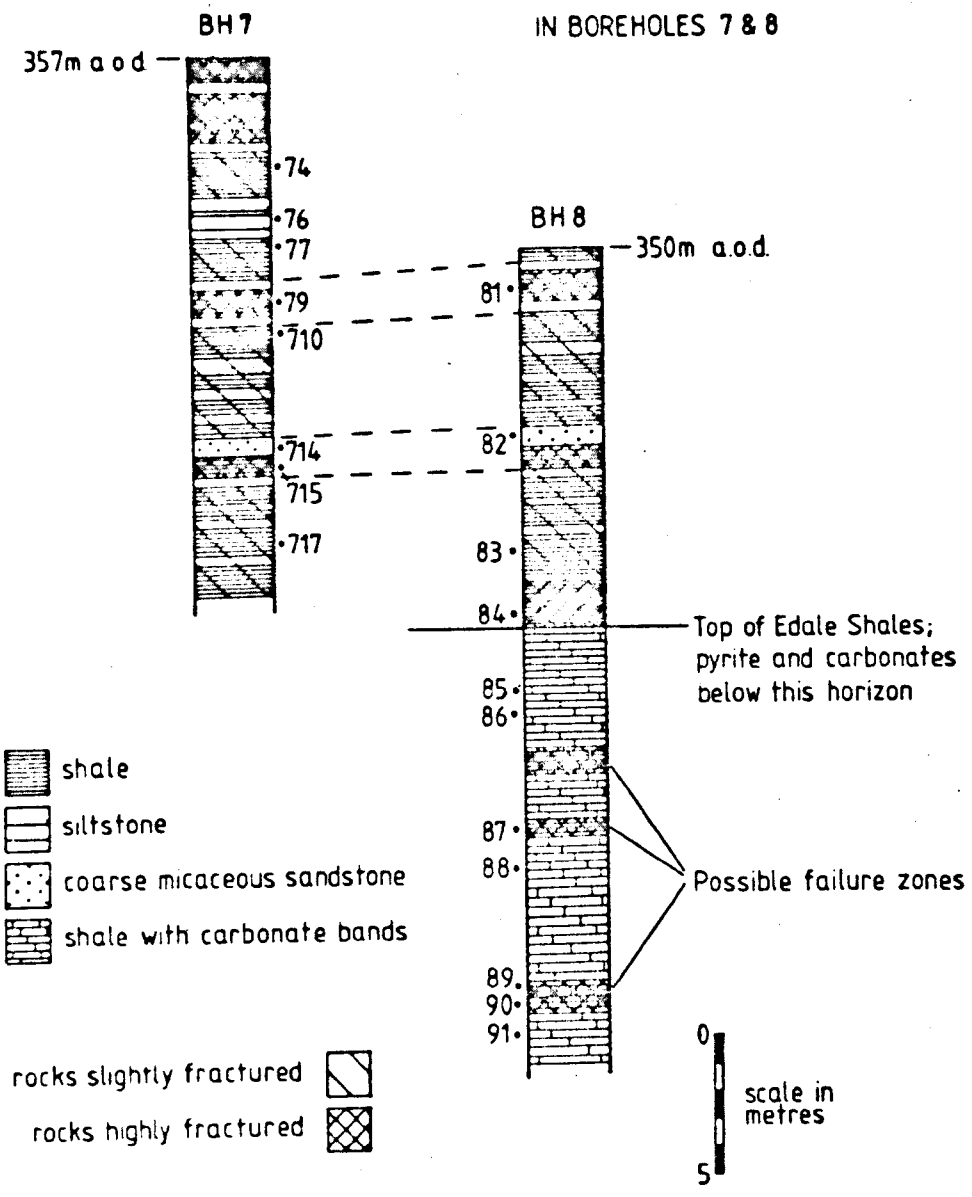

Borehole 8 was sunk to a depth of 30 m and samples were collected to 28 m. Not all the samples taken from these two boreholes were subjected to X-ray analysis - once again the emphasis was on comparing 'fresh' and the 'weathered' material.

A sketch log of the boreholes compiled from notes made at the time of sampling the cores is shown in Figure 24. Correlation between the boreholes is based on distinctive formations such as the coarse sandstone unit which contains large flakes of white mica.

Due to the lack of pyritic, carbonate-containing shales in Borehole 7, it is thought that the Edale Shales were not penetrated. The top of the Edale Shales is believed to be at a depth of 14 m in Borehole 8.

7.2 Particle Size Separation

7.2.1 Disaggregation

The shale samples described in 7.1 were to be subjected to two types of X-ray analysis; whole-rock and clay-mineral. For this reason the samples were divided into two parts. One part was treated as described in Section 7.3.2 and the other was disaggregated, in order to separate out those clay particles less than 2 μm in diameter.

Approximately 10 g of shale was lightly broken up using a geological hammer; for many of the weathered samples this procedure could be effected by crumbling the rock between the fingers. This material was then placed in clean, wide-necked polythene bottles of about 1 litre capacity and 300 ml of 'calgon' solution added. This dispersing agent, added to prevent the clay particles from flocculating, consists of 1.5 g sodium hexametaphosphate per litre of distilled water.

Tightly fitting lids were then placed on the bottles which were secured to a metal frame rotating about a central horizontal axis. The 'end-over-end' tumbling was continued until the samples had completely broken down to sand-, silt- and clay-sized particles. Anything from

between 1 to 24 hours of tumbling may be necessary, depending on the degree of consolidation.

When the shales were completely broken down they were transferred to sedimentation cylinders for further size separation.

7.2.2 Sedimentation

7.2.2.1 Theory

The following discussion concerning the separation of clay-, silt- and sand-sized materials is based on that presented by Blatt, Middleton and Murray (1972, Chapter 3).

The settling velocity of particles in solution is a function of particle size and fluid resistance. This resistance comprises both inertial and viscous forces which are proportional to the kinetic energy of the fluid ($\rho u^2/2$) and to the cross-sectional area of the particle, as follows:

$$F_R = C_D \cdot \frac{\rho u^2}{2} \cdot A \qquad (36)$$

where ρ is the mass density of the fluid

u the velocity of the fluid relative to the particle

A the cross-sectional area of the particle

C_D its 'drag coefficient'

This relationship is known as Newton's Law of Resistance.

The viscosity of the liquid determines the value of C_D. The cgs-system unit of viscosity is the 'poise' (g cm^{-1} s^{-1}) which can vary in a given fluid depending on the temperature and salt content. A relative measure of the total viscous forces of a fluid is the Reynolds number which is defined as:

$$R_e = \frac{ud\rho}{\mu} \qquad (37)$$

where d is the diameter of the particle

μ is the 'dynamic viscosity'.

It is found experimentally that the drag coefficient C_D is a unique function of the Reynolds number, for a constant particle shape.

Graf and Acaroglu (1966) have shown that for very fine-grained spherical particles settling in water at low concentrations:

$$C_D = \frac{24}{Re} \tag{38}$$

If this equation is combined with (36) above, we obtain:

$$F_R = 3\pi\, d\mu u \tag{39}$$

which is known as Stokes' Law of resistance. Following from this, for a particle settling in water with a constant velocity ω, Stokes' Law of settling can be written as:

$$\omega = \left[\frac{(\rho s - \rho)g}{18\mu}\right] \cdot d^2 \tag{40}$$

where $(\rho s - \rho)$ is the density difference between the particle and the fluid

g is the acceleration due to gravity.

This law is used as the basis of determining the size of clay and silt particles since the value inside the square bracket has the value of 0.892×10^4 at $20^\circ C$ (ω measured in cm s^{-1} and d in cm). Thus:

$$d = \sqrt{\left(\frac{\omega}{0.892 \times 10^4}\right)} \tag{41}$$

In practice the application of Stokes' Law is limited since clay particles are not spherical, their density is not precisely known, and high concentration of particles may retard settling. However, if the clay particles are adequately dispersed, and it is remembered that the

FIGURE 25: A method for separating < 2 μm clays from a sediment suspension using a graduated syphon tube.

FIG 25 A METHOD FOR SEPARATING <2μ CLAYS

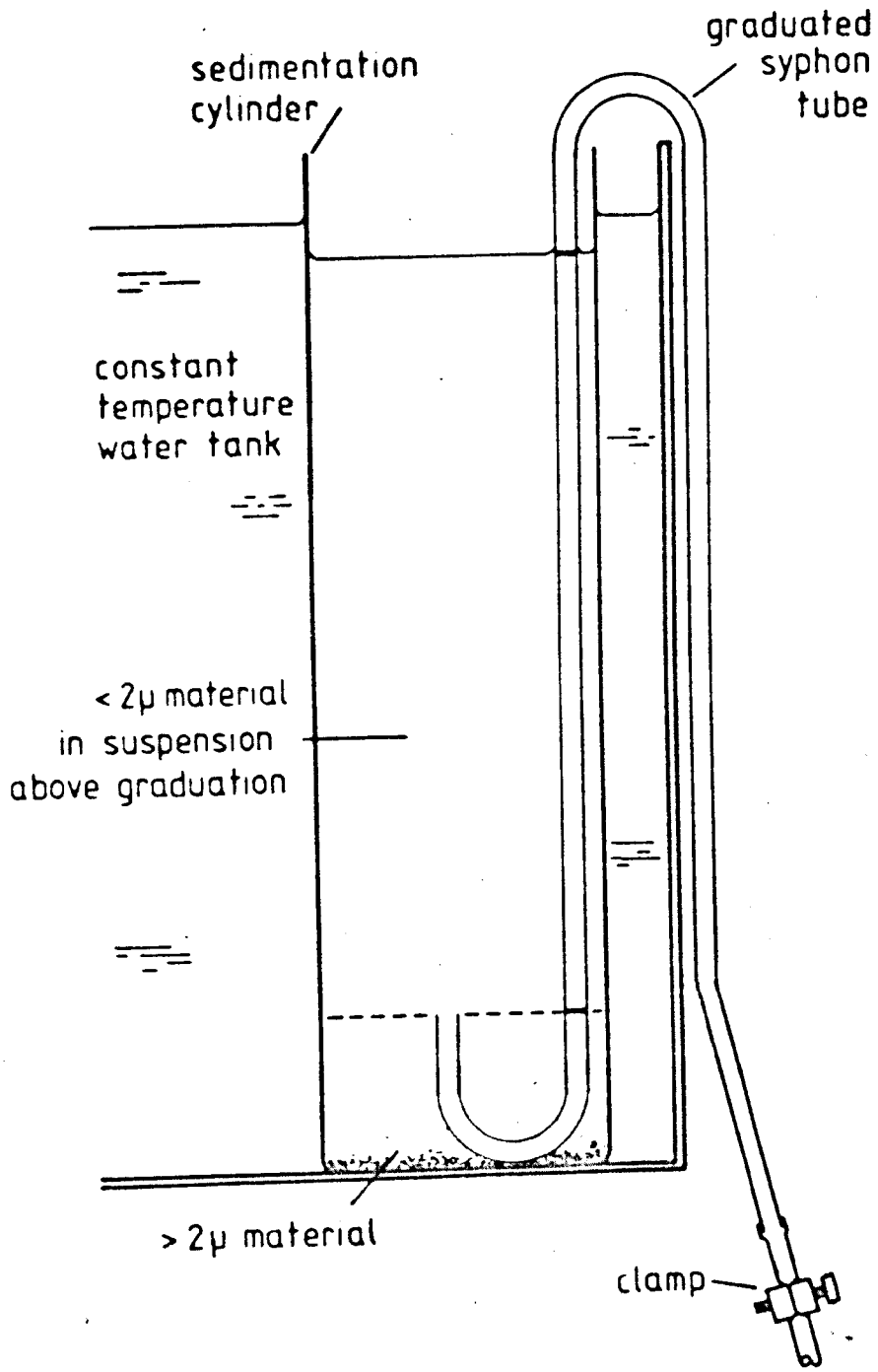

PLATE 22a: The Sedimentation Tank

PLATE 22b: Thin-section of Edale Shale.
x 5 Negative View.

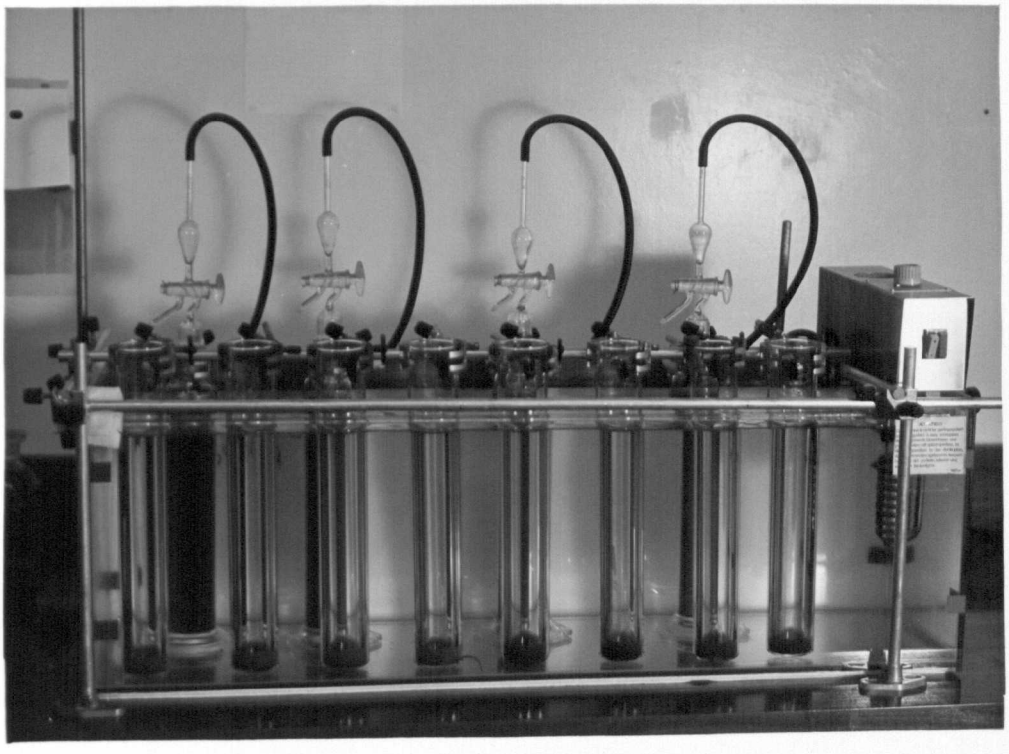

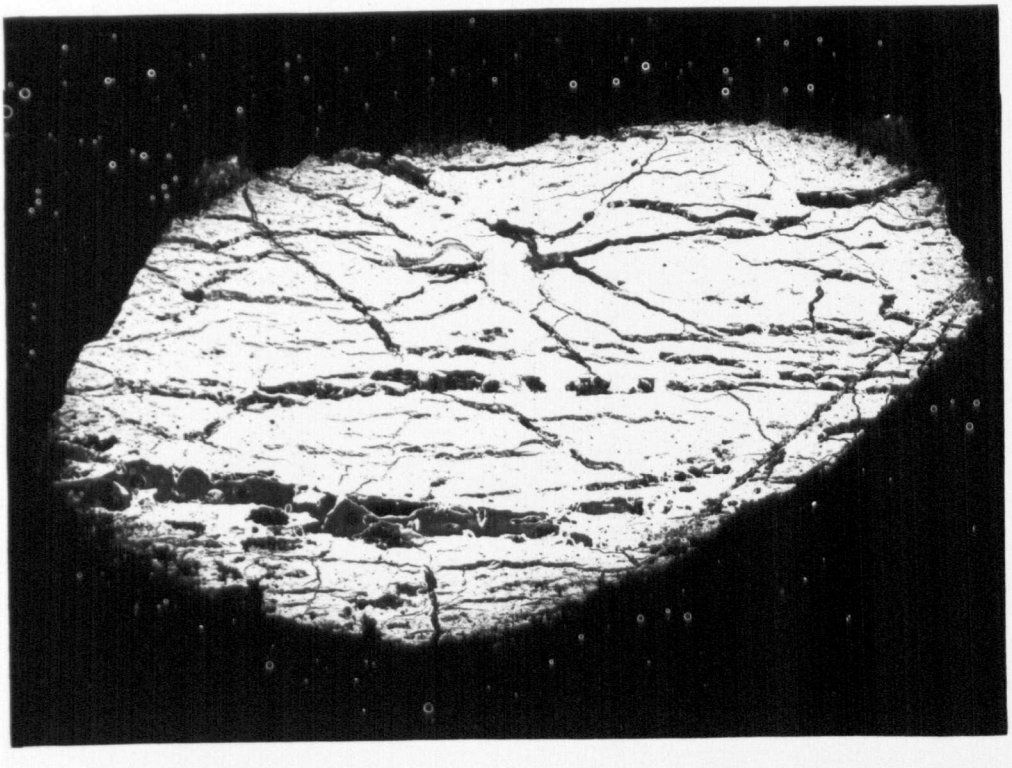

'equivalent diameter' (the diameter of a quartz sphere having the same settling velocity) is being measured then sedimentation is a perfectly acceptable technique of particle size determination.

7.2.2.2 Practice

From Stokes' Law can be calculated the time taken for particles of a known equivalent diameter to settle a given distance. Pure samples of clay <2 μm in diameter are most frequently used in X-ray diffraction studies of clay minerals. It was calculated that particles of this size will settle in a 'calgon' solution at a rate of 4.0277×10^{-4} cm s^{-1}. A convenient settling time in experimental studies is approximately 16 hours; samples can be mixed up at 5 p.m. and the fine fraction drawn off at 9 a.m. the following day. In sixteen hours 2 μm particles will settle a distance of 23.2 cm.

Consequently, sedimentation cylinders approximately 30 cm in length were obtained and syphon tubes constructed so as to draw off the top 23.2 cm of liquid from inside them. The whole apparatus was enclosed in a water bath kept at a constant temperature of 20°C by an electric thermostat. The set-up is shown diagrammatically in Figure 25 and also in Plate 22a.

At the commencement of sedimentation the samples from the 'end-over-end' tumbler were placed in the glass cylinders and made up to volume, according to the graduation on the syphon tube, as necessary. The cylinders were then inverted several times before leaving them to stand in the water bath.

After sixteen hours of undisturbed settling no material coarser than 2 μm remains in suspension above the lower graduation(Figure 25). The supernatant liquid, containing particles of 2 μm and smaller, is then drawn off by opening the clamp and activating the syphon (the syphon tubes are filled with distilled water before lowering them into the sedimentation cylinder).

Changes in clay mineralogy due to weathering are most noticeable in the finest size fractions (greatest surface area). Therefore, it was decided to separate out the <0.5 μm particles from the <2 μm cut. The sedimentation time required for this by the above procedure is far too long to be practicable. If the value of g in Equation 40 can be increased, by using a centrifuge, the time is reduced considerably.

Therefore, it was calculated that a spin-time of seven minutes and two seconds at 3000 rpm (for a 100 ml-capacity centrifuge head) would effectively bring down from suspension all particles coarser than 0.5 μm. The supernatant fluid, containing clay particles of <0.5 μm, was then further centrifuged at 4000 rpm for several hours until the liquid in the centrifuge tubes was clear and the clay particles had settled to the bottom and could be removed.

The subsequent treatment and analysis of these <2 μm and <0.5 μm sub-samples is discussed in Sections 7.3.2 and 7.4.

7.3 X-Ray Diffraction

7.3.1 Principles

X-rays consist of electromagnetic radiation of very short wavelength. This typically ranges from 2.5×10^{-8} m ('soft' X-rays) to about 1×10^{-11} m ('hard' X-rays). Visible light has a longer wavelength, and shorter overall range, in the order of 10^{-7} m. The very short wavelength of X-rays means that they can penetrate solid matter.

If monochromatic X-rays are incident upon a crystal surface at some angle θ, they will penetrate the solid to lower layers in the crystal lattice. They will penetrate further for higher angles of incidence and *vice versa*. If monochromatic, or 'coherent' X-rays emerge once again from the crystal, having been reflected from the lattice, then the path differences between the incident and reflected beams must be an integral

number of wavelengths. Otherwise destructive interference will lead to extinction in much the same way as happens to polarised light in transmitted light microscopy.

Bragg (1913) showed that the wavelength λ, and the angle of refraction θ are related to the crystal lattice spacing, d, in the following way:

$$n\lambda = 2d \sin \theta \qquad (42)$$

The X-ray source in modern X-ray diffractometers is held stationary and a device known as a 'goniometer' rotates both the sample and the X-ray analyser, a'proportional counter' (similar in principle to a Geiger-Müller counter), through various angles of incidence with the beam. Since the angle of reflection (θ) is equal to the angle of incidence (θ) the beam of X-rays is diverted through an angle 2θ in total. The counter, therefore, moves with twice the angular velocity of the sample.

The proportional counter records the intensity of the radiation it receives as a certain number of 'counts-per-second'. This information is sent to a chart recorder which gives a continuous visual reading of intensity. Peaks of X-ray intensity are observed, above a general low background level, when crystals of the same mineral in the sample are reflecting X-rays simultaneously and through the same angle. The different positions of these peaks on the chart, which has $^{o}2\theta$ along the horizontal axis and intensity along the vertical, indicate the presence of different mineral phases. Thus, if the goniometer is driven over a sufficient range of $^{o}2\theta$ to cover the possible peak positions of the minerals likely to be present, the overall mineralogy of the sample (assuming that its components are crystalline and not amorphous) can be determined.

TABLE 13: Operating Conditions for the X-ray Diffractometer

Tube Type	Cu
Voltage and Current	35 kV, 40 mA
Filter (secondary)	Ni
Pulse Height Analyser:	
Lower Level	180 divisions
Window	220 divisions x 10-100%
Gain	64
Range	4×10^3 c.p.s.
Time Constant	1 second
Chart Speed	2 cm per minute
Wavelength of $Cu_{K\alpha}$ Radiation	1.54 Å (1.54×10^{-10} m)

By altering the type or intensity of X-rays, the speed of rotation of the goniometer, and by using various methods of signal enhancement (such as filtration, 'pulse height analysis' and integration) satisfactory operating conditions can be obtained for most experimental situations. The standard operating conditions for the Philips diffractometer used in this study are shown in Table 13.

7.3.2 Mineral Identification in Whole-Rock Powder Samples

To analyse a whole-rock sample by XRD it is necessary to crush the rock to a very fine powder. This is most easily done in a mechanical 'Tema' grinder, after the rock has initially been broken up using a hammer or 'jaw' crusher.

After 'Tema' grinding the resulting powder is homogenised to produce a representative sample. Very little powder is needed to form the back-filled mount required for this type of analysis, although a considerable amount can be crushed at one time.

About 10g of the powder is ground still finer by hand in an agate mortar. This material is then pressed into a hole in a 1 mm-thick aluminium plate, which is covered on one side by a microscope slide cover glass. When the hole is full, a second solid plate is clipped on top and the mount turned over. On removing the cover slip the surface of the powder is found to be smooth and flat, although the mineral grains have random orientation. This powder mount is then placed in the sample chamber of the goniometer and analysed as described in the previous section.

Such a method of sample preparation gives good peak intensities on the chart because the powder is thick and many thousands of crystals will be reflecting X-rays at the same time. With such randomly-oriented grains, however, the resolution of separate peaks may be poor.

It is usual to scan such a sample from about 4^{o} to $45^{o}2\theta$. This range covers d-spacings from 22Å to 2Å; most common rock-forming and secondary minerals have lattice spacings in this range and will give one or more diffraction peaks. Each mineral has a number of possible peak positions corresponding to different crystal orientations.

A scanning rate of $1^{o}2\theta$ per minute is usually sufficient to produce an interpretable diffraction trace. If carbonate rocks are being analysed, however, it may be desirable to scan the specimen over a more limited 2θ range, and at a slower rate to obtain better resolution of the peaks. In this way subtle variations in composition between, say, dolomite, ferroan dolomite and ankerite (which have peaks very close together on a standard trace) may be discerned.

In this study most of the samples from 'Little Mam Tor', the retrogressive units and Borehole 7 were X-rayed using powder mounts. The samples were scanned from 4^{o} to $45^{o}2\theta$ at $1^{o}2\theta$ per minute. In addition, if carbonate was found to be present, the samples were scanned from 26^{o} to 33^{o} 2θ at $0.25^{o}2\theta$ per minute. Appendix Ci gives further details of these and any other analyses.

7.3.3 Identification and Estimation of Clay Minerals

There is considerable debate in the literature of sedimentary petrology as to the best way of preparing clay mineral samples for analysis by X-ray diffraction. The aim is to produce a highly oriented specimen so that only basal reflections are produced. Most authors agree that the use of<2 μm (or smaller)size fractions give the best results.

Perhaps the most commonly used preparation technique is that of smear mounting on a glass plate as described by Gibbs (1965). Kinter and Diamond (1956) however, believe that air drying on glass gives little better than random orientation and they propose a method involving suction of a clay-

water suspension through porous ceramic plates. This technique has the advantage that any dispersing agent or other chemical additive likely to affect the results can be washed off simply by sucking through distilled water. Such a technique is preferable, therefore, in cation replacement studies.

In a discussion of the various available mounting techniques, Gibbs (1968) recommends the use of only three; Kinter and Diamond's suction method, smear mounting on glass, or powder press mounting (as for whole rock analysis). The actual quantity of clay used in these techniques can also affect the results (Stokke and Carson, 1973).

Schultz (1975) believes that an overall accuracy in quantitative estimation of the minerals present better than $\pm$ 10% can be achieved with several techniques provided that sampling and preparation are standardised, the grinding procedure is controlled and uniform and that the results are consistently interpreted.

As a result of Cubitt's (1975) work it was decided in this study to use the glass smear mount of Gibbs (1965), which is also the most rapidly prepared type of sample. Cubitt concludes that: "Detailed statistical tests of competing sample preparation methods show that the commonly used smear technique is superior for distinguishing between shales on the basis of quantitative assessment of mineral content".

Since maximum structural information is required to determine subtle changes on weathering two size fractions - the $< 2\,\mu$ and $< 0.5\,\mu$ - were separated as described in Section 7.2. Each was allowed to almost completely dry before being lightly ground in an agate mortar to break up any aggregate which had formed. A very small amount of distilled water was then added to the clay to form a paste. If too much water is added at this stage the particles may actually go into suspension and, on drying, the very fine clay flakes will take longer to settle onto the plate. As a

result of adding too much water Gibbs (1965) observed enrichment of fine-grained montmorillonite in the surface layer of the mount.

After the paste has been thinly spread onto the glass slide using a small spatula the sample is quickly dried by passing a slight air stream over its surface. If this stream is too rapid, material may be built up more thickly at the edges of the mount. If the mount is successfully prepared a highly reflective and uniform surface, indicating good orientation, is achieved.

Basal reflections from the common clay minerals produce the most intense diffraction peaks in the range 4^{o} to about $30^{o}2\theta$. This is not to say, however, that each peak is at a distinct position on the trace. Rather, some peaks occur in the same place as, or very close to, those of other minerals. For example the [002] chlorite peak and the [001] kaolinite peak both occur at about 12.4^{o} 2θ (7.1Å d-spacing). Furthermore a fairly broad peak is often obtained at about 8.9^{o} 2θ (10Å d-spacing) which comprises both a [001] illite peak and a reflection from expandable clay material, often referred to as smectite, with a basal d-spacing anywhere between 10Å and 12Å.

To distinguish between these peaks and to determine whether in fact any expandable clays are present, a number of tests have been devised. The first of these involves solvating the smear-mounted sample with a molecule larger than the inter-layer cations, typically ethylene glycol. Any expandable clay minerals will swell in a saturated atmosphere of glycol as the molecule is pushed into inter-layer sites, expanding the crystal lattice from about 10Å to anything between 12Å and 14Å. Keeping the sample in glycol for about twenty minutes at $60^{o}C$ is usually sufficient to produce maximum swelling.

If the sample is subsequently heated the glycol is driven off and expandable clays dehydrate, collapsing back to the fundamental structure

with a 10Å d-spacing. The difference in area between the glycolated and heated 10Å peaks is commonly used as a quantitative measure of the relative proportions of expandable and illitic clays.

According to Austin and Leininger (1976): "The optimum temperature of collapse of illite-smectite mixed-layer clay minerals to 10Å ..... is about 375°C, and the maximum collapse of layers is complete after thirty minutes". They also note that maximum peak intensity is obtained if the sample is scanned when still at a temperature of over 100°C, so that even partial rehydration is prevented. Samples at such high temperatures are not to be recommended for use in standard X-ray diffractometers, however, and somewhat of a compromise was achieved in this study. The Mam Tor samples were heated to 550°C for one hour and then cooled rapidly in a dessicator before being quickly transferred to the sample chamber of the goniometer.

An intermediate heating to 250°C for one hour (thought to induce only partial collapse) was also conducted on certain samples. The relative merits of the two techniques together with a full description of results obtained will be discussed in Section 7.4.2.

The <2 μm and < 0.5 μm smear mounts were scanned from 4° to 30° 2θ and glycolated and heated specimens from 4° to about 20°2θ . Appendix Ci gives details of those samples treated in this way.

7.3.4 Other Materials

When only very small quantities of material are available for analysis it is not possible to produce a powder press mount. Although a highly oriented specimen is not necessarily desirable in many cases the only realistic alternative is to produce a smear mount (which in any case is far less time consuming).

FIGURE 26: Examples of typical powder mount diffraction traces for a carbonate (a) and mudstone (b). Samples MT2c and MT3, respectively.

a - ankerite; c - calcite; f - feldspar; g - gypsum; i - illite; j - jarosite; k - kaolinite; p - pyrite; q - quartz; s - siderite.

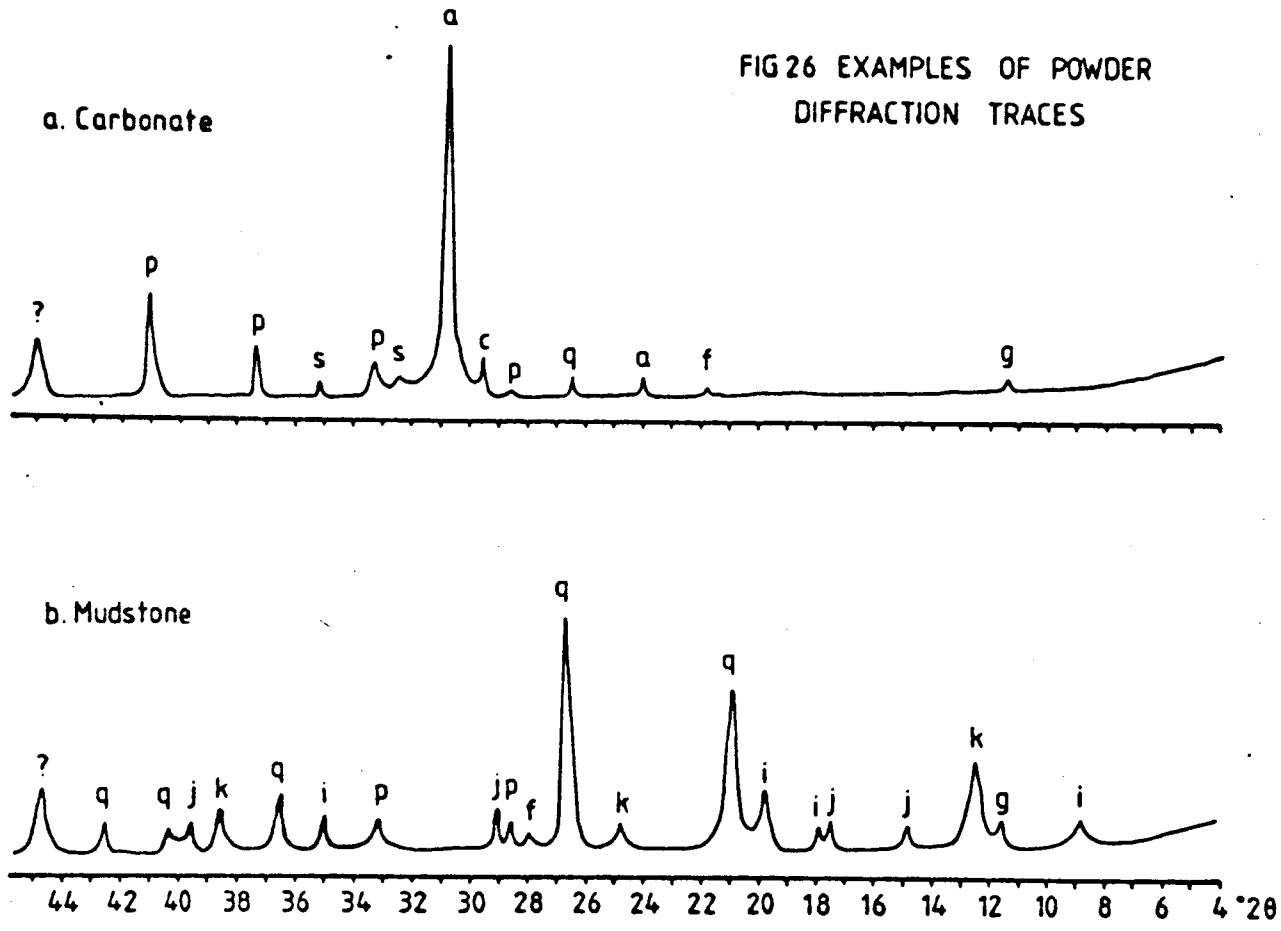

FIG 26 EXAMPLES OF POWDER DIFFRACTION TRACES

For the analysis of materials described in Section 7.1.3, particularly gypsum from the plant stems and surface deposits on the concretion, only small amounts were obtainable. These were ground to a paste with water and smeared onto a glass plate, as for oriented clay specimens, but without the preceding particle size separation.

These smears were subsequently scanned from 4^{o} to anything up to $50^{o}2\theta$ so that the presence of virtually any crystalline substance could be detected. The low intensity of peaks noted in many samples may be due to the fact that random orientation was not used. An alternative explanation for small peaks may be that the normally low background count rate was enhanced in many cases by the presence of iron-bearing minerals; $Cu_{K\alpha}$ - radiation is known to produce this effect. The influence of fluorescence was kept to a minimum by more precise signal discrimination, achieved by using an optimum combination of integration time, full-scale deflection and 'window' settings.

Results of these XRD investigations are considered in the following Sections, and shown in tabulated form by Appendix Cii.

7.4 XRD Results

7.4.1 Whole Rock

A typical XRD trace of a powder mount specimen is reproduced in Figure 26. Samples prepared in this way generally show peaks which are easily interpreted. The trace in Figure 26b, of sample MT3, is given as an example but the following discussion concerns the powder-mount samples in general.

The most noticeable features of the shale samples is that the dominant mineral present is quartz. This may be surprising since the Edale Shales, in particular, are very fine grained mudrocks which only occasionally contain more silty horizons. It is assumed, therefore, that most of this

quartz is of very small particle size. Alternatively, one or two fairly coarse detrital quartz grains, when ground to a fine powder would appear to be a major constituent of the rock.

The main quartz peak is at 3.35Å with much smaller peaks occurring at 4.21Å, 2.46Å, 2.29Å, 2.24Å and 2.13Å.

Kaolinite and illite are perhaps the two most abundant minerals after quartz. The main kaolinite peaks are at about 7.15Å (001) and 3.57Å (002). Illite peaks are at 10Å (002), 5Å (004), 4.48Å and 3.32Å. The latter peak coincides with the main quartz peak, but is usually much weaker, producing a bump on the high 2θ angle-side of the quartz peak.

The only other clay mineral detected using powder mounts, in this case, is chlorite at about 14Å.

In addition to these sharp peaks formed by the common silicate minerals certain of the Mam Tor samples (particularly borehole samples) show less pronounced X-ray peaks characteristic of the mineral goethite. Also the hydrous sulphate mineral jarosite ($KFe_2(SO_4)_2(OH)_6$) was present mainly in scree and other weathered surface material. Gypsum, which was noted as being a major constituent in weathered surface exposures, was also present in many of the samples containing jarosite.

Pyrite was not detected in samples from Borehole 7. This fact, combined with the higher quartz content of these samples, suggests that this borehole does not penetrate to sufficient depth to encounter the Edale Shales. Pyrite *was* present in samples of Edale Shale from surface exposures.

Feldspar was present in trace amounts in several instances.

In addition to those peaks accounted for by the minerals described here, one which appeared on every powder mount trace could not be ascribed to any mineral considered in standard X-ray mineralogy texts(see Brown, 1961;

Figure 27: The effects of glycolating and heating a <0.5 μm sample (Sample BH89)

X air dried

Y glycolated at 60°C for 20 minutes

Z heated to 550°C for one hour

C - Chlorite

I - Illite

J - Jarosite

K - Kaolinite

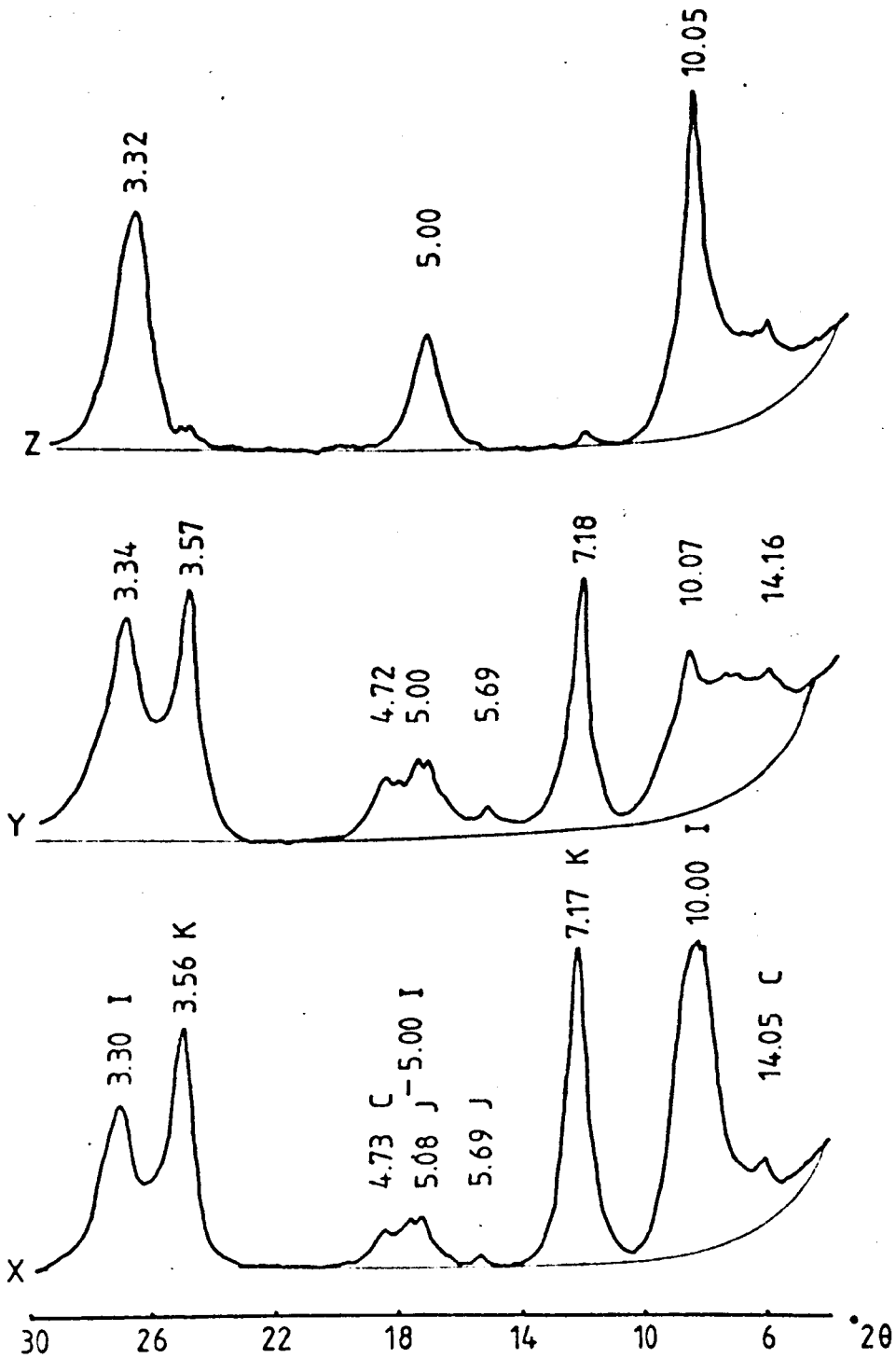
Z
3.32
5.00
10.05
Y
3.34
3.57
4.72
5.00
5.69
7.18
10.07
14.16
X
3.30 I
3.56 K
4.73 C
5.08 J
5.00 I
5.69 J
7.17 K
10.00 I
14.05 C
30
26
22
18
14
10
6
2θ

Figure 28: The effects of glycolating and heating a <0.5 μm sample (Sample SP2)

Lower Line - air dried

Middle Line - glycolated at 60°C for 20 minutes

Upper Line - heated to 550°C for one hour

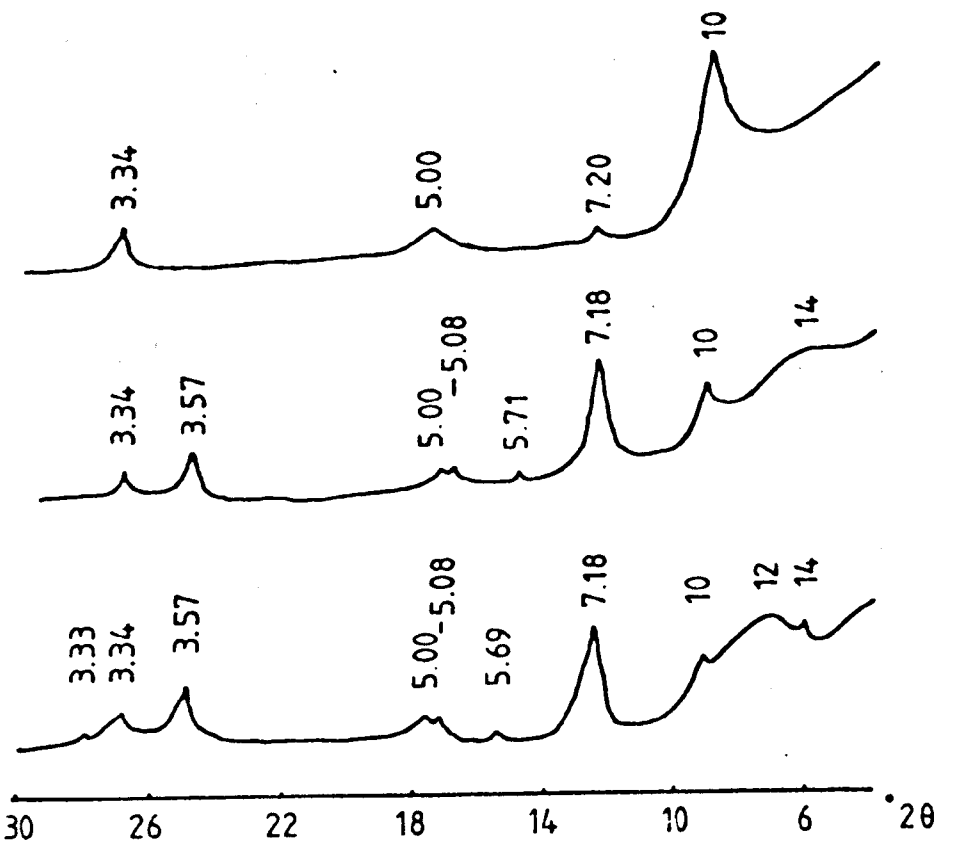
3.34
5.00
7.20
10
3.34
3.57
5.00_5.08
5.71
7.18
10
14
3.33
3.34
3.57
5.00_5.08
5.69
7.18
10
12
14
30
26
22
18
14
10
6
2θ

Brindley, 1955; Chao, 1969). This peak consistently appears at 44.64°2θ corresponding to a d-spacing of 2.03Å. The only mineral giving a peak at this position is elemental iron (ASTM Powder Diffraction Data File, Card No. 6-0696, according to Chao, 1969), but its presence in weathered sediments of this type is impossible.

The carbonates sampled are found to be of two distinct types. Those from Little Mam Tor are composed almost entirely of ankerite ($Ca(Mg,Fe)(CO_3)_2$), whereas both bands and concretions from the retrogressive units contain in addition a large proportion of dolomite ($CaMg(CO_3)_2$).

Calcite, siderite and pyrite are present in all the carbonates analysed. Quartz, feldspar, and clay minerals are also present in trace amounts as is gypsum, presumably from surface coatings. A typical carbonate X-ray trace is shown in Figure 26a.

7.4.2 Clay Minerals

Figures 27 and 28 illustrate the effects of glycolating and heating a <0.5 μm smear mount sample.

After solvating the 10Å peak diminishes as expandable clays absorb the glycol and swell to give a broad peak at between 12 and 14Å. The kaolinite and chlorite peaks are unaffected by this procedure.

Heating to 550°C restores the 10Å peak to its former proportions and in some cases it is even intensified as the expandable clay portion collapses back to 10Å (Figure 27). Kaolinite and jarosite are destroyed by the heating process and their peaks almost completely disappear. Chlorite is again unaffected.

An intermediate heating to 250°C for one hour produces only a partial collapse in the expandable clays and the kaolinite peak is hardly affected. No additional information or degree of discrimination is obtained.

TABLE 14: Peak Areas and Proportions of Clay Minerals in the < 0.5 μm Samples

A. Areas (cm^2)

Sample	Kaolinite (air dried)	Illite (heated)	Chlorite (air dried)	Total	Expandable Clay (air dried 10Å ∿ glycolated 10Å)
BH715	22.43	18.38	4.74	45.55	8.55
BH 86	3.82	3.93	0.00	7.75	2.20
BH 88	11.56	15.95	2.20	29.74	7.98
BH 89	19.54	44.86	5.20	69.60	14.80
G2	7.75	15.72	4.74	28.21	11.56
SP1	8.79	12.01	9.48	30.28	8.90
SP2	5.78	10.98	6.13	22.89	7.63
SP3	4.28	11.00	6.36	21.64	7.28

B. Percentages

Sample	Kaolinite%	Illite %	Chlorite %	*Expandable Clay %
BH715	49	40	11	47
BH 86	49	51	0	56
BH 88	39	54	7	50
BH 89	28	64	8	30
G2	27	56	17	74
SP1	29	40	31	74
SP2	25	48	27	69
SP3	20	51	29	66

C. Ratios

Sample	Kaolinite:Illite	Chlorite:Illite	Expandable:Illite	Expandable:Kaolinite
BH715	1.22	0.26	0.47	0.38
BH 86	0.97	0.00	0.56	0.58
BH 88	0.72	0.14	0.50	0.69
BH 89	0.43	0.12	0.33	0.76
G2	0.49	0.30	0.74	1.49
SP1	0.73	0.79	0.74	1.01
SP2	0.53	0.56	0.70	1.32
SP3	0.39	0.58	0.67	1.70

*Percent of 10Å peak, not of total clay

(see Appendix Ci for location of samples)

Most workers involved with clay mineral analysis use the <2 μm size fraction, presumably because it is more readily obtained. It was found during the course of this study, however, that the coarser material produced inferior diffraction traces to the < 0.5 μm smear mounts. Although the background level is reduced for the < 2 μm samples so too are peak intensities. Also, additional minerals are present in the coarser fraction and quartz and gypsum peaks - which are absent from the < 0.5 μm material - interfere with interpretation of the trace.

Since the finest particles will be more at equilibrium with the waters which contact them it was decided here to make semi-quantitative estimates of the proportions of various clay minerals on the < 0.5 μm samples only. It must be remembered that this is no indication of the proportion of minerals in the sample as a whole since the finest fraction is unrepresentative.

Pierce and Siegel (1969) studied several methods of quantitative analysis based on either peak-height or peak-area measurements (although they also used only the < 2 μm fraction). Their results are inconclusive and each technique yielded substantially different data. It appears, in fact, that any one procedure, if consistently applied, can be used to obtain an indication (but no more) of the varying proportions of clay minerals between samples.

In this study it was decided that peak areas would be used and that the total clay content would be taken as the sum of the 7.16Å kaolinite (air-dried trace), the 10Å (heated trace) and the 14Å chlorite peaks. The areas of each clay mineral were then calculated as a percentage of this total for each sample and the results obtained are shown in Table 14.

The peak areas were measured by cutting out the relevant portions of the diffraction trace - which had first been transferred onto draughting film - and comparing the weights of these pieces to the weight of a known

area of film. This technique is considered more accurate and is more rapidly performed than any other method of area measurement of complex shapes.

In addition, by superimposing the air-dried and glycolated traces the difference in the 10Å peaks, resulting from a shift in the position of the expandable clay peak, could be measured directly. This area was then calculated as a percentage of the 10Å peak (heated trace) in order to give an estimate of the proportion of expandable clay present in each sample. These percentages are given in Table 14B, Column 5.

In practice it was found to be extremely difficult to rapidly cool a smear mounted sample from 550°C to room temperature; many samples fractured due to contraction and could not be placed in the diffractometer. Consequently full analyses (air-dried, glycolated and successfully heated samples) were only performed on the eight samples for which results are given in Table 14.

These results show that there is a much greater proportion of chlorite and expandable clays in the surface weathered material and soil samples (G2, SP1-3) than in the shale from the borehole.

Assuming the mineralogy of both surface and deep material was originally similar the above observations can be explained in one of two ways. Firstly, the chlorite and expandable clays of the near-surface samples could be formed, by weathering, from both kaolinite and illite. Alternatively, kaolinite might be selectively leached out and the weathering products form entirely from illite. Although in most situations kaolinite is not preferentially removed this possibility must not be ruled out in solutions such as these where the high cation content might favour the persistence of dioctahedral clays.

Within the soil profile samples SP3→SP2→SP1 represent a weathering sequence, whereby illite appears to be transformed to expandable clays and

the proportion of kaolinite also increases.

The most obvious conclusion that can be drawn from the information of Table 14, is that the material at depth is very unlike the surface shales.

If weathering underground by percolating solutions containing inorganic acids produces the same results as surface weathering by organic soil acids (which Curtis (1975) believes to be the case - H^+ ion content alone being the important factor) then none of the borehole samples appear to be highly weathered. It might be expected that failure surfaces are, however, weathered due to the action of percolating solutions, in which case neither borehole contacted a failure surface. Alternatively, the irregular sampling might have failed to include material from such a failure zone, although the most fragmented shale *was* taken.

It is apparent that a major sampling programme and more detailed analysis of the clay minerals are needed in order to determine whether any of the boreholes encountered failure surfaces. The problem concerning chlorite which, although it is a less stable mineral than illite or kaolinite, increases in proportion on weathering also remains for the time being unresolved.

One observation which does make sense, however, is that the proportion of expandable clays increases on weathering. This is important in an engineering sense since clay swelling is frequently responsible for failure in rocks containing a high proportion of expandable clays (Nakano, 1967; Mielentz and King, 1955).

Chemical analyses earlier showed that the contribution of solutes from clay mineral transformations is small and it is thought that the overall degree of alteration on weathering is slight, except in the soil layers. This might be expected since the finest detrital clays have already undergone one cycle of weathering and transport prior to sedimentation, and should be reasonably stable in a weathering environment.

Accurate quantitative assessments of the amounts of various clay minerals present in a given sample are impossible to obtain. In the first place the proportion of < 0.5 μm clay which the sample contains is not known. Also peak intensities depend not only on the amount of each clay present but also on the degree of orientation, which is impossible to reproduce exactly in consecutive samples. In addition several subjective procedures are involved, such as the construction of a 'best-fit' background line and the terminating of peaks at abitrary 2θ values for the purpose of area measurement.

Despite these limitations the techniques outlined above do give an indication of inter-sample variations in the relative proportions of clay minerals.

7.4.3 Other Materials

7.4.3.1 Carbonate Coatings

Smear mounts of the various carbonate coatings described in Appendix Ci generally produced excellent diffraction traces.

Jarosite and goethite appear to be responsible for the orange and yellow-brown colouration in the weathered skin (Samples B, C, D), while the soft white efflorescences are composed entirely of gypsum (Samples A,F). The fibrous, white, crack-filling material from the concretion (Sample E) is found to be calcite. The similar-looking encrustation on plant stems in the seepages (Sample H) is confirmed as being gypsum.

7.4.3.2. 'Allophane'

Water at Site 11 on the main unit, having been supplied from Sites 7 and 8, flows through a drain beneath the upper section of the road before emptying into the Odin Sitch (see Figure 5 and Plate 12). Here the water meets a stream draining the limestone area to the south of the landslide and a spontaneous chemical reaction takes place.

From this point in the Odin Sitch downstream to Sites 13 and 1, and even beyond the toe of the landslide, a milky white precipitate lines the banks and bed of the stream (Plate 11b). In an accessible side-branch of the Odin Rake which lies directly beneath the Odin Sitch some water permeates the overlying limestone and the white precipitate is formed on the ceiling and walls of the worked-out vein.

Some of this material was collected and analysed by Wilkinson (1950). Although the author notes that the precipitate is "X-ray amorphous" he identifies it as being the mineral allophane (an aluminosilica gel) which is defined by Grim (1968) as the non-crystalline part of a clay that is soluble in hydrochloric acid.

Some of the precipitate was analysed in the present study and in addition a quantity was synthesised by mixing various proportions of water from Site 11 and from the limestone stream. The natural, stream precipitated, material indeed appears to be amorphous and no peaks are observed on the X-ray trace.

The laboratory precipitated material was allowed to dry completely before being ground and X-rayed in the normal way. This sample (Sample G) gave very strong gypsum peaks and no others. It would appear, therefore, that if the precipitate is given time to dehydrate it does become crystalline and is composed principally of gypsum rather than allophane.

7.4.3.3 Ochre

Samples of the ochre core described in Section 7.1.3 show a systematic variation in composition, as well as in appearance, with depth below the surface.

Brittle ochre at the top of the core is completely X-ray amorphous (Sample I) but gives a very high background reading suggesting fluorescence due to the presence of iron (see Section 7.3.4). Further down the core,

Figure 29: A comparison of four goethite samples
(letters refer to samples of Appendix C)

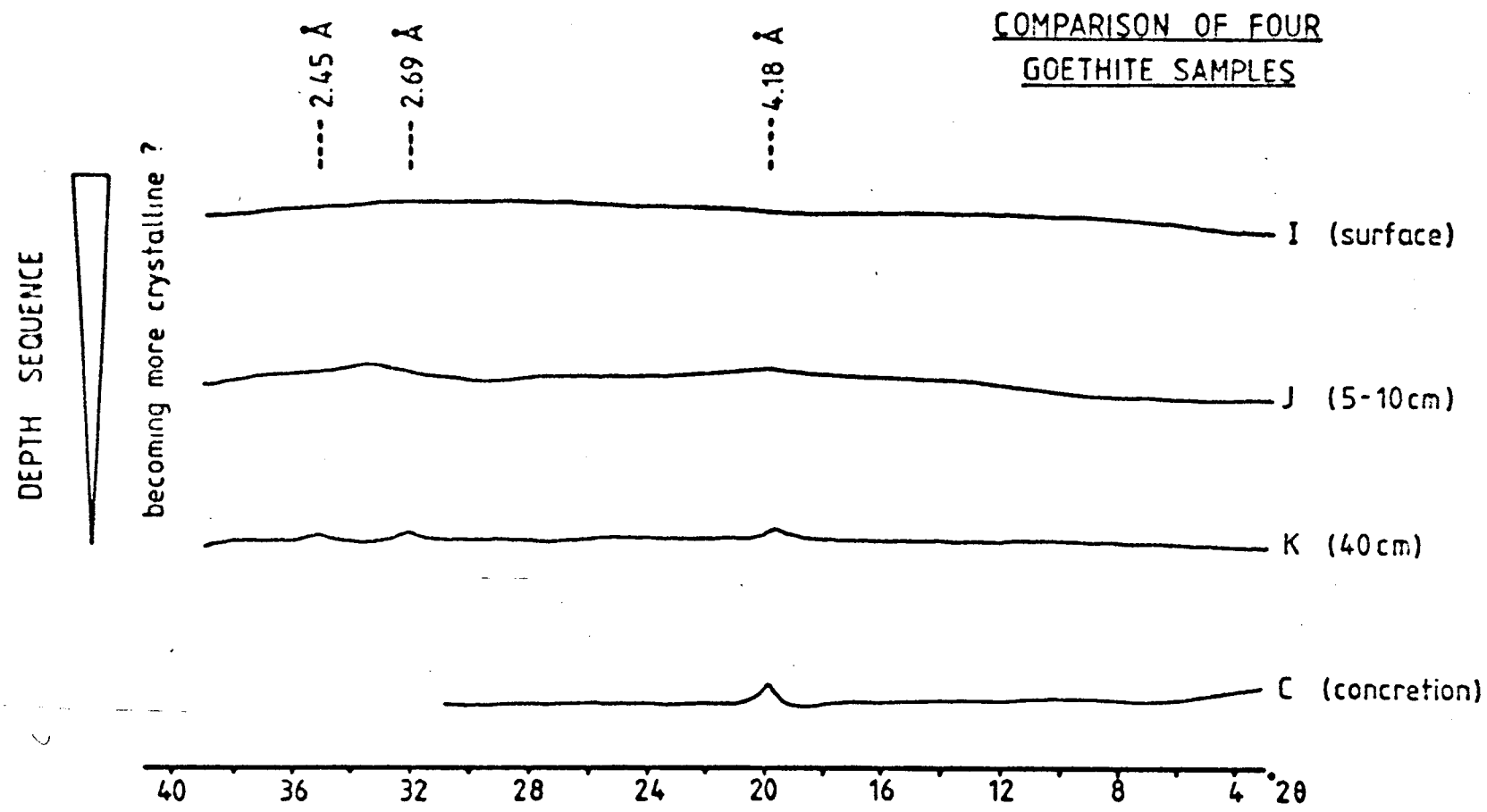
COMPARISON OF FOUR
GOETHITE SAMPLES
2.45 Å
2.69 Å
4.18 Å
DEPTH SEQUENCE
becoming more crystalline ?
I (surface)
J (5-10cm)
K (40cm)
C (concretion)
40
36
32
28
24
20
16
12
8
4
2θ

although fluorescence still occurs, distinct peaks begin to emerge above the background in the same position as those in Sample C (goethite).

Figure 29 shows this apparent sequence whereby material becomes progressively more crystalline with depth and, therefore, time.

The tables of Appendix Ciii show that the identification of selected minerals is consistent with published work (after Brown, 1961). The relative intensities of peaks are often different due to the fact that Brown uses powder press mounts and the samples from Mam Tor are mostly oriented smear mounts.

7.5 Thin Sections

The petrographic microscope is of limited use in the study of very fine grained rocks, and thin sections are often difficult to make since mudrocks break up very easily when cut using a diamond-edged wheel. Two thin sections of Edale Shales were prepared, however, in order to compare the fabric and texture of 'fresh' and 'weathered' samples.

'Fresh' Edale Shale was collected from Hope Cement Works - the same sample as was used for XRD analysis (HCW1). Plate 2b is a x 20 enlargement of part of this thinsection viewed in plane polarised light. The rock is extremely fine grained and the identification of individual crystals is, therefore, virtually impossible. Some larger-than-average quartz grains and some sericitic mica can be seen. Most of the dark colouration is thought to be due to the presence of carbonaceous material, the relative abundance of which distinguishes between the dark and light bands.

A few larger, subhedral grains of an opaque mineral can also be seen in Plate 2b. Observations in reflected light suggest that these grains, approximately 0.25 mm across, are pyrite.

The 'weathered' section of Edale Shale taken from the retrogressive unit above Site 7, was prepared by first impregnating the rock with 'Araldite'

resin so that it could withstand being cut and ground without disintegrating. Similar dark, fine-grained material as in Sample HCW1 makes up the bulk of this shale, but instead of a sharp transition from dark to light laminae highly crystalline material can be seen to clearly separate the two (Plate 3b). This mineral is identified as gypsum.

Inclusions of matrix material within these crystals give a sense of the gypsum forming between laminae and forcing the shale apart. Where larger cracks have opened well-formed euhedral crystals of gypsum, showing good cleavage, have developed (Plate 4a).

Plate 22b is a x 5 enlargement of the resin-impregnated section of shale, made by placing the thin section in a photographic enlarger. Although this results in a negative image the whole section can be studied at lower magnification than is possible with a microscope.

It is interesting to note that the gypsum (dark areas) not only forms along the (horizontal) bedding and laminations but also in cracks which intersect the bedding at between 40^{o} and 60^{o}. The presence of cracks on a much larger scale, but at a similar angle to bedding, were noted in exposure in the field (Section 2.2.1).

7.6 The Mechanism of Formation of Three Precipitate Minerals

7.6.1 Gypsum

Saas et al. (1965) report on the weathering of pyritic concretions in an arid area of southern Israel. Their description of the appearance of the concretions could be applied, without modification, to the weathered carbonate bands of the Edale Shales. According to these authors "the outer part of the concretions is usually composed of red to deep violet hematite and dull-brown goethite. Sometimes a coating of gypsum scales is found on the outside". (see page 19 for a description of the Mam Tor carbonates).

Saas et al. believe the gypsum is formed by acid (resulting from pyrite oxidation) attack on calcite in the country rocks. Where calcite is scarce the acid attacks clay minerals, leaching out the alkalis and alumina, to form jarosite and natrojarosite. Other alteration products are listed as alunite, baryte, celestine, goethite, hematite, sideronatrite and sulphur.

In more humid environments the presence of gypsum in surface material is generally thought to be only temporary and possibly even seasonal as a result of its high solubility (van Breemen, 1972). Where it is present in large amounts it is considered evidence that leaching is not taking place (Spears et al., 1971).

Smith and Drever (1976) and Vora and Raymahashay (1978) discuss the formation of gypsum in joints, similar to the situation at Mam Tor. They conclude that authigenic gypsum can form from undersaturated solutions due to "non-equilibrium evaporation" during dry periods. During winter rainfall the gypsum dissolves once again.

Gypsum crystals are present in the Edale Shales at Mam Tor, however, throughout the year; although a greater number of very fine rosettes do appear during warm summer weather. Downward leaching by rainfall must be considerable here due to the porous nature of this highly fractured material yet the gypsum still persists. It is thought that this may be in part due to a coating of less soluble material such as jarosite on the crystal surfaces, which also accounts for their yellow-brown colouration.

The precipitation of gypsum on the plants in the seepages is definitely related to dry weather evaporation and the crystals disappear even after moderate rainfall.

X-ray analysis also showed the white precipitate in the Odin Sitch to be composed of gypsum (page 107). This material is thought to be similar both in character and origin to the sludge formed during the lime and limestone treatment of acid mine drainage (see Section 6.2.2).

TABLE 15: Results of Gypsum Precipitation Experiment

Sample	Description	pH	Conductivity ($\mu S\ cm^{-1}$ at $25^{o}C$)
A	Site 11 water	3.3	2450
B	Odin Sitch water	7.5	520
C	50:50 mixture	4.4	1430
D	80:20 mixture	3.7	1800
C	(after 72 hours)	4.4	1360
D	(after 72 hours)	3.6	1840

The components necessary to form gypsum from solution - Ca^{2+} and SO_4^{2-} ions - are both contained in the waters emerging at Site 7 and flowing via Site 11 under the road to the Odin Sitch. No additional calcium is required, although a small amount is contained, in the water of the Odin Sitch.

In order to investigate the mechanism causing the rapid precipitation of gypsum where these streams mix, two 20-litre samples of the waters were collected and removed to the laboratory. Here they were mixed in 5-litre polythene beakers in 50:50 and 80:20 ratios of Site 11:Odin Sitch water. Changes in pH and electrical conductivity were monitored and the results are shown in Table 15.

After three days there was little change in pH and conductivity over the original change on mixing. Very little precipitate had formed in the 80:20 mix, whereas a considerable amount of orange 'gel' had accumulated in the bottom of the other beaker (50:50 mix). This precipitate was allowed to dry, after pouring off the supernatant liquid, before being subjected to XRD analysis as described in Section 7.4.3.2. It would appear from these simple experiments that a rise in pH from about 3.3 to 4.4 is needed to cause the gypsum (probably an impure form containing iron) to precipitate.

7.6.2 Jarosite

Another mineral which is known to precipitate from certain solutions after a change in pH is the hydrous sulphate of iron and potassium, jarosite. It has been suggested that this mineral is one end-member of a solid solution series and increasing Al^{3+} substitution tends to the other end-member, alunite ($KAl_3(SO_4)_2(OH)_6$). Intermediate minerals, however, are rare (Brophy et al. 1962).

Much of the work on the alteration of pyrite has been done in the USSR (see: Srebrodol'skiy, 1977; Yakhontova et al. 1979) where it is noted that jarosite is one of the most common oxidation products (Khlybov, 1976).

According to Nordstrom and Dagenhart (1978) there are two distinct types of pyrite weathering products. These are efflorescent crusts of sulphate minerals on the unoxidised sulphide and those minerals which precipitate directly from the drainage solutions. These authors suggest the following alteration sequence:

PYRITE→MELANTERITE→ROZENITE(+ SZOLMONOKITE)→COPIAPITE+COQUIMBITE

The final stage of this sequence "Is the formation of jarosite and hydrated iron oxides which have only been found as direct precipitates from water solutions".

In order to characterise the formation of such minerals, Bladh (1978) simulates the weathering of sulphide-bearing rocks in a rather unusual way - using differential equations describing equilibrium and non-equilibrium mass transfer between aqueous solutions and minerals. His calculations predict the formation of jarosite or alunite with the solution of only 1.8×10^{-8} g pyrite per litre of water being enough to precipitate geothite.

Brown (1971) considers the stability relationships between the three minerals; geothite, jarosite and pyrite. It is found that the dominating influence is pH although the activities of K^+ and SO_4^{2-} must also be high for jarosite, rather than geothite, to form (Kelly and Goddard, 1969). Brown notes that if the pH of the weathering solution is below 3.0 jarosite is the dominant phase. Above pH 3.0 goethite is the stable mineral. An increase or decrease in the activities of H^+, K^+ or SO_4^{2-} (perhaps caused by concentration or dilution) at a given Eh and activity

of iron will cause the precipitation of one or the other mineral. It is thought that bacterial activity, necessary in the first place for pyrite oxidation, can raise the Eh and lower the pH sufficiently to form jarosite rather than geothite.

Brown also notes that the replacement of jarosite by goethite has been observed and that jarosite precipitation is always limited to sites above the water table.

The formation of jarosite from goethite takes place according to the following reaction:

$$3FeOOH + K^{+} + 2SO_4^{2-} + 3H^{+} = KFe_3(SO_4)_2(OH)_6 \qquad (43)$$

This reaction must be spontaneous since the free energy is -19.7 kcal $mole^{-1}$ (Brown op.cit.).

7.6.3 Iron Hydroxides

The characteristic orange colour of the ochre deposits at Mam Tor is typical of the ferric hydroxide minerals 'limonite' and goethite and of the oxide hematite. There seems to be no consensus of opinion in the literature, however, as to which mineral will form in a given situation and the terms often appear to be interchangeable and are used loosely to describe a ferric hydroxide with indeterminate water content.

Here 'limonite' is taken to be the freshly-precipitated phase which is amorphous and, therefore, not a recognisable mineral; hence the use of quotation marks. Goethite is the crystalline ferric hydroxide with formula FeOOH (or $HFeO_2$). Hematite is the ferric oxide given by Fe_2O_3, although formulae of the type $Fe_2O_3 \cdot x\ H_2O$ may appear in later equations, representing a hydrated form.

In an article concerned with acid sulphate soil formation, which has been cited several times previously, Van Breemen (1972) states that the precipitation of iron minerals is pH-dependent. Below about pH 3 or 4

jarosite precipitates whereas above such values poorly-crystallised ('limonitic') goethite, lepidocrosite (γ Fe_2O_3) or hematite will form together with sulphate ions in solution. At Mam Tor, however, the pH of seepage waters is often as low as pH 3.0 and ferric hydroxides are the only minerals to precipitate. Jarosite is only found encrusting highly weathered shales where it is thought that evaporation and supersaturation play an important role (the availability of K^+ may also be greater here).

Changes in appearance and composition of the ochre formed in the seepages with depth as noted in Sections 7.13 and 7.43, are consistent with the observations of other workers. For example, Hanshaw (1974) notes that the first phase to precipitate is amorphous 'limonite' which, with time, dehydrates to form goethite as shown by reactions (19) and (20), page 65. This sequence is also recorded at Mam Tor where goethite X-ray peaks begin to emerge after prolonged burial (see Figure 29).

The persistence of organic matter at depth appears to contradict the common belief that red beds indicate oxidising conditions. It would appear that where ochre forms by chemical precipitation, as in this case, organic matter is preserved as long as anoxic conditions are maintained *inside* the deposit.

Hanshaw (op.cit.) reports organic matter being incorporated into a goethite deposit in much the same way as at Mam Tor. He was able to calculate a mean rate of accumulation of hydroxide of 0.9 mm per year, based on carbon-14 dates of the lowest organic materials. Carpenter and Hayes (1980) placed unglazed ceramic plates, which acted as artificial substrates, at various levels in a stream from the surface to below the sediment-water interface. The rate of iron oxide accumulation was found to be 120 µg cm^{-2} yr^{-1} near the surface and fell off to zero on the stream bed. The iron content of Carpenter and Hayes' streamwater is far lower than at Mam Tor and it is believed that the accumulation rate of goethite here is much greater.

Although there was insufficient time in this study to measure the accumulation rates it is thought that such work might be worthwhile in providing data concerning the age of the deposits and, ultimately, the age of the landslide (assuming the goethite began to form soon after the first movement opened up the rocks to acid attack). Hanshaw's goethite deposit is estimated to have first begun to accumulate some 9,500 years before present, corresponding to the retreat of the most recent mountain glaciers in that part of Colorado.

Iron hydroxide deposites are known to 'scavenge' and act as 'traps' for base metal ions (Jenne, 1968). Indeed Hanshaw (op.cit.) reports Cu, Pb, Zn-enrichment of goethite relative to the seepage water. Unfortunately, once again, there was not time to examine the trace element content of the Mam Tor ochres although several water samples were analysed for a total of eight base metals.

From Appendix Bxii it would appear that samples taken downstream from ochre deposits (Sites 2, 11 and 16) contain lower concentrations of trace metals than springs above the seepages (Site 7). This might suggest that these metals co-precipitate with the ochre, although the normal effects of dilution (as for other ions) must also be taken into account.

Also no definitive statement can be made based on such a small number of samples and anomalous values at certain sites (e.g. Zn at Site 2, Pb at Site 11) remain unexplained.

Future work, including more detailed sampling, could obviously be undertaken concerning these goethite deposits and it is hoped that some of the questions raised may subsequently be answered.

A more detailed knowledge of the various aqueous, crystalline and ionic species involved in the weathering reactions has now been obtained. Various inter-relations will be examined in the following Section from the thermochemical viewpoint and with special emphasis placed on iron chemistry.

8. CHEMICAL THERMODYNAMICS

One of the most important chemical approaches to hydrology is to establish whether or not natural water bodies approach equilibrium. By calculating equilibrium conditions and comparing them with observed conditions the degree of departure from equilibrium can be assessed, and from that the probable direction and extent of spontaneous reactions such as precipitation.

In this study it is essential to establish the state of equilibrium of emergent waters with respect to atmospheric oxygen and to precipitation of iron oxides and sulphates. Oxidation-reduction potential (Eh)is a good indicator of the P_{O_2} status of waters and the approach used here to examine pertinent equilibria is essentially the same as that of Garrels and Christ (1965), who describe the methods of construction of Eh-pH ('stability field') diagrams.

The heavy reliance on the above-cited work is easily explained. No other text describes the principles of construction of these diagrams so fully and in so logical a manner, and it is thought that a better understanding of the equilibria involved here will be obtained by following Garrels and Christ's methods fairly closely, with only slight modification to suit our particular needs.

In Section 8.2, equations marked with an asterisk are those given by Garrels and Christ (op.cit.). Many have been re-calculated using the recently revised data of Table 16.

Before considering these equilibria in detail the thermodynamic data of Table 16 will be used to calculate temperature changes induced by the reactionsdescribed in Section 6.

TABLE 16: Values of Standard Free Energies of Formation (kcal mole^{-1}, 25°C, 1 atmos)

Formula	State	ΔG^{o}_{f}	Source
Ca^{2+}	aq	-132.2	Latimer, 1952
Mg^{2+}	aq	-108.8	Langmuir, 1965
$CaMg(CO_3)_2$	c	-518.7	Robie, 1959
Fe^{2+}	aq	- 20.3	Latimer, 1952
Fe^{3+}	aq	- 2.52	Latimer, 1952
Fe_2O_3	c	-177.1	Rossini et al. 1952
Fe_3O_4	c	-242.4	Rossini et al. 1952
$Fe(OH)^{2+}$	aq	- 55.91	Rossini et al. 1952
$Fe(OH)_2$	c	-115.57	Rossini et al. 1952
$Fe(OH)_2^{+}$	aq	-106.2	Rossini et al. 1952
$Fe(OH)_3$	c	-166.0	Latimer,1952
FeOOH	c	-116.88	Berner, 1969
FeS	c	- 23.32	Rossini et al. 1952
FeS_2	c	- 38.29	Robie and Waldbaum, 1968
$KFe_3(SO_4)_2(OH)_6$	c	-794.0	Brown, 1970
H_2O	l	- 56.69	Kubaschewski and Evans, 1958
H_2S	aq	- 6.54	Rossini et al. 1952
HS^{-}	aq	3.01	Rossini et al. 1952
HSO_4^{-}	aq	-179.94	Rossini et al. 1952
SO_4^{2-}	aq	-177.97	Robie and Waldbaum, 1968

8.1 Temperature Considerations

Chemical reactions can be divided into two main categories - those which proceed spontaneously liberating heat (exothermic) and those which require heat energy to be supplied externally (endothermic). It has been noted previously that the oxidation of pyrite by atmospheric oxygen (Equation 26) is spontaneous and exothermic. The heat liberated is calculated from the free energy of formation of the reactants and products as described in Section 1.2.2:

$$2FeS_2 + 15(O) + H_2O = 2Fe^{3+} + 4SO_4^{2-} + 2H^+ \qquad (26)$$

$$\Delta G^\circ_f = -38.29 \quad 0 \quad -56.69 \quad -2.52 - 177.97 \quad 0$$

These values of ΔG°_f are in kcal mole^{-1}. The total energy liberated is calculated as:

$$\Delta G^\circ_r = \Sigma \Delta G^\circ_{f_{products}} - \Sigma \Delta G^\circ_{f_{reactants}} \qquad *(44)$$

$$= (2x(-2.52))+(4x(-177.97)) + 0 - (2x(-38.29)) + 56.69 + 0$$

$$= -583.368 \text{ kcal.}$$

Therefore, two moles of pyrite (2 x 119.97g) yield 583.368 kcal. Since 1.5596 g pyrite are consumed per litre of water at Site 7 (page 69) the total amount of heat liberated is given by:

$$\frac{1.5596}{2 \times 119.97} \times 583.368 = \underline{3.79^\circ C}$$

Thus the temperature of each litre of water at this site is raised by nearly $4^\circ C$ as a result of pyrite oxidation. Similarly, during goethite precipitation according to equation 28:

$$2Fe^{3+} + 2(O) + 5H_2O = 2FeOOH + 2H_2O + 4H^+ \qquad (28)$$

$$\Delta G^\circ_f = 12.52 \quad 0 \quad -56.69 \quad -116.88 \quad -56.69 \quad 0$$

$$\Delta G^{o}_{f} = (2x(-116.88)) + (2x(56.59)) + 0 - (2x(-2.52)) - (5x(-56.69)) - 0$$

$$= -58.646 \text{ kcal.}$$

Since 0.9816g goethite are precipitated the temperature rise is given by:

$$\frac{0.9816}{2x88.858} \times 58.646 = \underline{0.32^{o}C}$$

A substantial temperature rise can result from oxidation and precipitation reactions such as these, provided none of the energy is subsequently used up in endothermic reactions. Carbonate and silicate dissolution reactions generally have positive free energies, however, and require energy in order to proceed. For example, the dissolution of dolomite has the following free energy values:

$$CaMg(CO_3)_2 + 4H^{+} = Ca^{2+} + Mg^{2+} + 2H_2O + 2CO_2 \qquad *(45)$$

$$\Delta G^{o}_{f} = \quad -518.7 \qquad 0 \qquad -132.2 \quad -108.8 \quad -56.69 \quad 0$$

$$\Delta G^{o}_{r} = -132.2 + (-108.8) + (2x(-56.69)) + 0 - (-518.7) - 0$$

$$+ 164.32 \text{ kcal.}$$

This energy reduction corresponds to a temperature drop (for 1.688 g dolomite destroyed) of:

$$\frac{1.688}{184.41} \times -164.32 = \underline{-1.5^{o}C}$$

It is interesting to note at this stage that a set temperature rise of $2.6^{o}C$ is produced by these three reactions. The mean annual temperature of the water emerging from Site 7 is $9.5^{o}C$. If these reactions did not occur, therefore, and no others were involved, the temperature of the water underground would be approximately $7^{o}C$. This is the value said by Pitty (1976) to be the normal for this area (see also Pitty et al., 1979).

It is not intended to take these temperature considerations any further since additional reactions play a minor role and the quantities of mineral species involved are not so well known as those described above. It is worth noting simply that these reactions can account for the observed level and consistency of temperature of the waters emerging at Site 7.

In certain instances pyrite oxidation does not only raise the temperature of drainage waters. In highly porous surface material water may not be in direct contact with pyrite for more than a very short time during a rainfall event. In this case the heat of oxidation is released into the surrounding material which, in the case of spoil heaps, frequently is highly combustible. Both Winmill (1915) and Guney (1968) have examined the role played by this reaction in the spontaneous combustion of coal and coal slag.

As early as 1915, Winmill considers the "heats of formation" of various phases involved in the reactions given by Equations (9) and (10). He records a value of 623 kcal of heat produced in this way and describes laboratory experiments which produced results of a similar order. The discrepancy between this value and the one of 583 kcal given on page 117 is due to the refinement in free energy values over the years, and the slightly different reaction used in each case.

Winmill found that for crushed pyrite, assuming all the heat developed is used to raise the temperature of the material, a temperature rise of 60°C in three hours was obtained. The equivalent rise using oxidisable coal alone would take 48 hours. According to Winmill, "it is quite clear that where finely divided pyrites occurs in considerable proportion among coal, it may be the chief factor in originating combustion".

The amount of pyrite in the exposed Edale Shale at Mam Tor is far too small to engender such catastrophic events and readily combustible material

is not at hand. Nevertheless, pyrite oxidation could substantially raise the temperature of this material.

8.2 Mineral Stability and Eh-pH Diagrams

8.2.1 The Nernst and Debye-Hückel Equations

The relationships between pH and the oxidation potential (Eh) of an environment were first studied in detail by Clark and Cohen (1923) in the context of aquatic biochemistry. ZoBell (1946) reviews the early work on the subject related specifically to geological situations. Neither of these authors portray the stability fields of minerals in the now familiar form of Eh-pH diagrams, however, and the first publication in which these appear is the classic work of Pourbaix (1949).

As mentioned previously, principles of construction of Eh-pH diagrams described here are based on the method of Garrels and Christ (1965) who note that for every oxidation-reduction system the half-reaction can be written as:

$$\text{reduced state} = \text{oxidised state} + ne \qquad *(46)$$

where n denotes the number of electrons involved.

The oxidation-reduction potential, Eh, for such a half reaction is measured in volts relative to the standard hydrogen electrode and is given as:

$$Eh = E^{o} + \frac{RT}{nF} \ln \frac{[\text{Oxidised State}]}{[\text{Reduced State}]} \qquad *(47)$$

where E^{o} is the standard half-cell reaction
(The voltage of the half-cell when all the activities are unity)

R is the gas constant

T is the temperature in degrees Kelvin

n is the number of electrons

F is the Faraday constant

TABLE 17: Values of Parameter a_i in the Debye-Hückel Equation

a_i	ion
11	Th^{4+}, Sn^{4+}
9	Al^{3+}, Fe^{3+}, Cr^{3+}, H^{+}
8	Mg^{2+}, Be^{2+}
6	Ca^{2+}, Cu^{2+}, Zn^{2+}, Sn^{2+}, Mn^{2+}, Fe^{2+}, Ni^{2+}, Co^{2+}, Li^{+}
5	Sr^{2+}, Ba^{2+}, Cd^{2+}, Hg^{2+}, S^{2-}, Pb^{2+}, CO_3^{2-}, SO_3^{2-}, MoO_4^{2-}
4	SO_4^{2-}, SeO_4^{2-}, CrO_4^{2-}, Na^{+}, HCO_3^{-}, $H_2PO_4^{-}$
3	OH^{-}, F^{-}, HS^{-}, K^{+}, Cl^{-}, Br^{-}, I^{-}, NO_3^{-}, NO_2^{-}, Rb^{+}, Cs^{+}, NH_4^{+}, Ag^{+}

(after Kielland, 1937)

Square brackets indicate *activities* or *thermodynamic concentrations* of participating solutes.

Converting to base-10 logarithms at 25°C and 1 atmosphere total pressure for the reaction:

$$aA + bB = cC + dD \tag{48}$$

the half-reaction becomes:

$$Eh = E^o + \frac{0.0592}{n} \log \frac{[C]^c[D]^d}{[A]^a[B]^b} \tag{49}$$

This is known as the Nernst equation.

In addition, for E^o in volts:

$$E^o = \frac{\Delta G^o_r}{nF} = \frac{\Delta G^o_r}{nx23.06} \tag{50}$$

The only problem remaining is that actual quantities of solutes as determined by chemical analysis cannot be used in the Nernst equations. Instead such values must be converted to activities by multiplying the molar concentration by the corresponding *activity coefficient*. Activity coefficients are computed for each ion using the Debye-Hückel equation given as:

$$-\log \gamma_i = \frac{Az_i^2 \sqrt{I}}{1+Ba_i\sqrt{I}} \tag{51}$$

where γ_i is the activity coefficient of the ion

A is a constant relating to the solvent (for water at 25°C it is 0.5085)

z_i is the ionic charge

B is a constant relating to the solvent which for water at 25°C is 0.3281

a_i is a constant related to the effective diameter of the ion in solution (values of which are given in Table 17).

I is the ionic strength of the solution

TABLE 18: Molarities and Activities of Ions in the Site 7 Waters (based on the value of $I = 9.34 \times 10^{-2}$)

	Ca^{2+}	Mg^{2+}	Na^{+}	K^{+}	Fe^{2+}	Fe^{3+}	Cl^{-}	SO_4^{2-}
p.p.m. (annual mean)	404	185	14	5.4	85	29	42	2486
M litre^{-1} ($\times 10^{-3}$)	10.08	7. 1	0.61	0.04	1.52	0.52	1.18	25.88
Activity coefficient (γ)	0.873	0.8758	0.9662	0.9659	0.8737	0.7443	0.9659	0.8714
Activity (m litre^{-1} x 10^{-3})	8.8	6.7	0.59	0.04	1.3	0.4	1.1	22.55

The parameter I is computed from the expression:

$$I = \frac{\Sigma M_i Z_i^2}{2} \qquad (52)$$

where M is the concentration of a given ion, in moles per litre. The summation assumes that every ionic species present in solution is known. In practice only the ten or so major contributing ions are needed for a reasonably accurate estimate of ionic strength. Using mean compositional parameters for the Site 7 waters, I = 0.0934.

Table 18 shows the computed values of each ion in the Site 7 waters based on this value of I. In subsequent calculations activities of pure solids and pure liquids are taken to be unity and the activity of a gas phase equal to its pressure in atmosphere.

8.2.2 The Stability of Water

Since we are primarily interested in the stabilities of minerals in the presence of an aqueous phase the first stage in construction of an Eh-pH diagram is the plotting of the region in which liquid H_2O is itself stable. The reaction can be written:

$$2H_2O_l = O_{2g} + 4H^+_{aq} + 4e \qquad *(53)$$

$$\Delta G^o_f = -56.69 \qquad 0 \qquad 0$$

$$\Delta G^o_r = 0 + (4x0) - (2x(-56.69)) = +\ 113.4\ \text{kcal.}$$

$$E^o = \frac{\Delta G^o_r}{nx23.06} = \frac{113.4}{4x23.06} = 1.23\ \text{volt}$$

$$Eh = E^o + \frac{0.059}{n} \log \frac{P_{O_2} \left[H^+\right]^4}{\left[H_2O\right]^2} \qquad *(54)$$

Since P_{O_2} and H_2O are unity,

$$Eh = 1.23 + \frac{0.059}{4} \log \left[H^+\right]^4 \qquad *(55)$$

Figure 30 Eh-pH diagram for water and iron oxides

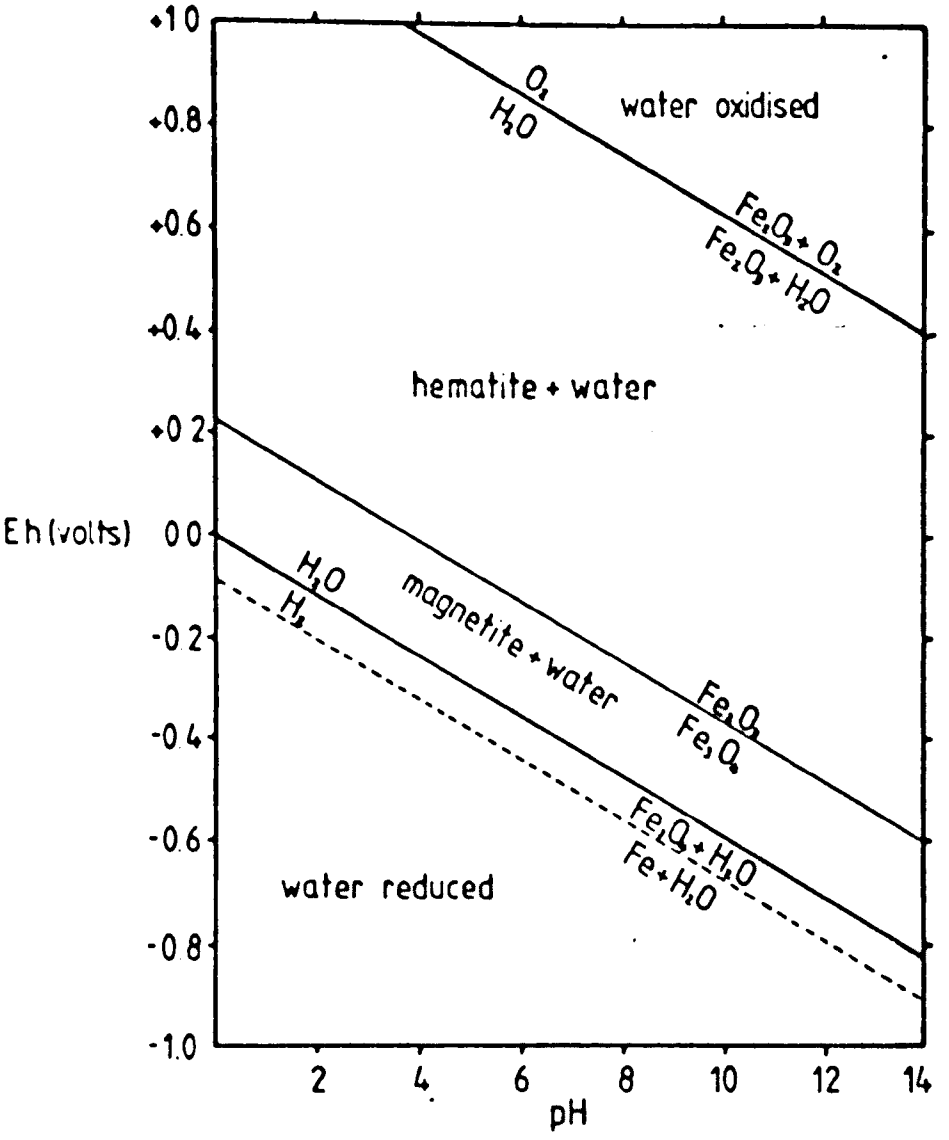
+1.0
+0.8
+0.6
+0.4
+0.2
0.0
-0.2
-0.4
-0.6
-0.8
-1.0
Eh (volts)
2
4
6
8
10
12
14
pH
O2
H2O
water oxidised
Fe2O3 + O2
Fe3O4 + H2O
hematite + water
H2O
H2
magnetite + water
Fe2O3
Fe3O4
Fe3O4 + H2O
Fe + H2O
water reduced

Substituting -pH for $[H^+]$

$$\underline{Eh = 1.23 - 0.059\ pH} \qquad *(56)$$

A line representing this equation can be plotted on an Eh-pH diagram, having an intercept of 1.23 volt Eh and a slope of -0.059 pH, (see Figure 30). This line represents the equilibrium between water and oxygen at 1 atmosphere total pressure. A similar line representing the lower stability limit of water (in equilibrium with hydrogen gas) can similarly be found from the half-reaction:

$$H_{2g} = 2H^+_{aq} + 2e \qquad *(57)$$

$$\Delta G^o_f = 0 \qquad 0 \qquad , \quad G^o_r = 0 - 0 = 0$$

and $$E^o = \frac{0}{2x23.06} = 0$$

Therefore:

$$Eh = 0 + \frac{0.059}{2} \log \frac{[H^+]^2}{P_{H_2}} \qquad *(58)$$

$$= \underline{0-0.059\ pH} \quad \text{for } P_{H_2} = 1 \qquad *(59)$$

The region between these two lines (shown on Figure 30) represents those conditions of Eh and pH under which water, at or near the surface of the earth, is stable.

8.2.3 The Iron Oxides

By expressing reactions between minerals (in the presence of water) in oxidation-reduction terms it is possible to calculate stability fields in much the same way as for water itself. Since iron minerals are of particular interest in this study the stability relationships between the various possible phases containing iron will be studied in more detail.

The stable iron oxides in surface environments are hematite and magnetite. By eliminating oxygen from the reaction describing the oxidation of iron to magnetite and adding in its place the water dissociation half-cell we can write:

$$3Fe_c + 4H_2O_l = Fe_3O_{4c} + 8H^+_{aq} + 8e \qquad *(60)$$

ΔG^o_f = 0 -56.69 -242.4 0

$\Delta G^o_r = -242.4 + (8x0) - (3x0) - (4x(-56.69)) = -15.6$ kcal.

$$E^o = \frac{-15.6}{8x23.06} = -0.084 \text{ volt}$$

$$Eh = -0.084 + \frac{0.059}{8} \log \frac{[Fe_3O_4][H^+]^8}{[Fe]^3 [H_2O]^4}$$

$$= -0.084 + \frac{0.059}{8} \log [H^+]^8 \qquad *(61)$$

Substituting -pH for $\log [H^+]$

$$Eh = \underline{-0.084 - 0.059 \text{ pH}} \qquad *(62)$$

Therefore, the reaction between iron and magnetite is a straight line with the same slope as the H_2O-H_2 boundary. Since the Fe-Fe_3O_4 line is below the lower stability limit of water, this reaction cannot take place in the presence of water if equilibrium is maintained.

The oxidation of magnetite to hematite can be represented by:

$$2Fe_3O_{4c} + H_2O_l = 3Fe_2O_{3c} + 2H^+_{aq} + 2e \qquad *(63)$$

ΔG^o_f = -242.4 -56.69 -177.1 0

$\Delta G^o_r = (3x(-177.1)) + (2x0) - (2x(-242.4)) - (-56.69) = +10.2$ kcal.

Figure 31 Eh-pH diagram for iron hydroxides

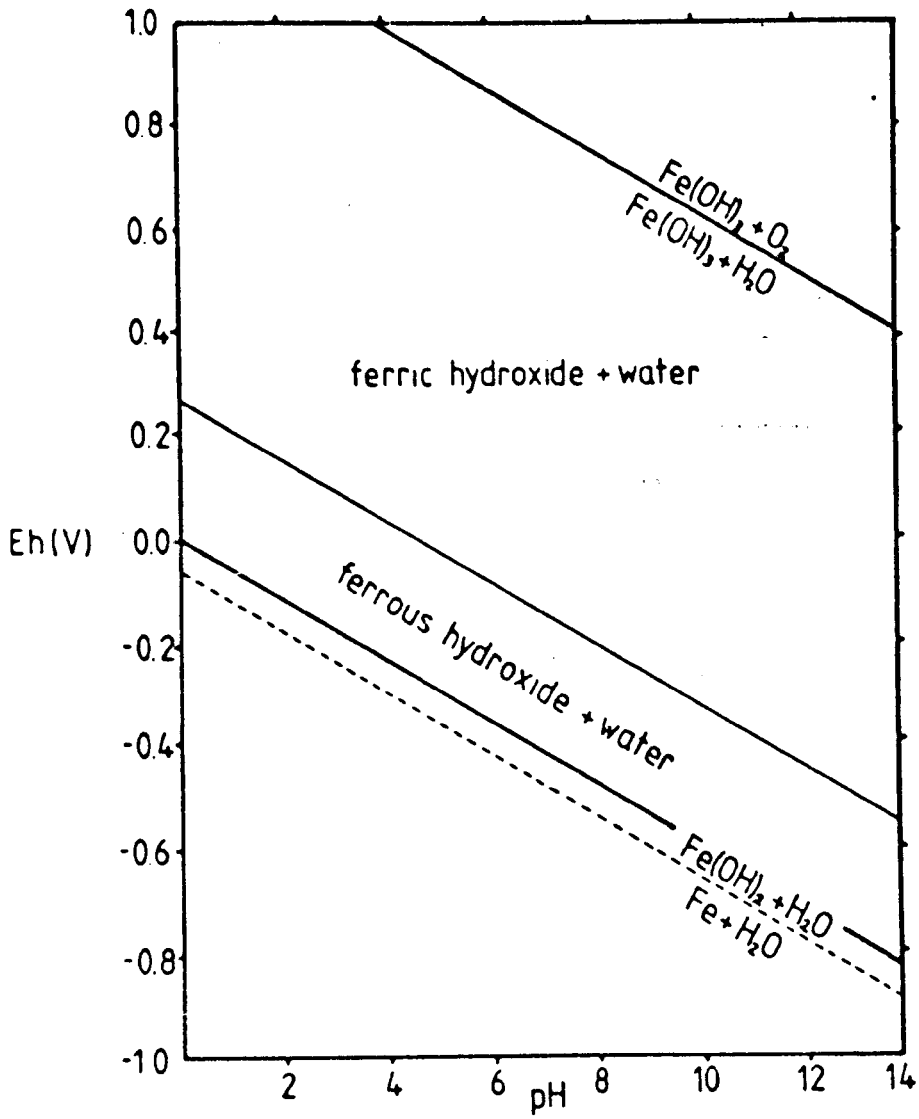
1.0
0.8
0.6
0.4
0.2
0.0
-0.2
-0.4
-0.6
-0.8
-1.0
Eh(V)
2
4
6
8
10
12
14
pH
Fe(OH)₂ + O₂
Fe(OH)₃ + H₂O
ferric hydroxide + water
ferrous hydroxide + water
Fe(OH)₂ + H₂O
Fe + H₂O

$$E^o = \frac{+10.2}{2x23.06} = 0.221 \text{ volt}$$

$$Eh = 0.221 + \frac{0.059}{2} \log \frac{[Fe_2O_3]^3 [H^+]^2}{[Fe_3O_4]^2 [H_2O]} \quad *(64)$$

$$= \underline{0.221-0.059 \text{ pH}} \quad *(65)$$

This line once again has the same slope but this time lies within the stability region for water (see Figure 30).

8.2.4 Iron Hydroxides

Hydroxides of iron are usually the first minerals to form as precipitates from solution. Both ferrous and ferric hydroxides, however, are unstable with respect to the more ordered forms considered above, but nevertheless may persist for some time as colloidal suspensions or stream bed (ochre) coatings. The fact that considerable periods of time are needed for the conversion to hematite or goethite has been noted in this study as well as in numerous others described in more detail in Section 7.6.3.

The stability fields for hydroxides of iron, although ephemeral, can be plotted in the same way as for the oxides. The reactions involved are given below, without the intermediate stages:

Ferrous hydroxide: $Fe_c + 2H_2O_l = Fe(OH)_{2c} + 2H^+_{aq} + 2e$ *(66)

$Eh = -0.047 - 0.059 \text{ pH}$ *(67)

Ferric hydroxide: $Fe(OH)_{2c} + H_2O_l = Fe(OH)_{3c} + H^+_{aq} + e$ *(68)

$Eh = 0.271 - 0.059 \text{ pH}$ *(69)

The resulting diagram (Figure 31) is remarkably similar to that for the oxides.

The fact that freshly precipitated ferric hydroxide will in time change to hematite or goethite is predicted by the negative free energy of reaction in the following equation:

$$2Fe(OH)_{3pptd} = Fe_2O_{3c} + 3H_2O_l \qquad *(70)$$

$$\Delta G^o_f = \quad -166.0 \qquad -177.1 \quad -56.69$$

$$\Delta G^o_r = -177.1 + (3x(-56.69)) - (2x(-166.0)) = -15.17 \text{ kcal.} \qquad *(71)$$

8.2.5 Relationships Among Ions

Since free energy data are also available for ions in aqueous solution it is possible to calculate fields of stability for ions in equilibrium with the solids. Certain of these reactions do not involve oxidation or reduction and are, therefore, independent of Eh. Such is that between the ferric ion and ferric oxide:

$$Fe_2O_{3c} + 6H^+_{aq} = 2Fe^{3+}_{aq} + 3H_2O_l \qquad *(72)$$

$$\Delta G^o_f = -177.1 \quad 0 \quad -2.53 \quad -56.69$$

$$\Delta G^o_r = (2x(-2.53)) + (3x(-56.69)) - (-177.1) - (6x0) = +2.0 \text{ kcal} \qquad *(73)$$

Since it is not possible to calculate Eh the equilibrium constant for the reaction must be used. For the reaction:

$$aA + bB = cC + dD \qquad (48)$$

the equilibrium constant is given by:

$$K = \frac{[C]^c [D]^d}{[A]^a [B]^b} \qquad (74)$$

and K is in turn related to the standard free energy as follows:

$$\Delta G^o_r = -RT \ln K \qquad (75)$$

where R and T are the gas constant and absolute temperature, as before. At 25°C:

$$\Delta G^{o}_{r} = -1.364 \log K \quad (76)$$

Therefore for the reaction of ferric iron with ferric oxide:

$$\log K = \frac{\Delta G^{o}_{r}}{-1.364} = \frac{2.0}{-1.364} = -1.45 \quad (77)$$

Since $[Fe_2O_3]$ and $[H_2O]$ are unity

$$\log \frac{[Fe^{3+}]^2}{[H^+]^6} = -1.45 \quad (78)$$

Rearranging and substituting -pH for $[H^+]$

$$2 \log [Fe^{3+}] = -1.45 - 6 \text{ pH} \quad *(79)$$

Thus, if the activity of ferric iron is stipulated then pH is fixed. Figure 32 shows contours of $[Fe^{3+}]$ plotted in this way. $[Fe^{3+}] = 10^{-3}$ is shown as a heavy line since this is approximately the value for Site 7 water (see Table 18).

Oxidation *is* involved in the reaction between ferric ions and magnetite which can be represented by:

$$Fe_3O_{4c} + 8H^+_{aq} = 3Fe^{3+}_{aq} + 4H_2O_l + e \quad *(80)$$

where $$Eh = 0.337 + 0.177 \log [Fe^{3+}] + 0.472 \text{ pH} \quad *(81)$$

Here a value of either Eh or pH must also be stipulated in addition to $[Fe^{3+}]$. The contours on Figure 32 are easily extended through the magnetite stability field by taking the pH values at the point where the Fe_2O_3-Fe_3O_4 line is reached.

The reactions necessary to calculate the relations of other possible ions to hematite and magnetite are given below without intermediate steps.

Figure 32 Composite Eh-pH Diagram Illustrating the 'Solubility' of Ferric and Ferrous Ions. Total Activity of Iron = 10^{-3} molar

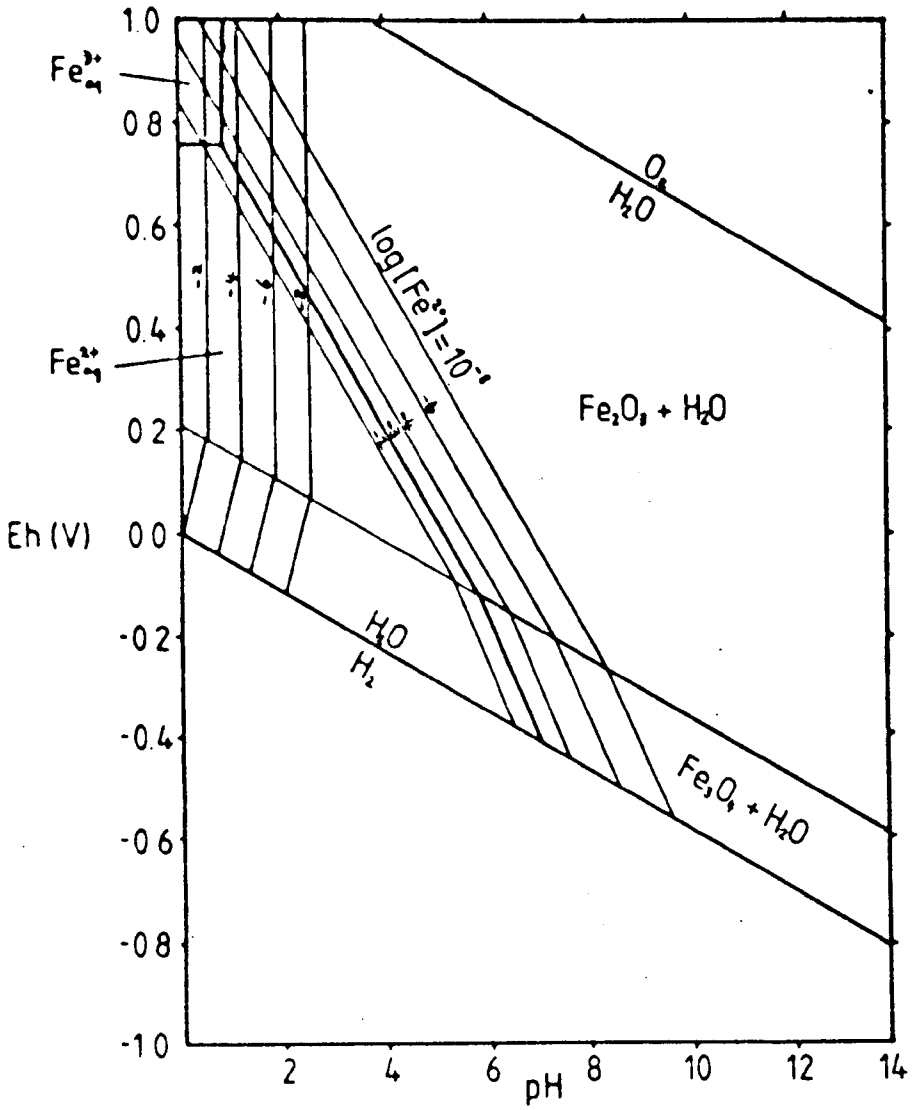
1.0
0.8
0.6
0.4
0.2
0.0
-0.2
-0.4
-0.6
-0.8
-1.0
Eh (V)
Fe^{3+}_{aq}
Fe^{2+}_{aq}
O_2
H_2O
H_2O
H_2
$Fe_2O_3 + H_2O$
$Fe_3O_4 + H_2O$
2
4
6
8
10
12
14
pH

TABLE 19: Reactions Relating Ionic Activities to Hematite and Magnetite
(After Garrels and Christ, 1965, page 189)

$Fe_2O_3 + 6H^+ = 2Fe^{3+} + 3H_2O$	$\log [Fe^{3+}] = -0.72 - 3\ pH$	(82)
$Fe_3O_4 + 8H^+ = 3Fe^{3+} + 4H_2O + e$	$Eh = 0.337 + 0.177 \log [Fe^{3+}] + 0.472\ pH$	(83)
$2Fe(OH)^{2+} + H_2O = Fe_2O_3 + 4H^+$	$\log [FeOH^{3+}] = -3.151 - 2\ pH$	(84)
$Fe_3O_2 + 5H^+ = 3Fe(OH)^{2+} + H_2O + e$	$Eh = 0.780 + 0.177 \log [FeOH^{2+}] + 0.259\ pH$	(85)
$Fe_2O_3 + H_2O + 2H^+ = 2Fe(OH)_2^+$	$\log [Fe(OH)_2^+] = -7.84\ 1\ pH$	(86)
$Fe_3O_4 + 2H_2O + 2H^+ = 3Fe(OH)_2^+ + e$	$Eh = 1.61 + 0.177 \log [Fe(OH)_2^+] + 0.118\ pH$	(87)
$2Fe^{2+} + 3H_2O = Fe_2O_3 + 6H^+ + 2e$	$Eh = 0.720 - 0.059 \log [Fe^{2+}] - 0.177\ pH$	(88)
$3Fe^{2+} + 4H_2O = Fe_3O_4 + 8H^+ + 2e$	$Eh = 0.980 - 0.088 \log [Fe^{2+}] - 0.236\ pH$	(89)
$2Fe(OH)^+ + H_2O = Fe_2O_3 + 4H^+ + 2e$	$Eh = 0.217 - 0.059 \log [Fe(OH)^+] - 0.118\ pH$	(90)
$3Fe(OH)^+ + H_2O = Fe_3O_4 + 5H^+ + 2e$	$Eh = 0.214 - 0.088 \log [Fe(OH)^+] - 0.148\ pH$	(91)
$2HFeO_2^- = Fe_2O_3 + H_2O + 2e$	$Eh = -1.139 - 0.059 \log [HFeO_2^-]$	(92)
$2HFeO_2^- + H^+ = Fe_2O_4 + 2H_2O + 2e$	$Eh = -1.819 - 0.088 \log [HFeO_2^-] + 0.029\ pH$	(93)

All this information is brought together into a composite diagram in Figure 32. Boundaries are drawn in by joining points of equal activity at their intersection, as illustrated in the case of Fe^{2+} and Fe^{3+} in Figure 35, and represent a set of points where the activity of the ion dominant in the field on one side is equal to the activity of that dominant on the other side.

The fields of many of the ions considered in Table 16 do not appear in the final diagram (Figure 32). This is due to the fact that they occupy parts of the fields already assigned to Fe^{2+} and Fe^{3+}. The latter ions dominate these fields and the effect of other ions is negligible. Thus, very few of the total possible species are in fact present in appreciable amounts within the stability field of water. Possibly the two most striking features of Figure 32 are the small field of Fe^{3+} at highly acid, oxidising conditions and the large field of hematite which is stable over a considerable range of conditions from acid-oxidising to alkaline-reducing.

A line representing the stability of ferrous ions in equilibrium with goethite rather than hematite is shown on Figure 34 as calculated from the relationship:

$$Fe^{2+}_{aq} + 2H_2O_l = HFeO_{2c} + 3H^+_{aq} + e \qquad (94)$$

$$Eh = 0.73 - 0.118 \log Fe^{2+} - 0.177\ pH \qquad (95)$$

This lies very close to the Fe^{2+}-Fe_2O_3 boundary for $[Fe^{2+}] = 10^{-3}$ and shows that the minerals hematite and goethite have virtually identical stability fields.

8.2.6 Dissolved Sulphur Species

By adding sulphur to the iron-oxygen-water system which has been developed here, information can be obtained regarding the iron sulphide

Figure 33 Eh-pH diagram for dissolved sulphur species. Total activity of sulphur = 10^{-1} molar.

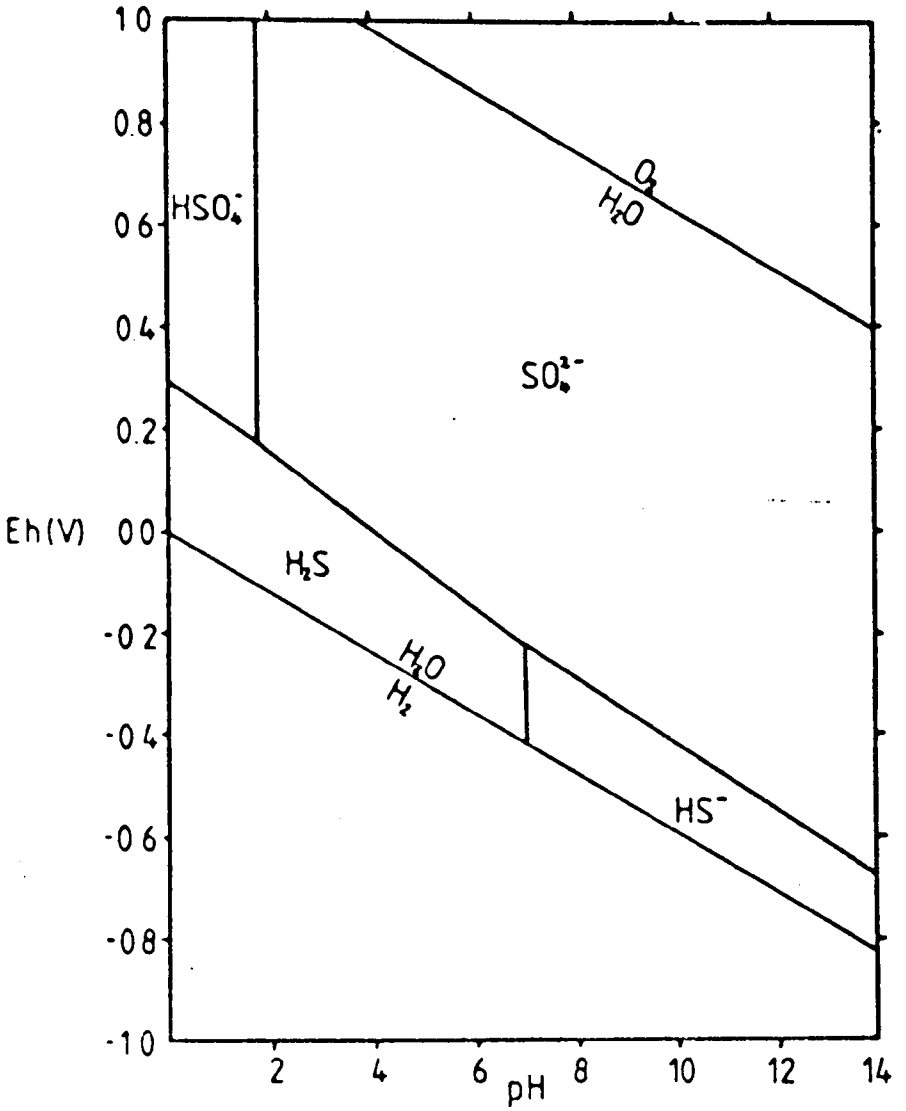
1.0
0.8
0.6
0.4
0.2
0.0
-0.2
-0.4
-0.6
-0.8
-1.0
Eh(V)
2
4
6
8
10
12
14
pH
HSO_4^-
O_2
H_2O
SO_4^{2-}
H_2S
H_2O
H_2
HS^-

Figure 34 Composite Eh-pH diagram for the system S-Fe-H_2O. Activity of sulphur = 10^{-1} molar; activity of iron = 10^{-3} molar.

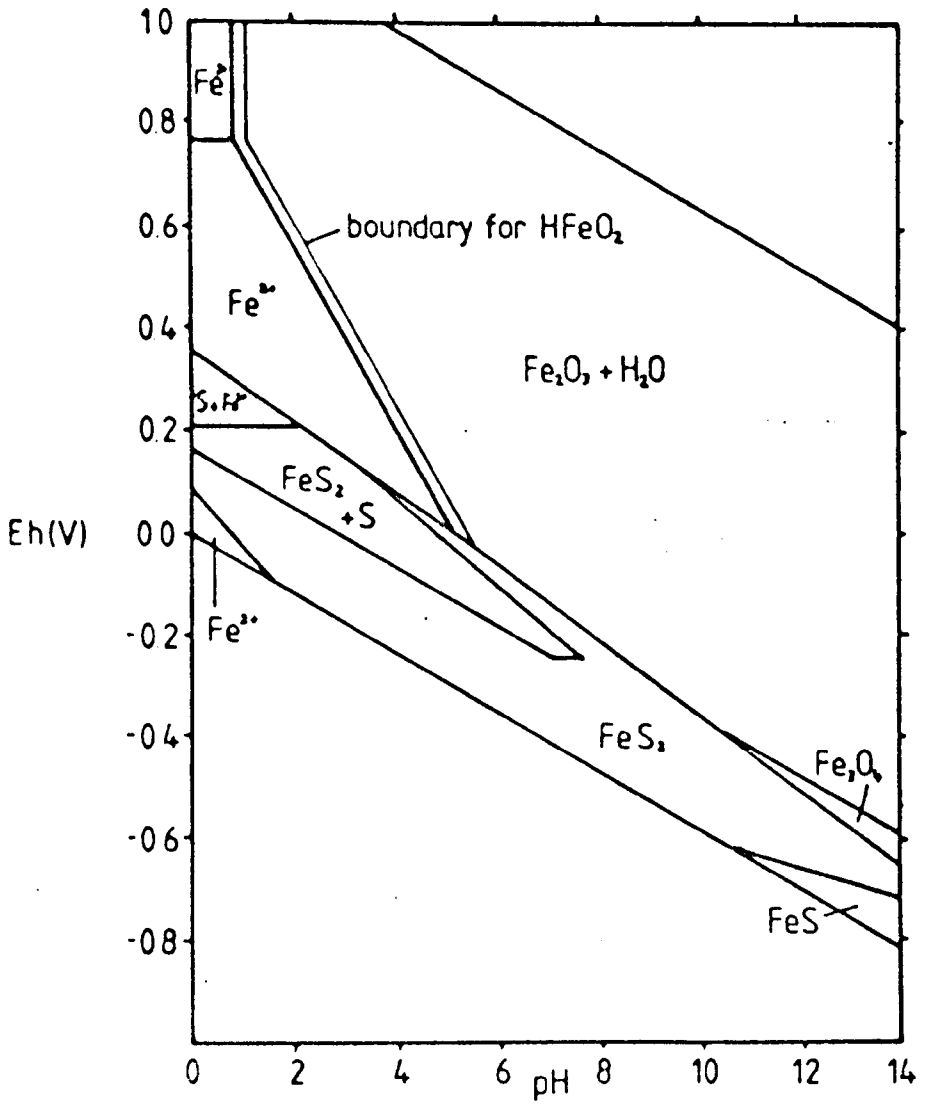
Eh(V)
1.0
0.8
0.6
0.4
0.2
0.0
-0.2
-0.4
-0.6
-0.8
0
2
4
6
pH
8
10
12
14
Fe
boundary for HFeO2
Fe3+
Fe2O3 + H2O
S, H+
FeS2 + S
Fe2+
FeS2
Fe3O4
FeS

Figure 35 Method of construction of field boundaries and the plotting of Eh-pH values of Mam Tor waters. See Table 22 for description of Samples 1-4.

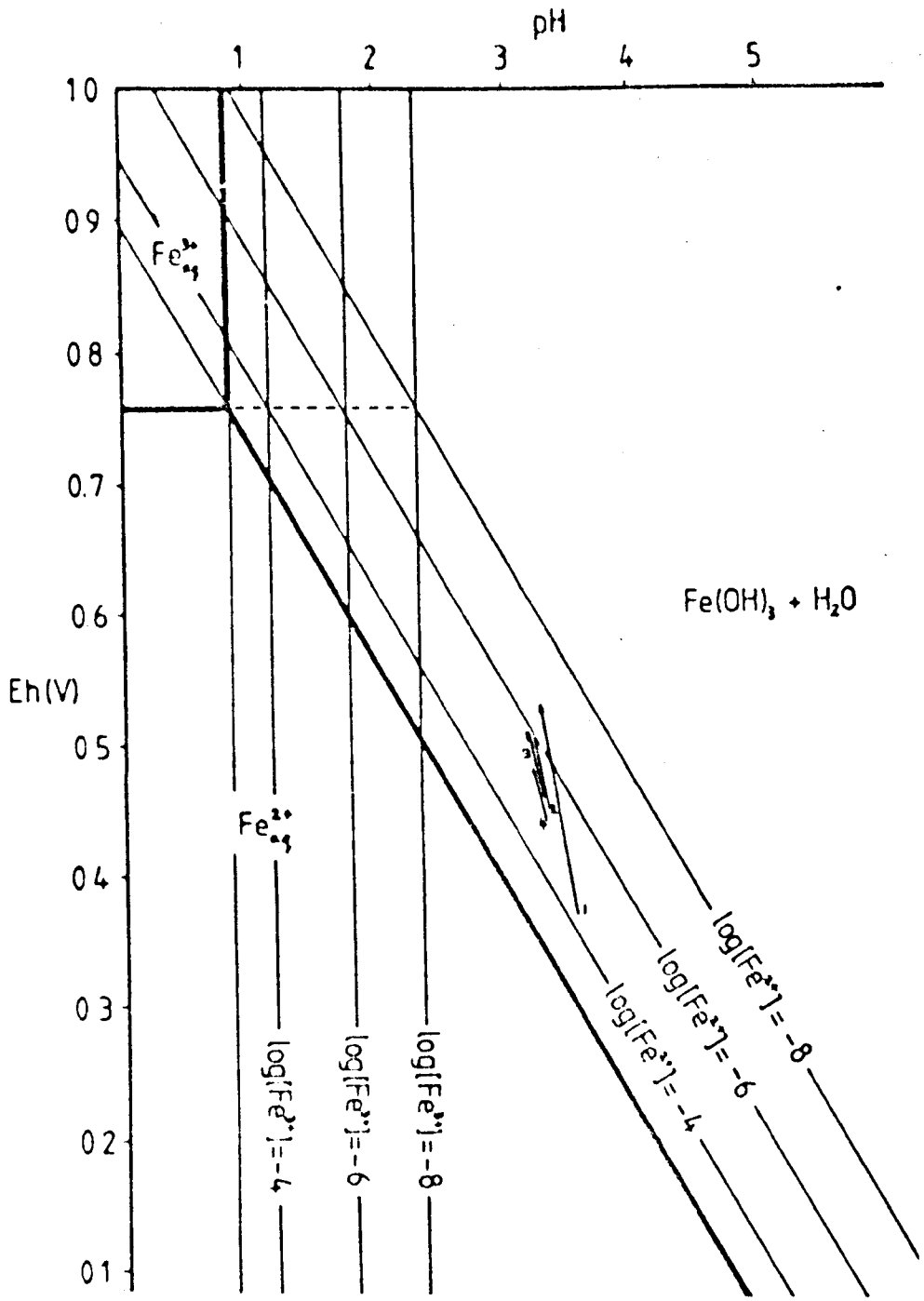
pH
1
2
3
4
5
10
09
08
0.7
0.6
Eh(V)
0.5
0.4
0.3
0.2
0.1
Fe^{3+}_{aq}
Fe^{2+}_{aq}
log[Fe²⁺]=-4
log[Fe²⁺]=-6
log[Fe²⁺]=-8
log[Fe²⁺]=-4
log[Fe²⁺]=-6
log[Fe²⁺]=-8
$Fe(OH)_3 + H_2O$

TABLE 20: Reactions Between Dissolved Sulphur Species for $[\text{Total Sulphur}] = 10^{-1}$

$$H_2S + 4H_2O = HSO_4^- + 9H^+ + 8e \qquad Eh = 0.290 - 0.066\ pH + 0.007 \log \frac{[HSO_4^-]}{[H_2S]} \qquad *(96)$$

$$H_2S + 4H_2O = SO_4^{2-} + 10H^+ + 8e \qquad Eh = 0.303 - 0.074\ pH + 0.007 \log \frac{[SO_4^{2-}]}{[H_2S]} \qquad *(97)$$

$$HS^- + 4H_2O = SO_4^{2-} + 9H^+ + 8e \qquad Eh = 0.252 - 0.066\ pH + 0.007 \log \frac{[SO_4^{2-}]}{[HS^-]} \qquad *(98)$$

$$S^{2-} + 4H_2O = SO_4^{2-} + 8H^+ + 8e \qquad Eh = 0.148 - 0.059\ pH + 0.007 \log \frac{[SO_4^{2-}]}{[S^{2-}]} \qquad *(99)$$

minerals pyrite and pyrrhotite. The reactions listed in Table 20 help delimit the stability fields of the various dissolved sulphur species plotted on Figure 33.

At the boundaries the activities of sulphur species on each side are equal and lines can be drawn as simple functions of Eh and Ph. The boundary between HSO_4^- and SO_4^{2-} is obtained from the relation:

$$HSO_{4\ aq}^- = H^+_{aq} + SO_{4\ aq}^{2-} \qquad *(100)$$

$$\frac{[SO_4^{2-}]}{[HSO_4^-]} = \frac{K_{HSO_4}}{[H^+]} = \frac{10^{-1.9}}{[H^+]} \qquad *(101)$$

Since the activity of SO_4^{2-} in the Site 7 water is approximately 10^{-1} moles per litre the boundaries of Figure 33 are drawn for this value.

8.2.7 The Composite Diagram

In considering reactions between the sulphides and iron oxides it is found that many of the theoretical boundaries lie outside the stability field of water, and pyrite is the stable mineral throughout the H_2S field. The reactions and Eh equations used to calculate the boundaries on the composite diagram (Figure 34) are given in Table 21.

The Eh-pH diagrams presented here are the simplest that can be drawn based on the water compositional parameters of Table 18. Other dissolved species included in Table 16 could be incorporated into the diagram together with dissolved CO_2 and other gaseous phases which are undoubtedly present before the Site 7 waters emerge at the surface.

It is, however, beyond the scope of this study to do so since the final composite diagram (Figure 34) adequately describes the relationships which have been observed in the field. Discussion of these observations in terms of Eh and pH follows in the next Section.

Figure 36 Eh-pH diagram for iron hydroxides and sulphides, including jarosite. After van Breemen, 1972.

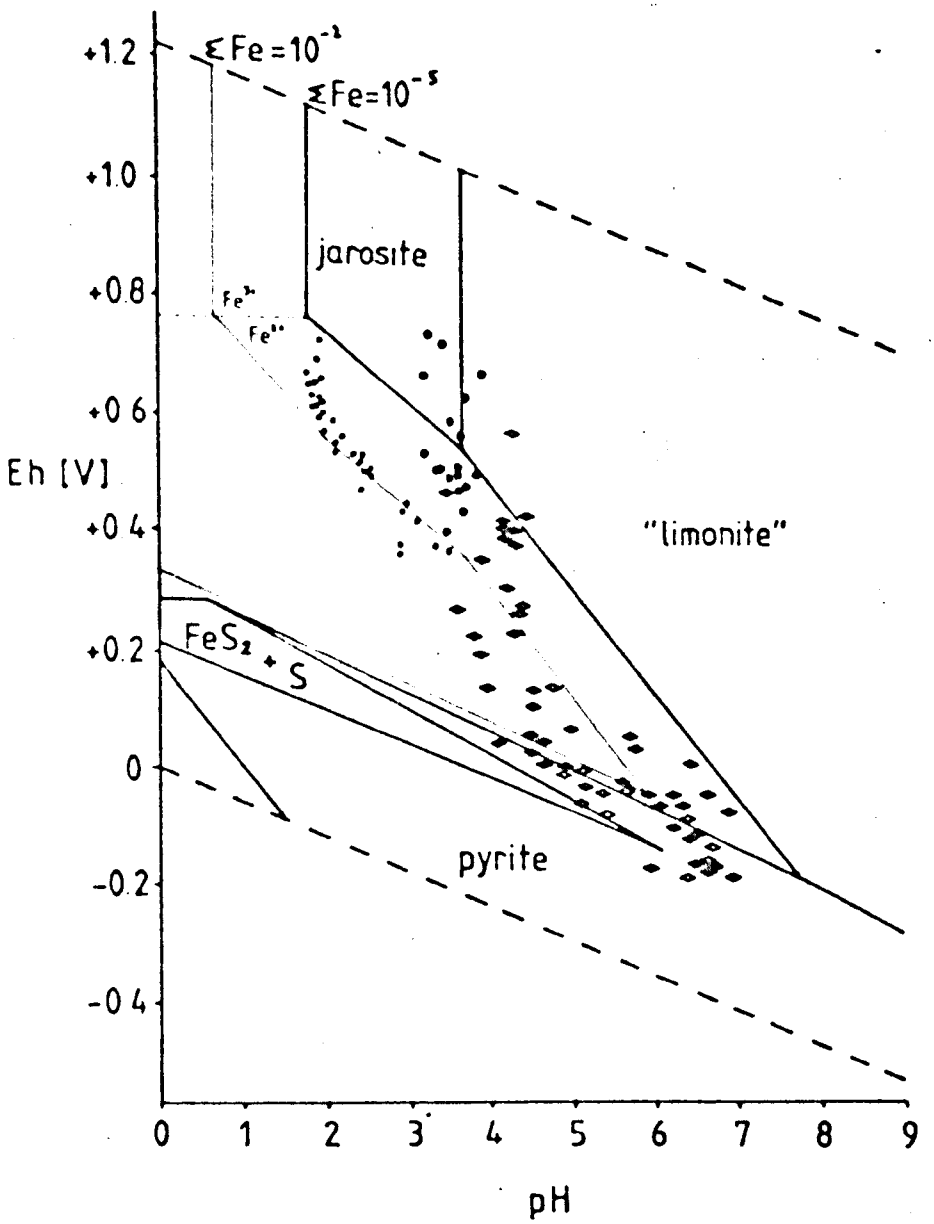
+1.2
+1.0
+0.8
+0.6
+0.4
+0.2
0
-0.2
-0.4
Eh [V]
0
1
2
3
4
5
6
7
8
9
pH
ΣFe=10⁻²
ΣFe=10⁻⁵
jarosite
Fe³⁺
Fe²⁺
"limonite"
FeS₂ + S
pyrite

TABLE 21: Reactions between Ions, Dissolved Sulphur Species and Solids

$FeS + HS^- = FeS_2 + H^+ + 2e$	$Eh = -0.340 - 0.029\ pH - 0.029\ \log 10^{-1}$	*(102)
$2FeS_2 + 19H_2O = Fe_2O_3 + 4SO_4^{2-} + 28H^+ + 30e$	$Eh = 0.380 - 0.075\ pH + 0.008\ \log 10^{-1}$	*(103)
$3FeS_2 + 28H_2O = Fe_3O_4 + 6SO_4^{2-} + 56H^+ + 44e$	$Eh = 0.384 - 0.075\ pH + 0.008\ \log 10^{-1}$	*(104)
$2FeS_2 + 19H_2O = 4HSO_4^- + Fe_2O_3 + 34H^+ + 30e$	$Eh = 0.366 - 0.067\ pH + 0.008\ \log 10^{-1}$	*(105)
$2H_2S + Fe^{2+} = FeS_2 + 4H^+ + 2e$	$Eh = 0.057 - 0.118\ pH - 0.059\ \log 10^{-1} - 0.029\ \log[Fe^{2+}]$	*(106)
$FeS_2 + 8H_2O = 2HSO_4^- + Fe^{2+} + 14H^+ + 14e$	$Eh = 0.339 - 0.059\ pH + 0.008\ \log 10^{-1} + 0.004\ \log[Fe^{2+}]$	*(107)
$FeS_2 + 8H_2O = 2SO_4^{2-} + Fe^{2+} + 16H^+ + 14e$	$Eh = 0.354 - 0.067\ pH + 0.008\ \log 10^{-1} + 0.004\ \log[Fe^{2+}]$	*(108)
$2HS^- + Fe^{2+} = FeS_2 + 2H^+ + 2e$	$Eh = -0.470 - 0.059\ pH - 0.059\ \log 10^{-1} - 0.029\ \log[Fe^{2+}]$	*(109)
$FeS_2 = Fe^{2+} + 2S + 2e$	$Eh = 0.340 + 0.029\ \log[Fe^{2+}]$	*(110)
$FeS + H^+ = Fe^{2+} + HS^-$	$\log[Fe^{2+}] = -4.4 - pH - \log 10^{-1}$	*(111)

The reader interested in Eh-pH diagrams in general, and their extension to other systems, is referred to the following publications. General and iron system diagrams: Hem, 1961; Hem, 1970; Hem and Cropper, 1959; Barnes and Back, 1964. Aluminium, fluoride and sulphate: Hem, 1968. Bicarbonate and iron: Hem, 1960a. Manganese: Hem, 1972. Sulphur species: Garrels and Naeser, 1958; Hem, 1960b. Trace metals: Hem, 1977.

Van Breemen (1972) considers the mineral jarosite in an iron stability field diagram. This is reproduced in Figure 36 purely for interest, as the activities of certain species are far removed from those used in this study. The jarosite field would be appreciably smaller had Van Breemen constructed the diagram for the stable minerals goethite and hematite rather than for the metastable 'limonitic Fe_2O_3'.

8.3 Further Consideration of the Eh-pH Diagrams

The measurement of oxidation-reduction (redox) potentials depends on the use of an electrode made from a noble metal, commonly platinum. When such an electrode is placed in a solution containing, say, ferric ions the rod becomes positively charged as the Fe^{3+} ions react with electrons from the platinum:

$$Fe^{3+} + e^{-} = Fe^{2+} \qquad (112)$$

Conversely, when the electrode is placed in a solution containing only Fe^{2+} ions it becomes negatively charged.

The amount of negative or positive charge developed, measured relative to a zero reference electrode (commonly of calomel), is dependent upon the ratio of reduced to oxidised species present. A solution having a negative redox potential is reducing, and one with a positive potential is oxidising.

TABLE 22: pH and Redox Measurements on Four Mam Tor Samples

Sample Number	Location	Eh (volt)[1]	Eh (volt)[2]	pH[1]	pH[2]
1	Site 7	+0.365	+0.535	3.5	3.2
2	10 m downstream from Site 7	+0.448	+0.506	3.3	3.2
3	Site 11	+0.459	+0.510	3.3	3.1
4	Waterfall above mixing site (Odin Sitch)	+0.439	+0.477	3.3	3.2

Suffixes: 1 = 40 minutes after sampling on 23rd January, 1980

2 = two weeks after sampling - 6th February, 1980

In highly oxygenated waters a layer of oxide may form on the surface of the electrode and reactions such as that given above (Equation 112) may become irreversible. It is essential, therefore, to periodically clean the Pt in a strong acid solution, such as hot H_2SO_4.

Many systems of interest to the geologist, such as dilute aqueous solutions and soft sediments, present problems in measuring redox potential and in the interpretation of results (see Golterman, 1975; Schindler and Honick, 1971). Complex ions and ions with valencies greater than about 3 are often responsible for inconsistent and ambiguous readings.

The aqueous system presented by Spring 7, however, appears to be one which can, at least in part, be adequately described in terms of Eh and pH. This is due to the fact that the ionic strength of the solution is relatively high (facilitating accurate redox measurements) and the system is dominated by a few simple ions.

In addition to illustrating the method of construction of field boundaries, Figure 35 also contains plots of Eh-pH values recorded at Mam Tor. Redox potentials were measured using platinum and calomel electrodes on an Orion Research Microprocessor ionalyser (Model 901). This instrument is fragile and requires an electrical power supply and, therefore, could not be taken into the field. Instead samples were collected in airtight polythene bottles, from which all the air was excluded, and returned to the laboratory for analysis within forty minutes of collection.

Values plotted on Figure 35 are from Table 22. The four sites are located at irregular intervals along the stream flowing between Site 7 and the Odin Sitch. In addition to readings taken immediately on return to the laboratory corresponding measurements were made, two weeks after collection, on the same samples. During the interim period the sample bottles were left covered but not sealed and placed in full light (not direct sunlight) on a windowsill.

These solutions originally plot on Figure 35 in the stability field of ferric hydroxide. Since ochre can be seen to precipitate along the length of the stream this is not entirely unexpected, and the water must be supersaturated with respect to ferric hydroxide.

With continued oxidation, presumably caused by mixing with atmospheric oxygen, the waters attain higher redox potentials while at the same time pH falls slightly. The precipitation reaction has been given previously as:

$$2Fe^{2+} + \tfrac{1}{2}O_2 + 5H_2O = 2Fe(OH)_3 + 4H^+ \qquad (19)$$

and it was noted in Section 4.4.2, that with time ferrous ions are indeed lost from solution. This cannot be accounted for, however, by simple oxidation to ferric ions as seems to be suggested in Table 4. The generation of hydrogen ions by reaction (19) clearly illustrates why ferric hydroxide precipitation makes the solution more acid.

Buffering of the waters to the narrow pH range of 3 to 3.5 (noted in Section 4.4.1 and illustrated by Figure 11) can also be explained in terms of the stability field diagram. It can be seen that as the solutions move up towards higher Eh and lower pH values the solubility of ferrous iron becomes vanishingly small. Once a pH of about 3.0 is reached the log of the activity of ferrous iron is less than 10^{-8}, so small that further ochre precipitation is precluded and the pH can fall no more.

Extrapolating back from the initial pH and Eh values of Figure 35 the 'starting point' for the oxidation of these waters can be found (or more precisely, the region in which the starting point will lie). This can be seen from Figures 33 and 34. to be the region where pyrite is in equilibrium with SO_4^{2-} and Fe^{2+} ions - the precise environment produced by pyrite oxidation according to the mechanism discussed in Section 6.

Baas Becking et al. (1960), have accumulated most of the Eh-pH data available from the literature on natural waters up to 1960. This inform-

Figure 37 Eh-pH diagram showing the field of natural waters. After Baas-Becking et al., 1960.

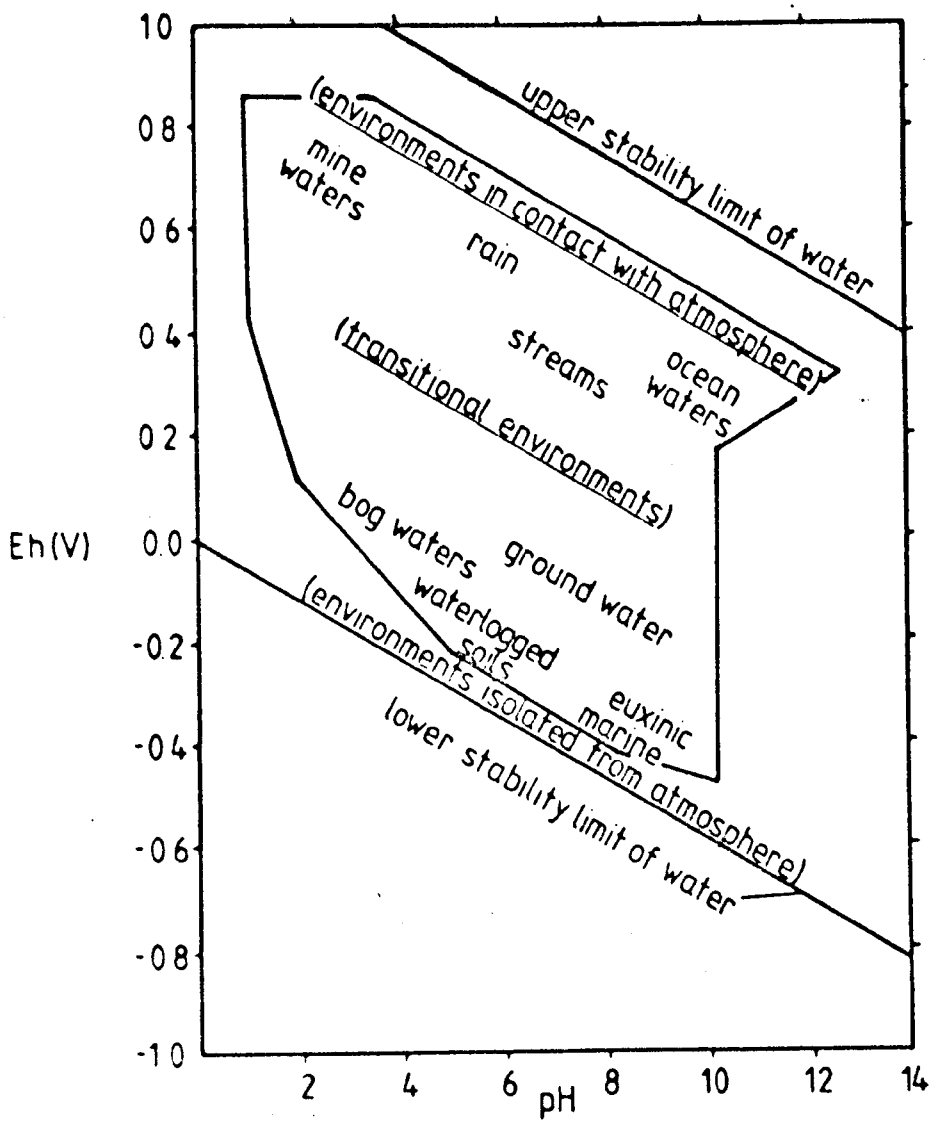
Eh(V)
10
0.8
0.6
0.4
0.2
0.0
-0.2
-0.4
-0.6
-0.8
-1.0
2
4
6
pH
8
10
12
14
upper stability limit of water
(environments in contact with atmosphere)
mine waters
rain
streams
ocean waters
(transitional environments)
bog waters
ground water
waterlogged soils
euxinic marine
(environments isolated from atmosphere)
lower stability limit of water

ation is reproduced in diagrammatic form in Figure 37.

It can be seen that highly oxygenated surface waters (including acid mine drainage) plot along a line parallel to the upper stability of water itself. Sato (1960) believes that this represents the true upper limit of water in as much as further oxidation can only proceed via a rate-determining, intermediate hydrogen peroxide step.

From Figure 37 it is apparent that the 'starting point' of the (underground) Mam Tor waters is in the region which overlaps the three labels, 'ground water', 'bog water' and 'waterlogged soils'. After emergence and continued oxidation the Eh and pH approach the region labelled 'mine waters' at the extreme upper limit of aqueous environments. This once again reaffirms the similarity between these and acid mine drainage solutions.

8.4 Gypsum Solubility

The only other mineral which can be seen to precipitate directly from solution in the seepage areas is gypsum (see Section 7.6.1). Since only a short dry spell of weather is required for this mineral to begin to precipitate on the seepage vegetation by non-equilibrium evaporation (Smith and Drever, 1976), it is thought that the waters must already be close to saturation with $CaSO_4$.

Table 18 lists the activities of the major solutes in the Site 7 waters. From these figures can be calculated the *solubility product* of gypsum as follows:

$$K = [Ca^{2+}] \; [SO_4^{2-}] \qquad (113)$$

$$= 0.0088 \times 0.0225$$

$$= 1.98 \times 10^{-4}$$

$$= \underline{10^{-3.7}}$$

From published equilibrium constant data, however, the solubility product of gypsum is given as $10^{-4.6}$ (Sillen and Martell, 1964). The value calculated for Site 7 is nearly eight times greater than this, which predicts that the seepage waters are supersaturated with respect to gypsum.

This clearly is incorrect since gypsum only precipitates after capillary rise up the plant stems and subsequent evaporation. Any crystals falling back into the water are re-dissolved, proving that the waters are undersaturated.

One possible explanation of this anomaly is that the ion pair $CaSO_4^o$ (zero charge), or more complex ligands, are forming in solution. These would have the effect of lowering the solubility of gypsum whilst at the same time contributing to the Ca^{2+} and SO_4^{2-} content of the waters during chemical analysis. Thepresence of other species such as $MgSO_4$ or $FeSO_4$ are also known to lower the solubility of gypsum in high ionic strength solutions (Tanji and Doneen,1966).

Alternatively, gypsum solubility might be a function of Eh, pH and ionic content of the waters, in much the same way as for ferrous iron, and may not be explained in terms of simple solubility products.

The conclusions that can be drawn from this Section on thermodynamic chemistry are four-fold.

In the first place, the elevated and constant temperature of the waters emerging at Site 7 can be accounted for. Chemical reactions raise the temperature some 2.5°C above the normal groundwater value in this area of 7°C. The importance of such reactions in the spontaneous combustion of certain coal spoils is also noted.

Secondly, oxygenation of these waters causes supersaturation with respect to ferric hydroxide and deposits of ochre form in the seepage

areas. With time this freshly precipitated 'limonite' will convert to the more stable forms goethite or hematite (see Section 7.6.3).

The precipitation of ferric hydroxide liberates H^+ ions and greatly acidifies the solutions. A natural lower limit on the acidity is imposed by decreasing solubility of ferrous ions in high Eh environments and the system is buffered at values around pH 3.0. This is in close agreement with the observations made in Section 4.4.1.

Finally calculations of the solubility of gypsum appear to be complicated by the presence of ionic $CaSO_4^o$ or other species containing calcium or sulphate. Gypsum does precipitate with increasing pH and on evaporation which suggests the solution must be at least close to saturation.

TABLE 23: Volume Changes Involved in the Three Principle Reactions

		SG	ΔV (ml)
1.5596 g	pyrite destroyed	5.0	-0.31
1.6880 g	dolomite destroyed	2.9	-0.58
0.9816 g	goethite precipitated	4.2	+0.23
		Total:	-0.66

9. CHEMICAL WEATHERING AND SLOPE STABILITY

This Section considers some of the ways in which chemical weathering could possibly influence the stability of the landslide. Mechanisms involving the dissolution and precipitation of minerals, the alteration of clays, and forces induced by repeated wetting and drying, and the maintenance of failure surfaces will be discussed. Finally, the importance of identifying the true cause of landslide movement will be stressed with reference to past management policies at Mam Tor.

9.1 Dissolution and Precipitation

Quantities of various mineral phases involved in the weathering sequence proposed in this study were calculated in Section 6.2. By considering the specific gravities (relative densities) of these minerals the volume changes involved in their formation or destruction can be calculated by simple division.

Table 23 lists the amounts of pyrite, dolomite and goethite involved together with average specific gravities (individual mineral specimens can show a range of values) and approximate volume changes incurred.

These reactions result in a net porosity increase of 0.66 ml per litre of percolating groundwater. With a calculated flow rate of 0.43 l sec^{-1} at Site 7 this means a net void creation of 0.89 m^3 per year accounted for by this stream alone. Volume changes induced by jarosite precipitation and clay mineral transformations are not taken into account as the effects are considered small in relation to the three dominant processes of Table 23.

Dissolution of pyrite and dolomite is probably not occurring at the same sites as secondary mineral precipitation. Once the various ions have entered into solution migration through pore spaces and fissures can

occur prior to secondary mineral growth. Other authors have also reported the formation of alteration products of these and similar reactions some distance from the source of the primary reactants (see Grattan-Bellew and Eden, 1975; Nordstrom and Dagenhart, 1968).

This implies that internal stresses may be built up within the rocks as voids are created in some areas and precipitating minerals create pressures in others (particularly along joint planes). Individually these internal stresses must be very slight, but the cumulative effect might be great enough to influence the stability of the mass as a whole or at least the most intensely weathered parts of it.

One of the most expansive weathering products of pyritic, calcareous shales is the sulphate gypsum. Pressures induced by the precipitation and growth of this mineral have been described previously (Section 1.2.3) in an engineering context.

At Mam Tor gypsum is only found near the surface and is not thought to form at depth. Nevertheless the nature of the surface accumulations, in joints and on bedding planes (Plate 4b, 5 and 21) must contribute to instability of the exposures particularly on steep slopes.

The appearance of this joint-filling gypsum is remarkably similar to that which causes floor heave (Grattan-Bellew and Eden, 1975; Quigley et al. 1973). Excellent scanning electron micrographs of gypsum crystals prising apart shale laminations are included in the former article (particularly that on p.375). The similarity between these pictures and the photomicrographs of weathered Edale Shales shown in Plates 3 and 4a is obvious. A further similarity is that Grattan-Bellew and Eden also also observe crystal growth in cracks both normal and at steep angles to bedding, similar to those shown in Plate 22b.

9.2 The Mechanism of Shale Breakdown

It was noted in the Introduction (Section 1.2.3) that certain authors believe purely chemical weathering processes to be of secondary importance in the breakdown of mudrocks (see, for example, Spears and Taylor, 1972). Essentially physical processes such as expansion in mixed-layer clays are thought to be rate-determining and after an initial rapid breakdown along joints and bedding planes further weathering (solution and cation exchange) proceeds relatively slowly.

In the shale samples from Mam Tor the quantity of expansive clays is generally small and only reaches significant proportions in the soil layers (Section 7.4.2). It is thought, therefore, that a much more effective process than clay mineral swelling might be the formation of expansive minerals in the natural fissures and discontinuities of the rocks, as described in Section 1.2.3 with reference to Goudie et al. (1970) and Cooke and Smalley (1968). Initial swelling of the expandable clay components,however, may create the necessary space for these minerals to begin to precipitate.

Spears et al. (1971) observe the presence of gypsum in coal mine spoil heaps and suggest that since it is a soluble mineral its occurrence implies insignificant leaching. It was noted in Section 7.6.1 that euhedral crystals of gypsum also persist in surface exposures of Edale Shales at Mam Tor. Here,rapid leaching takes place during heavy rainfall, since the material is so fragmented, but the exposures dry out rapidly when the rain stops and it is thought that the overall rate of gypsum precipitation (during evaporation and capillary rise of solutions through the shale) exceeds removal by percolating waters. A surface coating of iron oxide on the crystals, which appear red-brown, might also protect them from dissolution.

Spears et al. (op.cit.) also note that pyrite is abundant even in material at the surface of the spoil heaps and they propose that this is

further evidence of very slow weathering. Pyrite is also found in the exposures of Edale Shales (see Appendix Ci), usually in close association with carbonates which themselves have undergone intense weathering. Its appearance at the surface is somewhat of a mystery since it might be expected that over the years it would have been completely oxidised.

It is suggested that the persistence of pyrite could be due to the absence of *Thiobacilli* from these surface environments, where the pH may be too high to support them. Oxidation by atmospheric oxygen alone is too slow to completely remove pyrite in the space of a few years.

The repeated wetting and drying thought to account for the persistence of gypsum might in itself cause breakdown of shales, at least near to the surface. Taylor and Spears (1970), for example, conduct slaking tests on various Coal Measures rocks. They observe that breakdown is arrested if the tests are carried out *in vacuo*.

The mechanism causing air breakage is explained by Taylor and Spears as follows. During dry periods the shear resistance of rock fragments is increased by high contact pressures caused by surface evaporation. Any voids become filled with air which, when the water returns, as during a heavy rainfall event, is pressurised due to capillary forces in the outer pores. Failure along the weakest planes results, which further opens up the material. Taylor and Spears note that this mechanism is similar to that of soil slaking reported by Terzaghi and Peck (1967).

Since effective breakdown *in vacuo* has only occasionally been reported (see Badger et al. 1956; Berkovitch et al. 1959) air breakage of shales is considered an important mechanism and may contribute to instability at Mam Tor since oxygenated waters can readily gain access through the major joint systems and failure surfaces.

Once again there is clearly scope for further work concerning the breakdown mechanism of the Edale Shales. Engineering tests, which are

not considered here, could also prove useful if representative samples can be found and access gained to unweathered material.

9.3 Pore Water Pressure and Failure Surfaces

In surface exposures of weathered shales gypsum, jarosite and goethite can be seen to form along bedding planes and in joints. By contrast gypsum is not encountered in the borehole cores and jarosite is found only infrequently, presumably due to the fact that it only precipitates above the zone of groundwater saturation (Brown, 1971).

Goethite, however, is found at considerable depth within the landslide and although failure surfaces could not be positively identified (Figure 24) it is thought that this mineral is occurring principally as joint-fill or along surfaces of rupture. Hanshaw (1974) also observes ferric hydroxide in fissures of old mine workings well below the zone of aeration, illustrating that oxidation is possible so long as oxygenated waters can gain access.

Failure surfaces are often developed during times of unusually high pore water pressures resulting from a rise in the water table. Conditions at the end of the Pleistocene glaciation were favourable for the initiation of mass movements and many landslides in the Southern Pennines were activated at this time, later becoming covered by end-Pleistocene solifluction deposits (Said, 1969). Landslides resting on top of such solifluction mantles, as in the case of Mam Tor, must be younger although a more precise dating is often not possible (see Section 1.1.1).

At exactly what time and however the surface (or surfaces) of rupture was established does not concern us here. Rather we have been considering processes which can maintain such a surface on the verge of failure for many hundreds of years, to be activated at regular intervals where conditions are favourable, i.e. when the water table rises after the spring thaw or during any 'freak' rainfall events.

In order to predict the stability of slopes and the likelihood of failure, Hodge and Freeze (1977) believe that information concerning the nature and position of the water table is essential. From observations made in this study it would also appear that information concerning groundwater chemistry might be equally important in certain geologic situations.

Subsequent to the drilling of the boreholes at Mam Tor piezometers were placed in the ground by the County Council in order to monitor fluctuations in ground water level. Results of these piezometric investigations would be invaluable in assessing the effectiveness of any drainage scheme but, in common with the pending report, they have not been released.

It must be stressed once again that water in the failure zones does not act as a lubricant but rather reduces the internal strength and shear resistance of the rock mass. Changes in groundwater level are only a trigger mechanism, as suggested by Nakano (1967) and graphically demonstrated by Curtis and Williams (1978).

9.4 Future Management

Cooke and Doornkamp (1974) perhaps make the most pertinent comment concerning landslide management, in view of the information obtained on the Mam Tor slide. They state that "The physical control of landslides is an engineering problem whose solution lies in the correct identification of the causes of movement".

It is clear from the small amount of literature, mainly in the form of newspaper articles, concerning Mam Tor that the true cause of movement is not generally understood. For example, a typical article concerning one period of rapid movement states that "Flood water has loosened the sides of the 1700 ft. mountain" and goes on to describe the remedial measures taken by County Council workmen who "dumped 300 tons of gravel at the edge of the road to prevent further subsidence" (Anon, 1965).

Equally futile and short-sighted maintenance work is described in another article concerned with the January, 1966, movement which states that "Teams of Council workmen have been working round the clock to seal cracks (*in the road*) as they appear, to stop water getting into them" (Anon, 1966 - my italics). Clearly the highway engineers did not understand that the cracks are a *manifestation* of the movement and not the real cause; although it is accepted that a certain amount of oxygenated water will gain access to the failure surfaces in this way.

In 1977 it was commonly believed that heavy lorries using the Mam Tor road (in particular lorries from the Hope Cement Works) were the cause of repeated failure. After two years of closure to all but light traffic, however, the latest and most dramatic damage occurred (Plates 16 to 19). Once again the nature and scale of the true situation was not realised.

The drainage scheme proposed for Mam Tor (discussed in Section 3.3) although on a very large scale would, in the opinion of the author, have also proved unsuccessful in stabilising the slide. Apart from the supply of deep groundwater irrespective of infiltration it has been shown in several instances that the opening up of pyritic materials of this type can actually increase the rate of weathering and, ultimately, the scale of the problem. For example, Bloomfield (1972b) notes that considerably more ochre than naturally precipitates in pyritic soils is deposited in field drains installed specifically to alleviate the problem. Such drains can become completely blocked by iron hydroxides and are rendered useless.

Although it is accepted that excessive pore water pressures can be relieved by adequate drainage, in a chemical system so active as that at Mam Tor other effects could be intensified. Not only would pyrite oxidation speed up but also the products of reaction would be more efficiently transported away from the reaction sites and might not precipitate again within the landslide. In this event the amount of void space created would be greatly increased.

Several million pounds have been spent over the years on repairs to the Mam Tor road. These maintenance operations have been strictly short-term, aimed at getting the road open again to traffic as soon as possible, and none has had the slightest effect on long-term stability. Since the landslide poses no direct threat to any major structures or community (other than the road, and the barn in Plate 15) it is unlikely that any effective long-term remedial measures will be taken. This is even more evident in view of the recent decision to build a permanent alternative route at a cost of at least 2½ to 3 million pounds.

Figure 38 Pyrite oxidation model.

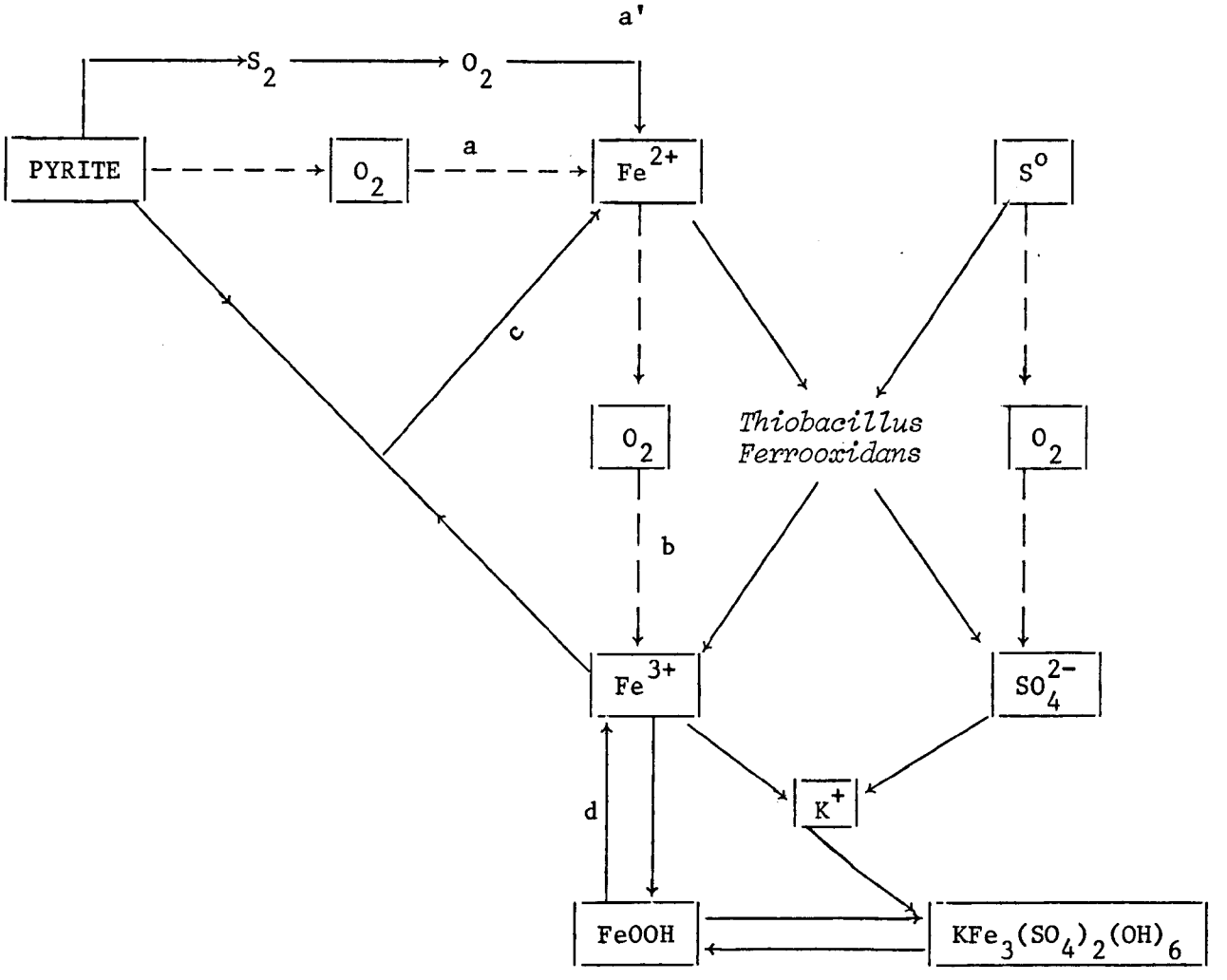

⟶ Slow reaction

⟶ Fast reaction

10. FINAL CONCLUSIONS

The following is a brief account of the major conclusions that can be drawn from the preceding chapters. Special emphasis is placed on certain points but generally a more detailed account can be found at the end of the relevant Section in the text.

Precipitates of ochre and gypsum in the seepages at Mam Tor suggest that the composition of drainage waters is somewhat unusual. Detailed analyses reveal that these streamwaters closely resemble so-called acid mine drainage, the root cause of which is pyrite oxidation catalysed by the presence of iron-oxidising bacteria.

Although the precise mechanistic steps are not considered in detail the model illustrated in Figure 38 (similar to that proposed by Temple and Delchamps, 1953) represents, schematically, the oxidation of pyrite as thought to be occurring within the fractured Edale Shales at Mam Tor. The pathways involving elemental sulphur and jarosite are added from van Breemen (1972).

The rate-determining step in this model is step b, the oxidation of ferrous iron, which is extremely slow under natural conditions. By contrast the oxidation of pyrite by ferric iron can be up to 1000 times faster (Garrels and Thompson, 1960).

Stumm and Morgan (1970) believe that the sequence is initiated by the direct oxidation (a) or dissolution and oxidation (a') of pyrite. The ferrous iron formed is slowly oxidised to ferric iron (b) which in turn is rapidly reduced in the presence of pyrite (c) releasing acidity and more Fe^{2+} for use in step b. Once the sequence is started atmospheric oxygen is only indirectly involved.

Step d, the precipitation of ferric hydroxide, appears to be incidental. Goethite may, however, act as a reservoir for soluble Fe^{3+}. If step b

becomes insignificant or if the pH falls dramatically ferric iron may be supplied by the dissolution of goethite. At lower pH jarosite may become the dominant solid Fe^{3+} phase.

The significance of microbial activity cannot be over-emphasised. Organisms act as catalysts in the oxidation of both ferrous iron and sulphur and are, therefore, responsible for the rate at which the whole model operates.

Many workers reporting on the weathering of sulphide-rich rocks refer to acid production without realising the true scale of the process. Water with a pH of about 3.0 is not so uncommon as these authors would have us believe; for example Hargreaves, et al. (1975) report many examples of highly acidic streams in England and Wales. The most interesting point concerning the acid waters at Mam Tor, therefore, is not that their acidity is unusually great but that the rate of production of that acid is so rapid.

It is noted that pyrite oxidation and the accompanying release of H^+ ions can proceed very rapidly in the presence of catalytic bacteria. Subsequent reactions involving carbonates and silicates which consume H^+ ions and release others into solution must proceed at *strictly comparable rates* to produce waters whose chemical composition varies so little.

The fact that the vast majority of H^+ ions (99% at least) are consumed in these additional reactions has not been stressed by other researchers. Van Breemen (1972) is one of the few who acknowledge this fact - he quotes a figures of 99.7% of the acid produced by pyrite oxidation being inactivated by dissolved (carbonate) alkalinity or consumed by mineral weathering.

The residual 1% acidity is sufficient to give the waters a pH of about 3 to 3.5. Thermodynamic calculations suggest that this buffering is a function of decreasing Fe^{2+} solubility as ferric hydroxide precipitates and the redox potential rises. The effectiveness of this mechanism can be

seen from the great many values of Appendix Bii, which fall in this narrow pH range.

Wider consideration of the results of chemical analyses indicates that different streams respond differently to changes in climatic variables. By using cluster analysis - a technique of hierarchical classification - the streams can be split into a number of distinct 'groups' which derive their waters from different sources. Some are merely surface runoff streams which have a composition close to that of rainfall while others obtain their water from deep underground after a long residence time in contact with pyritic shales. The majority of sites demonstrate mixing of waters from both sources and as a result show marked dilution when the surface contribution is large.

A series of chemical reactions, loosely termed a 'weathering model', is suggested to account for the composition of waters emerging at one of the spring sites - Site number 7 - which is least diluted by surface runoff. Quantitative values can be fitted at each step in this model and the resulting composition of the water can be explained. X-ray analysis of the solid materials generally confirms the accuracy of the weathering model, with a few minor qualifications for jarosite precipitation.

Analysis of the precipitate minerals indicates that the first-formed phase 'limonite' gradually converts to the more stable hydroxide goethite. Jarosite precipitation appears to be restricted to sites above the zone of permanent water saturation, and gypsum is only found at the surface.

The chemical alteration of clay minerals does not appear to be responsible for shale breakdown; only minor amounts of cations are derived in this way. Surface weathering occurs principally as a result of the growth of alteration products on bedding planes and in joints. At depth such precipitation is still possible where aerated waters can penetrate

the strata but processes of clay swelling (expandable fraction only) and air breakage are also thought to be important. Long term chemical alteration would appear to proceed much more slowly than the initially rapid breakdown into angular fragments. Internal stresses produced by solution and precipitation of minerals may be important locally.

Large scale and often rapid landslide movements occur periodically at Mam Tor and appear to be triggered by changes in pore water pressures. Such movements take place along pre-determined failure surfaces which are maintained by deep chemical weathering.

The correlation between physical instability and extreme chemical instability at this site is fascinating. The area is a vast 'geochemical factory',and affords many excellent examples for teaching purposes; the reactions can be 'seen' to be taking place. This thesis has done no more than demonstrate and carefully document these chemical changes which could conceivably contribute to the maintenance of instability; there is no question of being able to link them with the original failure.

It is sincerely hoped that this research will prompt further work into the links between chemical weathering and slope stability.

T H E E N D

11. REFERENCES

ALLEN, J.R.L. 1960. The Mam Tor Sandstones: A turbidite facies of the Namurian Deltas of Derbyshire. Journ. Sed. Pet. 30, 193-208.

ALLEN, S.E. (ed.) 1974. Chemical Analysis of Ecological Materials. Blackwell Scientific Publications, Oxford.

ALLEN, S.E., CARLISLE, A., WHITE, E.J. and EVANS, C.C. 1968. The plant nutrient content of rainwater. J. Ecol. 56, 497-504.

AMIN, M.A. 1979. Geochemistry and mineralogy of Namurian sediments in the Pennine Basin, England. Ph.D. Thesis, Univ. Sheffield.

ANDERSON, W.C. and YOUNGSTROM, M.P. 1976. Coal pile leachate quantity and quality characteristics. 6th Symposium on Coal Mine Drainage Research. NCA/BCR Coal Conference, Kentucky, 17-33.

ANDERSSON, A. and WIKLANDER, L. 1975. Release of crystal constituents by chemical weathering of some soil minerals. Soil Sci., 120, 13-19.

ANON. 1960. Structures don't settle in this shale, but watch out for heave. Engineering News-Record, 164, 46-48.

ANON. 1965. Mountain blamed for road closure. Article appearing in The Sheffield Morning Telegraph, 30th December, 1965.

ANON. 1966. Mam Tor Road Closed. Article appearing in The Star (Sheffield Newspapers Ltd.), 17th January, 1966.

APPALACHIAN REGIONAL COMMISSION. 1969. Acid Mine Drainage in Appalachia. Washington, D.C.

ASHMEED, D. 1955. The influence of bacteria on the formation of acid mine waters. Colliery Guardian, 190, 694-698.

AUSTIN, G.C. and LEININGER, R.K. 1976. The effect of heat treating sedimented mixed layer illite-smectite as related to quantitative clay mineral determinations. Journ. Sed. Pet., 46, 206-215.

BAAS BECKING, L.G.M., KAPLAN, I.R. and MOORE, D. 1960. Limits of the natural environment in terms of pH and oxidation-reduction potential. J. Geol., 68, 243-284.

BADGER, C.W., CUMMINGS, A.D. and WHITMORE, R.L. 1956. The disintegration of shales in water. J. Inst. Fuel. 29, 417-423.

BANERJEE, A.C. 1971. Mechanism of oxidation of iron pyrites. Chem. Commun. 1006-1007.

BARNES, H.L. and ROMBERGER, S.B. 1968. Chemical aspects of acid mine drainage. Jour. Water Pollution Control Federation, 40, 371-384.

BARNES, I. and BACK, W. (1964). Geochemistry of iron rich groundwater of southern Maryland. J. Geol., 72, 435-447.

BARNES, I., STUART, W.T. and FISHER, D.W. 1964. Field investigations of mine waters in the Northern Anthracite Field, Pennsylvania. U.S. Geol. Surv., Prof. Pap. 473-B, 8 pp.

BARNHISEL, R.I. and ROTROMEL, A.L. 1974. Weathering of clay minerals by simulated acid coal spoil bank solutions. Soil Sci. 118, 22 pp.

BERKOVITCH, I., MANACKERMAN, M. and POTTER, N.M. 1959. The shale breakdown problem in coal washing. Part 1 - Assessing the breakdown of shales in water. J. Inst. Fuel. 32, 579-589.

BERNER, R.A. 1964. Iron sulfides formed from aqueous solution at low temperatures and atmospheric pressure. Jour. Geol. 72, 293-306.

BERNER, R.A. 1969. Goethite stability and the origin of red beds. Geochim. et Cosmochim Acta, 33, 267-273.

BERNER, R.A. 1970. Sedimentary pyrite formation. Amer. Jour. Sci., 268, 1-23.

BIESECKER, J.E. and GEORGE, J.R. 1966. Stream quality in Appalachia as related to coal mine drainage. U.S. Geol. Surv. Circ., 526, Washington, D.C.

BISHOP, A.W., HUTCHINSON, J.N., PENMAN, A.D. and EVANS, H.E. 1969. Geotechnical investigation into the causes and circumstances of the disaster of 21st October, 1966. Item 1, 1-80. A selection of technical reports submitted to the Aberfan Tribunal. Welsh Office, London. HMSO.

BLADH, K. 1978. Formation of goethite, jarosite and alunite during 25°C weathering of felsic rocks containing pyrite and chalcopyrite. Geol. Soc. Am. Abstracts with Programs, 10, p.368.

BLATT, H., MIDDLETON, G. and MURRAY, R. 1972. Origin of Sedimentary Rocks. Prentice Hall, New Jersey, 634 pp.

BLOOMFIELD, C. 1972(a). The oxidation of iron sulfides in soils in relation to the formation of acid sulphate soils and of ochre deposits in field drains. J. Soil. Sci., 23, 1-16.

BLOOMFIELD, C. 1972(b). Acidification and ochre formation in pyritic soils. Proc. Int. Symp. Acid Sulph. Soils, Wageningen.

BOWEN, N.L., 1928. The evolution of the igneous rocks. Princeton Univ. Press, Princeton, N.J.

BRAGG, W.L. 1913. X-ray diffraction and crystal structures. Proc. Roy. Soc. A., 89, 248-277.

van BREEMEN, N. 1972. Soil forming processes in acid sulphate soils. In: H. Dost (ed.), Acid Sulphate Soils. Proc. Int. Symp. on Acid Sulphate Soils, Wageningen, Netherlands, 1972.

BRICKER, O.P., GODFREY, A.E. and CLEAVES, E.T., 1968. Mineral water interaction during the chemical weathering of silicates. Am. Chem. Soc. Advances, Chemistry Ser. 73, 128-142.

BRINDLEY, G.W. 1955. Identification of clay minerals by X-ray diffraction analysis. In: Pask and Turner, 1955.

BRITISH STANDARDS INSTITUTION, 1964. Methods of measurement of liquid flow in open channels. Part 2A - Dilution Method, constant rate injection. B.S. 3680, PE2A, BSI, London, 39p.

BRITISH STANDARDS INSTITUTION, 1965. Methods of measurement of liquid flow in open channels. B.S. 3680 4A.

BROCK, T.D. 1969. Microbial growth under extreme conditions. Symp. Soc. Gen. Microbio. 19, 15-41.

BROPHY, G.P., SCOTT, E.S. and SNELLGROVE, R.A. 1962. Sulfate Studies II. Solid solution between alunite and jarosite. Am. Min. 47, 112-126.

BROWN, G. 1961. The X-ray Identification and Crystal Structures of Clay Minerals. Mineralogical Society, London.

BROWN, J.B. 1970. A chemical study of some synthetic potassium-hydronium jarosites. Can. Mineral., 48, 703-706.

BROWN, J.B. 1971. Jarosite-goethite stabilities at 25°C, 1 atm. Mineral Deposits (Berl.), 6, 245-252.

BROWN, R.D. 1977. Excursion itineraries for the 6th British Polish Seminar, Sheffield 1977. Sheffield University, Geography Department.

BRYNER, L.C. and JAMERSON, A.K. 1958. Micro-organisms in leaching sulphide minerals. Appl. Microbiol. 6, 281-287.

CARPENTER, R.H. and HAYES, W.B. 1980. Annual accretion of Fe-Mn oxides and certain associated metals in a stream environment. Chem. Geol. 29, 249-260.

CARUCCIO, F.T., GEIDEL, G. and SEWELL, J.M. 1976. The character of drainage as a function of the occurrence of framboidal pyrite and groundwater quality in eastern Kentucky. 6th Sumposium on Coal Mine Drainage Research. NCA/BCR Coal Conference, Kentucky, 1-16,

CHAO, G.Y. 1969. 2θ(Cu) table for common minerals. Carleton Univ., Department of Geology, Geological Paper, 69-2, Ottawa, Canada.

CHRISTIAN, G.D. and FELDMAN, F.J. 1970. Atomic Absorption Spectroscopy. Applications in Agriculture, Biology and Medicine. Wiley-Interscience, New York, 490 pp.

CLARK, W.M. and COHEN, B. 1923. An analysis of the theoretical relations between reduction potentials and pH. Public Health Reps. Repr., 826.

CLEAVES, E.T., GODFREY, A.E. and BRICKER, O.P. 1970. Geochemical balance of a small watershed and its geomorphic implications. Geol. Soc. Am. Bull. 81, 3015-3032.

COLLINSON, J.D. and WALKER, R.G. 1967. Namurian sedimentation in the High Peak. In: Geol. Excursions in the Sheffield Region. C. Downie and R. Neves (Eds) Univ. Sheffield, 1967, 163 p.

COLMER, E.R. and HINKLE, M.E. 1947. The role of micro-organisms in acid mine drainage. Science, 106, 253 p.

COOKE, R.U. and DOORNKAMP, J.C. 1974. Geomorphology in Environmental Management. Oxford University Press, 413 p.

COOKE, R.U. and SMALLEY, I.J. 1968. Salt weathering in deserts. Nature, 220, 1226-1227.

COOMBS, D. 1971. Mam Tor: A Bronze Age Hillfort? C. Arch. 27, 100-102.

CORRENS, C.W. 1961. The experimental chemical weathering of silicates. Clay Minerals Bull. 4, 249-265.

CORRENS, C.W. 1963. Experiments on the decomposition of silicates and discussion of chemical weathering. Clays Clay Minerals, Proc. Natl. Conf. Clays Clay Minerals, 10, 443-59. Pergamon Press, New York.

COVENEY, R.M. and PARIZEK, E.J. 1977. Deformation of mine floors by sulfide alteration. Bull. Assoc. Eng. Geol. 14, 131-156.

CRISP, D.T. 1966. Input and output of minerals for an area of Pennine moorland: The importance of precipitation, drainage, peat erosion and animals. J. Appl. Econ. 3, 327-348.

CROUSE, H.L. and ROSE, A.W. 1976. Natural beneficiation of acid mine drainage by interaction of stream water with stream sediment. Proc. 6th Symp. Coal Mine Drainage Res., Kentucky, 237-269.

CRUICKSHANK, J.G. 1972. Soil Geography. David and Charles Ltd., Newton Abbot, 256 pp.

CRYER, R. 1976(a) A study of the sources and variations of major solutes in selected mid-Wales catchments. Ph.D. Thesis, University of Wales, 1978.

CRYER, R. 1976(b). The significance and variation of atmospheric nutrient inputs in a small catchment system. J. Hydrol. 29, 121-137.

CUBITT, J.M. 1975. A regression technique for the analysis of shales by X-ray diffraction. Jour. Sed. Pet. 45, 546-553.

CURTIS, C.D. 1975. Chemistry of rock weathering fundamental reactions and controls. In: Geomorphology and Climate. E. Derbyshire (ed.) Wiley, London.

CURTIS, C.D. 1976. Stability of minerals in surface weathering reactions: A general thermochemical approach. Earth Surface Processes, 1, 63-70.

CURTIS, G.D. and WILLIAMS, J.W. 1978. Dynamic demonstration of pore pressure's role in slope instability. J. Geol. Educ., 26, 111-113.

DEPARTMENT OF THE ENVIRONMENT 1972. Determination of Sulphate. In: Analysis of raw, potable and waste waters. HMSO, London, 78-79.

DEUL, M. 1974. Limestone for controlling acid mine drainage and for treatment of acid mine water. 10th Forum Geol. Ind. Miner. (Columbus USA), 43-46.

DOUGHERTY, M.T. and BARSOTTI, N.J. 1972. Structural damage and potentially expansive sulfide minerals. Bull. Assoc. Eng. Geol. 9, 105-125.

DUGAN, P.R. 1972. Biochemical Ecology of Water Pollution. Plenum Publishing Corp, New York, 159 pp.

DUNN, A. 1979. Mam Tor to get by-pass. Article appearing in The Guardian, 13th February, 1979.

EARLY, K.R. and SKEMPTON, A.W. 1972. Investigations of the landslide at Walton's Wood, Staffordshire. Q.Jl. Eng. Geol., 5, 19-41.

EDEN, R.A., ORME, G.R., MITCHELL, M. and SHIRLEY, J. 1962. A study of part of the margin of the Carboniferous limestone massif in the Pin Dale area, Derbyshire. Bull. Geol. Surv. 21, 73-118.

EMMONS, W.H. 1917. The enrichment of ore deposits. U.S. Geol. Surv. Bull. 625, 530 p.

FASSISKA, E.J., WAGENBLAST, H. and DOUGHERTY, M.T. 1974. The oxidation mechanism of sulfide minerals. Bull. Assoc. Engineering Geologists, 11, 75-82.

FORBES, H. 1947. Landslide investigation and correction. Am. Soc. Siv. Eng., Tr. 112, 377-442.

FORD, T.D. 1976. Geochemical prospecting over Odin Rake. Chapter 6. In: Ford T.D. and Rieuwerts, J.H., 1976. Bull. Peak Dist. Mines Hist. Soc. 6, No.4.

FORD, T.D. and RIEUWERTS, J.H. 1975. Lead Mining in the Peak District. Peak Park Joint Planning Board, Bakewell.

FORD, T.D. and RIEUWERTS, J.H. 1976. Odin Mine, Castleton, Derbyshire. Bull. Peak Dist. Mines Hist. Soc., 6, No. 4.

GARRELS, R.M. and CHRIST, C.L. 1965. Solutions, Minerals and Equilibria. Harper and Row, New York, 450 p.

GARRELS, R.M. and NAESER, C.R. 1958. Equilibrium distribution of dissolved sulphur species in water at 25°C and one atmosphere total pressure. Geochim et Cosmochim. Acta 15, 113-130.

GARRELS, R.M. and THOMPSON, M.E. 1960. Oxidation of pyrite by iron sulfate solutions. Am. J. Sci. 258A, 57-67.

GIBBS, R.J. 1965. Error due to segregation in quantitative clay mineral X-ray diffraction mounting techniques. Am. Min. 50, 741-751.

GIBBS, R.J. 1968. Clay mineral mounting techniques for X-ray diffraction analysis. Jour. Sed. Pet., 38, 242-243.

GOLDICH, S.S. 1938. A study in rock weathering. J. Geol. 46, 17-58.

GOLTERMAN, H.L. 1975. Physiological Linmology. Elsevier, New York, 489 p.

GOLTERMAN, H.L., CLYMO, R.S. and OHNSTAD, M.A.M. 1978. Methods of physical and chemical analysis of fresh waters (2nd Ed.). International Biological Programme Handbook No. 8.

GORE, A.J.P. 1968. The supply of six elements by rain to an upland peat area. J. Ecol. 56, 483-495.

GOUDIE A., COOKE R.U. and SMALLEY, I. 1970. Experimental investigation of rock weathering by salts. Area. 42-48.

GRAF, W.H. and ACAROGLU, E.R. 1966. Settling velocities of natural grains. Bull. Intern. Assoc. Sci. Hydrology, 11, 27-43.

GRATTAN-BELLEW, P.E. and EDEN, W.J. 1975. Concrete deterioration and floor heave due to biogeochemical weathering of underlying shale. Can. Geotech. J., 12, 372-378.

GREGORY, S. 1963. Statistical methods and the geographer. (3rd Ed., 1973). Longman, London, 271 p.

GRIM, R.E. 1968. Clay Mineralogy (2nd Ed.) McGraw Hill (International Series In Earth and Planetary Sciences).

GUNEY, M. 1968. Oxidation and spontaneous combustion of coal: Review of individual factors. Colliery Guardian, February, 1968, 137-143.

GUTSCHICK, K.A. 1974. Lime and limestone. Mining Engineering, 26, 113-114.

HANSHAW, B. 1974. Geochemical evolution of a goethite deposit. In: Proc. International Symposium on Water-Rock Interaction, 70-75.

HARGREAVES, J.W., LLOYD, E.J.H. and WHITTON, B.A. 1975. Chemistry and vegetation of highly acidic streams. Freshwat. Biol. 5, 563-576.

HARRER, C.M. and TESCH, W.J. 1959. Reconnaissance of iron occurrences in Colorado. U.S. Bureau of Mines, Information Circ. 7918.

HARRISON, A.D. 1958. The effects of sulphuric acid pollution on the biology of streams in the Transvaal, South Africa. Verh. Int. Verein. theor. angew. Limnol., 13, 603-610.

HEM, J.D. 1960(a). Restraints on dissolved ferrous iron imposed by bicarbonate, redox potential and pH. U.S. Geol. Surv. Water-Supply Paper 1459-B, 33-55.

HEM, J.D. 1960(b). Some chemical relationships among sulphur species and dissolved ferrous iron. U.S. Geol. Surv. Water Supply Paper 1459, 57-73.

HEM, J.D. 1961. Stability field diagrams as aids in iron chemistry studies. Amer. Water Works Assoc. J. 53.

HEM, J.D. 1968. Graphical methods for studies of aqueous aluminium hydroxide fluoride and sulphate complexes. U.S. Geol. Surv. Water Supply Paper 1827B.

HEM, J.D. 1970. Study and interpretation of the chemical characteristics of natural water. U.S. Geol. Surv. Water Supply Paper 1473.

HEM, J.D. 1972. Chemical factors thatinfluence the availability of iron and manganese in aqueous systems. Bull. Geol. Soc. Amer., 83, 443-450.

HEM, J.D. 1977. Reactions of metal ions at surfaces of hydrous iron oxide. Geochim. et Cosmochim. Acta, 41, 527-538.

HEM, J.D. and CROPPER, W.H. 1959. A survey of ferric-ferrous chemical equilibria and redox potential. U.S. Geol. Surv. Water Supply Paper 1459A, 1-31.

HILL, R.D. 1974. Overview of use of carbonate rocks for controlling acid mine drainage. 10th Forum, Geol. Ind. Miner. Columbus, USA) 25-29.

HILL, R.D. and WILMOTH, R.C. 1971. Limestone treatment of acid mine drainage. Trans. Soc. Min. Eng. 250, 162-166.

HODGE, R.A.L. and FREEZE, R.A. 1977. Groundwater flow systems and slope stability. Can. Geotech. J., 14, 466-476.

HOLLAND, H.D. 1979. Metals in Black Shales: A reassessment. Econ. Geol. 74, 1676-1680.

HUDSON, R.G.S. and COTTON, G. 1945. The Carboniferous rocks of the Edale Anticline, Derbyshire. Quart. Jour. Geol. Soc. Lond., 101, 1-36.

HUTCHINSON, J.N. 1968. Mass movement. In: Fairbridge, R.W. (Ed.), Encyclopedia of Geomorphology.

JACKSON, M.L. and SHERMAN, G.D. 1953. Chemical weathering of minerals in soils. Advances in Agronomy, 5, Academic Press, N.Y., 219-318.

JACKSON, W. 1927. The succession below the Kinderscout Grit in North Derbyshire. Manchester Geol. Soc. Jour. 1, 15-32.

JENNE, E.A. 1968. Controls on Mn, Fe, Co, Ni, Cu, Zn concentrations in soils and water: The significant role of hydrous Mn and Fe oxides. in: Gould, R.F. (ed), Trace inorganics in water. Am. Chem. Soc., Advances in Chemistry Series, 73, 337-387.

JOHNSON, L.J., MATELSKI, R.P. and ENGLE, C.F. 1963. Clay mineral characterisation of modal soil profiles in several Pennsylvanian counties. Proc. Soil Sic. Soc. Am., 27, 568-572.

JOHNSON, N.M., LIKENS, G.E., BORMANN, F.H., FISHER, D.W., and PIERCE, R.S. 1969. A working model for the variation in stream water chemistry at the Hubbard Brook Experimental Forest, New Hampshire. Water Resources Research, 5, 1353-1363.

JOHNSTON, R.J. 1978. Multivariate Statistical Analysis in Geography. Longman, London. 280 pp.

KAPLAN, I.R., EMERY, K.O. and RITTENBERG, S.C. 1963. The distribution and isotopic abundance of sulphur in recent marine sediments off southern California. Geochim. et Cosmochim. Acta, 27, 297-332.

KELLY, W.C. and GODDARD, E.N. 1969. Telluride ores of Boulder County, Colorado. Geol. Soc. America Memoir, 109, 237 p.

KHLYBOV, V.V. 1976. Yarozit iz zony okisleniya piritizirovanykh porod Zapadnogo Piritman ya (Jarosite from the oxidation zone of pyritised rocks in the West Timan Region). In: Mineralogiya rudnykh mestorochdeniy Severa Urala i Pay-Khoya (Yushkin, N.P. - Ed.). Akad. Nauk SSSR, Komi Fil. Inst. Geol. Tr, 20, 65-67.

KIELLAND, J. 1937. Individual activity coefficients of ions in aqueous solutions. Am. Chem. Soc. Jour. 59, 1675-1678.

KINTER, E.B. and DIAMOND, S. 1956. A new method for preparation and treatment of oriented-aggregate specimens of soil clays for X-ray diffraction. Soil Sci. 81, 111-120.

KITANO, Y., KATO, K., KANAMORI, S., KANAMORI, N. and YOSHIOKA, R., 1967. Rockslides resulting from the geochemical weathering of parent materials. Annals, Disaster Prevention, Res. Inst. Kyoto Univ. 10A, 557-587 (in Japanese).

KRAUSKOPF, K.B. 1967. Introduction to Geochemistry. McGraw-Hill, New York, 721 p.

KUBASCHEWSKI, O. and EVANS, E.L. 1958. Metallurgical Thermochemistry. 3rd Ed., Pergamon Press, New York, 226-343.

KUZNETSOV, S.I., IVANOV, M.V. and LYALIKOVA, N. 1963. Introduction to Geological Microbiology. English Edition - C.H. Oppenheimer (Ed.), McGraw-Hill, New York, 252 pp.

LACKEY, J.B. 1938. The fauna and flora of surface waters polluted by acid mine drainage. U.S. Publ. Hlth. Rep., 53, 1499-1507.

LAGUROS, J.G., KUMAR, S. and ANNAMALA, M. 1974. Comparative study of simulated and natural weathering of some Oklahoma shales. Clay, Clay Min., 22, 111-115.

LANGMUIR, D. 1965. Stability of carbonates in the system $MgO-CO_2-H_2O$. Jour. Geology, 73, 730-754.

LATIMER, W.M. 1952. Oxidation Potentials. Prentice Hall, New Jersey, 392 p.

LAU, C.M., SHUMATE, K.S. and SMITH, E.E. 1970. The role of bacteria in pyrite oxidation kinetics. Proc. 3rd Symp. Coal Mine Drainage Res., Mellon Institute,Pittsburgh, Pa., 114-122.

LAZAROFF, N. 1963. Sulphate requirements for iron oxidation by *Thiobacillus ferrooxidans*. J. Bacteriol. 85, 78-83.

LEATHEN, W.W., KINSEL, N. and BRALEY, S.A. 1956. *Ferrobacillus ferrooxidans* - A chemosynthetic autotrophic bacterium. J. Bateriol. 72, No. 5.

LEE, G.F. and HOADLEY, A.W. 1967. Biological activity in relation to the chemical equilibrium composition of natural waters. In: Equilibrium Concepts in Natural Water Systems. Am. Chem. Soc. Advances in Chemistry Ser., 67, 319-338.

LIND, C.J. 1970. Specific conductance as a means of estimating ionic strength. USGS Prof. Paper 700-D, D272-D280.

LOUGHNAN, F.C. 1962. Some considerations in the weathering of silicate minerals. Jour. Sed. Pet., 32, 284-290.

LOVELL, H.L. and LACHMAN, R.I. 1970. An investigation of the natural beneficiation of coal mine drainage. Special Research Report, SR-76, Coal Research Section, Pennsylvania State University, 187 pp.

MAPSTONE, G.E. 1954. The weathering of pyrite. Chem. Ind. 577-578.

MASON, M.H. 1961. The Mam Tor sandstones: A turbidite facies of the Namurian of North Derbyshire. Ph.D. Thesis, University of Manchester.

McARTHUR, J.L. 1970. A geomorphological study of the Upper Derwent Basin, Derbyshire. Ph.D. Thesis, University of Sheffield.

MIELENTZ, R.C. and KING, M.E. 1955. Physical-chemical properties and engineering performance of clays. Bull. Div. Mines Calif., 169, 196-254.

NAMBU, M. 1957. Hydrated Fe-oxides. 1. Hydrated ferric oxide minerals altered from pyrite by weathering. Sci. Rep. Res. Inst., Tokoku Univ., Ser. A, 9, 215-226.

NAKANO, R. 1967. On weathering and change of properties of Tertiary mudstones related to landslide. Soil and Fdn., 7, 1-14.

NONVEILLER, E. 1967. Shear strength of bedded and jointed rocks as determined from the Salesina and Vajont Slides. Proc. Geotechnical Conference, Oslo 1967. Norwegian Geotech. Inst., 289-294.

NORDSTROM, D.K. and DAGENHART, T.V. 1978. Hydrated iron sulfate minerals associated with pyrite oxidation. Field relations and thermodynamic properties. Geol. Soc. Am. Abstracts with programs, 10, p.464.

OBORN, E.T. 1960. A survey of pertinent biochemical literature. U.S. Geol. Surv. Water Supply Paper 1459F, 111-190.

OBORN, E.T. and HEM, J.D. 1962. Some effects of the larger types of aquatic vegetation on iron content of water. U.S. Geol. Surv. Water Supply Paper 1459I, 237-268.

OHIO STATE UNIVERSITY RESEARCH FOUNDATION 1971. Acid mine drainage formation and abatement. Washington (US) Environmental Protection Agency Grant 14010, FPR, DAST-42, 82 p.

PEAK PARK JOINT PLANNING BOARD 1977. Mam Tor: The Alternatives. Peak Park News (Journal of the Peak National Park), Autumn, 1977, p.4.

PERKIN-ELMER 1976. Analytical methods for atomic absorption spectrophotometry. Perkin Elmer, September 1976.

PIERCE, J.W. and SIEGEL, F.R. 1969. Quantification in clay mineral studies and sedimentary rocks. Jour. Sed. Set., 39, 187-193.

PITEAU, D.R. 1970. Geological factors significant to the stability of slopes cut in rock. In: van Rensburg, P.W.J. (Ed.), Planning Open Pit Mines. S. Afr. Inst. Min. Met.

PITTY, A.F. 1976. Water temperatures in the limestone areas of the central and southern Pennines. Proc. Yorks. Geol. Soc., 40, 601-612.

PITTY, A.F., HALLIWELL, R.A. and TERNAN, J.L. 1979. The range of water temperature fluctuations in the limestone waters of the central and southern Pennines. J. Hydrol., 41, 157-160.

POTTER, R.W. 1976. The weathering of sulfide ores in Shasta County, California and its relationship to pollution associated with acid mine drainage. Open File Report, U.S. Geol. Surv. 76, 18 p.

POURBAIX, M.J.N. 1949. Thermodynamics of Dilute Aqueous Solutions. Edward Arnold & Co., London, 136 pp.

QUIGLEY, R.M. and VOGAN, R.W. 1970. Black shale heaving at Ottawa, Canada. Canadian Geotechnical Journal, 7, 106-115.

QUIGLEY, R.M., ZAJIC, J.E., McKYES, E. and YONG, R.N. 1973. Biochemical alteration and heave of black shale: Detailed observations and interpretations. Can. J. Earth Sci., 10, 1005-1006.

QUISPEL, A., HARMSEN, G.W. and OTZEN, D. 1952. Contribution to the chemical and bacteriological oxidation of pyrite in soils. Pl. and Soil, 4, 43-55.

RAE, G. 1977. Computer analysis of information on acid mine-drainage waters. In: Optimatl Development and Management of Groundwater (Buchan, S., Chairperson). Int. Assoc. Hydrogeol. Mem., 13, B39-B49.

RAE, G. 1978. Mine drainage from coalfields in England and Wales: A summary of its distribution and relationship to water resources. G.B. Cent. Water Plann. Unit., Tech. Note, No.24, 21 pp.

RAINWATER, F.H. and THATCHER, L.L. 1960. Methods for collection and analysis of water samples. A.S. Geol. Surv. Water Supply Paper, 1454.

READ, H.H. 1970. Rutley's Elements of Mineralogy. 26th Ed., Allen and Unwin, London, 560 pp.

READING, H.G. 1964. A review of factors affecting the sedimentation of the Millstone Grit in the Southern Pennines. In: Deltaic and Shallow Marine Deposits. L.M.J.V. van Straaten (Ed.), Elsevier, Amsterdam, 340-346.

REED, C. 1977. An article concerning alternative routes to the Mam Tor road. In: The Morning Telegraph (Sheffield Newspapers Ltd.), June 10th, 1977.

RICCA, V.T. and CHOW, K. 1974. Acid mine drainage quantity and quality generation model. Trans. Soc. Min. Eng. AIME (New York), 256, 328-336.

RICKARD, D.T. 1969. The chemistry of iron sulphide formation at low temperatures. Stockholm Contr. Geology, 20, 67-95.

RIPPON, J.E. 1980. Studies of acid rain on soils and catchments. NATO Conference Series No.1, Ecology, 4, 499-

ROBIE, R.A. 1959. Thermodynamic properties of selected minerals and oxides at high temperatures. U.S. Geol. Surv. Trace Elements Inv. Rept., 609.

ROBIE, R.A. and WALDBAUM, D.R. 1968. Thermodynamic properties of minerals and related substances at 298.15 K (25^{o}C) and one atmosphere (1.013 bars) pressure and at higher temperatures. U.S. Geol. Surv. Bull., 1259, 256 p.

RORISON, I.H. 1973. The effect of extreme soil acidity on the nutrient uptake and physiology of plants. Acid Sulphate Soils, Proc. Int. Symp. 18.

ROSSINI, F.D., WAGMAN, D.D., EVANS, W.H., LEVINE, S. and JAFFE, I. 1952. Selected values of chemical thermodynamic properties. Natl. Bur. Standards Circ. 500, U.S. Dept. Commerce.

ROYSTER, D.L. 1979. Landslide remedial measures. Assoc. Eng. Geol. Bull., 16, 301-352.

RUTTNER, F. 1953. Fundamentals of Limnology. University of Toronto Press, Toronto.

SAAS, E., NATHAN, Y. and NISSENBAUM, A. 1965. Mineralogy of certain pyrite concretions from Israel and their alteration products. Min. Mag., 35, 84-87.

SAID, M. 1969. The Pleistocene geomorphology of the Burbage Basin. Ph.D. Thesis, University of Sheffield.

REED, C. 1977. An article concerning alternative routes to the Mam Tor road. In: The Morning Telegraph (Sheffield Newspapers Ltd.), June 10th, 1977.

RICCA, V.T. and CHOW, K. 1974. Acid mine drainage quantity and quality generation model. Trans. Soc. Min. Eng. AIME (New York), 256, 328-336.

RICKARD, D.T. 1969. The chemistry of iron sulphide formation at low temperatures. Stockholm Contr. Geology, 20, 67-95.

RIPPON, J.E. 1980. Studies of acid rain on soils and catchments. NATO Conference Series No.1, Ecology, 4, 499-

ROBIE, R.A. 1959. Thermodynamic properties of selected minerals and oxides at high temperatures. U.S. Geol. Surv. Trace Elements Inv. Rept., 609.

ROBIE, R.A. and WALDBAUM, D.R. 1968. Thermodynamic properties of minerals and related substances at 298.15 K (25^{o}C) and one atmosphere (1.013 bars) pressure and at higher temperatures. U.S. Geol. Surv. Bull., 1259, 256 p.

RORISON, I.H. 1973. The effect of extreme soil acidity on the nutrient uptake and physiology of plants. Acid Sulphate Soils, Proc. Int. Symp. 18.

ROSSINI, F.D., WAGMAN, D.D., EVANS, W.H., LEVINE, S. and JAFFE, I. 1952. Selected values of chemical thermodynamic properties. Natl. Bur. Standards Circ. 500, U.S. Dept. Commerce.

ROYSTER, D.L. 1979. Landslide remedial measures. Assoc. Eng. Geol. Bull., 16, 301-352.

RUTTNER, F. 1953. Fundamentals of Limnology. University of Toronto Press, Toronto.

SAAS, E., NATHAN, Y. and NISSENBAUM, A. 1965. Mineralogy of certain pyrite concretions from Israel and their alteration products. Min. Mag., 35, 84-87.

SAID, M. 1969. The Pleistocene geomorphology of the Burbage Basin. Ph.D. Thesis, University of Sheffield.

SAKSELA, M. 1952. Weathering of sulfide minerals. Geologi, 4, 23.

SATO, M. 1960(a). Oxidation of sulphide ore bodies. I. Geochemical environments in terms of Eh and pH. Econ. Geol. 55, 928-961.

SCHINDLER, J.E. and HONICK, K.R. 1971. Oxidation-reduction determination at the mud-water interface. Limnol. Oceanogr. 16, 837.

SCHRAMM, J.R. 1966. Plant colonisation studies on black wastes from anthracite mining in Pennsylvania. Trans. Am. Phil. Soc. 56, 194 pp.

SCHULTZ, L.G. 1964. Quantitative interpretation of the mineralogical composition from X-ray and chemical data for the Pierre Shale. U.S. Geol. Surv. Prof. Paper, 391C, 1-31.

SHARPE, C.F.S. 1960. Landslides and Related Phenomena. Pageant, New York, 137 pp.

SILLEN, L.G. and MARTELL, A.E. 1964. Stability constants of metal-ion complexes. Sec.1: Inorganic ligands. Chem. Soc. (London), Spec. Pub. 17, 754 p.

SIMPSON, E. 1954. The Speedwell Cavern and some North Derbyshire drainage problems. Cave Sci. 3, 267-273.

SINGER, P.C. and STUMM, W. 1970. Acidic mine drainage: The rate determining step. Geochim. et Cosmochim Acta, 40, 441-447.

SLACK, K.V. and FISHER, D.W. 1965. Light dependent quality changes in stored water samples. U.S. Geol. Surv. Prof. Paper 525C. C190-C192.

SMITH, C.H. and DREVER, J.I. 1976. Control on the chemistry of springs at Teels Marsh, Mineral County, Nevada. Geochim. et Cosmochim. Acta, 40, 1081-1093.

SMITH, K. and LAVIS, M.E. 1975. Environmental influences on the temperature of a small uplant stream. Oikos, 26, 228-236.

SPEARS, D.A. and TAYLOR, R.K. 1972. The influence of weathering on the composition and engineering properties of in-situ Coal Measures rocks. Int. J. Rock Mech. Min. Sci., 9, 729-756.

SPEARS, D.A., TAYLOR, R.K. and TILL, R. 1971. A mineralogical investigation of a spoil heap at Yorkshire Main Colliery. Q. Jl. Eng. Geol., 3, 239-252.

SREBRODOL'SKIY, B.I. 1977. Mineral formation from sulfate solutions. Acad. Sci. USSR, Dokl, Earth Sci. Sect. 226, 121-122.

STEGER, H.F. and DESJARDINS, L.E. 1978. Oxidation of sulfide minerals: 4. Pyrite, chalcopyrite and pyrrhotite. Chem. Geol. 23, 225-237.

STEINBACK, J.T. 1966. An ecological investigation of the alga genera and other biota in waters polluted by mineral acid-drainage from coal mines in Vintan Co., Ohio. M.Sc. Thesis, Ohio State University, U.S.A.

STEVENSON, C.M. 1968. An analysis of the chemical composition of rainwater and air over the British Isles and Eire for the years 1959-64. Quart. Jour. Met. Soc., 94, 56-70.

STEVENSON, I.P. 1967. The Castleton Reef Belt and adjoining areas. In: Geological Excursions in the Sheffield Region. C. Downie and R. Neves (Eds.) Univ. of Sheffield, 1967, 163 p.

STEVENSON, I.P. and GAUNT, G.D. 1971. Geology of the country around Chapel-en-le-Frith. Mem. Geol. Surv. Gt. Br.

STOKKE, P.R. and CARSON, B. 1973. Variation in clay mineral X-ray diffraction results with the quantity of sample mounted. Jour. Sed. Pet., 43, 957-964.

STUMM, W. and MORGAN, J.J. 1970. Aquatic Chemistry - An introduction emphasising chemical equilibria in natural waters. Wiley-Interscience, New York, 583 p.

SYKORA, J.L., SMITH, E.H., SHAPIRO, M.A. and SYNAK, M. 1972. Chronic effect of ferric hydroxide on certain species of aquatic animals. Proc. 4th Symp. Coal Mine Drainage Res., Pittsburgh, Pa.

TANJI, K.K. and DONEEN, L.D. 1966. Predictions on the solubility of gypsum in aqueous salt solutions. Water Resources Research, 2, 543-548.

TAYLOR, R.K. and SPEARS, D.A. 1970. The breakdown of British Coal Measure rocks. Int. J. Rock Mech. Min. Sci., 7, 481-501.

TEMPLE, K.L. and COLMER, A.R. 1951. The autotrophic oxidation of iron by a new bacterium: *Thiobacillus ferrooxidans*. J. Bact., 62, 605-611.

TEMPLE, K. and DELCHAMPS, E. 1953. Autotrophic bacteria and the formation of acid in bituminous coal mines. Appl. Microbiol. 1, p.225.

TERZAGHI, K. 1950. Mechanism of Landslides. In: Application of Geology to Engineering Practice. Berkey Volume, Geol. Soc. Am., 83-125.

TERZAGHI, K. and PECK, R.B. 1967. Soil Mechanics in Engineering Practice. Wiley, New York, 729 p.

TREXLER, B.D., RALSTON, D.R., REECE, D.R. and WILLIAMS, R.E. 1975. Sources and causes of acid mine drainage. Pam. Idaho Bur. Mines. Geol. 165, 129 p.

VARNES, D.J. 1958. Landslides and Engineering Practice. In: Eckel,E.J. (Ed.) Highway Research Board, Washington, Special Report 29, NAS-NRC Publ. 544, 323 p.

VINE, J.D. and TOURTELOT, E.B. 1970. Geochemistry of Black Shale Deposits: A summary report. Econ. Geol. 65, 253-272.

VORA, K.H. and RAYMAHASHAY, B.C. 1978. Gypsum-jarosite incrustation on limestone; an unusual occurrence. Geol. Soc. India J., 19, 228-230.

WALKER, R.G. 1966. Shale grit and Grindslow shales: Transition from turbidite to shallow water sediments in the upper Carboniferous of northern England. J. Sed. Pet., 36, 90-114.

WALKER, R.G. 1967. Turbidite sedimentary structures and their relationship to proximal and distal depositional environments. J. Sed. Pet. 37, 25-43.

WARD, J.H. 1963. Hierarchical grouping to optimise an objective function. Jour. Am. Stat. Assoc., 58, 236-244.

WARNER, R.W. 1968. Preliminary report on the biology of acid mine drainage at Grassy Run and Roaring Creek, W. Virginia. Fed. Wat. Poll. Cont. Admn, Cincinnati, Ohio (Nov. 1968).

WENTZ, D.A. 1974. Effect of mine drainage on the quality of streams in Colorado, 1971-1972. Colo. Water Resour. Circ. 21, 117 p.

WHALEY, P.W., CLARK, H.R. and WIRAM, V.P. 1977. Field assessment of acid mine drainage potential of overburden materials encountered in strip mining. Geol. Soc. Am. Abstr. Progr. 9, 665-666.

WHITTON, B.A. 1972. Environmental limits of plants in flowing waters. Symp. Zool. Soc. Lond. 29, 3-19.

WILKINSON, P. 1950. Allophane from Derbyshire. Clay Min. Bull. 1, 122-123.

WILSON, M.J. 1975. Chemical weathering of some primary rock forming minerals. Soil Sci. 119, 349-355.

WINMILL, T.F. 1915-16. Atmospheric oxidation of iron pyrites. Pt. IV. Trans. Inst. Min. Engrs., 51, 500.

YAKHONTOVA, L.K., GRUDEV, A.P. and NESTEROVICH, L.G. 1979. Mekhanizm okisleniya pirita (The mechanism of pyrite oxidation). Geol. Rud. Mestorochd., 21, 63-68.

YOSHIOKA, R. 1975. Estimation of amounts of weathered products through chemical composition of waters in the Kamenose landslide area. Bull. Disaster Preven. Res. Inst. Kyoto Univ., 25.

ZoBELL, C.E. 1946. Studies on redox potentials of marine sediments. Bull. Am. Assoc. Petrol. Geol., 30, 477-513.

ZoBELL, C.E. and BROWN, B.F. 1944. Studies on the chemical preservation of water samples. Jour. Mar. Res., 5, 178-184.

APPENDIX A

Wet Chemistry Analytical Procedures

Ai DETERMINATION OF CALCIUM

By Atomic Absorption Spectrophotometry.

Sample Treatment: 1% w/v lanthanum chloride was added to the filtered and acidified field samples. These were then diluted 1 to 50 with distilled water so that Ca^{2+} concentration fell within the range of the standard solutions.

Standard Solutions: A commercial stock solution of 1000 µg ml^{-1} Ca was diluted to give a number of standards ranging from 0 to 10 µg ml^{-1}. In this analysis standards of 2.0, 6.0 and 10.0 µg ml^{-1} Ca were used.

Operating Parameters:

Wavelength	422.7 nm
Slit Setting	0.7 nm
Light Source	Hollow cathode lamp
Flame Type	Air-acetylene flame, oxidising (lean, blue)

Sensitivity: For the standard conditions above, the sensitivity is about 0.08 µg ml^{-1} Ca for 1% absorption.

Interferences: Silicon, aluminium, phosphate and sulphate depress the sensitivity for calcium. This can be remedied by the addition of lanthanum chloride or the use of a nitrous oxide-acetylene flame.

N.B. The acid concentration of the standards should be matched with that of the samples.

Source: Perkin-Elmer, 1976.

Aii DETERMINATION OF MAGNESIUM

By Atomic Absorption Spectrophotometry

Sample Treatment: As for calcium, 1% w/v lanthanum chloride was added to the samples which were then diluted either 1 to 50 or 1 to 100 to fall within the range of the standards.

Standard Solutions: A commercial stock solution of 1000 μg ml^{-1} Mg was diluted to give standards ranging from 0 to 3 μg ml^{-1} Mg. Standards of 0.5, 1.5 and 2.5 μg ml^{-1} Mg were used here.

Operating Parameters:

Wavelength	285.2 nm
Slit Setting	0.7 nm
Light Source	Hollow cathode lamp
Flame Type	Air-acetylene flame, oxidising (lean, blue)

Sensitivity: For the standard conditions above the sensitivity is about 0.007 μg ml^{-1} Mg for 1% absorption.

Precision: About 0.5%

Interferences: Silicon and aluminium depress the absorption of magnesium in an air-acetylene flame. Lanthanum chloride can be added or a nitrous oxide-acetylene flame used.

Source: Perkin-Elmer, 1976.

Aiii DETERMINATION OF SODIUM

By Atomic Absorption Spectrophotometry

Sample Treatment: The filtered and acidified samples were diluted 1 to 50 with distilled water.

Standard Solutions: A commercial stock solution of 1000 μg ml^{-1} Na was diluted to give standards of 2.0, 6.0 and 10.0 μg ml^{-1} Na.

Operating Parameters:

Wavelength	589.2 nm
Slit Setting	0.7 nm
Light Source	Hollow cathode lamp
Flame Type	Air-acetylene flame, oxidising (lean, blue)

Sensitivity: For the standard conditions above the sensitivity is about 0.015 μg ml^{-1} Na for 1% absorption.

Precision: About 2%.

Interferences: Sodium is partially ionised in an air-acetylene flame. This may be overcome by the addition of another alkali in excess of 1000 or 2000 μg ml^{-1}, but this was not done in this case.

Source: Perkin-Elmer, 1976.

Aiv DETERMINATION OF POTASSIUM

By Atomic Absorption Spectrophotometry

Sample Treatment: The original filtered and acidified samples were used undiluted.

Standard Solutions: A commercial stock solution was diluted to give standards of 2.0, 6.0 and 10.0 $\mu g\ ml^{-1}$ K.

Operating Parameters:

Wavelength	766.5 nm
Slit Setting	2.0 nm
Light Source	Hollow cathode lamp
Flame Type	Air-acetylene flame, oxidising (lean, blue)

Sensitivity: For the standard conditions above the sensitivity is about 0.04 $\mu g\ ml^{-1}$ K for 1% absorption.

Precision: About 2%.

Interference: Potassium is partially ionised in an air-acetylene flame. This may be overcome by the addition of another alkali in excess of 1000 $\mu g\ ml^{-1}$, but this was not done in this case.

Source: Perkin-Elmer, 1976.

Av DETERMINATION OF TOTAL IRON

Reagents:

Colour-developing reagent: (a) Hydroxylamine hydrochloride, 25%

(b) Sodium acetate, 0.5 N

(c) Dipyridyl solution: dissolve 0.2 g 2.2'-dipyridyl in 100 ml 0.2 N hydrochloric acid. Mix 2g (a), 6.8g (b), and 40 ml (c) and dilute to 200 ml with distilled water. The reagent is stable for at least one month.

Standard iron solution: Dilute commercial 1000 $\mu g\ ml^{-1}$ Fe standard to give a 100 $\mu g\ ml^{-1}$ standard solution.

Procedure: Into a 100 ml volumetric flask pipette 10 ml sample solution. Add 5 ml colour-developing reagent and make up the volume with distilled water. For standard solution add 5 ml colour-developing reagent to 10 ml of standard solution and dilute to 100 ml. A reagent blank should also be made consisting of 5 ml colour-developing reagent diluted to 100 ml. A deep red colour developes if any iron is present in solution. Measure the optical density of blank, standard and sample solutions in a 2 cm cell at 522 nm*. Determinations must be made within 24-hours of colour development.

Calculation:

$$\mu g\ ml^{-1}\ Fe \text{ in sample} = \frac{\mu g\ ml^{-1} Fe \text{ in standard} \times \text{sample sp reading} \times \text{Dilution factor}}{\text{standard sp reading} - \text{blank sp reading}}$$

$$= \frac{10 \times \text{sample sp reading}}{(\text{standard} - \text{blank})\ \text{sp reading}} \times 10$$

$$= \frac{\text{sample sp. reading}}{(\text{standard} - \text{blank})\ \text{sp reading}} \times 100$$

Precision: Approximately 1-2%.

Source: Sheffield University, Geology Department - Analytical Laboratory Handbook.

*Using a Pye Unicam SP 500 spectrophotometer.

Avi DETERMINATION OF FERROUS IRON

Reagents:

Potassium dichromate standard: Weigh 0.2728g dry potassium dichromate and dilute to 1 litre in a volumetric flask. 1 ml of this solution ≡ 0.31 mg Fe^{2+}.

Indicator Solution: Dissolve 0.1 g sodium diphenylamine sulphonate in 500 ml distilled water. Add 500 ml orthophosphoric acid and mix well.

Procedure: Add 5 ml indicator to 50 ml sample and titrate against $K_2Cr_2O_7$ to purple end-point.

Calculation:

$\mu g\ ml^{-1}\ Fe^{2+}$ in sample = volume of titre x 0.31 x dilution factor

= volume of titre x 6.10

Precision: 1-2% if dichromate indicator is carefully made up and checked against a Fe^{2+} standard solution such as ammonium ferrous sulphate (0.7021 g → 1 litre = 100 $\mu g\ ml^{-1}\ Fe^{2+}$).

Source: Sheffield University, Geology Department - Analytical Laboratory Handbook.

Avii DETERMINATION OF ALUMINIUM

By Atomic Absorption Spectrophotometry

Sample Treatment: With the exception of sample No. 7, which was diluted 1 to 50, all samples were analysed undiluted.

Standard Solutions: A commercial stock solution of 1000 μg ml^{-1} Al was diluted to give standards covering the range 0 to 50 μg ml^{-1} Al. Standards of 10, 20 and 50 μg ml^{-1} Al were used here.

Operating Parameters:

Wavelength	309.3 nm
Slit Setting	0.7 nm
Light Source	Hollow cathode lamp
Flame Type	Nitrous oxide-acetylene flame, reducing (rich,red)

Sensitivity: For the standard conditions above the sensitivity is about 1.0 μg ml^{-1} Al for 1% absorption.

Precision: 2-5%.

Interferences: Hydrochloric acid and iron greater than 0.2% decrease aluminium sensitivity. Sulphuric acid has a similar effect. Aluminium is also partially ionised in the flame unless total salts exceed 1000 μg ml^{-1}.

Source: Perkin-Elmer, 1976.

Aviii DETERMINATION OF CHLORIDE

Reagents:

Silver nitrate, 0.1 N

Methyl orange indicator: dissolve 0.04 g methyl orange in 20 ml alcohol. Add 80 ml distilled water and mix well.

Precipitated calcium carbonate.

Potassium chromate indicator: dissolve 5 g K_2CrO_4 in 100 ml water.

Sodium carbonate 0.02 N.

Procedure: Pour 50 ml sample into a 100 ml beaker. Add three drops methyl orange indicator and neutralise acidity by the addition of 0.02 N sodium carbonate (the orange colour will disappear). Add approximately 5 ml K_2CrO_4 indicator and titrate with 0.1 N $AgNO_3$ until yellow colour is tinged with a reddish brown.

Calculation:

$$\mu g\ ml^{-1}\ Cl^- \text{ in sample} = \frac{ml\ AgNO_3 \times 3550}{ml\ of\ sample}$$

$$= ml\ AgNO_3 \times 71$$

Interference: It is possible that Fe^{3+} in excess of 10 $\mu g\ ml^{-1}$ may interfere. The accuracy of samples high in ferric iron may, therefore,be considerably less than stated below.

Precision: Approximately 5%.

Source: Allen, 1974.

Aix DETERMINATION OF SULPHATE

Reagents:

Conditioning reagent:	Dissolve 75 g NaCl in 300 ml distilled water. Add 30 ml conc. HCl, 100 ml 95% 1-propanol (isopropyl alcohol), and 50 ml glycerol. Mix well.
Barium chloride:	Sieved to produce crystals of uniform size (300-500 μ).
Sulphate standard:	Dissolve 0.1479 g anhydrous sodium sulphate in water and make up to 1 litre (1 ml = 0.1 mg SO_4^{2-}).

Procedure:

1. Measure maximum of 100 ml sample containing not more than 4 mg SO_4^{2-} (40 μg ml^{-1}) into 250 ml conical flask. Make to 100 ml as necessary.

   N.B. Considerable dilution was needed for many of the Mam Tor samples (up to 100 x).

2. Add 5 ml conditioning reagent and mix using magnetic stirrer.
3. Add 0.5 g barium chloride and stir for one minute.
4. Measure absorption on spectrophotometer at wavelength of 420 nm. Continue to take readings at 30-second intervals for approximately 5 minutes, noting the maximum value (normally at c.2 min).
5. Subtract absorption due to colour and turbidity in original sample.
6. Prepare calibration curve using various dilutions of SO_4^{2-} standard for range 0.0 to 40 μg ml^{-1} SO_4^{2-}. Treat calibration samples exactly as described above but use blank determination with distilled water to set zero.
7. Read SO_4^{2-} concentration in sample from calibration curve and multiply by dilution factor to obtain value in μg ml^{-1}.

Interferences:

(a) Silica in excess of 500 µg ml^{-1}.

(b) Precipitation may be retarded by high concentrations of dissolved organic matter.

(c) Extreme colour and turbidity in original sample.

Precision: 5-10%.

Source: Adapted from Department of the Environment 1972; Analysis of Raw, Potable and Waste Waters. HMSO, London, p.78-79.

Ax DETERMINATION OF TRACE METALS

By Atomic Absorption Spectrophotometry

Trace metals were determined using a high-temperature graphite furnace in conjunction with the 'Perkin-Elmer 400' spectrophotometer. In all cases the purge gas was argon and the gas interrupt 3 seconds during atomisation, unless otherwise stated.

Copper (Sample dilution x 1)

Operating Parameters:	Wavelength	324.7 nm
	Slit Setting	0.7 nm
	Drying	105°C for 50 seconds
	Charring	1000°C for 20 seconds
	Atomising	2700°C for 10 seconds
Standards:	0.05 and 0.10 μg ml^{-1} Cu.	

Nickel (Sample dilution x 10)

Operating Parameters:	Wavelength	232.0 nm
	Slit Setting	0.2 nm
	Drying	105°C for 50 seconds
	Charring	1000°C for 20 seconds
	Atomising	2700°C for 10 seconds
Standards:	0.05 and 0.10 μg ml^{-1} Ni.	

Zinc (Sample dilution x 50)

Operating Parameters:	Wavelength	294.0 nm
	Slit Setting	0.7 nm
	Drying	105°C for 50 seconds
	Charring	1000°C for 20 seconds
	Atomising	2700°C for 10 seconds
Standards:	0.5 and 1.0 μg ml^{-1} Zn.	

Chromium (Sample dilution x 1)

Operating Parameters:	Wavelength	357.9 nm
	Slit Setting	0.7 nm
	Drying	105°C for 50 seconds
	Charring	1350°C for 20 seconds
	Atomising	2700°C for 10 seconds
Standards:	0.02 and 0.05 μg ml^{-1} Cr.	

Manganese (Sample dilution x 100)

Operating Parameters:	Wavelength	279.5 nm
	Slit Setting	0.2 nm
	Drying	105°C for 50 seconds
	Charring	1100°C for 20 seconds
	Atomising	2700°C for 10 seconds
Standards:	0.02 and 0.05 μg ml^{-1} Mn.	

Lead: (Sample dilution x 10)

Operating Parameters:	Wavelength	283.3 nm
	Slit Setting	0.7 nm
	Drying	105°C for 50 seconds
	Charring	500°C for 90 seconds
	Atomising	2700°C for 10 seconds
Standards:	0.05 and 0.10 μg ml^{-1} Pb.	

N.B. Gas interrupt 7 seconds during atomisation.

Cadmium: (Sample dilution x 10)

Operating Parameters:	Wavelength	228.8 nm
	Slit Setting	0.7 nm
	Drying	105°C for 50 seconds
	Charring	300°C for 90 seconds
	Atomising	2000°C for 10 seconds
Standards:	0.02 and 0.05 μg ml^{-1} Cd.	

Vanadium: (Sample dilution x 1)

Operating Parameters:	Wavelength	318.4 nm
	Slit Setting	0.2 nm
	Drying	105°C for 50 seconds
	Charring	1300°C for 20 seconds
	Atomising	2700°C for 10 seconds
Standards:	0.50 and 1.00 µg ml^{-1} V.	

APPENDIX B

Results of the Water Analyses

Bi TEMPERATURE (°C)

Sampling Date	Code	Site Number														
		1	2	3	4	6	7	8	11	13	16	17	18	100	101	3a
24.10.78	D	9.7	10.8	10.5	10.4	10.4	9.6	10.1	10.5	10.7	11.4	9.8	10.3	9.6	9.1	-
31.10.78	E	9.8	10.4	9.6	10.1	9.9	9.6	9.9	10.0	10.0	10.0	9.8	10.1	9.1	9.2	9.8
07.11.78	F	9.5	9.3	9.5	8.9	9.1	9.5	8.6	8.8	8.5	8.8	9.2	9.3	8.9	8.8	9.6
14.11.78	G	8.3	-	-	8.6	-	-	-	-	-	8.9	8.4	8.8	-	-	-
21.11.78	H	8.5	8.7	9.1	8.8	9.3	9.5	8.4	8.8	8.8	9.1	8.5	9.0	9.0	8.7	9.2
28.11.78	I	2.5	2.8	4.3	1.9	5.0	9.2	1.5	5.0	1.8	3.2	2.2	3.9	6.9	6.9	4.2
05.12.78	J	2.1	1.6	4.5	1.1	3.8	8.9	1.7	4.4	1.9	4.3	1.1	2.4	6.4	6.9	1.8
12.12.78	K	6.8	6.9	7.8	6.9	7.8	9.2	6.6	7.4	6.8	7.7	7.0	7.3	7.8	7.8	6.9
19.12.78	L	1.9	1.7	4.5	0.9	4.9	9.1	1.2	4.3	1.8	4.7	0.5	2.8	7.0	7.0	2.5
09.01.79	M	1.9	1.8	4.7	1.1	4.4	9.1	0.4	3.3	1.7	3.8	1.0	2.4	5.0	6.8	1.8
06.02.79	N	0.9	1.4	4.8	0.1	2.5	8.7	*	3.9	1.3	5.3	0.0	1.6	-	6.6	1.4
27.02.79	O	1.4	1.8	6.5	2.8	3.3	8.7	*	2.8	1.1	7.1	0.6	2.6	-	6.9	*
13.03.79	P	4.4	4.1	6.3	3.4	5.5	9.2	4.1	5.4	4.0	6.5	3.4	4.2	5.2	7.2	3.9
27.03.79	Q	2.0	2.4	4.8	2.2	3.8	9.0	1.5	1.9	1.8	4.8	2.0	2.5	4.5	6.4	2.3
11.04.79	R	-	-	-	-	-	-	-	-	-	-	-	-	-	-	-
24.04.79	S	6.1	6.4	6.6	5.9	5.6	9.0	5.0	6.3	5.1	7.1	6.0	6.0	5.2	5.6	6.0
08.05.79	T	-	-	-	-	-	-	-	-	-	-	-	-	-	-	-
22.05.79	U	11.2	12.6	10.8	10.8	10.0	9.4	12.6	10.5	10.0	10.9	10.0	8.6	8.2	8.8	15.5
05.06.79	V	13.8	14.9	12.8	14.5	12.9	9.8	17.8	14.6	14.0	12.0	14.6	12.0	9.0	9.2	16.9
19.06.79	W	13.9	17.2	14.0	16.7	12.9	10.0	22.7	16.8	16.2	14.8	15.1	13.3	11.5	9.1	24.2
03.07.79	X	11.0	12.4	10.1	12.0	10.0	9.9	13.0	11.8	11.3	10.8	12.1	11.5	9.1	9.0	*
24.07.79	Y	11.2	*	10.4	*	10.8	10.0	12.2	11.9	11.5	11.4	13.0	12.0	10.6	9.0	*
07.08.79	Z	12.8	*	11.4	*	11.9	10.2	14.0	13.2	13.2	13.9	14.5	13.7	12.8	9.5	*
21.08.79	AA	11.4	12.2	10.3	*	11.1	10.0	12.8	11.0	11.0	10.8	12.8	11.3	10.0	8.9	*
04.09.79	BB	12.0	12.5	11.4	*	11.7	10.2	14.5	12.1	12.0	11.9	12.2	11.8	11.7	9.0	15.1
18.09.79	CC	11.6	11.4	10.7	*	11.2	10.0	11.6	11.2	11.4	11.4	11.8	12.0	11.0	9.0	*
02.10.79	DD	9.0	o.1	8.6	*	9.0	9.9	9.8	8.8	8.9	7.3	9.0	8.7	10.0	8.1	*

- Temperatures not measured

* Stream frozen or dry

Bii pH($-\log_{10}[H^+]$) AND RAINFALL (mm)

Sampling Date	Code	Site Number															Precipitation*	
		1	2	3	4	6	7	8	11	13	16	17	18	100	101	3a		
24.10.78	D	5.1	3.2	2.9	3.3	5.2	3.4	5.6	3.0	6.0	2.8	3.2	5.3	5.0	6.9	-	0.0	(1 week)
31.10.78	E	5.2	3.0	3.1	3.6	4.7	3.5	5.2	3.3	5.9	3.0	3.0	5.9	5.5	6.9	3.0	0.0	(1 week)
07.11.78	F	5.2	3.3	3.2	3.4	3.5	3.3	5.2	3.1	4.8	3.0	3.2	5.2	5.4	6.6	2.9	0.6	(1 week)
14.11.78	G	5.4	3.4	3.0	3.6	3.9	3.5	5.4	3.2	4.8	3.2	3.2	5.5	5.6	6.8	3.2	7.5	(1 week)
21.11.78	H	5.5	3.0	2.8	3.6	5.4	3.3	5.1	3.4	5.6	3.0	3.2	5.6	5.3	6.6	3.2	58.1	(1 week)
28.11.78	I	5.2	3.6	3.3	3.5	4.6	3.3	4.7	3.1	4.6	3.2	3.5	5.2	5.2	6.2	3.4	19.9	(1 week)
05.12.78	J	4.9	2.9	3.0	3.4	3.4	3.2	4.4	3.1	5.6	3.1	3.0	5.0	5.4	6.2	3.2	13.1	(1 week)
12.12.78	K	5.2	3.3	3.4	3.6	5.4	3.8	4.4	3.2	6.1	3.3	3.2	5.1	5.5	6.2	3.5	44.0	(1 week)
19.12.78	L	-	-	-	-	-	-	-	-	-	-	-	-	-	-	-	44.1	(1 week)
09.01.79	M	4.9	3.3	2.8	3.2	4.4	3.3	4.8	3.3	3.6	3.2	3.4	5.0	5.0	6.8	3.4	135.4	(3 weeks)
06.02.79	N	-	-	-	-	-	-	-	-	-	-	-	-	-	-	-	-	
27.02.79	L	5.1	3.7	3.5	4.0	5.5	3.6	-	3.6	5.1	3.4	3.6	5.2	-	6.4	-	104.0	(7 weeks)
13.03.79	P	5.2	3.5	3.4	3.8	5.1	3.5	5.8	3.3	4.9	3.4	3.4	5.1	5.9	5.5	3.7	90.5	(2 weeks)
27.03.79	Q	5.0	3.5	3.4	3.8	5.2	3.4	4.6	3.7	5.1	3.2	3.5	5.4	4.8	5.6	3.7	55.0	(2 weeks)
11.04.79	R	4.9	3.2	3.2	3.5	5.2	3.2	4.7	3.4	5.1	3.2	3.3	5.0	4.7	5.7	3.6	87.6	(2 weeks)
24.04.79	S	5.2	3.4	3.4	3.6	5.2	3.4	5.2	3.2	4.4	3.3	3.0	5.4	5.0	5.6	3.6	16.7	(2 weeks)
08.05.79	T	5.6	3.0	3.0	3.7	3.6	3.4	5.6	3.4	5.4	3.3	3.3	5.2	5.7	6.2	3.5	47.8	(2 weeks)
22.05.79	U	-	-	-	-	-	-	-	-	-	-	-	-	-	-	-	51.4	(2 weeks)
05.06.79	V	5.9	3.3	3.4	3.6	5.8	3.7	6.2	3.4	5.1	3.4	3.2	6.5	6.1	6.6	3.6	58.7	(2 weeks)
19.06.79	W	5.6	3.5	3.2	3.5	5.8	3.6	6.2	3.2	5.6	3.0	3.0	5.8	6.0	6.7	3.4	45.3	(2 weeks)
03.07.79	X	5.2	3.2	3.4	3.6	5.6	3.6	6.1	3.2	4.7	3.3	3.2	6.1	6.1	7.0	-	30.0	(2 weeks)
24.07.97	Y	5.4	-	3.3	-	4.3	3.8	6.1	3.3	4.8	3.3	3.1	5.7	6.1	7.0	-	16.6	(3 weeks)
07.08.79	Z	5.7	-	3.4	-	4.1	3.8	6.2	3.2	4.9	3.2	3.2	5.8	6.2	7.0	-	30.6	(2 weeks)
21.08.79	AA	5.6	3.1	3.2	-	5.8	3.2	5.4	3.3	5.9	3.2	3.0	5.8	-	-	-	102.4	(2 weeks)
04.09.79	BB	5.7	3.5	3.4	-	5.8	3.7	5.9	3.3	6.0	3.2	3.2	6.6	6.5	6.7	3.5	44.7	(2 weeks)
18.09.79	CC	5.8	3.3	3.4	-	5.5	3.6	6.1	3.2	5.5	3.4	3.3	6.2	5.8	6.9	-	8.6	(2 weeks)
02.10.79	DD	5.8	3.4	3.5	-	5.3	3.6	5.9	3.1	5.5	3.3	3.5	5.9	5.6	6.9	-	24.9	(2 weeks)

*Total collected since last emptying of rain gauge

Biii CONDUCTIVITY ($\mu S\ cm^{-1}$ at $25^{o}C$)

Sampling Date	Code	Site Number														
		1	2	3	4	6	7	8	11	13	16	17	18	100	101	3a
24.10.78	D	750	1230	1370	1300	900	2440	160	1750	700	1540	1170	390	104	350	-
31.10.78	E	750	1240	1550	1300	850	2350	160	1600	670	1580	1140	300	106	350	1530
07.11.78	F	810	1240	1480	1270	870	2250	190	1700	760	1540	1140	360	106	350	1500
14.11.78	G	730	1100	1460	1190	820	1920	170	1580	690	1430	1000	340	60	320	1390
21.11.78	H	410	1000	1320	1040	710	1900	170	740	340	1370	930	160	97	290	850
28.11.78	I	540	960	1190	990	680	1750	140	1140	450	1030	770	180	110	280	940
05.12.78	J	630	1080	1380	1110	780	2120	170	1110	555	1410	980	290	115	340	1160
12.12.78	K	555	1020	1190	985	695	2300	190	940	470	1100	790	165	90	345	790
19.12.78	L	610	1040	1350	1020	730	2170	180	1480	580	1300	850	230	90	350	790
09.01.79	M	740	860	1360	1050	710	2300	125	1180	770	1220	770	200	65	370	610
06.02.79	N	765	890	1280	1040	770	1750	-	1100	620	1220	790	235	-	330	730
27.02.79	O	660	890	1400	1180	730	2260	-	930	600	1500	830	225	-	380	-
13.03.79	P	660	980	1470	1140	730	2330	130	1400	580	1470	790	185	80	350	730
27.03.79	Q	410	830	1360	1070	650	2280	110	640	310	1330	670	160	80	310	550
11.04.79	R	355	830	1310	1170	660	2460	115	740	270	1320	780	185	80	340	660
24.04.79	S	770	1040	1500	1350	760	2400	130	1670	790	1530	950	360	80	390	1120
08.05.79	T	-	-	-	-	-	-	-	-	-	-	-	-	-	-	-
22.05.79	U **	635	1120	1510	1360	820	2460	135	1410	555	1650	1010	310	80	360	1130
05.06.79	V **	710	1250	1680	1430	950	2580	160	1730	730	1750	1090	310	90	400	1060
19.06.79	W ++	700	1020	2000	1280	840	3900	150	2440	700	2280	1030	280	78	330	990
03.07.79	X **	930	1220	1500	1360	850	2350	150	1820	975	1610	1070	360	93	335	-
24.07.79	Y **	1010	-	1400	-	870	2500	160	2120	1000	1730	1280	430	80	390	-
07.08.79	Z **	1050	-	1580	-	890	2450	170	2160	1060	1740	1300	470	100	380	-
21.08.79	AA**	640	1240	1500	-	850	2350	150	1400	600	1630	1100	240	75	320	-
04.09.79	BB**	650	1370	1750	-	950	2600	160	1340	580	1840	1280	330	85	380	1400
18.09.79	CC**	730	1240	1500	-	860	2210	170	1690	700	1560	1130	400	85	335	-
02.10.79	DD**	860	1270	1500	-	850	2260	170	1820	870	1550	1090	420	130	350	-

** Meter No. 2

++ Meter damaged, suspect readings

Biv CALCIUM Ca^{2+} ($\mu g\ ml^{-1}$)

Sampling Date	Code	Site Number														
		1	2	3	4	6	7	8	11	13	16	17	18	100	101	3a
24.10.78	D	97	193	189	178	100	393	13	245	99	244	167	48	7	78	-
31.10.78	E	95	190	234	177	95	386	10	208	97	219	163	39	9	74	226
07.11.78	F	118	207	252	195	106	415	23	278	132	268	188	52	9	85	256
14.11.78	G	113	197	234	185	99	389	19	262	118	246	181	49	6	77	232
21.11.78	H	68	177	236	176	52	344	15	117	39	250	144	24	7	75	132
28.11.78	I	81	188	241	185	97	386	16	190	85	242	152	27	5	77	171
05.12.78	J	81	181	231	165	96	376	33	157	75	216	153	37	9	78	178
12.12.78	K	66	171	234	149	84	394	18	135	62	219	118	22	4	79	79
19.12.78	L	99	184	248	161	96	428	18	234	92	253	149	29	6	93	128
09.01.79	M	94	163	298	194	109	500	7	183	85	243	133	23	8	83	100
06.02.79	N	100	161	234	185	111	385	-	202	93	238	129	26	-	71	117
27.02.79	O	77	146	250	201	108	408	-	125	55	287	172	31	-	90	-
13.03.79	P	86	153	235	167	91	400	14	187	80	254	123	23	10	82	106
27.03.79	Q	50	128	216	205	80	415	12	78	42	224	100	20	10	77	79
11.04.79	R	52	127	211	183	86	419	2	85	32	230	123	19	2	108	97
24.04.79	S	136	219	274	338	104	450	10	289	134	289	166	46	2	108	202
08.05.79	T	60	170	227	203	86	402	7	86	41	267	136	18	4	79	103
22.05.79	U	83	168	222	185	94	383	8	189	73	261	136	34	7	70	172
05.06.79	V	85	155	217	195	99	353	8	201	82	254	121	25	1	69	123
19.06.79	W	100	215	235	213	122	417	14	265	109	278	148	41	6	76	168
03.07.79	X	146	194	250	213	102	377	14	281	157	281	161	45	5	77	-
24.07.79	Y	157	1	259	1	95	430	16	333	161	281	182	56	8	85	-
07.08.79	Z	*	*	*	*	*	*	*	*	*	*	*	*	*	*	*
21.08.79	AA	*	*	*	*	*	*	*	*	*	*	*	*	*	*	*
04.09.79	BB	80	329	247	-	118	411	15	160	79	314	170	37	9	80	205
18.09.79	CC	124	222	279	-	144	451	20	350	128	288	297	56	7	95	-
02.10.79	DD	177	413	235	-	110	389	17	270	133	246	189	52	8	79	-

\- Not sampled

* Not analysed

Bv MAGNESIUM Mg^{2+} ($\mu g\ ml^{-1}$)

Sampling Date	Code	Site Number														
		1	2	3	4	6	7	8	11	13	16	17	18	100	101	3a
24.10.78	D	24	41	49	57	26	194	11	115	36	62	36	13	4	4	-
31.10.78	E	23	40	61	48	26	179	5	101	28	56	33	11	5	2	58
07.11.78	F	27	42	62	50	182	11	120	38	60	37	13	3	3	2	59
14.11.78	G	28	43	62	50	26	187	11	118	36	60	39	13	4	2	60
21.11.78	H	13	36	60	36	4	175	7	30	6	58	28	6	3	2	22
28.11.78	I	19	37	60	47	25	172	10	89	23	59	31	8	4	3	44
05.12.78	J	17	38	61	46	25	168	16	72	17	55	32	10	4	3	48
12.12.78	K	13	34	57	39	22	167	9	62	13	54	22	6	3	2	17
19.12.78	L	24	36	60	42	24	190	11	102	28	58	29	8	4	3	32
09.10.79	M	21	30	85	49	33	239	8	83	22	55	24	7	3	2	25
06.02.79	N	25	32	59	50	22	184	-	96	28	59	27	8	-	2	31
27.02.79	O	16	29	61	51	23	174	-	45	9	64	32	7	-	3	-
13.03.79	P	20	30	58	41	21	182	7	88	25	58	23	7	5	2	25
27.03.79	Q	10	25	54	43	19	188	6	37	9	54	20	6	5	2	20
11.04.79	R	9	24	50	46	19	186	3	37	5	50	21	5	4	3	22
24.04.79	S	35	40	60	82	23	192	8	118	41	62	29	12	4	4	45
08.05.79	T	14	36	58	55	20	194	6	45	9	67	27	6	3	3	27
22.05.79	U	21	36	63	55	24	202	3	96	22	70	29	9	3	2	55
05.06.79	V	24	36	61	63	28	217	7	107	31	69	28	8	3	1	37
19.06.79	W	25	40	59	51	30	196	8	118	32	65	23	10	3	2	39
03.07.79	X	40	38	60	51	24	188	9	120	53	63	31	12	3	2	-
24.07.79	Y	42	-	59	-	25	176	10	138	49	63	35	15	4	2	-
07.08.79	Z	42	-	60	-	25	177	11	137	52	60	37	15	3	2	-
21.08.79	AA	23	35	55	-	28	161	9	81	26	57	29	9	3	2	-
04.09.79	BB	19	71	64	-	25	175	9	68	18	75	32	10	4	2	47
18.09.79	CC	31	41	63	-	31	180	11	135	34	62	68	14	4	3	-
02.10.79	DD	37	97	64	-	28	176	11	121	46	65	44	16	4	3	-

Bvi SODIUM Na^+ ($\mu g\ ml^{-1}$)

Sampling Date	Code	Site Number														
		1	2	3	4	6	7	8	11	13	16	17	18	100	101	3a
24.10.78	D	53	36	43	72	82	11	4	7	23	58	30	20	6	9	-
31.10.78	E	50	32	50	64	73	8	2	6	19	53	25	13	3	8	50
07.11.78	F	59	36	53	68	78	13	10	11	23	57	31	22	8	12	50
14.11.78	G	54	37	52	68	79	13	10	13	26	59	33	32	9	13	52
21.11.78	H	53	37	57	65	20	16	11	8	25	60	32	16	10	14	33
28.11.78	I	52	38	53	75	81	18	12	12	30	60	31	18	13	16	40
05.12.78	J	72	39	56	71	85	15	13	12	51	62	33	21	11	16	44
12.12.78	K	52	35	52	56	70	14	10	11	37	56	22	15	8	14	16
19.12.78	L	48	30	56	66	74	15	11	11	27	63	29	19	9	15	32
09.01.79	M	84	30	38	64	66	19	10	12	70	54	26	14	10	23	27
06.02.79	N	74	21	51	63	87	14	-	12	53	56	27	18	-	20	30
27.02.79	O	84	32	58	66	73	18	-	12	79	60	36	20	-	28	-
13.03.79	P	60	30	53	57	66	14	10	12	26	54	24	16	10	15	26
27.03.79	Q	40	26	49	60	62	16	10	11	34	51	23	16	11	19	22
11.04.79	R	39	25	46	55	60	14	6	9	24	47	22	14	9	14	23
24.04.79	S	63	43	56	110	72	14	10	15	33	57	29	25	10	17	41
08.05.79	T	50	34	52	63	69	16	10	12	34	59	34	18	11	19	28
22.05.79	U	42	32	54	65	76	11	5	11	30	58	27	20	8	15	42
05.06.79	V	43	35	54	78	71	14	11	13	25	60	28	20	10	15	33
19.06.79	W	44	40	55	68	84	14	9	12	26	57	27	20	8	12	37
03.07.79	X	49	36	55	70	77	19	11	12	22	59	31	23	10	15	-
24.07.79	Y	54	-	55	-	75	11	8	14	27	51	32	23	11	13	-
07.08.79	Z	66	-	57	-	80	17	12	15	35	60	40	33	10	16	-
21.08.79	AA	40	40	55	-	89	17	16	15	34	55	35	24	16	18	-
04.09.79	BB	39	62	55	-	77	15	12	12	28	59	31	21	12	16	42
18.09.79	CC	43	42	56	-	80	22	12	15	29	54	60	28	11	16	-
02.10.79	DD	50	77	53	-	93	15	10	13	26	55	47	25	10	14	-

Bvii POTASSIUM K^+ ($\mu g\ ml^{-1}$)

Sampling Date	Code	Site Number														
		1	2	3	4	6	7	8	11	13	16	17	18	100	101	3a
24.10.78	D	2.9	7.7	6.4	4.7	4.0	5.5	2.2	5.9	2.2	6.0	7.7	2.2	0.8	1.4	-
31.10.78	E	2.7	7.1	6.5	4.4	3.8	5.4	2.1	4.0	1.9	5.9	7.1	1.9	0.9	1.2	5.9
07.11.78	F	2.9	6.6	6.5	4.0	3.8	5.2	2.2	4.2	2.3	5.8	7.2	2.0	0.7	1.0	5.6
14.11.78	G	2.8	8.4	6.9	4.8	4.2	5.6	2.6	4.8	2.6	6.1	9.4	2.7	0.8	1.1	6.5
21.11.78	H	2.0	8.1	6.6	5.4	3.9	5.3	2.3	3.3	1.4	5.9	7.9	1.6	0.7	1.4	4.3
28.11.78	I	2.2	7.7	6.5	4.7	4.0	5.3	2.1	3.8	1.7	6.0	7.1	1.6	0.7	1.1	5.3
05.12.78	J	2.3	10.0	6.5	7.2	4.1	5.2	2.6	4.0	2.0	6.3	11.0	2.6	0.7	1.3	6.2
12.12.78	K	2.1	9.2	6.8	5.0	4.1	5.5	2.3	3.5	1.6	6.4	8.5	1.6	0.7	1.4	4.1
19.12.78	L	2.2	7.5	6.5	4.6	3.8	5.4	2.1	3.6	1.8	6.1	6.8	1.7	0.6	1.3	3.9
09.01.79	M	2.7	6.0	6.0	5.0	3.9	5.7	1.8	3.3	1.9	5.9	5.5	1.5	0.7	1.5	2.9
06.02.79	N	2.7	6.0	5.8	4.6	3.5	5.5	-	4.0	2.0	6.0	5.3	1.7	-	1.4	3.5
27.02.79	O	1.9	5.2	5.9	4.5	3.4	5.4	-	3.1	1.5	6.0	5.2	1.7	-	1.7	-
13.03.79	P	2.5	5.5	6.4	4.5	3.4	5.5	1.9	3.0	1.8	5.9	4.6	1.3	0.6	1.1	3.2
27.03.79	Q	1.7	4.7	6.0	4.5	3.3	5.5	1.7	2.4	1.3	5.4	4.1	1.3	0.7	1.3	2.5
11.04.79	R	1.6	4.4	5.6	4.5	3.1	5.5	1.8	2.5	1.3	5.2	4.0	1.7	0.6	1.1	2.4
24.04.79	S	2.8	5.4	6.9	5.3	3.4	5.6	1.6	4.1	2.2	6.2	5.2	2.1	0.6	1.2	4.9
08.05.79	T	1.7	4.6	5.3	4.1	3.1	4.9	1.5	2.7	1.3	5.3	4.0	1.2	0.7	1.5	2.3
22.05.79	U	2.0	4.8	5.7	4.1	3.3	5.0	1.4	3.2	1.3	5.4	4.1	1.5	0.7	1.3	3.2
05.06.79	V	2.1	4.5	5.3	3.4	3.2	5.0	1.7	3.5	1.7	5.4	3.4	1.3	0.7	1.1	1.4
19.06.79	W	2.1	4.8	6.4	3.7	3.0	5.7	1.7	3.7	1.7	5.9	2.8	1.0	0.6	1.2	1.9
03.07.79	X	3.0	5.2	6.3	3.5	3.1	5.7	1.4	4.2	2.5	6.0	2.3	1.3	0.6	1.1	-
24.07.79	Y	3.3	-	6.8	-	3.8	5.8	1.7	4.9	2.6	6.3	3.1	1.8	0.7	1.0	-
07.08.79	Z	3.5	-	6.5	-	4.1	5.5	1.8	4.7	2.7	6.0	3.2	2.0	0.7	1.2	-
21.08.79	AA	2.0	6.9	6.5	-	4.4	5.7	1.9	3.8	1.6	6.1	5.7	1.6	0.7	1.3	-
04.09.79	BB	2.0	7.2	6.1	-	4.3	5.2	1.8	3.2	1.3	5.6	5.5	1.5	0.6	1.0	1.6
18.09.79	CC	2.4	6.5	6.2	-	7.1	5.1	2.2	4.6	2.0	5.4	5.6	3.0	0.8	1.0	-
02.10.79	DD	2.7	6.8	5.9	-	3.9	4.9	1.7	4.0	2.0	5.4	5.9	1.9	0.6	0.9	-

Bviii TOTAL IRON $Fe^{2+} + Fe^{3+}$ ($\mu g\ ml^{-1}$)

Sampling Date	Code	Site Number														
		1	2	3	4	6	7	8	11	13	16	17	18	100	101	3a
24.10.78	D	6.7	93.7	32.6	1.0	4.8	110.9	1.3	107.9	2.2	77.3	22.9	1.0	0.7	2.3	-
31.10.78	E	8.9	91.0	80.0	2.0	1.4	112.1	1.1	104.8	2.3	86.4	22.8	2.1	3.3	1.2	29.3
07.11.78	F	11.8	104.0	81.0	2.6	4.0	110.0	2.2	113.0	5.2	86.2	25.1	3.0	1.6	0.8	31.8
14.11.78	G	12.4	101.0	91.4	1.9	3.4	113.0	1.9	114.0	4.2	83.2	26.9	2.5	1.1	0.2	30.9
21.11.78	H	1.4	53.3	65.1	2.0	3.6	109.2	2.7	54.6	0.5	75.5	18.2	2.5	0.6	1.5	4.0
28.11.78	I	8.3	97.4	81.6	4.6	9.2	110.8	8.0	109.4	9.9	81.5	23.1	5.2	4.1	5.4	9.5
05.12.78	J	4.8	75.9	86.9	4.2	4.8	111.6	4.5	102.8	3.6	85.5	22.7	5.2	1.0	4.4	7.2
12.12.78	K	5.2	44.5	68.8	5.2	8.1	107.5	6.8	73.7	8.1	69.5	14.9	6.2	2.9	5.8	8.4
19.12.78	L	5.8	46.2	77.0	3.2	6.1	105.7	2.3	98.6	9.5	59.9	9.0	4.5	1.3	2.9	0.9
09.01.79	M	5.5	59.3	69.6	3.9	11.2	107.6	3.3	111.7	12.2	63.8	13.2	4.2	2.9	2.6	5.5
06.02.79	N	4.2	65.5	79.8	0.8	6.5	109.2	-	105.9	5.9	75.2	10.7	0.8	-	0.0	0.0
27.02.79	O	0.0	7.1	80.6	2.2	0.5	111.9	-	56.8	1.3	66.1	13.2	2.9	-	1.5	-
13.03.79	P	8.5	33.0	88.0	1.0	6.2	114.0	1.0	121.0	15.0	97.0	9.8	1.7	2.8	1.3	2.4
27.03.79	Q	2.3	17.0	70.0	1.3	5.1	110.0	2.1	42.0	1.9	77.0	8.9	1.7	3.4	2.1	2.1
11.04.79	R	2.6	18.0	60.0	3.0	7.1	114.0	3.9	38.0	3.2	65.0	8.6	5.5	1.7	1.7	0.9
24.04.79	S	7.7	53.0	92.0	1.5	2.3	104.0	1.0	99.0	4.0	108.0	15.0	1.6	0.0	1.9	3.7
08.05.79	T	2.0	19.0	65.0	4.5	6.7	116.0	6.3	29.0	5.7	86.0	16.0	5.5	5.3	5.0	6.2
22.05.79	U	4.1	37.0	68.0	1.3	2.4	106.0	2.5	49.0	4.0	83.0	18.0	0.3	1.0	1.0	2.4
05.06.79	V	10.0	75.0	76.0	5.3	3.3	109.0	2.8	73.0	5.1	95.0	20.0	4.2	0.3	1.5	7.1
19.06.79	W	7.0	98.0	85.0	5.7	4.3	102.0	2.3	77.0	5.7	102.0	34.0	1.9	0.7	1.7	10.0
03.07.79	X	10.0	123.0	113.0	4.1	8.1	119.0	2.6	114.0	12.0	53.0	55.0	4.1	2.0	3.3	-
24.07.79	Y	10.0	-	115.0	-	13.0	113.0	0.6	114.0	5.9	84.0	66.0	3.0	0.4	0.2	-
07.08.79	Z	12.0	-	103.0	-	17.0	97.0	3.5	101.0	7.3	38.0	66.0	3.9	0.2	0.8	-
21.08.79	AA	5.4	87.0	96.0	-	8.9	95.0	1.8	76.0	7.3	54.0	44.0	2.0	0.0	1.3	-
04.09.79	BB	2.5	119.0	109.0	-	14.6	105.0	3.3	75.0	2.9	90.0	53.0	4.7	1.6	2.1	2.3
18.09.79	CC	5.9	115.0	106.0	-	22.0	106.0	3.7	104.0	2.8	73.0	56.0	6.4	1.4	1.4	-
02.10.79	DD	10.7	121.0	110.0	-	35.0	110.0	1.0	112.0	8.6	52.0	58.0	6.1	1.5	1.5	-

Bix ALUMINIUM Al^{3+} ($\mu g\ ml^{-1}$)

Sampling Date	Code	Site Number														
		1	2	3	4	6	7	8	11	13	16	17	18	100	101	3a
19.06.79	W	1.3	3.1	11.8	10.5	0.0	68.5	0.0	43.9	4.2	12.5	2.3	0.0	0.0	0.0	5.4
03.07.79	X	4.6	1.4	11.0	10.5	0.3	76.1	0.0	47.9	13.8	11.9	1.9	0.0	0.0	0.0	-
24.07.79	Y	2.0	-	10.4	-	1.4	73.1	0.0	52.4	7.3	11.8	0.9	0.0	0.0	0.0	-
07.08.79	Z	2.0	-	13.8	-	3.0	81.0	0.0	58.0	9.8	15.0	2.0	0.0	0.0	0.0	-
21.08.79	AA	3.5	4.8	14.0	-	0.3	88.0	0.0	35.5	5.6	15.0	2.6	0.0	0.0	0.0	-

Bx CHLORIDE Cl^- ($\mu g\ ml^{-1}$)

Sampling Date	Code	Site Number														
		1	2	3	4	6	7	8	11	13	16	17	18	100	101	3a
24.10.78	D	89	99	103	149	128	71	23	35	53	135	78	64	21	32	-
31.10.78	E	85	92	124	149	121	71	21	28	43	135	78	57	21	28	117
07.11.78	F	92	92	121	149	128	67	21	28	43	135	82	64	18	21	114
14.11.78	G	92	99	114	149	128	85	21	35	50	128	85	71	14	28	121
21.11.78	H	64	82	114	135	103	27	17	14	39	121	71	35	14	28	71
28.11.78	I	78	85	114	135	121	114	21	28	50	121	71	57	18	32	89
05.12.78	J	85	85	114	149	121	21	21	28	92	135	78	60	14	32	89
12.12.78	K	85	85	106	135	114	28	21	28	64	117	67	42	18	28	64
19.12.78	L	71	82	114	121	110	75	18	35	42	121	67	43	18	28	64
09.01.79	M	170	75	111	124	129	31	17	28	135	104	60	44	18	43	57
06.02.79	N	131	76	124	121	168	30	-	28	100	112	70	56	-	40	66
27.02.79	O	146	75	117	111	123	35	-	28	148	106	63	48	-	58	-
13.03.79	P	97	74	119	103	116	35	21	53	47	101	53	35	25	34	56
27.03.79	Q	67	65	104	104	99	23	21	23	51	94	53	39	21	33	47
11.04.79	R	65	64	104	105	96	21	17	23	50	92	55	35	21	35	49
24.04.79	S	112	74	116	119	106	39	23	48	90	112	70	61	21	36	71
08.05.79	T	74	67	108	116	104	28	21	31	83	105	71	45	18	36	55
22.05.79	U	71	64	112	121	116	25	15	28	74	105	61	45	17	32	67
05.06.79	V	71	67	110	121	119	31	18	31	59	116	67	45	16	33	46
19.06.79	W	74	77	110	138	127	30	21	27	61	114	65	44	18	32	56
03.07.79	X	76	80	110	120	123	34	21	28	53	118	80	49	19	32	-
24.07.79	Y	81	-	109	-	121	28	19	33	63	96	83	50	22	28	-
07.08.79	Z	89	-	112	-	132	40	23	35	76	110	96	69	23	31	-
21.08.79	AA	65	71	110	-	136	39	26	35	76	101	88	54	27	33	-
04.09.79	BB	63	83	108	-	125	37	23	27	65	103	86	54	22	30	-
18.09.79	CC	70	72	108	-	128	41	24	35	64	97	111	63	22	29	-
02.10.79	DD	80	110	109	-	138	34	22	32	60	112	106	54	22	29	-

Bxi SULPHATE SO_4^{2-} ($\mu g\ ml^{-1}$)

Sampling Date	Code	Site Number														
		1	2	3	4	6	7	8	11	13	16	17	18	100	101	3a
24.10.78	D	454	680	692	634	322	2820	80	1600	346	900	572	120	66	58	-
31.10.78	E	278	613	804	690	352	2180	118	1300	346	850	596	80	100	120	780
07.11.78	F	356	732	794	726	330	2800	130	1420	506	770	526	170	84	84	795
14.11.78	G	340	706	890	596	326	2260	118	1290	416	930	594	130	54	80	900
21.11.78	H	178	570	792	524	110	2050	140	950	174	790	400	96	90	96	442
28.11.78	I	250	634	925	640	322	2290	102	870	206	870	494	102	90	110	830
05.12.78	J	224	720	1100	706	350	2360	170	925	210	890	542	118	60	72	720
12.12.78	K	185	570	910	622	366	2060	110	890	160	950	478	92	90	80	680
19.12.78	L	252	544	850	567	260	1900	100	1060	262	890	390	56	31	53	560
09.01.79	M	320	638	1030	756	353	3320	92	1320	357	1030	462	99	50	87	700
06.02.79	N	350	632	1090	782	310	2540	-	1360	391	1140	516	102	-	73	800
27.02.79	O	197	396	760	688	257	2230	-	592	147	1000	494	66	-	70	-
13.03.79	P	233	514	806	574	253	2450	45	1175	292	965	430	48	36	38	550
27.03.79	Q	160	458	870	636	265	2430	44	700	143	980	414	46	38	40	344
11.04.79	R	172	480	1000	613	281	2710	47	760	150	975	426	59	30	39	378
24.04.79	S	370	600	990	780	350	2670	48	1335	450	885	454	80	18	29	650
08.05.79	T	127	556	900	775	264	2490	36	585	184	1025	430	57	25	32	372
22.05.79	U	302	610	1020	700	274	2490	48	1125	256	900	500	75	25	32	554
05.06.79	V	308	680	755	755	414	2430	53	1425	410	1045	498	80	23	35	684
19.06.79	W	360	675	1010	820	404	2760	61	1095	390	1065	574	99	26	36	700
03.07.79	X	580	675	1010	830	336	2720	68	1545	695	1200	602	116	26	36	-
24.07.79	Y	642	-	1245	-	435	2350	68	1950	706	1245	710	132	32	36	-
07.08.79	Z	650	-	1105	-	505	2440	66	1550	630	1245	690	130	27	33	-
21.08.79	AA	440	560	655	-	475	2540	5	715	370	1165	605	79	26	37	-
04.09.79	BB	425	590	630	-	475	2460	59	1130	415	1190	615	75	28	35	-
18.09.79	CC	520	710	890	-	560	2760	65	1180	465	1115	585	70	31	38	-
02.10.79	DD	500	680	910	-	490	2620	64	960	485	1175	610	71	30	40	-

Bxii TRACE METALS ($\mu g\ ml^{-1}$)

Ion	Sample Number							
	1	2	3	7	8	11	16	100
Cu^{2+}	0.000	0.029	0.000	0.265	0.000	0.098	0.015	0.047
Ni^{2+}	0.020	0.090	0.300	1.900	0.000	0.390	0.360	0.000
Zn^{2+}	0.350	3.900	0.090	1.700	0.050	0.030	0.040	0.100
Cr^{3+}	0.000	0.001	0.001	0.450	0.001	0.003	0.001	0.000
Mn^{2+}	3.200	*5.000	*5.000	*5.000	2.200	*5.000	*5.000	1.500
Pb^{2+}	0.000	0.800	0.630	0.570	0.650	1.030	0.470	0.980
Cd^{2+}	0.000	0.010	0.020	0.070	0.010	0.030	0.010	0.000
V^{3+}	0.024	0.007	0.114	0.626	0.000	0.049	0.061	0.000

*Concentration above upper detection limit of 5.00 $\mu g\ ml^{-1}$

APPENDIX C

Mineral Analysis

Ci SAMPLE DESCRIPTION AND TREATMENT

Sample	Location	Description of Material	Mount Type	Scan Width	Scan Rate
MT1	'Little Mam Tor' face	Relatively 'fresh' mudstone from partially-cemented horizon	Powder Powder	4^{o}-$45^{o}2\theta$ 26^{o}-$33^{o}2\theta$	1^{o} 2θ min^{-1} $0.25^{o}2\theta$ min^{-1}
MT2a	'Little Mam Tor' face	Upper portion of light grey carbonate band	Powder Powder	4^{o}-$45^{o}2\theta$ 26^{o}-$33^{o}2\theta$	$1^{o}2\theta$ min^{-1} $0.25^{o}2\theta$ min^{-1}
MT2b	'Little Mam Tor' face	Centre portion of carbonate band; darker grey than 2a	Powder Powder	4^{o}-$45^{o}2\theta$ 26^{o}-$33^{o}2\theta$	$1^{o}2\theta$ min^{-1} $0.25^{o}2\theta$ min^{-1}
TT2c	'Little Mam Tor' face	Lower portion of carbonate band, light grey	Powder Powder	4^{o}-$45^{o}2\theta$ 26^{o}-$33^{o}2\theta$	$1^{o}2\theta$ min^{-1} $0.25^{o}2\theta$ min^{-1}
MT2x	'Little Mam Tor' face	Weathered shale in contact with top of MT2 carbonate sample	Powder	4^{o}-$45^{o}2\theta$	$1^{o}2\theta$ min^{-1}
MT3	'Little Mam Tor' face	Weathered shale from joint surface; yellow/brown staining	Powder <2μ smear <2μ smear(G)	4^{o}-$45^{o}2\theta$ 4^{o}-$30^{o}2\theta$ 4^{o}-$13^{o}2\theta$	$1^{o}2\theta$ min^{-1} $1^{o}2\theta$ min^{-1} $1^{o}2\theta$ min^{-1}
MT4	'Little Mam Tor' face	'Average'sample of weathered shale; scraped from across numerous horizons, c.10 cm below surface	Powder Powder	4^{o}-$45^{o}2\theta$ 26^{o}-$33^{o}2\theta$	$1^{o}2\theta$ min^{-1} $0.25^{o}2\theta$ min^{-1}
MT5	'Little Mam Tor'	Scree material below face; from c.5 cm below surface	Powder <2μ smear <2μ smear(G)	4^{o}-$45^{o}2\theta$ 4^{o}-$30^{o}2\theta$ 4^{o}-$13^{o}2\theta$	$1^{o}2\theta$ min^{-1} $1^{o}2\theta$ min^{-1} $1^{o}2\theta$ min^{-1}
MT6	'Little Mam Tor'	Highly broken down shale; from below grass covered scree	<2μ smear <2μ smear(G)	4^{o}-$30^{o}2\theta$ 4^{o}-$13^{o}2\theta$	$1^{o}2\theta$ min^{-1} $1^{o}2\theta$ min^{-1}
MT7	'Retrogressive unit' (above Site 7)	Brown weathered carbonate band from top of scarp face	Powder Powder	4^{o}-$45^{o}2\theta$ 26^{o}-$33^{o}2\theta$	$1^{o}2\theta$ min^{-1} $0.25^{o}2\theta$ min^{-1}

Sample	Location	Description of Material	Mount Type	Scan Width	Scan Rate
MT8	Retrogressive unit (above Site 7)	Dark grey carbonate band from centre of face	Powder Powder	4^{o}-$45^{o}2\theta$ 26^{o}-$33^{o}2\theta$	$1^{o}2\theta\ min^{-1}$ $0.25^{o}2\theta\ min^{-1}$
MT9	Retrogressive unit (above Site 7)	Fragments of weathered carbonate from scree below face	Powder Powder	4^{o}-$45^{o}2\theta$ 26^{o}-$33^{o}2\theta$	$1^{o}2\theta\ min^{-1}$ $0.25^{o}2\theta\ min^{-1}$
MT10	Retrogressive unit	Samples broken from very hard carbonate concretion lying at base of scree	Powder Powder	4^{o}-$45^{o}2\theta$ 26^{o}-$33^{o}2\theta$	$1^{o}2\theta\ min^{-1}$ $0.25^{o}2\theta\ min^{-1}$
BH74	Borehole 7 (depth 3.9m)	Small grey/brown shale fragments set in muddy material	Powder	4^{o}-$45^{o}2\theta$	$1^{o}2\theta\ min^{-1}$
BH76	Borehole 7 (depth 6.0 m)	Similar to BH74. Also contains coarse sandstone fragments	Powder	4^{o}-$45^{o}2\theta$	$1^{o}2\theta\ min^{-1}$
BH79	Borehole 7 (depth 9.0 m)	Grey and red-brown shale and very fine mud	Powder	4^{o}-$45^{o}2\theta$	$1^{o}2\theta\ min^{-1}$
BH710	Borehole 7 (depth 10.5 m)	More massive shale 'blocks', red and yellow surface weathering	Powder <0.5μ smear <0.5μ smear(G)	4^{o}-$45^{o}2\theta$ 4^{o}-$30^{o}2\theta$ 4^{o}-$28^{o}2\theta$	$1^{o}2\theta\ min^{-1}$ $1^{o}2\theta\ min^{-1}$ $1^{o}2\theta\ min^{-1}$
BH714	Borehole 7 (depth 14 m)	Brown sandy material and fine, dark grey mud	Powder	4^{o}-$45^{o}2\theta$	$1^{o}2\theta\ min^{-1}$
BH715	Borehole 7 (depth 15 m)	Fragmented dark grey shale	Powder Whole rock smear <0.5μ smear <0.5μ smear(G) <0.5μ smear(H)	4^{o}-$45^{o}2\theta$ 4^{o}-$45^{o}2\theta$ 4^{o}-$30^{o}2\theta$ 4^{o}-$28^{o}2\theta$ 4^{o}-$30^{o}2\theta$	$1^{o}2\theta\ min^{-1}$ $1^{o}2\theta\ min^{-1}$ $1^{o}2\theta\ min^{-1}$ $1^{o}2\theta\ min^{-1}$ $1^{o}2\theta\ min^{-1}$
BH717	Borehole 7 (depth 17.25 m)	Finely fragmented shale and siltstone	Powder	4^{o}-$45^{o}2\theta$	$1^{o}2\theta\ min^{-1}$

Sample	Location	Description of Material	Mount Width	Scan Width	Scan Rate
BH86	Borehole 8 (Depth 16.8 m)	Compact shale. Brown weathering and mica crystals	<0.5μ smear	4^{o}-$30^{o}2\theta$	$1^{o}2\theta\ min^{-1}$
			<0.5μ smear (G)	4^{o}-$28^{o}2\theta$	$1^{o}2\theta\ min^{-1}$
			<0.5μ smear (H)	4^{o}-$28^{o}2\theta$	$1^{o}2\theta\ min^{-1}$
BH88	Borehole 8 (Depth 22 m)	Compact 'fresh' grey shale	<0.5μ smear	4^{o}-$30^{o}2\theta$	$1^{o}2\theta\ min^{-1}$
			<0.5μ smear (G)	4^{o}-$28^{o}2\theta$	$1^{o}2\theta\ min^{-1}$
			<0.5μ smear (H)	4^{o}-$30^{o}2\theta$	$1^{o}2\theta\ min^{-1}$
BH89	Borehole 8 (Depth 27 m)	Highly fragmented grey shale; ? failure surface	<0.5μ smear	4^{o}-$30^{o}2\theta$	$1^{o}2\theta\ min^{-1}$
			<0.5μ smear (G)	4^{o}-$30^{o}2\theta$	$1^{o}2\theta\ min^{-1}$
			<0.5μ smear (H)	4^{o}-$30^{o}2\theta$	$1^{o}2\theta\ min^{-1}$
HCW1	Hope Cement Works Quarry	'Fresh'-looking compact light grey shale from unknown horizon	Whole rock smear	4^{o}-$47^{o}2\theta$	$1^{o}2\theta\ min^{-1}$
FS1	Failure surface	Slickensided surface of main shear plane as exposed along scree	<0.5μ smear	4^{o}-$30^{o}2\theta$	$1^{o}2\theta\ min^{-1}$
			<0.5μ smear (G)	4^{o}-$30^{o}2\theta$	$1^{o}2\theta\ min^{-1}$
			<0.5μ smear (H)	4^{o}-$30^{o}2\theta$	$1^{o}2\theta\ min^{-1}$
SP1	Soil pit above retrogressive units	Finely fragmented shale from turf layer	Heavy fraction smear	4^{o}-$44^{o}2\theta$	$1^{o}2\theta\ min^{-1}$
			<2 μ smear	4^{o}-$30^{o}2\theta$	$1^{o}2\theta\ min^{-1}$
			<0.5μ smear	4^{o}-$32^{o}2\theta$	$1^{o}2\theta\ min^{-1}$
			<0.5μ smear (G)	4^{o}-$20^{o}2\theta$	$1^{o}2\theta\ min^{-1}$
			<0.5μ smear (H')	4^{o}-$20^{o}2\theta$	$1^{o}2\theta\ min^{-1}$
SP2	Soil pit above retrogressive units	Light grey brown shale; 25 cm down in soil pit	Heavy fraction smear	4^{o}-$44^{o}2\theta$	$1^{o}2\theta\ min^{-1}$
			<2 μ smear	4^{o}-$30^{o}2\theta$	$1^{o}2\theta\ min^{-1}$
			<0.5μ smear	4^{o}-$32^{o}2\theta$	$1^{o}2\theta\ min^{-1}$
			<0.5μ smear (G)	4^{o}-$20^{o}2\theta$	$1^{o}2\theta\ min^{-1}$
			<0.5μ smear (H)	4^{o}-$20^{o}2\theta$	$1^{o}2\theta\ min^{-1}$
			<0.5μ smear (H')	4^{o}-$20^{o}2\theta$	$1^{o}2\theta\ min^{-1}$

Sample	Location	Description of Material	Mount Type	Scan Width	Scan Rate
SP3	Soil pit above retrogressive units	Weathered shale at base of soil pit (45 cm down)	Heavy fraction smear	4^{o}-$44^{o}2\theta$	$1^{o}2\theta$ min^{-1}
			<2 μ smear	4^{o}-$30^{o}2\theta$	$1^{o}2\theta$ min^{-1}
			<0.5μ smear	4^{o}-$32^{o}2\theta$	$1^{o}2\theta$ min^{-1}
			<0.5μ smear (G)	4^{o}-$20^{o}2\theta$	$1^{o}2\theta$ min^{-1}
			<0.5μ smear (H')	4^{o}-$20^{o}2\theta$	$1^{o}2\theta$ min^{-1}
G2	Retrogressive units	Highly weathered, gypsiferous shale from face below soil pit	Heavy fraction smear	4^{o}-$44^{o}2\theta$	$1^{o}2\theta$ min^{-1}
			<2 μ smear	4^{o}-$44^{o}2\theta$	$1^{o}2\theta$ min^{-1}
			<0.5μ smear	4^{o}-$32^{o}2\theta$	$1^{o}2\theta$ min^{-1}
			<0.5μ smear (G)	4^{o}-$20^{o}2\theta$	$1^{o}2\theta$ min^{-1}
			<0.5μ smear (H')	4^{o}-$20^{o}2\theta$	$1^{o}2\theta$ min^{-1}
			<0.5μ smear (H)	4^{o}-$20^{o}2\theta$	$1^{o}2\theta$ min^{-1}
A	Carbonate concretion	Spherical white masses, c. 2 mm in diameter from surface of large concretion	Smear	4^{o}-$30^{o}2\theta$	$1^{o}2\theta$ min^{-1}
B	Carbonate concretion	Soft yellow surface coating	Smear	4^{o}-$35^{o}2\theta$	$1^{o}2\theta$ min^{-1}
C	Carbonate concretion	Hard orange surface coating	Smear	4^{o}-$32^{o}2\theta$	$1^{o}2\theta$ min^{-1}
D	Carbonate concretion	Hard purplish-red surface layer	Smear	4^{o}-$35^{o}2\theta$	$1^{o}2\theta$ min^{-1}
E	Carbonate concretion	Fibrous white surface and synaresis crack material	Smear	4^{o}-$44^{o}2\theta$	$1^{o}2\theta$ min^{-1}
F	Carbonate concretion	White powdery surface coating	Smear	4^{o}-$30^{o}2\theta$	$1^{o}2\theta$ min^{-1}
G	Odin Sitch	White precipitate from stream	Smear	4^{o}-$45^{o}2\theta$	$1^{o}2\theta$ min^{-1}
H	Seepage at Site 3	White crystalline coating on plant stems	Smear	4^{o}-$50^{o}2\theta$	$1^{o}2\theta$ min^{-1}

Sample	Location	Description of Material	Mount Type	Scan Width	Scan Rate
I	Seepage at Site 3	Purplish-red ochre on stream bed	Smear	4^{o}-$45^{o}2\theta$	$1^{o}2\theta$ min^{-1}
J	Seepage at Site 3	Orange-red ochre from 10 cm down in auger core	Smear	4^{o}-$45^{o}2\theta$	$1^{o}2\theta$ min^{-1}
K	Seepage at Site 3	Orange ochre from 40 cm down in auger core	Smear	4^{o}-$45^{o}2\theta$	$1^{o}2\theta$ min^{-1}

Explanation of Symbols:

(G) Sample placed in atmosphere saturated with ethylene glycol at $60^{o}C$ for 20 minutes

(H') Sample heated at $250^{o}C$ for 1 hour

(H) Sample heated at $550^{o}C$ for 1 hour

Cii MINERALOGY OF SAMPLES

XXX very strong peak XX strong peak X good peak t very slight peak

	MT1	MT2a	MT2b	MT2c	MT2x	MT3	MT4	MT5	MT6	MT7	MT8	MT9	MT10	BH74	BH76	BH77	BH79	BH710	BH714	BH715	BH717	SP1	SP2	SP3	G2	BH86	BH88	BH89	HCW1	FS1	A	B	C	D	E	F	G	H	I	J	K
Chlorite														X	X	X	X		X	X	X	X	X	t		X	X	X	X	X											
12Å Clay						X		X	t											t		X	X	X	X	t	X	X		X											
Illite	X	t				X	X	X	X					X	X	X	X	X	X	X	X	X	X	X	X	X	X	X	X	X	X											
Kaolinite	X	t			X	X	X	X	X					X	X	X	X	X X	X	X X	X	X	X	X	X	X	X	X	X	X											
Quartz	X X	X	t	t	X	X X	X X	X X	X	t	t	X	t	X X	X X X	X X	X X	X	X X X	X X	X X		X	X	X	X			X	X	X X											
Feldspar			X	t		t			t	X				X	X	t	t	X	X	X	X																				
Siderite		X	X	X					X	X	X	t																													
Ankerite	X	X X	X X	X X					X X X	X X X	X X	X X																													
Dolomite									X X	X	X	X X																													
Calcite	X X	X	X	X					X	X	X	X																						X X X							
Pyrite	X X	X X	X	X X	X	X	X	t	X	X X	X	X X																t												
Goethite														t	t	t	t	X	t	t	t								X			X	X					t	X	
Jarosite					X	X	X	X	t							t				t		X	X	X		t	X		t	X		X								
Gypsum	X	X	t	t	X X	X	X	X		t	t	X	X											X X X					X X X					X X X	X X X	X X X				
2.03Å ?	X	X	X	X	X	X	X	X	X	X	X	X	X	X	X	X	X	X	X	X	X	X																		

Ciii COMPARISON OF PURE MINERAL SAMPLES (AFTER BROWN, 1961) WITH SELECTED SAMPLES FROM MAM TOR

1. Pyrite (FeS_2)

hkl	Brown		MT1		MT2a		MT2b		MT2c		MT2x	
	d(Å)	I	d(Å)	I	d(Å)	I	d(Å)	I	d(Å)	I	d(Å)	I
(111)	3.13	36	3.14	40	-	-	-	-	3.14	Trace	3.13	Trace
(200)	2.71	84	2.71	100	2.71	30	2.69	25	2.70	25	2.71	Trace
(210)	2.42	66	2.42	60	2.42	60	2.42	50	2.42	45	2.42	Trace
(211)	2.21	52	2.21	50	2.21	100	2.20	100	2.21	100	2.22	Trace
(220)	1.92	40	-	-	-	-	-	-	-	-	-	-
(311)	1.63	100	-	-	-	-	-	-	-	-	-	-

2. Jarosite ($KFe_3(SO_4)_2(OH)_6$)

	Brown		G2		SP2		SP1		BH89	
	d(A)	I	d(A)	I	d(A)	I	d(A)	I	d(A)	I
(101)	5.93	/7	-	-	-	-	-	-	-	-
(003)	5.70	5	5.71	5	5.71	5	5.71	6	5.69	4
(012)	5.09	8	5.08	10	5.08	10	5.08	10	5.08	10
(021)	3.11	8	-	-	-	-	3.11	3	-	-
(113)	3.07	10	3.08	8	3.08	6	3.08	5	3.08	1
(006)	2.85	8	2.86	2	-	-	-	-	-	-
(107)	2.28	8	2.28	4	-	-	-	-	-	-

hkl	3. Gypsum ($CaSO_4.2H_2O$)											
	Brown		H		A		F		G		MT2a	
	d(A)	I	d(A)	I	d(A)	I	d(A)	I	d(A)	I	d(A)	I
(020)	7.56	100	7.56	100	7.56	100	7.56	100	7.56	100	7.63	100
(12$\bar{1}$)	4.27	51	4.28	20	4.28	15	4.27	5	4.27	1	4.28	25
(031) (040)	3.79	21	3.79	35	3.79	25	3.79	10	3.79	5	3.80	30
(14$\bar{1}$)	3.06	57	3.08	30	3.07	25	3.06	8	3.06	2	3.07	15
(002)	2.87	27	2.88	5	-	-	-	-	-	-	2.87	Trace
(022) (051)	2.68	28	2.68	5	-	-	-	-	-	-	2.68	Trace